UNCLASS

SECURITY CLASSIFICATION OF THIS PAGE (When Data Entered)

REPORT DOCUMENTATION PAGE	READ INSTRUCTIONS BEFORE COMPLETING FORM
1. REPORT NUMBER: AFIT/CI/NR 84-9D	2. GOVT ACCESSION NO. / 3. RECIPIENT'S CATALOG NUMBER
4. TITLE (and Subtitle): Response and Performance of Contingency Airfield Pavements Containing Stabilized Material Layers	5. TYPE OF REPORT & PERIOD COVERED: THESIS/DISSERTATION
	6. PERFORMING ORG. REPORT NUMBER
7. AUTHOR(s): Robert Riddick Costigan	8. CONTRACT OR GRANT NUMBER(s)
9. PERFORMING ORGANIZATION NAME AND ADDRESS: T STUDENT AT: University of Illinois at Urbana-Champaign	10. PROGRAM ELEMENT, PROJECT, TASK AREA & WORK UNIT NUMBERS
CONTROLLING OFFICE NAME AND ADDRESS: T/NR, FB OH 45433	12. REPORT DATE: April 1984
	13. NUMBER OF PAGES: 267
MONITORING AGENCY NAME & ADDRESS (if different from Controlling Office)	15. SECURITY CLASS. (of this report): UNCLASS
	15a. DECLASSIFICATION/DOWNGRADING SCHEDULE

DISTRIBUTION STATEMENT (of this Report)

PROVED FOR PUBLIC RELEASE; DISTRIBUTION UNLIMITED

17. DISTRIBUTION STATEMENT (of the abstract entered in Block 20, if different from Report)

18. SUPPLEMENTARY NOTES

APPROVED FOR PUBLIC RELEASE: IAW AFR 190-1

LYNN E. WOLAVER 14 May 84
Dean for Research and
Professional Development
AFIT, Wright-Patterson AFB OH

19. KEY WORDS (Continue on reverse side if necessary and identify by block number)

20. ABSTRACT (Continue on reverse side if necessary and identify by block number)

ATTACHED

DTIC FILE COPY

DTIC ELECTE MAY 29 1984 S D A

PII Redacted

AD-A141 466

DD FORM 1 JAN 73 1473 EDITION OF 1 NOV 65 IS OBSOLETE

UNCLASS

SECURITY CLASSIFICATION OF THIS PAGE (When Data Entered)

84 05 21 139

RESPONSE AND PERFORMANCE OF CONTINGENCY AIRFIELD PAVEMENTS CONTAINING STABILIZED MATERIAL LAYERS

Robert Riddick Costigan, Ph.D.
Department of Civil Engineering
University of Illinois at Urbana-Champaign, 1984

The purpose of this study was to validate the mechanistic approach for the design and evaluation of Contingency Airfield Pavements (CAPs) containing stabilized material layers. The mechanistic approach was validated by relating predicted first pass structural response parameters (stress and strain) to observed performance of field test items.

Eleven CAP test items were constructed; eight two-layer items containing a rigid cement aggregate mixture and two inverted pavement items containing stone base and stabilized subbase courses. Items were subjected to simulated channelized F-4 main gear traffic using a load cart.

Stabilized material layer modulus was back-calculated using Falling Weight Deflectometer load-deflection data. First pass predicted structural response was determined using finite element computer programs. The test items were thin by conventional design standards and had predicted first pass stress ratios in the stabilized material layers greater than one. Transfer functions were developed relating predicted first pass crack stress or strain ratios to passes to functional failure.

This document has been approved for public release and sale; its distribution is unlimited.

DTIC ELECTE MAY 2 3 1984 A

Major study findings included: 1) Subgrade characteristics control performance in pavements with predicted first pass crack stress ratio greater than one. 2) CAPs should be designed and evaluated using an intact slab concept. 3) Design of CAPs should be based on stress or strain ratios less than one. 4) The presence of a crushed stone base course over a stabilized subbase course in an inverted pavement has a bridging effect at transfer cracks in the stabilized subbase and inhibits the rate of crack propagation to the surface.

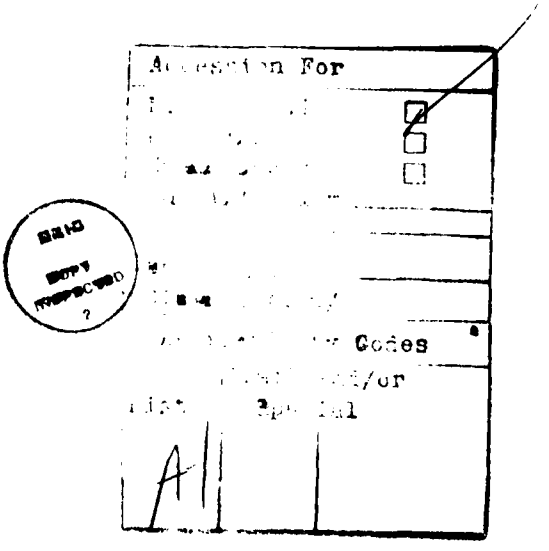

AFIT RESEARCH ASSESSMENT

The purpose of this questionnaire is to ascertain the value and/or contribution of research accomplished by students or faculty of the Air Force Institute of Technology (ATC). It would be greatly appreciated if you would complete the following questionnaire and return it to:

AFIT/NR
Wright-Patterson AFB OH 45433

RESEARCH TITLE: Response and Performance of Contingency Airfield Pavements Containing Stabilized Material Layers

AUTHOR: Robert Riddick Costigan

RESEARCH ASSESSMENT QUESTIONS:

1. Did this research contribute to a current Air Force project?

( ) a. YES ( ) b. NO

2. Do you believe this research topic is significant enough that it would have been researched (or contracted) by your organization or another agency if AFIT had not?

( ) a. YES ( ) b. NO

3. The benefits of AFIT research can often be expressed by the equivalent value that your agency achieved/received by virtue of AFIT performing the research. Can you estimate what this research would have cost if it had been accomplished under contract or if it had been done in-house in terms of manpower and/or dollars?

( ) a. MAN-YEARS _____ ( ) b. $_____

4. Often it is not possible to attach equivalent dollar values to research, although the results of the research may, in fact, be important. Whether or not you were able to establish an equivalent value for this research (3. above), what is your estimate of its significance?

( ) a. HIGHLY SIGNIFICANT ( ) b. SIGNIFICANT ( ) c. SLIGHTLY SIGNIFICANT ( ) d. OF NO SIGNIFICANCE

5. AFIT welcomes any further comments you may have on the above questions, or any additional details concerning the current application, future potential, or other value of this research. Please use the bottom part of this questionnaire for your statement(s).

NAME GRADE POSITION

ORGANIZATION LOCATION

STATEMENT(s):

RESPONSE AND PERFORMANCE OF CONTINGENCY AIRFIELD PAVEMENTS CONTAINING STABILIZED MATERIAL LAYERS

BY

ROBERT RIDDICK COSTIGAN

B.S., Virginia Military Institute, 1970
M.S., University of Missouri-Columbia, 1974

THESIS

Submitted in partial fulfillment of the requirements
for the degree of Doctor of Philosophy in Civil Engineering
in the Graduate College of the
University of Illinois at Urbana-Champaign, 1984

Urbana, Illinois

UNIVERSITY OF ILLINOIS AT URBANA-CHAMPAIGN

THE GRADUATE COLLEGE

APRIL 1984

WE HEREBY RECOMMEND THAT THE THESIS BY

ROBERT RIDDICK COSTIGAN

ENTITLED RESPONSE AND PERFORMANCE OF CONTINGENCY AIRFIELD PAVEMENTS CONTAINING STABILIZED MATERIAL LAYERS

BE ACCEPTED IN PARTIAL FULFILLMENT OF THE REQUIREMENTS FOR THE DEGREE OF DOCTOR OF PHILOSOPHY

Marshall R Thompson
Director of Thesis Research

Ernest J Barenberg
Head of Department

Committee on Final Examination†

Marshall R Thompson
Chairman

Michael I. Darter

Barry J Dempsey

† Required for doctor's degree but not for master's.

O-517

ACKNOWLEDGMENT

The author gratefully acknowledges the advice, support, and encouragement of Professor Marshall R. Thompson during the course of this research. Appreciation is expressed to the U.S. Army Engineer Waterways Experiment Station, Pavement Systems Division, Prototype Testing and Evaluation Unit and especially Albert J. Bush, III for their support in providing the field data used in this research. Special thanks are extended to Ruth Pembroke for her assistance throughout the course of this research. The author wishes to thank his wife, Judy, for her support, understanding, and love. Finally, the author must acknowledge the spiritual support of God, without which this endeavor would not have been completed.

TABLE OF CONTENTS

Page

LIST OF TABLES

LIST OF FIGURES

Figure | Page

Figure | Page

RESPONSE AND PERFORMANCE OF CONTINGENCY AIRFIELD PAVEMENTS CONTAINING STABILIZED MATERIAL LAYERS

Robert Riddick Costigan, Ph.D.
Department of Civil Engineering
University of Illinois at Urbana-Champaign, 1984

The purpose of this study was to validate the mechanistic approach for the design and evaluation of Contingency Airfield Pavements (CAPs) containing stabilized material layers. The mechanistic approach was validated by relating predicted first pass structural response parameters (stress and strain) to observed performance of field test items.

Eleven CAP test items were constructed; eight two-layer items containing a rigid cement aggregate mixture and two inverted pavement items containing stone base and stabilized subbase courses. Items were subjected to simulated channelized F-4 main gear traffic using a load cart.

Stabilized material layer modulus was back-calculated using Falling Weight Deflectometer load-deflection data. First pass predicted structural response was determined using finite element computer programs. The test items were thin by conventional design standards and had predicted first pass stress ratios in the stabilized material layers greater than one. Transfer functions were developed relating predicted first pass crack stress or strain ratios to passes to functional failure.

Major study findings included: 1) Subgrade characteristics control performance in pavements with predicted first pass crack stress ratio greater than one. 2) CAPs should be designed and evaluated using an intact slab concept. 3) Design of CAPs should be based on stress or strain ratios less than one. 4) The presence of a crushed stone base course over a stabilized subbase course in an inverted pavement has a bridging effect at transfer cracks in the stabilized subbase and inhibits the rate of crack propagation to the surface.

CHAPTER 1

INTRODUCTION

A. BACKGROUND ON CONTINGENCY AIRFIELD PAVEMENTS

1. Requirement

The North Atlantic Treaty Organization's plan for defending Western Europe relies on air superiority and close air support provided by fighter aircraft stationed at airbases in Western Europe. The majority of these fighter aircraft were made in the United States and include the F-4, F-15, and the F-16. Compared to earlier generation aircraft, these modern fighter aircraft need smoother and stronger airfield pavements despite their increased sophistication (Reference 1). The requirements of high quality smooth surfaces and continued use of fixed airfields make the airfield's pavements a prime target. An enemy can neutralize the effectiveness of another's air force by damaging the airfield pavements so planes cannot takeoff or land. The vulnerability of the airfield pavements has been further increased in recent years by construction of hardened aircraft shelters which greatly reduce the vulnerability of aircraft on the ground (Reference 1).

Over the past 6 years (1977-1983), considerable progress has been made in developing new procedures, equipment, and materials for repairing large and small bomb craters as well as rocket and cannon spalls. Although these improvements have increased the Rapid Runway Repair capability of base recovery forces, resumption of even limited fighter aircraft operations within the desired limit after sustaining an attack is still questionable.

Although research is continuing in the areas of protective clothing, equipment hardening, unexploded ordnance disposal, and bomb crater repair, a very attractive alternative of meeting the desired time limit for resumption of aircraft operations exists. Construction of contingency airfield pavements (CAPs) during peacetime for immediate availability after an attack provides a feasible alternative to the resource intense Rapid Runway Repair. The increased surface redundancy provided by from 1 million to 10 million square feet of additional prepositioned pavement, properly located, can insure the availability of an undamaged section large enough to support aircraft operations (Reference 2). Increased surface redundancy greatly complicates the enemy's targeting problems and reduces the probability of achieving a total airfield closure. Feasibility of the CAPs concept depends upon pavements that are inexpensive to build, reliable, and easy to inspect and maintain.

2. CAP User Requirements

It is anticipated contingency airfield pavements will be used only in wartime and then only until the primary runway and taxiway are repaired. Traffic levels will be much less than on the primary airfield pavements. Considering the expected level of damage, available repair resources, and aircraft sortie rates, these CAPs are currently expected to safely support approximately 150 fighter aircraft sorties. These aircraft will be loaded to their maximum allowable takeoff weight.

Expected aircraft ground operations on the CAPs include the normal taxi and takeoff modes. Landing operations, however, may be more severe because of the shorter distances available for landing.

3. Previous Research

The US Air Force and the US Army conducted research in the 1960s and 1970s on expedient construction of unsurfaced and stabilized airfields for forward operating bases (References 3, 4, 5, 6). The bulk of the effort was for expedient construction under severe time and material constraints. The peacetime construction of CAPs allows the use of high quality materials and better quality control. The traffic levels considered in the previous research were much greater than now envisioned for the CAPs. CAPs designed using the results of the previous research would be conservative because of the use of higher quality materials can now be used and lower pass levels are expected.

The US Air Force has also conducted extensive research in aircraft/soil response and interaction. The goal of this research was to characterize the forces involved in this complex interaction and to quantify them so criteria could be developed for the emergency operation of fighter aircraft on unimproved soil surfaces. Project SAFE, Soil Airfield Fighter Environment, was completed in 1983 by the Air Force Wright Aeronautical Laboratories, Wright-Patterson AFB, Ohio (Reference 7). Since the purpose of this research was emergency aircraft operation on unimproved soil surfaces, the results of this research have limited applicability for the design of CAPs containing stabilized material layers.

In 1981, the US Air Force contracted with the US Army Engineer Waterways Experiment Station (WES) to conduct field tests of conventional flexible pavements with a thin asphalt concrete wearing course and a granular base course. The purpose of the test was to

determine the minimum asphalt concrete wearing course thickness needed for fighter aircraft traffic. Preliminary indications are the minimum asphalt concrete wearing course thickness for F-4 aircraft can be reduced from the current 3 inch requirement.

Thompson and Dempsey (Reference 8) demonstrated the feasibility of a mechanistic design approach for CAPs containing stabilized material layers in their "ALRS Stabilized Material Pavement Analysis System (SPAS)." Stabilized material properties, structural modeling and behavior concepts, and environmental factors were considered in this system. They recommended further research and development to validate the approach.

B. CONTINGENCY AIRFIELD PAVEMENT FIELD TEST

In early 1981, the US Air Force concurred with the recommendation for validation testing of the SPAS. The University of Illinois was directed to design several CAP test pavements using the SPAS, and WES was directed to build the test items and conduct field traffic testing. Eleven CAP pavement test items containing stabilized material layers were constructed at Vicksburg, Mississippi. The test items were subjected to simulated channelized F-4 passes until failure or 1000 passes. Nine two-layer cement stabilized pavement test items of different strength and thickness and two inverted pavement test items containing crushed stone base courses and stabilized material subbase courses were constructed on a CBR 5-6 subgrade. Stabilized material layer thickness was selected to provide structural response and

performance data for failure pass levels ranging from less than 100 to over 1000 passes.

The data collected from laboratory materials testing and field measurements will be published by the US Air Force. Preliminary data are available in unpublished form (Reference 9) and are the focus of the research contained in this report.

C. RESEARCH OBJECTIVE

Stabilized materials offer excellent potential for constructing CAPs (Reference 8). They can be built easily and inexpensively with locally available materials and conventional techniques. A validated mechanistic design approach for CAPs containing stabilized material layers is not currently available for the conditions of low volume traffic, high gear loads, and high tire pressures. The tools are available for refining, improving, expanding, and validating such a mechanistic design approach.

The overall objective of this research is to relate predicted first pass structural response parameters with observed field performance of CAPs containing stabilized material layers. Predicted structural response parameters include stresses, strains, deflections, and ultimate load capacity. Field response and performance data were obtained during the CAP field test at WES (Reference 9). Relating predicted first pass response parameters with observed performance provides the information necessary for evaluating, refining, and validating the mechanistic design approach.

D. REPORT ORGANIZATION

Chapter 2 contains a detailed description of the CAP field test conducted at WES. Laboratory and field data are presented as well as the mechanistic design approach used to select stabilized material layer thickness and strength. Material characterization is covered in Chapter 3 and includes the subgrade, cement and lime stabilized mixtures, crushed limestone, and asphalt concrete used to construct the test items. Chapter 4 introduces general response and performance concepts applicable to the CAP test items. These include phases of item performance, crack effects, structural and functional failure, and stress and strain transfer functions. Chapters 5 and 6 cover the detailed response and performance of the two-layer and inverted pavement test items respectively. An overall discussion of test item response and performance is covered in Chapter 7. Chapter 8 presents the report findings and their implications relative to the mechanistic design and evaluation of CAPs containing stabilized material layers.

CHAPTER 2

CONTINGENCY AIRFIELD PAVEMENT FIELD TEST

A. GENERAL TEST DESCRIPTION

Eleven 30 foot long by 12 foot wide test items (Figures 2-1, 2-2) were constructed at the Waterways Experiment Station (WES), Vicksburg, Mississippi. Construction began on 27 October and was completed on 31 October, 1982. A mechanically processed medium strength heavy clay was used for the subgrade in all the items. The processed clay was placed on undisturbed lean clay underlying the test site. Items 1 through 8 were cement aggregate mixture (CAM) rigid two-layer pavements of different strength and thickness. Item 11 was similar except it was surfaced with a 1 inch asphalt concrete wearing course. The inverted pavement test items had a 1 inch asphalt concrete wearing course, 4 inches of crushed limestone base course, and 12 inches of either lime stabilized clay (item 9) or CAM (item 10) subbase course.

Simulated F-4 aircraft traffic was applied in a single channelized lane down the center of the item using a load cart fitted with an F-4 main gear tire loaded to 27,000 pounds and pressurized to 265 psi. Items were trafficked from 10 January until 26 January, 1983. The traffic was applied until structural failure or 1000 passes whichever occurred first. Extensive amounts of field and laboratory data were collected before, during, and after traffic and are contained in a data report prepared by WES (Reference 9).

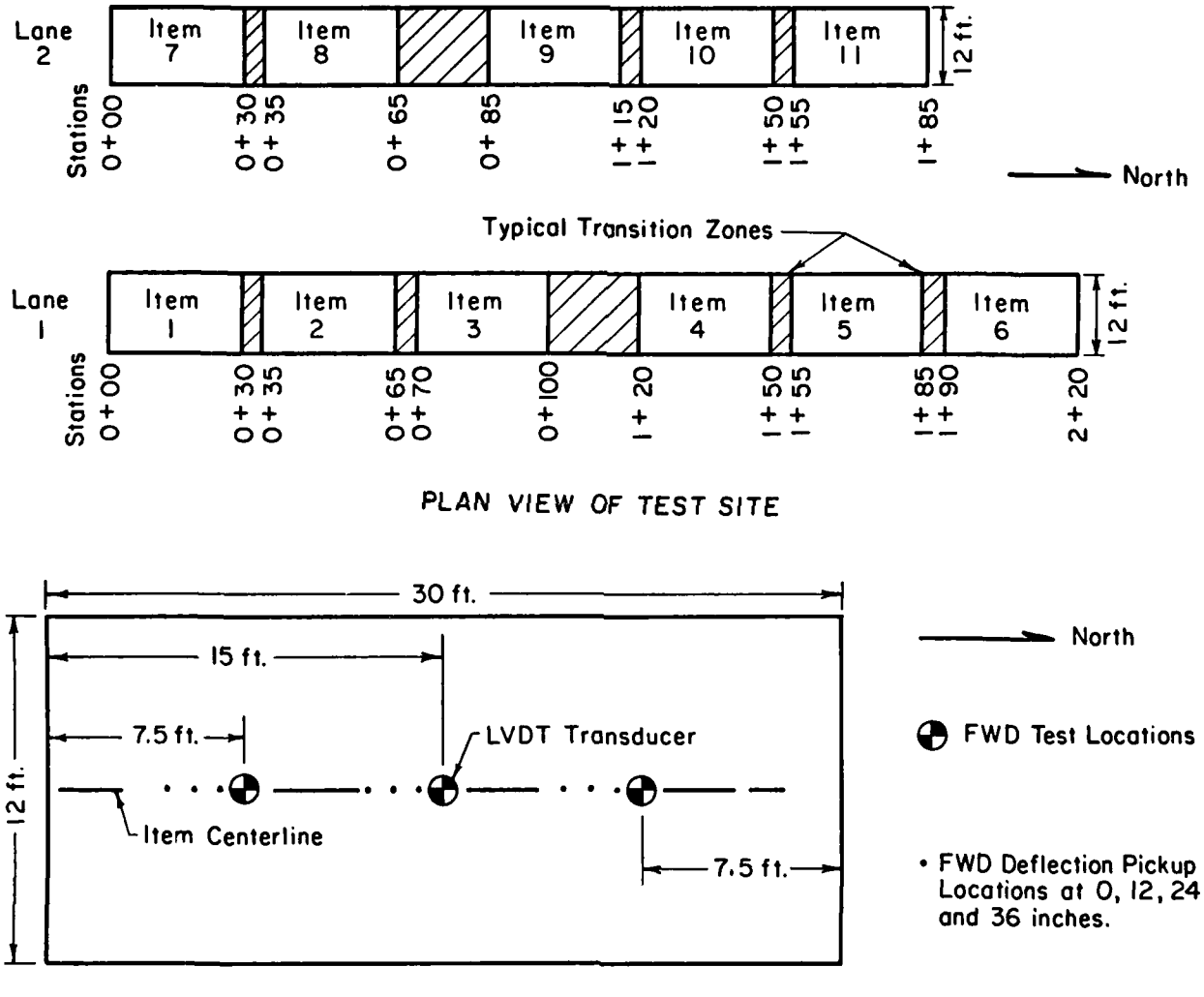

Figure 2-1. Contingency Airfield Pavement (CAP) Test Site Layout

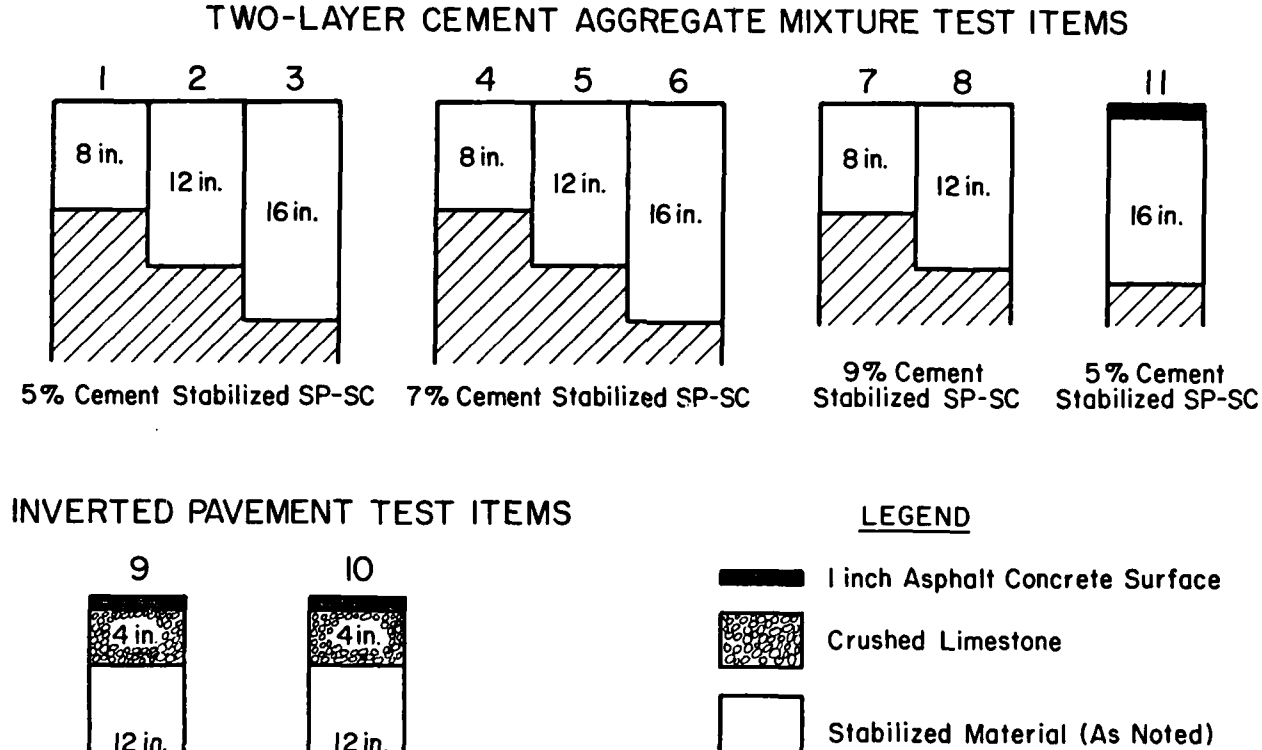

Figure 2-2. Description of CAP Test Items

B. MECHANISTIC DESIGN OF CAP TEST ITEMS

A mechanistic design approach (Figure 2-3) was used to design the 11 CAP test items (Reference 8). A mechanistic design approach permits the extrapolation of material strength and thickness effects over a broader range than used in the test items.

The ILLI-PAVE finite element structural model (Reference 10) was used to develop a structural response data base for two-layer pavements subjected to F-4 interior loading of 27,000 pounds and 265 psi tire pressure. The F-4 ILLI-PAVE data base (Appendix C) contains 96 combinations of stabilized material layer modulus, thickness, and subgrade support. The parameters considered were:

Stabilized material layer thickness: 9, 12, 15 and 18 inches.
Stabilized material layer modulus: 100, 200, 500, 1,000 and 2,000 ksi.
Standard subgrade models: very soft, soft, medium and stiff.

The F-4 ILLI-PAVE data base shows the major factor affecting the flexural stress in the rigid stabilized material layer is layer thickness. E_{ri} has very little effect.

The standard medium subgrade was selected as representative of the expected CAP subgrade. ILLI-PAVE interior flexural (tensile) stress at the bottom of the stabilized material layer was increased by 50 percent to account for increased stress at the expected transverse shrinkage cracks.

A range of CAM strengths was considered by varying the percent cement content. Figure 2-4 shows the assumed modulus-strength

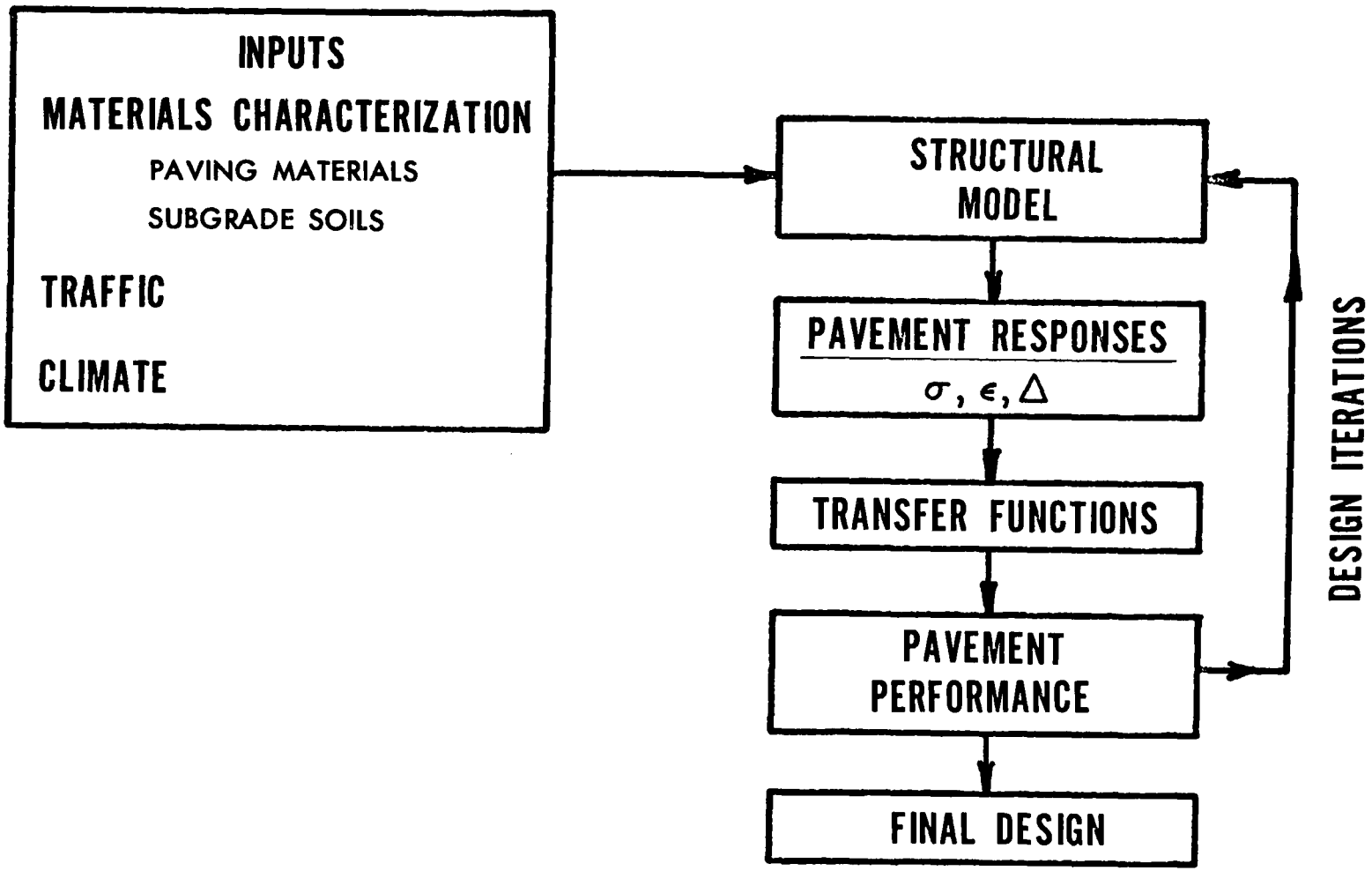

Figure 2-3. Mechanistic Design Approach

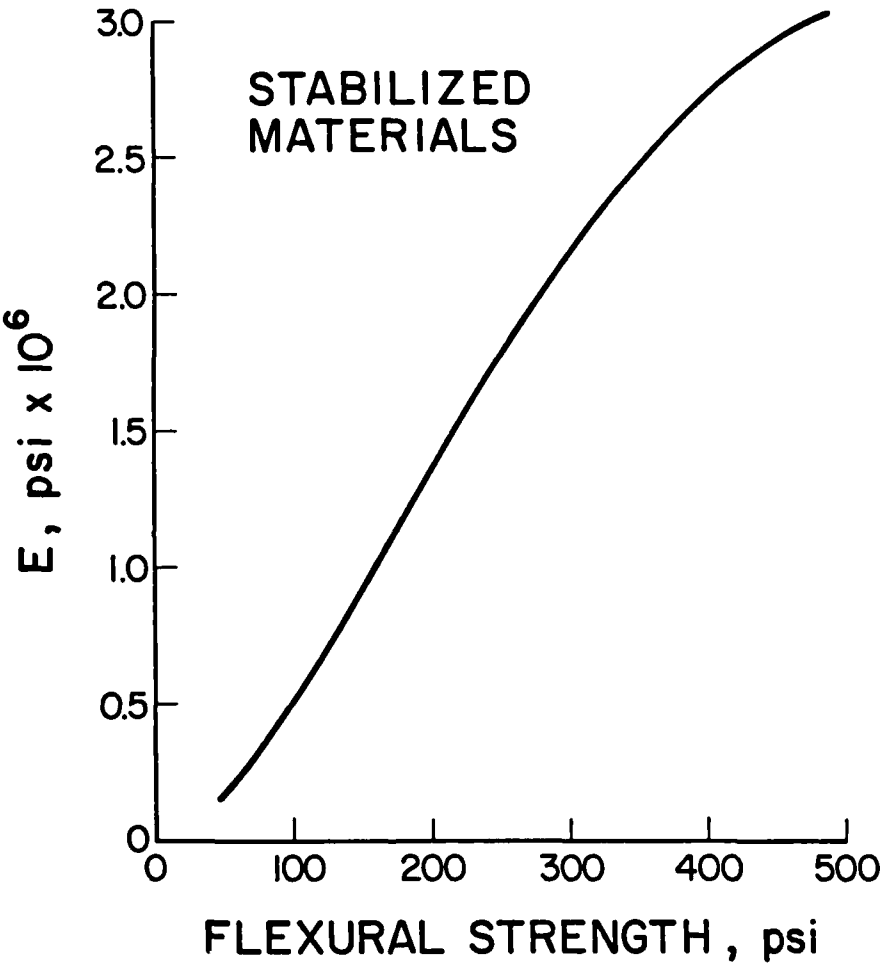

Figure 2-4. Generalized Material Modulus-Flexural Strength for Cement Stabilized Materials (Reference 8)

relationship for the CAM material. Performance was predicted by relating the predicted first pass crack stress ratio (tensile stress/flexural strength) in the stabilized material layer to the number of load applications to failure using the transfer function in Figure 2-5. Design thicknesses were then selected to produce failures below, at, and above the desired 150 passes. CAM cement content and thickness design values for the 11 CAP test items are shown in Figure 2-2.

C. MATERIALS AND CONSTRUCTION PROCEDURES

A detailed description of the construction procedures used in the CAP field test is contained in Reference 9. A summary of the more important points is included herein.

A heavy clay (classified CH by WES on the Unified Soil Classification System, Figure 2-6) was used as the subgrade material for all test items. The clay was also lime treated (Figures 2-7) and used as a stabilized subbase course in item 9.

A poorly graded gravelly clayey sand (classified SP-SC by WES on the Unified Soil Classification System, Figure 2-6) was used for the cement aggregate mixture (CAM) layers in the remaining items (Figure 2-7). The base course of the inverted pavement items was a crushed limestone (Figure 2-6).

The 11 CAP test items were built in two 12 foot wide test lanes (Figure 2-1) under a large hanger for protection from the weather. Each lane was excavated 4 feet below grade and lined with polyethylene to minimize moisture loss in the subgrade. The CH soil used for the subgrade was processed offsite on a mixing pad to the required moisture

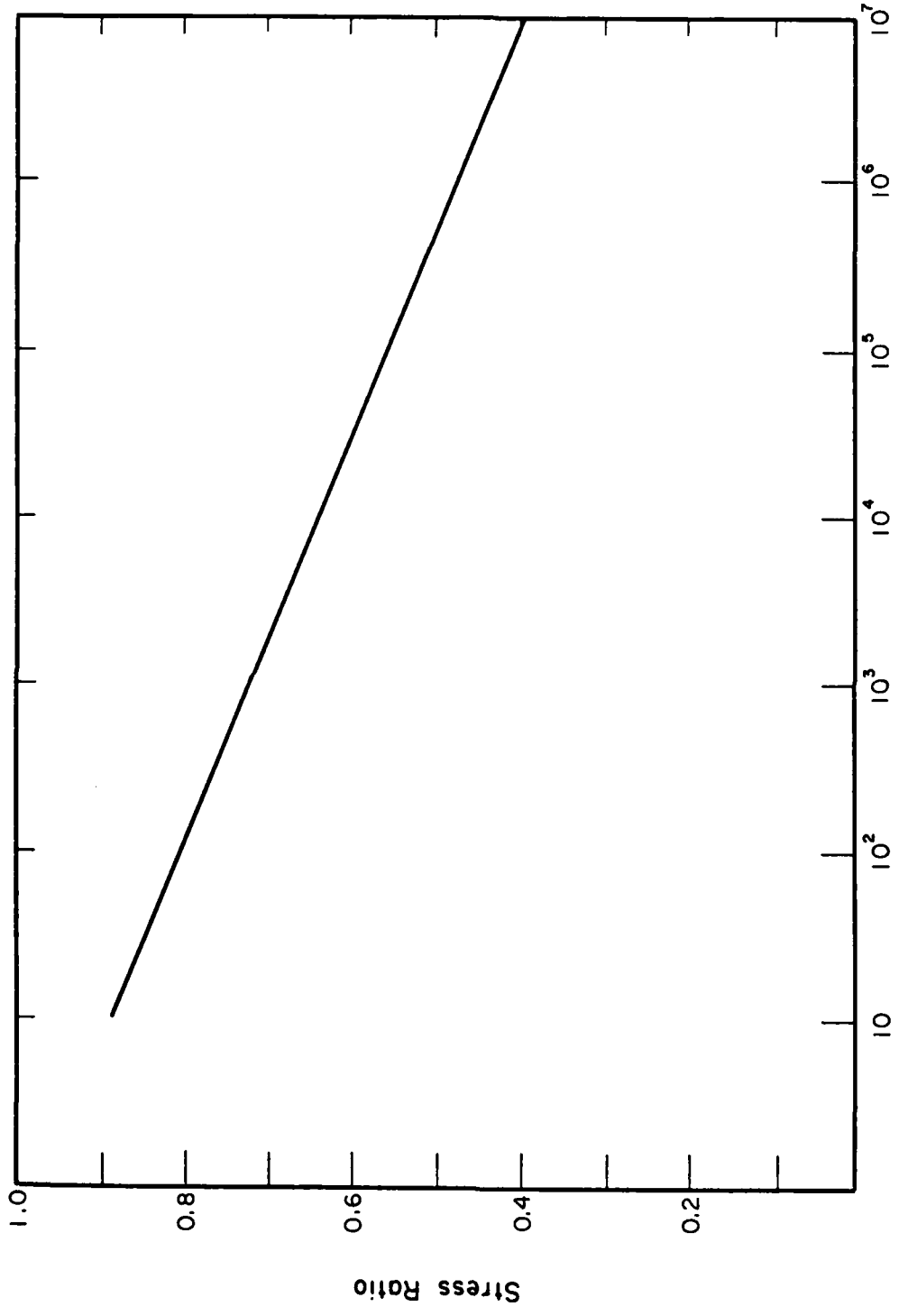

Figure 2-5. Stress Ratio-Fatigue Relation for Cementitiously Stabilized Materials (Reference 8)

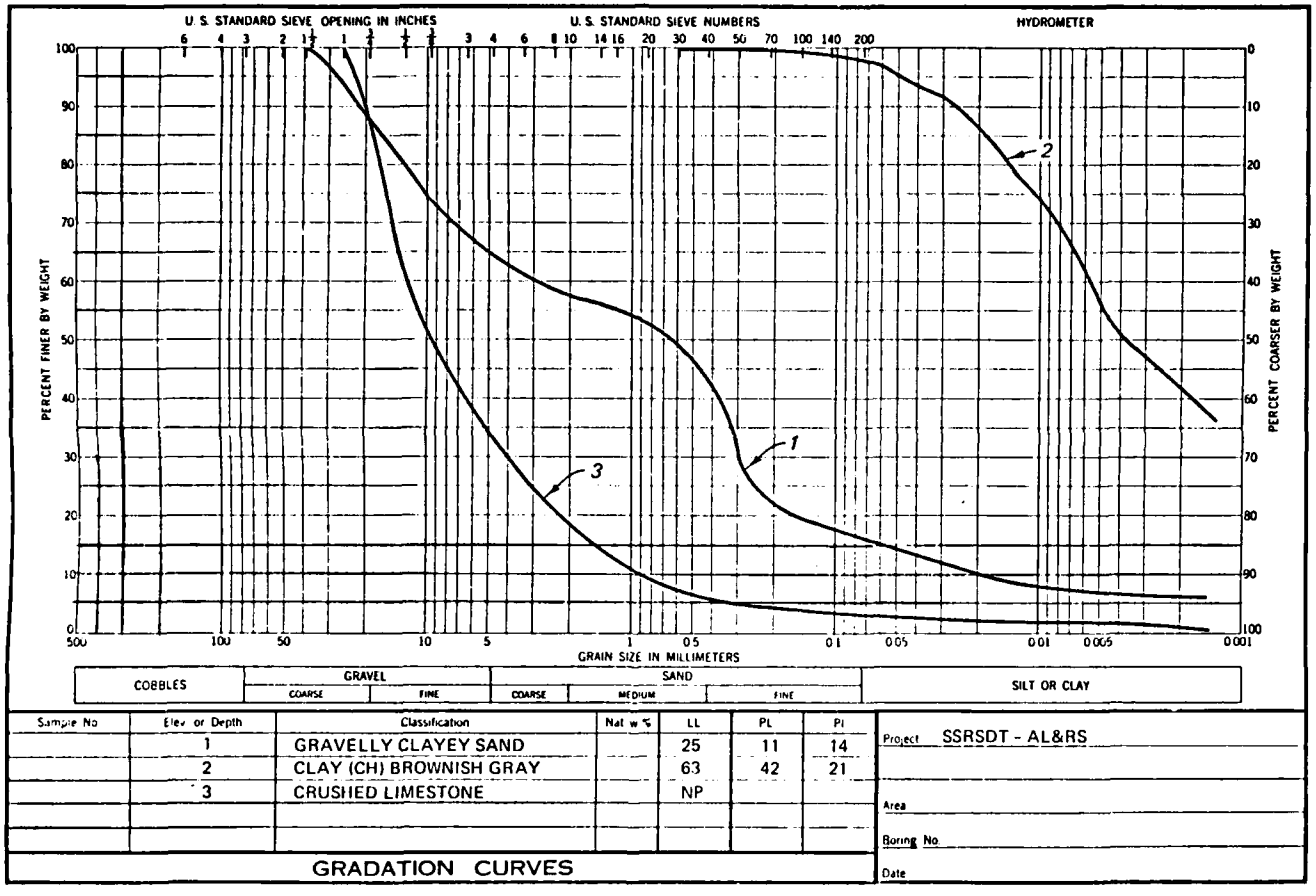

Sample No	Elev or Depth	Classification	Nat w %	LL	PL	PI
	1	GRAVELLY CLAYEY SAND		25	11	14
	2	CLAY (CH) BROWNISH GRAY		63	42	21
	3	CRUSHED LIMESTONE		NP		

GRADATION CURVES

Project SSRSDT - AL&RS

Area

Boring No.

Date

Figure 2-6. Gradation Curves and Laboratory Test Results on CAP Construction Materials (Reference 9)

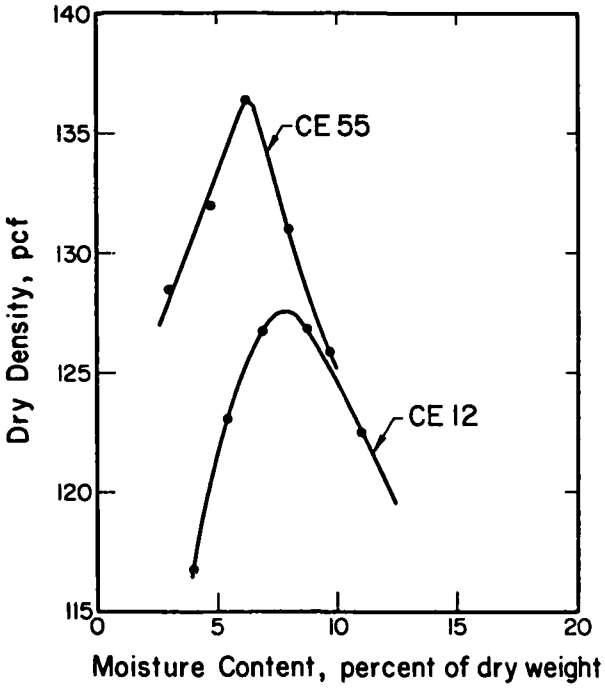

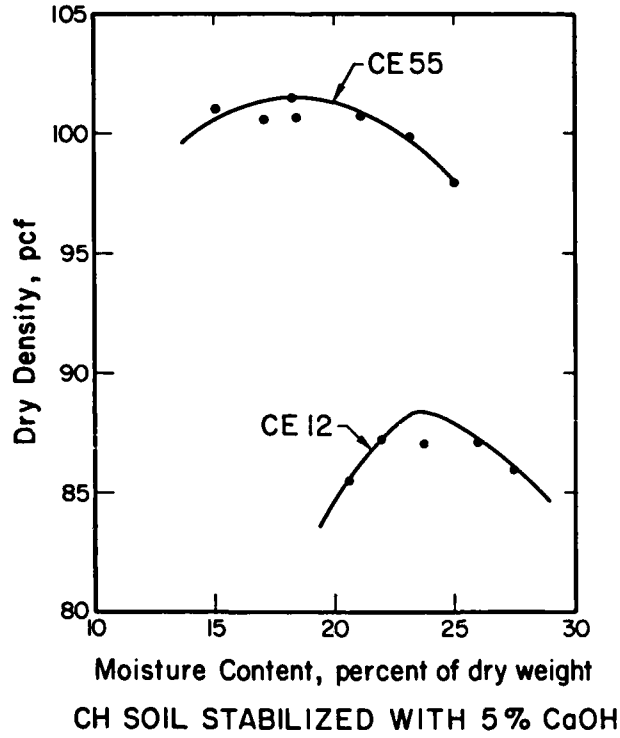

Figure 2-7. Laboratory Compaction Curves (Reference 9)

content, placed in the excavation in 6 inch lifts and compacted to the density required to produce a 5-6 CBR. Direct current linear variable differential transformer (LVDT) displacement transducers were then installed at the geometric center of each item for deflection and deformation measurements. The CAM was field mixed offsite on a mixing pad and then placed with a paver in 5-6 inch lifts. Difficulties were experienced in compacting the CAM to the desired density on the soft subgrade. The lime stabilized CH clay was also field mixed offsite and then spread over the subgrade in item 9 and compacted in three lifts. The crushed limestone base and asphalt concrete surface were then placed on items 9 and 10 with the paver.

D. FIELD MEASUREMENTS AND OBSERVATIONS

1. Stationing

The beginning and end of each item are denoted by station numbers as shown in Figure 2-1. Locations down the centerline of each item are referenced to the station numbers.

2. Subgrade

Prior to placement of the stabilized materials, CBR, modulus of subgrade reaction (k), dry density, and moisture content tests were conducted on the processed subgrade (Table 2-1).

3. Layer Thickness

The average constructed thickness of each pavement layer is listed in Table 2-2. Layer thickness was determined by recording elevations at 1 foot intervals along transverse survey lines at item quarter points immediately before and after the construction of each

TABLE 2-1. BEFORE TRAFFIC SUBGRADE TEST RESULTS (REFERENCE 9)

Item	Depth (in.)	CBR (%)	Dry Density (pcf)	Moisture (%)	k (psi/in.)
1	0	4.9	88.7	29.8	N/A
	6	5.0	87.9	29.6	
	12	4.1	85.6	31.5	
2	0	5.7	89.3	28.9	N/A
	6	5.3	88.5	29.3	
	12	8.3	89.4	28.5	
3	0	5.3	89.0	28.6	121
	6	4.3	85.6	31.4	
	12	6.3	88.8	29.1	
4	0	5.3	88.5	29.8	114
	6	4.5	88.9	28.8	
	12	5.3	88.5	29.7	
5	0	4.8	87.9	29.5	116
	6	4.2	85.8	31.0	
	12	4.7	86.6	31.5	
6	0	6.0	88.4	29.6	N/A
	6	4.8	85.7	31.7	
	12	4.5	86.0	31.7	
7	0	6.3	90.1	27.9	118
	6	4.7	86.1	30.4	
	12	5.3	90.9	28.6	
8	0	5.2	89.7	28.8	120
	6	5.2	88.7	30.3	
	12	6.0	90.0	27.9	
9	0	5.2	90.5	28.4	96
	6	5.3	88.5	29.2	
	12	3.3	86.0	32.4	
10	0	5.7	90.4	27.9	N/A
	6	6.3	89.9	27.5	
	12	4.3	86.9	31.5	
11	0	5.3	90.2	27.9	N/A
	6	4.8	88.5	29.5	
	12	6.7	89.9	28.0	

TABLE 2-2. CONSTRUCTED LAYER THICKNESS

Item	Overall Item[1] Mean (in.)	Overall Item[1] S.D. (in.)	Station	Center 4 feet[2] Mean (in.)	Center 4 feet[2] S.D. (in.)	Thickness for Use In Analysis (in.)
For items 1 - 8, thickness is for cement stabilized SP-SC.						
1	8.93	0.55	0+7.5	8.86	0.26	8.8
			0+15	8.56	0.31	8.4
			0+22.5	8.80	0.42	8.8
2	12.65	0.46	0+42.5	13.16	0.32	13.2
			0+50	12.14	0.43	12.2
			0+57.5	12.42	0.33	12.4
3	16.48	0.75	0+77.5	16.50	0.63	16.4
			0+85	16.62	0.66	16.6
			0+92.5	16.14	0.39	16.1
4	7.81	0.52	1+27.5	8.34	0.56	8.3
			1+35	7.72	0.41	7.6
			1+42.5	7.74	0.34	7.8
5	11.70	0.93	1+62.5	12.64	0.86	12.6
			1+70	11.88	0.83	11.9
			1+77.5	10.92	0.75	10.9
6	16.4	0.59	1+97.5	16.76	0.69	16.6
			2+05	16.24	0.43	16.2
			2+12.5	17.04	0.57	17.0
7	8.49	0.54	0+7.5	8.04	0.27	8.0
			0+15	8.48	0.28	8.4
			0+22.5	9.14	0.24	9.1
8	11.72	0.92	0+42.5	10.74	0.23	10.7
			0+50	11.60	0.23	11.6
			0+57.5	12.80	0.17	12.7
9	Lime Stabilized CH Soil					
	13.07	0.26	0+92.5	13.18	0.11	13.2
			1+00	12.88	0.04	12.9
			1+07.5	12.78	0.08	12.9

TABLE 2-2. (CONTINUED)

Item	Overall Item[1] Mean (in.)	S.D. (in.)	Station	Center 4 feet[2] Mean (in.)	S.D. (in.)	Thickness for Use In Analysis (in.)
9 Crushed Limestone	3.56	0.34	0+92.5	3.72	0.26	3.7
			1+00	3.74	0.13	3.7
			1+07.5	3.40	0.14	3.4
9 Asphalt Concrete	1.42	0.26	0+92.5	1.74	0.13	1.7
			1+00	1.46	0.05	1.4
			1+07.5	1.10	0.10	1.1
10 Cement Stabilized SP-SC	10.99	0.35	1+27.5	11.16	0.11	11.2
			1+35	10.96	0.11	11.0
			1+42.5	11.0	0.34	11.0
10 Crushed Limestone	3.81	0.42	1+27.5	3.96	0.18	4.0
			1+35	3.92	0.15	3.9
			1+42.5	3.40	0.10	3.4
10 Asphalt Concrete	1.04	0.23	1+27.5	0.80	0.12	0.8
			1+35	0.96	0.05	0.9
			1+42.5	1.30	0.12	1.3
11 Cement Stabilized SP-SC	11.28	1.16	1+62.5	12.60	0.21	12.6
			1+70	11.42	0.43	11.4
			1+77.5	9.98	0.16	10.0
11 Asphalt Concrete	1.38	0.21	1+62.5	1.22	0.18	1.2
			1+70	1.32	0.11	1.3
			1+77.5	1.58	0.08	1.5

(1) Thickness measurements at the item edges not included.
(2) Includes centerline and 2 feet each side of centerline.

layer. Since only the centerline of the item was trafficked, the thickness of the center 4 feet of the item is relevant in structural analysis. Small differences in layer thickness between the center 4 feet of the item and the outer 4.5 feet will not affect the structural response of the item when trafficked down the centerline.

4. CAM Density

After traffic, the dry density (water balloon method) and moisture content of the cured CAM layers were determined (Table 2-3). These tests were performed outside the traffic lanes and represent typical values.

5. LVDT Deflections

As the traffic was applied, pavement deflections were registered by the LVDT transducers installed at the item center. The LVDT transducers were mounted on steel reference rods extending to reference flanges located 6 feet into the subgrade. A complete description of the LVDT and the installation procedures are presented in Reference 11. LVDTs were installed:

At the subgrade surface in items 1 through 8.

At the asphalt concrete surface in items 9, 10, and 11.

The LVDT transducers measured vertical movement under the moving F-4 wheel load. LVDT pass deflection is the maximum vertical movement (deflection) of the gage under the moving F-4 wheel load and includes both resilient deflection and permanent deformation. LVDT cumulative permanent deformation is the total permanent deformation that

TABLE 2-3. CAM LAYER DENSITIES AFTER TRAFFIC (REFERENCE 9)

Item	Depth (inches)	Dry Density[1,2] (pcf)	Moisture[1] (percent)
1	0-2	119.5	4.3
	3-5	113.3	4.9
	6-8	112.6	7.2
2	0-4	117.8	3.9
	4-8	116.8	6.3
	8-11	118.2	6.6
3	0-3	116.2	4.0
	8-11	114.0	6.3
	13-15	118.9	5.8
5	0-3	119.8	4.4
	3-6	113.0	6.1
	8-11	120.7	6.6
6	0-3	116.4	5.0
	7-10	113.6	6.4
	13-15	125.8	6.2
7	0-2.5	114.6	4.1
	2.5-5	108.6	6.2
	5.7(5)	113.2	6.2
8	0-4	118.2	3.8
	4-8	113.9	5.7
	8-12	127.3	5.9

(1) Average of 2 measurements at each depth.
(2) Water Balloon Method, ASTM D2167-66.

accumulated from the start of traffic. Tables A-1 through A-4 and Figures A-1 through A-11 in Appendix A contain the LVDT data for various pass levels up to item or gauge failure.

6. FWD Deflections

Falling weight deflectometer (FWD) non-destructive testing load-deflection measurements were obtained at item quarter points (Figure 2-1). The FWD applies an impulse load up to 15,000 pounds to the pavement surface through an 11.8 inch diameter plate. The FWD loads used in this study were 9,000 and 15,000 pounds compared to the 27,000 pound F-4 load. The FWD loads were large enough to produce the desired responses in the CAP test items. The surface deflections are measured by velocity transducers under the center of the load and at radial distances of 12, 24 and 36 inches, denoted D0, D1, D2, and D3 respectively (Figure 2-8). Deflections were measured along the item centerline south of the FWD load. The FWD load-deflection data for each item at various pass levels are listed in Tables A-5 through A-15 of Appendix A.

7. Surface Cracking

Transverse shrinkage cracks were observed and recorded prior to traffic. Load related surface cracking was monitored throughout the traffic period. Figures B-1 through B-11 of Appendix B present the surface cracking data.

The load transfer efficiency (LTE) of selected transverse shrinkage cracks was measured prior to traffic and at various pass levels (Table B-1). Load transfer efficiency (LTE) is a deflection based measure of the crack shear transfer efficiency. The FWD load

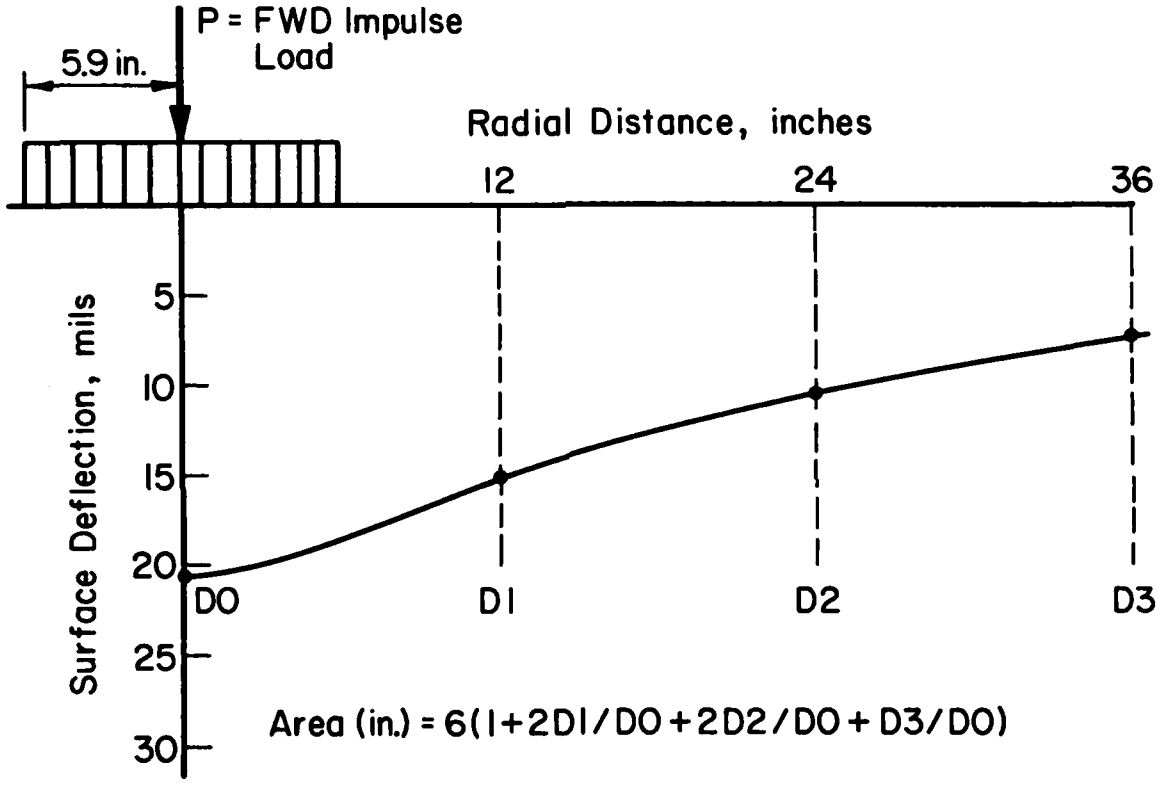

Figure 2-8. FWD Deflection Basin

plate is placed tangent to the crack and deflections recorded on each side of the crack in the immediate vicinity of the load. LTE is then determined by:

$$LTE = (\Delta_u/\Delta_l)100 \qquad (2\text{-}1)$$

where:

LTE = load transfer efficiency, percent

Δ_u = crack deflection of unloaded slab

Δ_l = crack deflection of the loaded slab.

When no load transfer exists across the crack, the LTE is zero. When $\Delta_u = \Delta_l$, the LTE is 100 percent.

8. Longitudinal Surface Profiles

The surface profiles down the center of the traffic lane in each item was taken prior to traffic and after failure or 1000 passes. This data are presented in Figures A-12 through A-17 of Appendix A.

9. Ultimate Load Test Data

Ultimate load tests were performed on items 1, 2, 3, 5, 6 and 7. A 12 inch diameter plate was loaded to ultimate load or up to the test limit of 50 kips. The load was applied at a steady rate and the maximum load was reached within one minute. Figures 2-9, 2-10 and 2-11 and Table 2-4 contain the results of these tests.

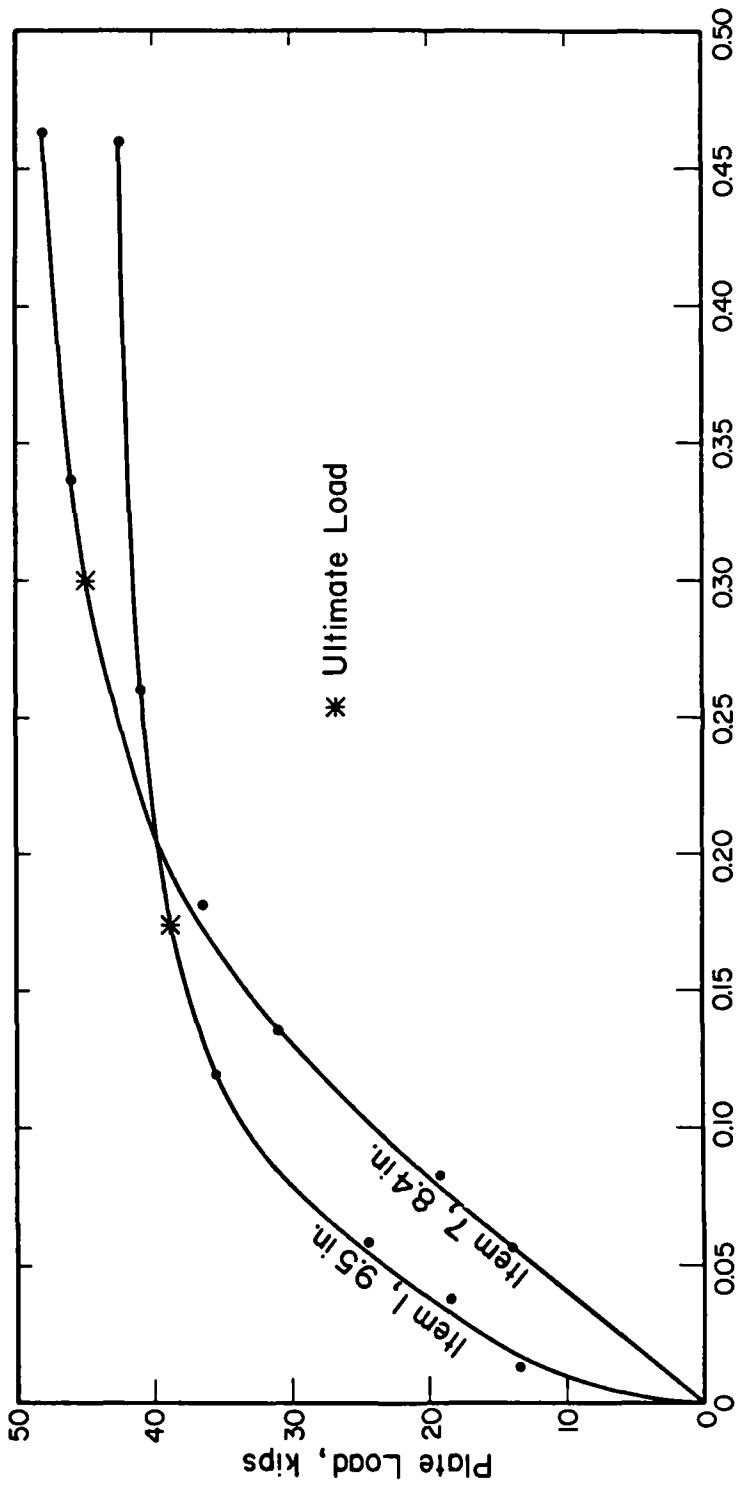

Figure 2-9. Ultimate Load Test Data for Items 1 and 7 (Reference 9)

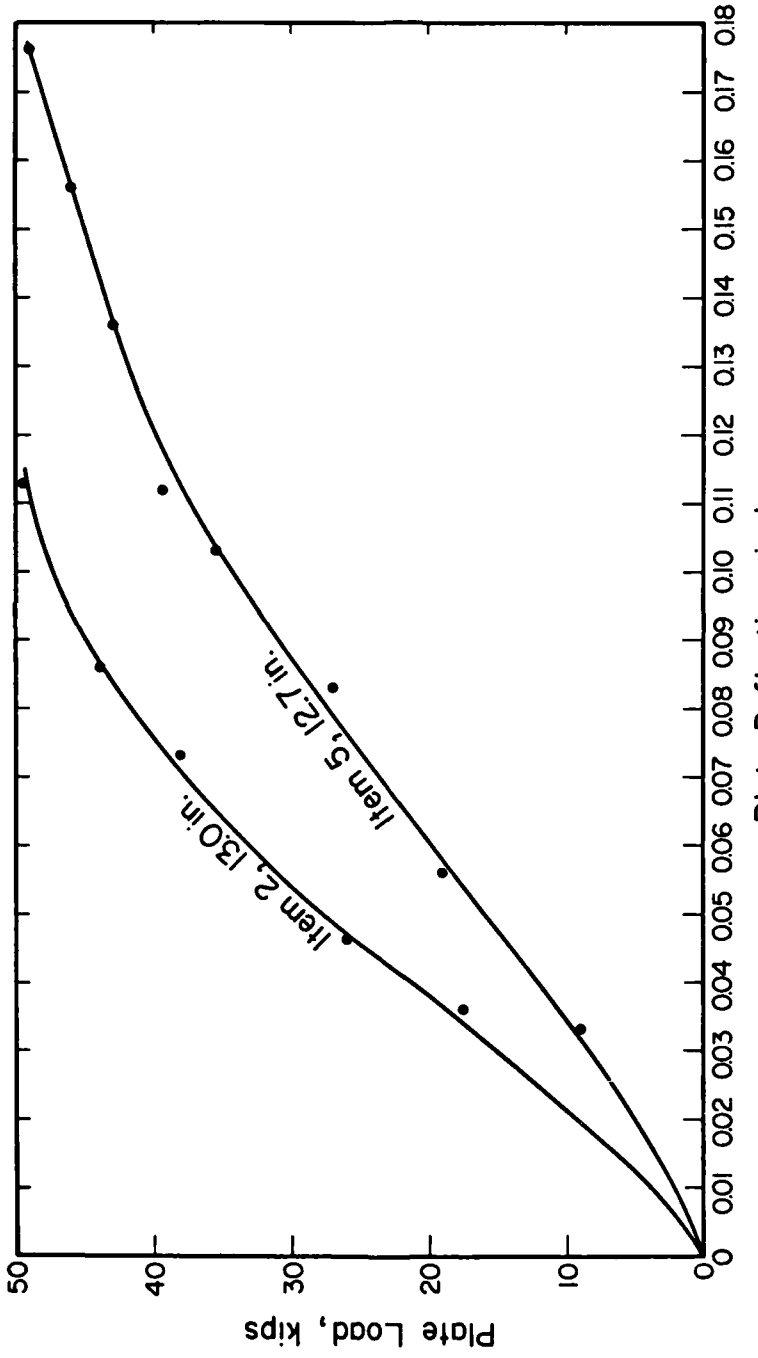

Figure 2-10. Ultimate Load Test Data for Items 2 and 5 (Reference 9)

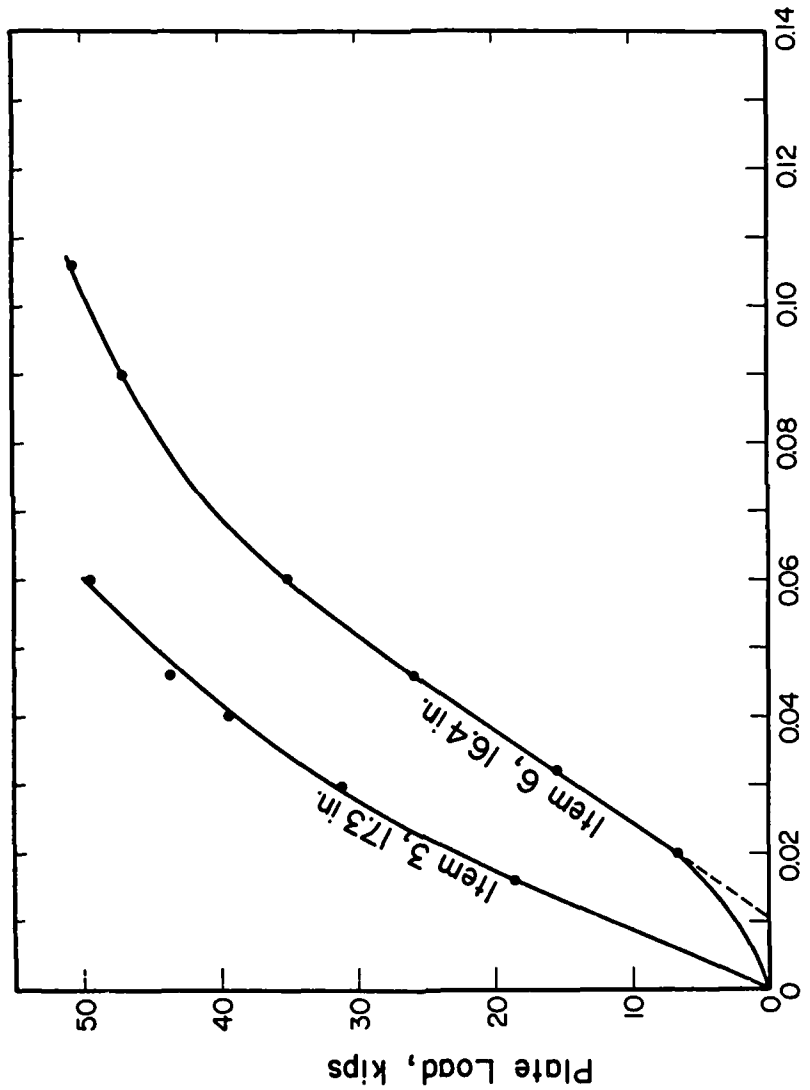

Figure 2-11. Ultimate Load Test Data for Items 3 and 6 (Reference 9)

TABLE 2-4. ULTIMATE LOAD TEST RESULTS (REFERENCE 9)

Item	Plate Location		Thickness of Stabilized Mat. (in.)	Ultimate Load[1] (kips)
	Station	Feet West of Centerline		
1	0+20	3	9.5	39
2	0+43	3	13.0	45
3	0+82	3	17.3	>50
5	1+61	3	12.7	>50
6	1+96	3	16.4	>50
7	0+18	3	8.4	>50

(1) Figures 2-9, 2-10 and 2-11.

CHAPTER 3

MATERIALS CHARACTERIZATION

A. GENERAL CONCEPTS

The ILLI-PAVE (Reference 10) and ILLI-SLAB (Reference 12) structural models require material characteristics of the various layers as inputs. Depending on the sensitivity of the pavement response and performance, material characteristics may be determined from direct laboratory testing, back calculated from NDT data, or estimated from compressive strength data.

1. Resilient Modulus

A measure of the elastic modulus of untreated cohesive soils and granular materials is the resilient modulus, E_R. It is determined from repeated load tests and is defined by:

$$E_R = \frac{\text{repeated axial compressive stress}}{\text{recoverable axial strain}} \qquad (3\text{-}1)$$

E_R is recommended for use in elastic analysis of pavements subjected to moving wheel loads. The ILLI-PAVE finite element program can accommodate stress dependent modulus relationships for cohesive soils and granular materials.

2. Back-Calculated Layer Modulus Using FWD Deflections

Moving wheel load pavement deflections are influenced by loading conditions, modulus and thickness of the pavement layers, size of the loaded pavement section, and the load transfer across the joints and cracks. Items 1 through 8 are two-layer pavements consisting of a rigid CAM layer over a subgrade (Figure 3-1). If all the pavement

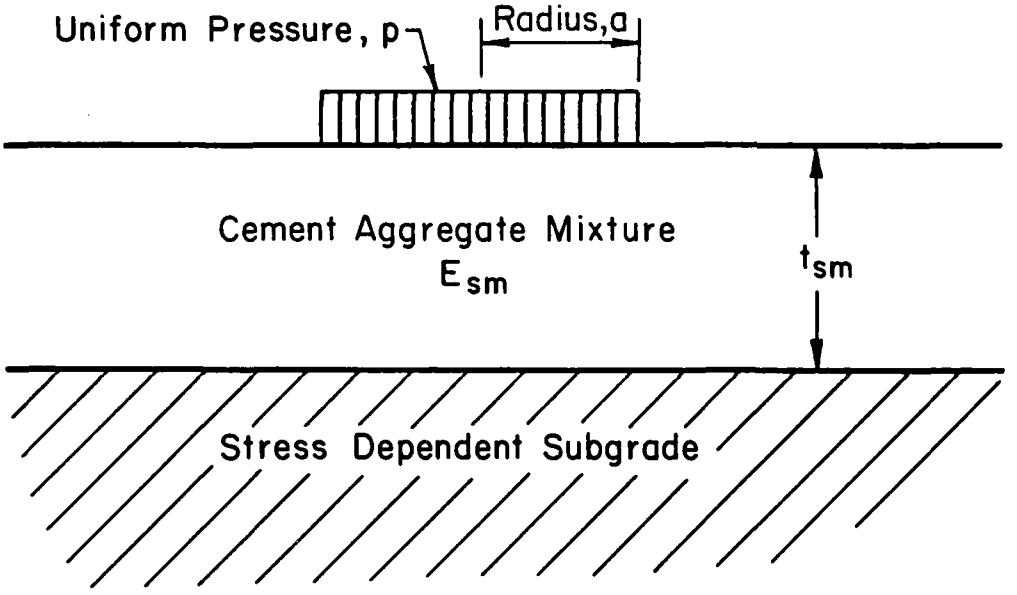

Figure 3-1. Two-Layer Pavement with Rigid Stabilized Material Layer

structure variables are known except the modulus of the CAM layer, it can be "back calculated" from FWD deflection data. This is accomplished by modeling the known properties of the pavement structure in the ILLI-PAVE structural model. The modulus of the CAM layer is varied until the ILLI-PAVE predicted deflection basin matches the FWD deflection basin. The back-calculated modulus is an "effective" layer modulus since the presence of minute cracks and irregularities in the stabilized layer affect the FWD deflections.

The D0 deflection for a given load and subgrade is primarily influenced by the modulus of the CAM layer while the D3 deflection is largely influenced by the subgrade modulus (Figures 3-2, 3-3). If the predicted D0 and D3 deflections match the FWD deflections, then both the rigid CAM layer and the subgrade are being accurately modeled.

The back-calculation procedure is also applicable for inverted pavements, items 9 and 10 (Figure 3-4). The modulus of the stabilized layer is varied until the predicted and measured deflection basins match. As in the two-layer pavement, large variation in the modulus of the CAM layer has a small effect on surface deflections in an inverted pavement for an FWD load (Figure 3-5). The deflection basin match will not be as exact as in the two-layer items because transverse shrinkage cracks in the stabilized layers could not be recorded and these affect the FWD deflections.

This back-calculation procedure is illustrated in Figure 3-6. The FWD deflection basin for the center of item 8 and ILLI-PAVE predicted deflection basins for various CAM layer modulus are shown. By matching the deflection basins, the back-calculated CAM modulus is

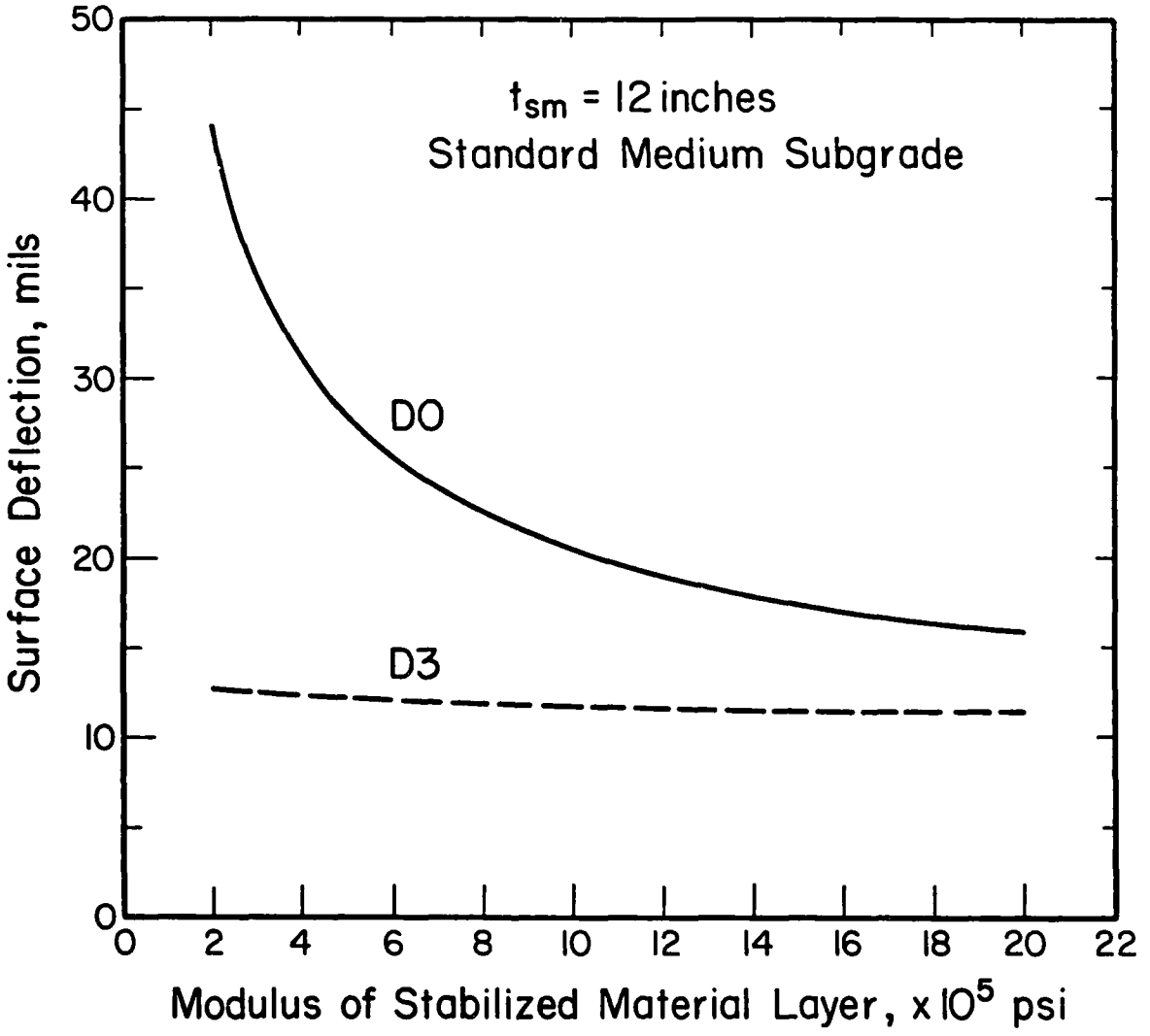

Figure 3-2. Effect of Stabilized Material Layer Modulus on D0 and D3 Deflection in Two-Layer Pavements (F-4 ILLI-PAVE Data Base, Appendix C)

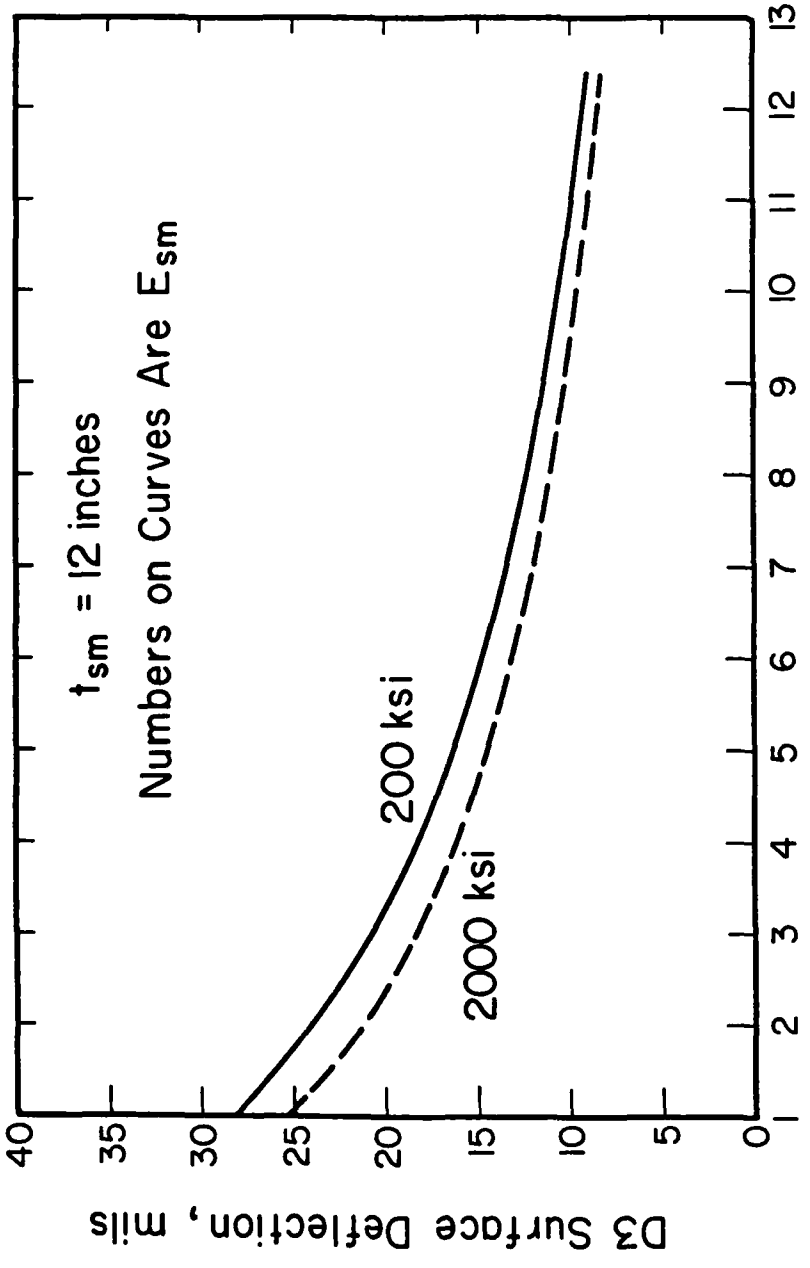

Figure 3-3. Effect of Subgrade E_{ri} on D3 Deflection in Two-Layer Pavement (F-4 ILLI-PAVE Data Base, Appendix C)

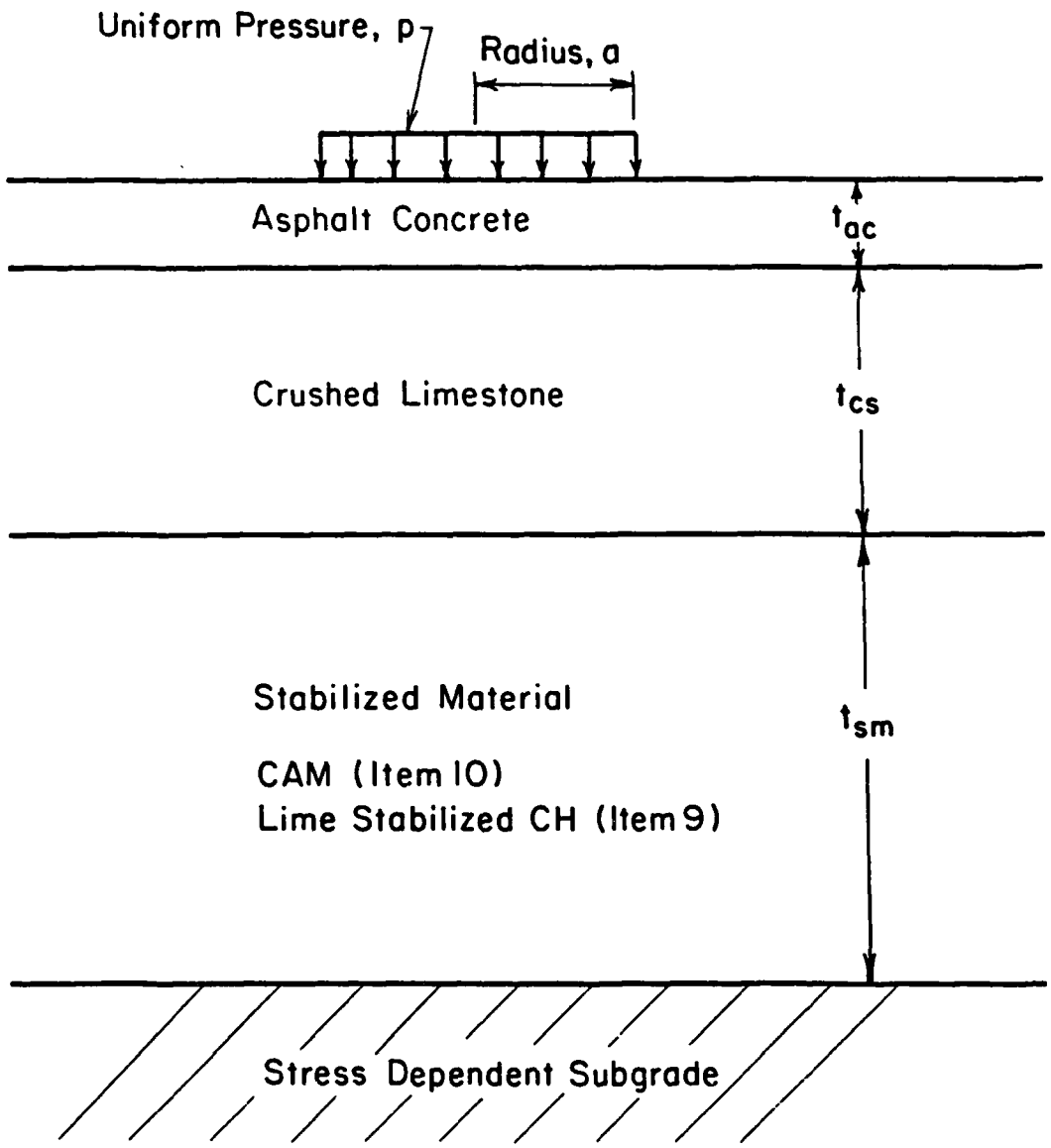

Figure 3-4. Inverted Pavement with Crushed Stone Base Course and Stabilized Material Subbase Course

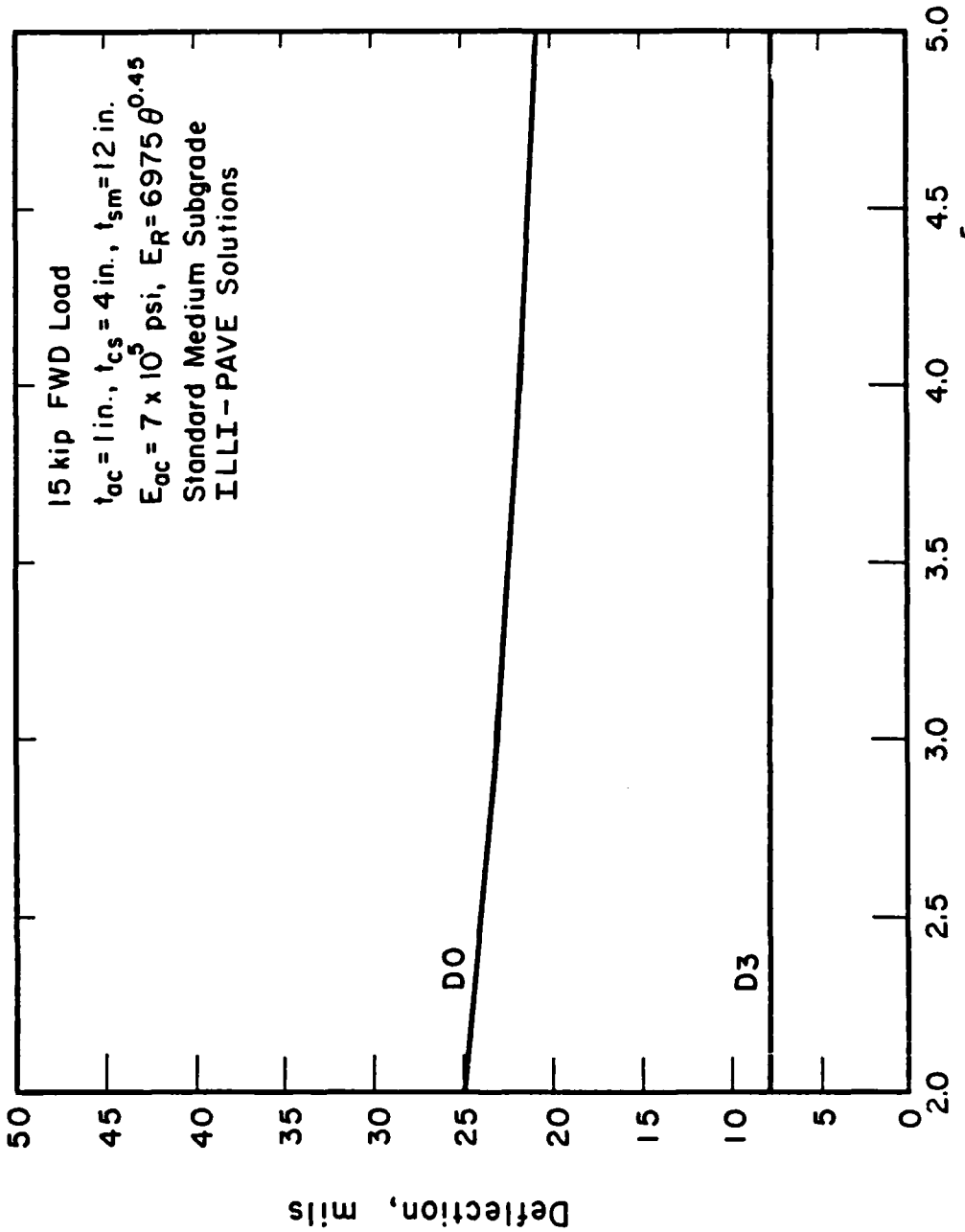

Figure 3-5. Effect of E_{sm} on D0 and D3 Deflection in Inverted Pavement (F-4 ILLI-PAVE Inverted Pavement Data Base, Appendix E)

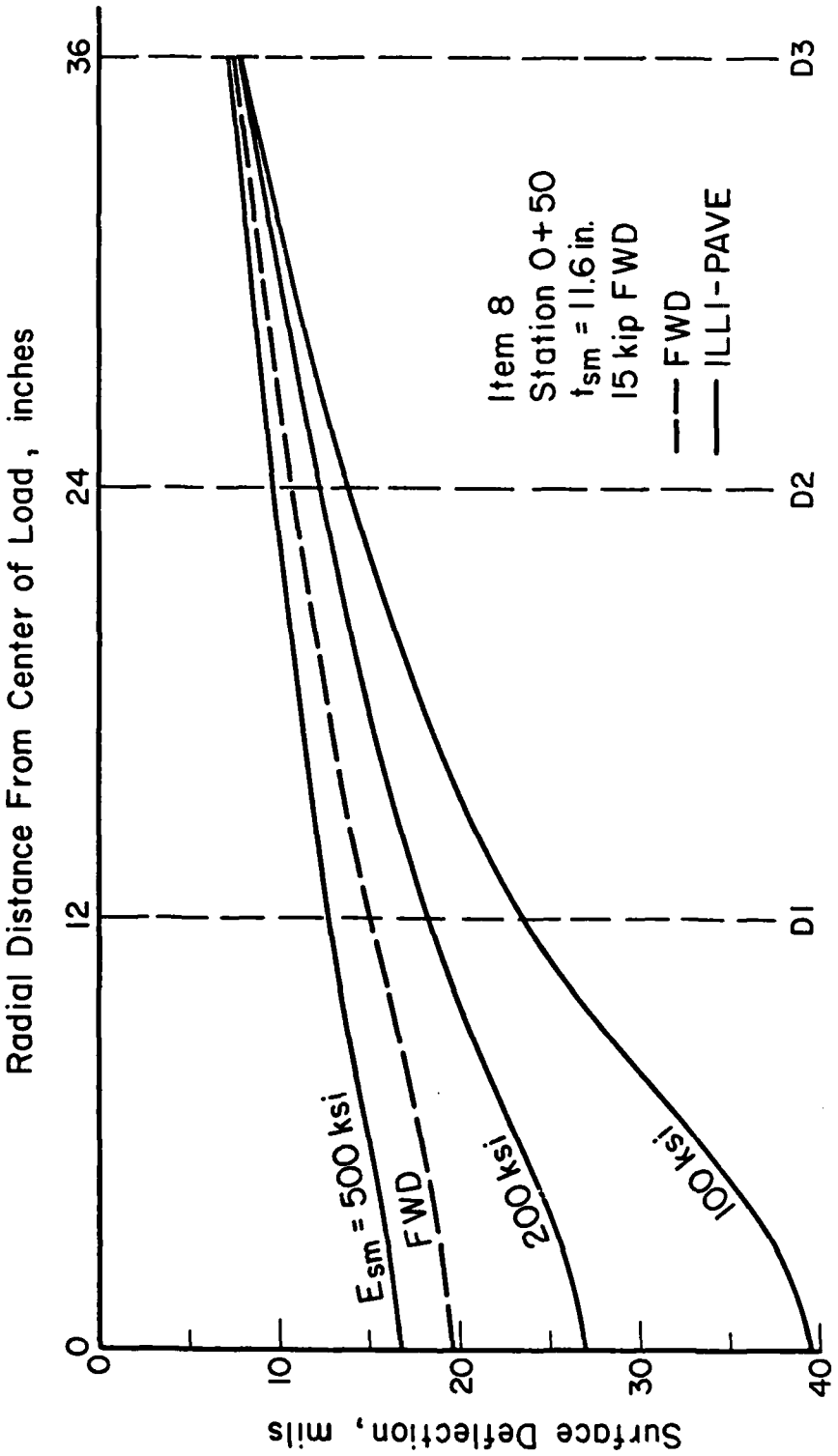

Figure 3-6. Comparison of FWD and Predicted ILLI-PAVE Deflection Basins

approximately 400 ksi. The near exact match of the D3 deflection indicates the subgrade is properly modeled.

The ILLI-PAVE structural model represents an interior load condition. Cracks near the FWD load influence the FWD deflections and distort the shape of the deflection basin. The ILLI-SLAB program can model this condition and show the effect of cracks on the deflection basin. In ILLI-SLAB, an iterative process was used to simulate a stress dependent dynamic subgrade response of medium stiffness (resilient modulus ot subgrade reaction approximately 720 psi/inch) under a rigid pavement. Figure 3-7 shows different deflection basins for a rigid two-layer pavement with cracks near the load. The crack is 12 inches from the load center and the D1 pickup measures deflection at the crack on the loaded slab. For a LTE of 33 percent, the D0 and D1 deflections are larger than predicted for the interior load condition while the D2 and D3 deflections are smaller. Deflection magnitude is affected by crack LTE. The deflection basin has a different shape than for the interior load condition indicating cracking in the vicinity of the FWD load. Thus, interior load condition assumptions are not met.

The ILLI-SLAB and ILLI-PAVE programs can be used to back calculate stabilized material layer modulus even if a crack is affecting the FWD deflections. If the crack location and LTE are known, the absolute values of deflection from ILLI-PAVE are adjusted by deflection ratios determined from ILLI-SLAB and then compared to the FWD deflections.

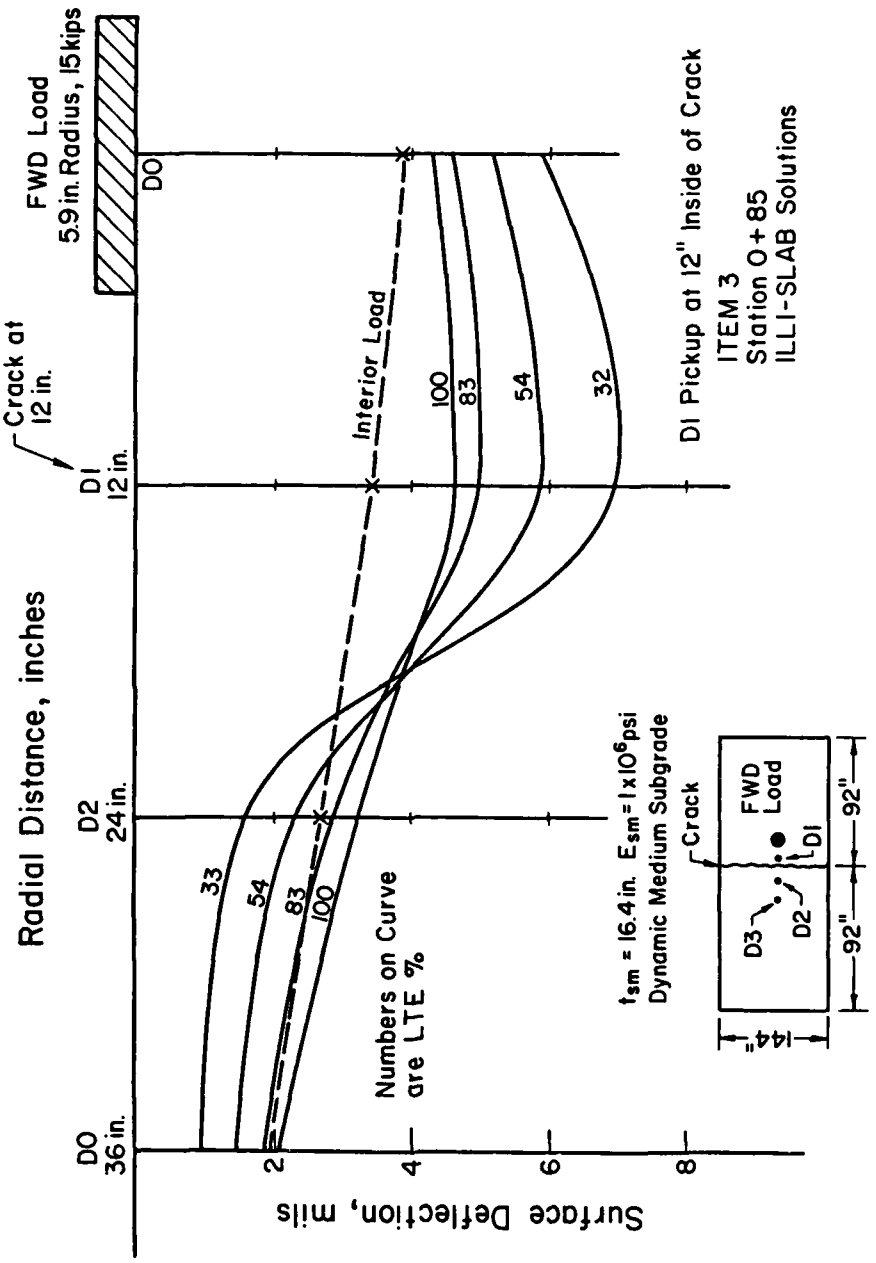

Figure 3-7. Effect of a Crack on the FWD Deflection Basin

B. SUBGRADE

1. Resilient Modulus

Proper characterization of the stress dependent resilient modulus behavior of the subgrade is needed for using the FWD deflections to back calculate the modulus of the stabilized layers. In general, the resilient modulus of cohesive soils decreases with increasing deviator stress and is relatively unaffected by small changes in the confining pressure (References 13, 14). Figure 3-8 shows the general stress dependent resilient modulus behavior for cohesive soils (E_R is in ksi and σ_d is in psi).

a. Laboratory Repeated Load Tests

Repeated load unconfined triaxial tests were performed at the University of Illinois on 2.85 inch diameter tube samples of the subgrade taken by WES. Tube samples from each item were cut into several 5.5 inch long samples representing various depths in the subgrade. Samples were conditioned at 6 psi for 200 repetitions and then axially loaded at 2, 4, 6, 8, 10, 14, and 18 psi deviator stress ($\sigma_1-\sigma_3$). The deflections for about 10 repetitions at each load level were recorded. The slope of the resilient response curve for less than 6 psi deviator stress, denoted K_1, and the slope for greater than 6 psi, denoted K_2, are shown in Table 3-1.

b. Subgrade Behavior Model for Back-Calculation Procedure

The different resilient modulus behavior of each layer in the processed subgrade, as determined by the subgrade samples taken at various depths, produce very similar surface deflections in the pavement test items if replaced by a single layer of equal thickness but with the

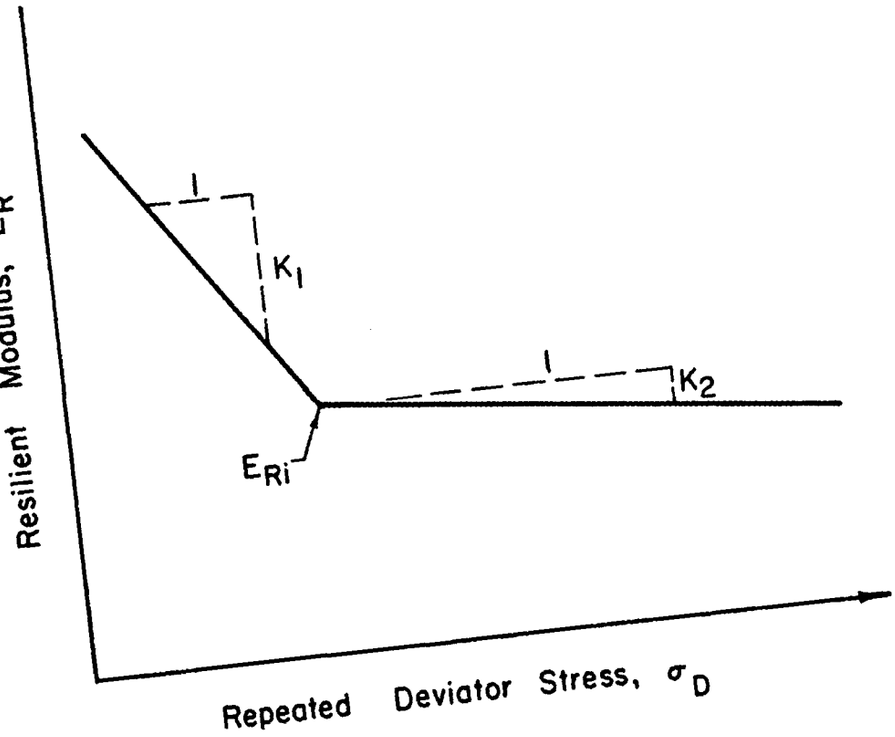

Figure 3-8. Typical Resilient Modulus-Repeated Deviator Stress Relation (Reference 8)

TABLE 3-1. LABORATORY TEST RESULTS ON SUBGRADE TUBE SAMPLES (UNIVERSITY OF ILLINOIS STUDY)

Item-Sample	Sample Mid-depth (in.)	Dry Density (pcf)	Moisture (percent)	Degree Saturation (percent)	E_{ri}[1] (ksi)	K_1 (ksi/psi)	K_2 (ksi/psi)	q_u (psi)
1D	10.8	91.4	29.9	94.5	6.47	1.01	0.24	28.4
1D	16.3	92.8	30.2	98.7	5.59	0.30	0.15	27.8
1E	16.3	93.2	30.1	99.3	6.89	0.30	0.19	37.1
2B	9.6	92.6	30.7	99.8	6.54	0.54	0.25	25.4
2C	15.2	93.0	30.1	98.8	7.43	0.25	0.20	30.1
2D	20.7	92.8	30.0	98.0	9.85	0.21	0.24	33.9
3A	3.8	94.3	29.7	100.5	6.79	0.86	0.22	29.2
3B	9.3	93.3	30.0	99.2	9.27	0.39	0.30	29.6
3C	14.7	94.4	29.4	99.8	8.51	0.01	0.10	37.2
3D	20.2	95.0	28.8	99.1	10.4	0.01	0.22	38.1
4A	2.7	93.8	29.3	98.0	6.51	0.69	0.19	26.3
4B	9.2	93.4	30.2	100.1	6.84	0.87	0.30	25.4
4C	14.6	92.8	30.1	98.3	7.28	0.00	0.30	28.2
4D	20.1	93.7	30.0	100.1	6.80	0.35	0.10	30.1
5A	2.7	94.3	29.4	99.5	4.68	0.55	0.16	24.5
5B	10.1	93.5	30.0	99.7	6.65	0.45	0.23	24.9
5C	15.5	92.9	30.3	99.2	9.18	0.38	0.32	25.9
5D	20.9	92.2	30.0	97.6	8.88	0.09	0.25	19.7
6A	2.8	94.0	28.8	96.8	7.99	0.68	0.29	32.5
6B	9.5	93.0	30.3	99.5	6.03	0.61	0.16	24.0
6C	14.9	91.4	30.4	96.1	7.04	0.89	0.23	31.5
6D	20.5	92.0	29.5	94.6	9.84	0.21	0.25	27.3
7A	3.0	93.9	29.9	100.3	6.27	0.63	0.21	31.0
7B	8.5	92.9	30.4	99.5	6.36	0.53	0.22	24.0
7C	14.0	93.8	29.7	99.3	8.07	0.52	0.19	33.2
7D	19.5	91.2	28.8	90.6	6.28	0.54	0.20	25.4
8A	3.3	91.7	29.7	94.5	4.66	0.76	0.19	21.6
8B	8.9	93.1	28.9	95.1	6.00	0.26	0.28	29.2
8C	14.3	93.9	28.6	95.9	4.40	0.63	0.18	24.0
8D	19.8	91.5	30.9	97.9	4.54	0.53	0.25	21.6
9B	7.2	93.9	29.2	97.9	6.10	0.76	0.21	22.1
9C	12.6	91.1	31.2	97.9	5.96	0.83	0.32	18.3
9D	18.0	90.6	31.9	98.9	7.50	0.13	0.46	19.8
10A	4.3	94.0	30.0	100.8	6.97	0.91	0.34	26.3
10B	9.9	92.4	30.2	97.7	6.61	0.45	0.24	26.8
10C	15.3	90.6	31.7	98.3	5.44	0.90	0.30	17.9
10D	20.7	90.4	32.4	100.0	5.09	0.79	0.27	18.8
11A	3.3	92.9	30.6	100.2	3.14	0.39	0.14	21.2
11B	8.9	92.4	31.0	100.3	4.65	0.55	0.24	22.0
11C	14.3	92.0	30.1	96.5	4.60	0.28	0.21	22.6
11D	19.7	90.7	31.9	99.2	3.76	1.16	0.28	19.8

(1) E_{ri} is resilient modulus at 6 psi deviator stress.

average response of the various layers. Figure 3-9 shows item 5 modeled two different ways. Both models are 300 inches thick since studies using finite element stress dependent programs have shown the thickness of the subgrade in a rigid type pavement has an important effect on the magnitude of the surface deflections (Reference 15). The upper layer is 12 inches of CAM with a modulus, E_{sm}, of 130 ksi. This low value of E_{sm} was selected to get surface deflections large enough to determine any difference resulting from the different subgrade models. The top 23.5 inches of the subgrade is the depth of processed CH subgrade represented by the tube sample data. This layer in model 1 is subdivided into four layers, each with a different resilient modulus behavior as determined by the sample for that depth. Since the processed subgrade was about 38 inches thick, a 14.5 inch layer having the average resilient modulus behavior of all the samples in items 1-10 (denoted average CAP subgrade) was used to bring the thickness to the full 38 inches. Item 11 is not included in the average CAP subgrade because later analysis determined the subgrade in item 11 is not as soft as represented by the tube sample. Model 2 replaces these five layers in the top 38 inches of the subgrade with a single layer having the average resilient modulus behavior of the samples in item 5.

The lower 250 inches of subgrade was modeled using the standard medium subgrade of the F-4 ILLI-PAVE data base study (Appendix C). WES studies of the CH soil show a resilient modulus behavior very similar to that of the standard medium subgrade at deviator stress levels less than 5 psi. Since the deviator stress at 38 inches into the subgrade is well below 5 psi, using the standard medium subgrade for the lower 250 inches in all analyses using ILLI-PAVE is justified. Figure

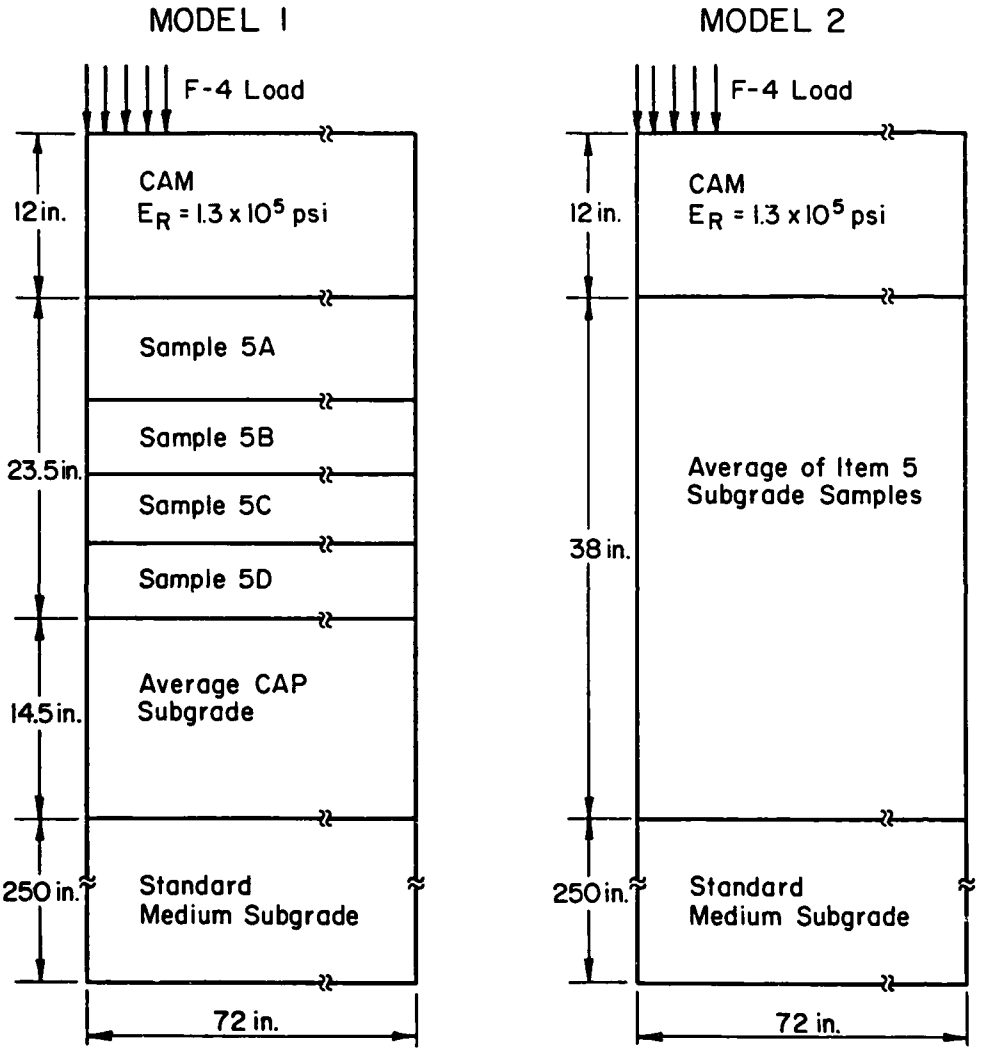

Figure 3-9. ILLI-PAVE Models for Subgrade Study

3-10 shows the stress dependent resilient modulus behavior of the various subgrade layers used in the models.

A load of 27,000 pounds and 265 psi contact pressure was used in each model. The surface deflection responses are shown below where D0, D1, D2 and D3 are surface deflections in mils at 0, 12, 24 and 36 inches from the center of the load. Area is the normalized area of the surface deflection basin as shown in Figure 2-8.

Model	D0	D1	D2	D3	Area, in.
1	64.2	40.5	26.5	17.7	20.18
2	63.0	39.7	26.1	17.6	20.21

A review of the responses shows no significant difference in surface deflections using either model. Therefore, the 36-38 inches of processed subgrade in each item can be represented by a single layer having the average resilient modulus behavior of the samples from various depths in that item. Figures 3-11 through 3-13 show the average subgrade resilient modulus behavior for each item. Figure 3-14 shows the resilient modulus behavior for both the average CAP subgrade and the standard medium subgrade.

2. Strength

Subgrade shear strength facilitates consideration of permanent deformation behavior. Unconfined compressive tests were performed on the subgrade tube samples following the resilient modulus testing. The samples were loaded at 0.05 inches per minute to failure and the resulting stress-strain curves plotted. Unconfined compressive strength, q_u, was taken at 5 percent total axial strain. The data are shown in Table 3-2. Regression analysis of the relation between q_u

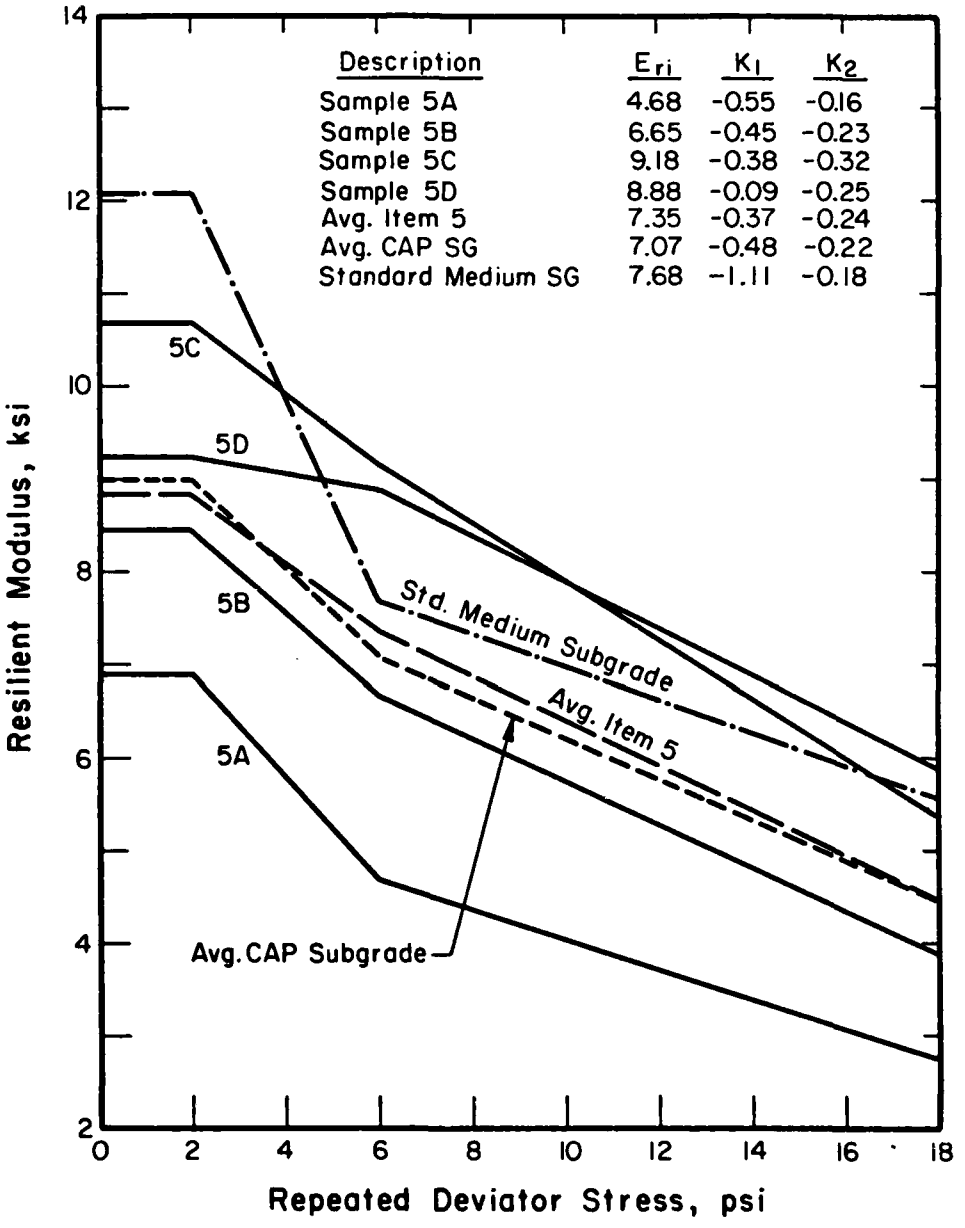

Figure 3-10. Subgrade Soil Models for ILLI-PAVE Subgrade Study

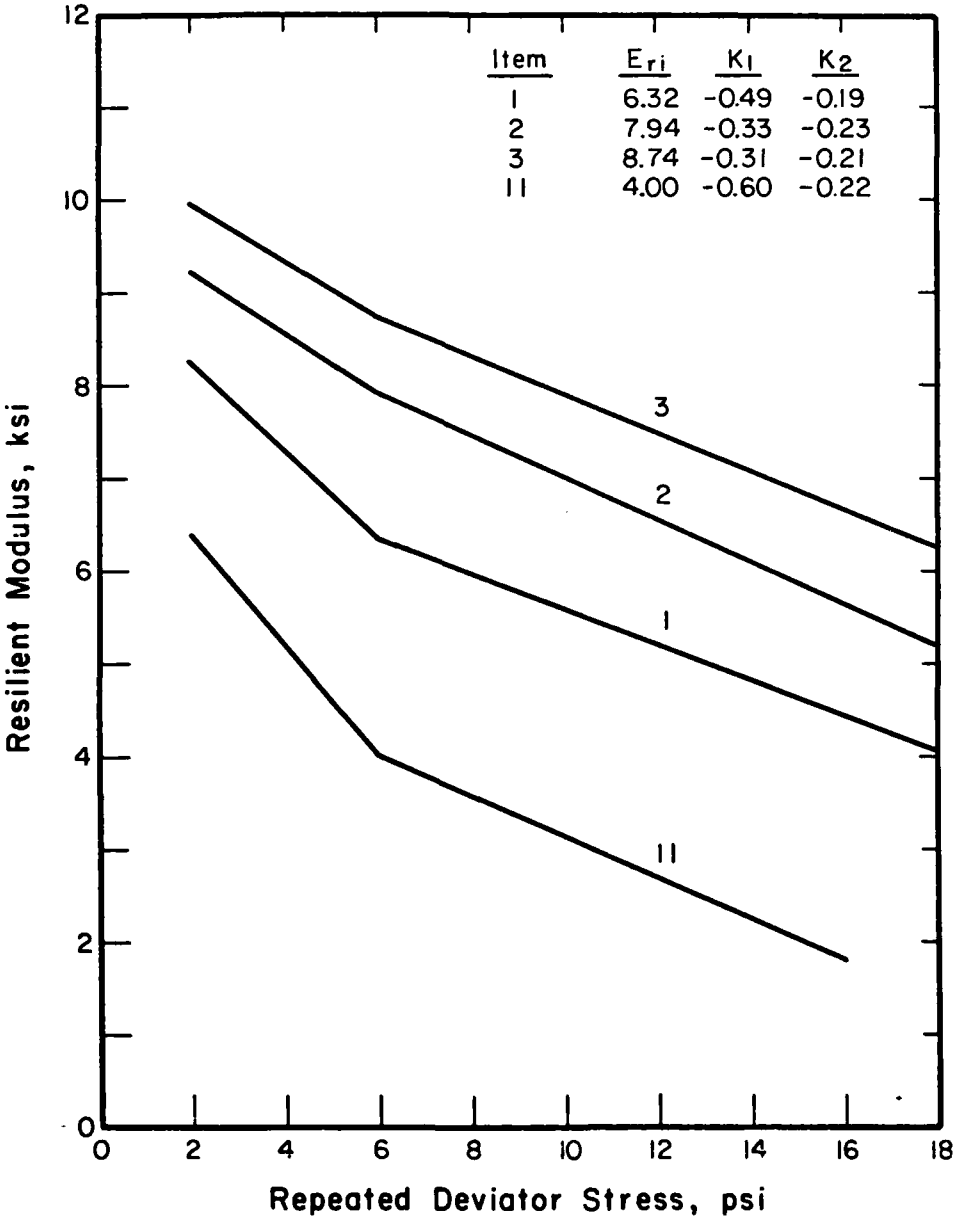

Figure 3-11. Average Subgrade Resilient Modulus Behavior, Items 1, 2, 3 and 11

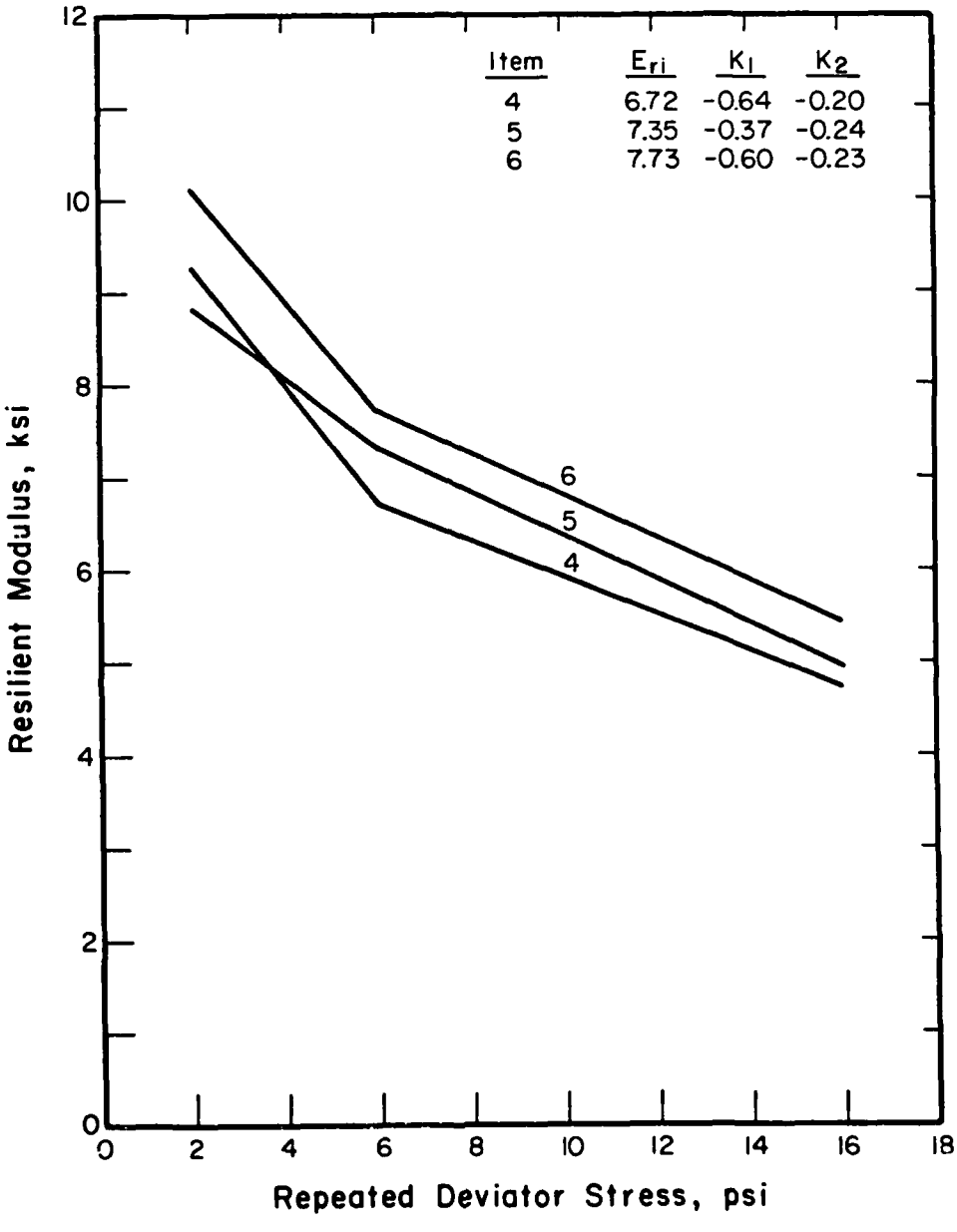

Figure 3-12. Average Subgrade Resilient Modulus Behavior, Items 4, 5 and 6

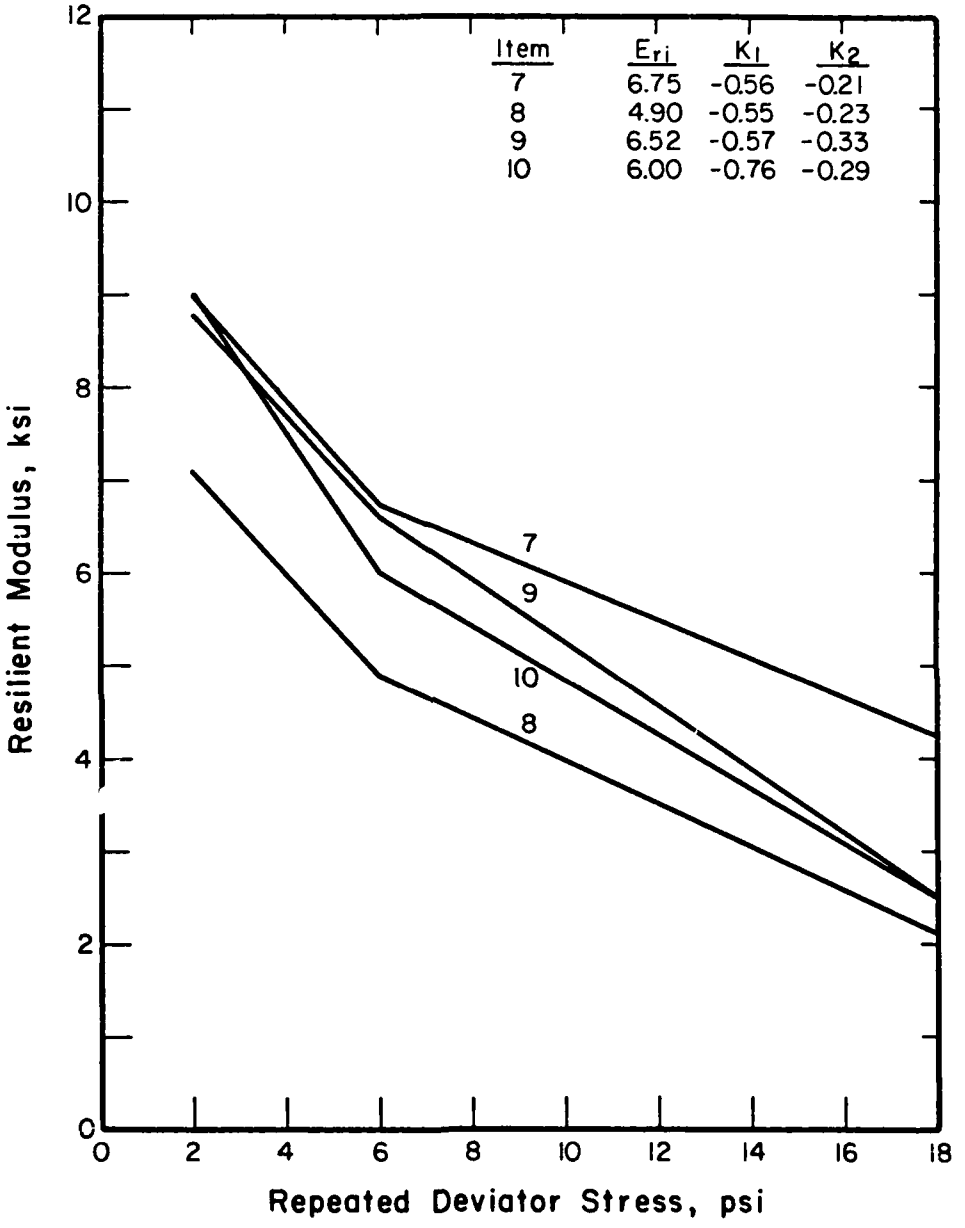

Figure 3-13. Average Subgrade Resilient Modulus Behavior, Items 7, 8, 9 and 10

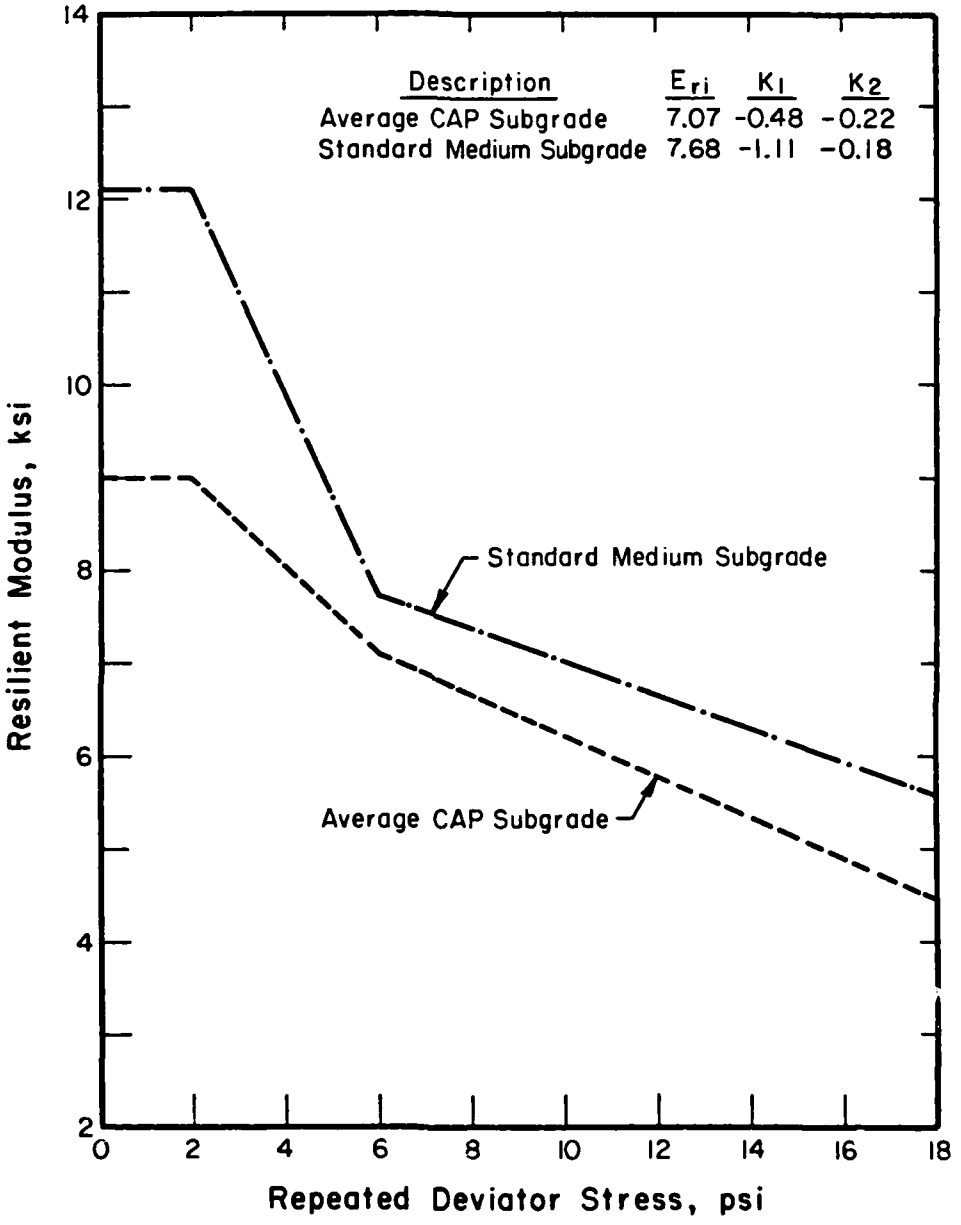

Figure 3-14. Subgrade Models for Back-Calculation Procedure

TABLE 3-2. ITEM SUBGRADE STRENGTH (UNIVERSITY OF ILLINOIS)

Item	Unconfined[1] Compressive Strength (psi)	Undrained[1,2] Shear Strength (psi)
1	31.0	15.5
2	29.9	14.9
3	33.6	16.8
4	27.4	13.7
5	23.6	11.8
6	28.8	14.4
7	28.4	14.2
8	24.2	12.1
9	20.1	10.0
10	22.5	11.2
11	21.4	10.7

(1) Strengths are for mean of tube samples for that item.

(2) Undrained shear strength is unconfined compressive strength divided by 2.

and sample depth showed no correlation. The average of the sample strengths for an item were used in the analyses.

C. ASPHALT CONCRETE

The nominal 1 inch thick asphalt concrete wearing course on items 9, 10 and 11 is too thin to provide any structural load carrying benefit. Therefore, the stiffness of the asphalt concrete can vary considerably and not affect the overall structural response. During trafficking, the daily air temperature of the CAP field test site was approximately 50 degrees F (Reference 9). The modulus of the asphalt concrete was estimated at 700 ksi.

D. CRUSHED LIMESTONE

1. Resilient Modulus

The resilient modulus, E_R, of unstabilized granular materials is stress dependent (Reference 16). The resilient response of granular materials can be represented by $E_R = K\theta^n$ where K and n are material constants evaluated from repeated load triaxial compression tests and θ is the sum of the principal stresses ($\theta = \sigma_1 + 2\sigma_3$).

WES (Reference 17) and the University of Illinois conducted repeated load triaxial tests on the crushed limestone to determine the stress dependent resilient modulus behavior. The tests were performed at similar densities and degrees of saturation. The results of these tests are shown by least squares regression lines in Figure 3-15. The WES test results show a stone much stiffer than comparable granular materials studied by other researchers. For comparison, the resilient

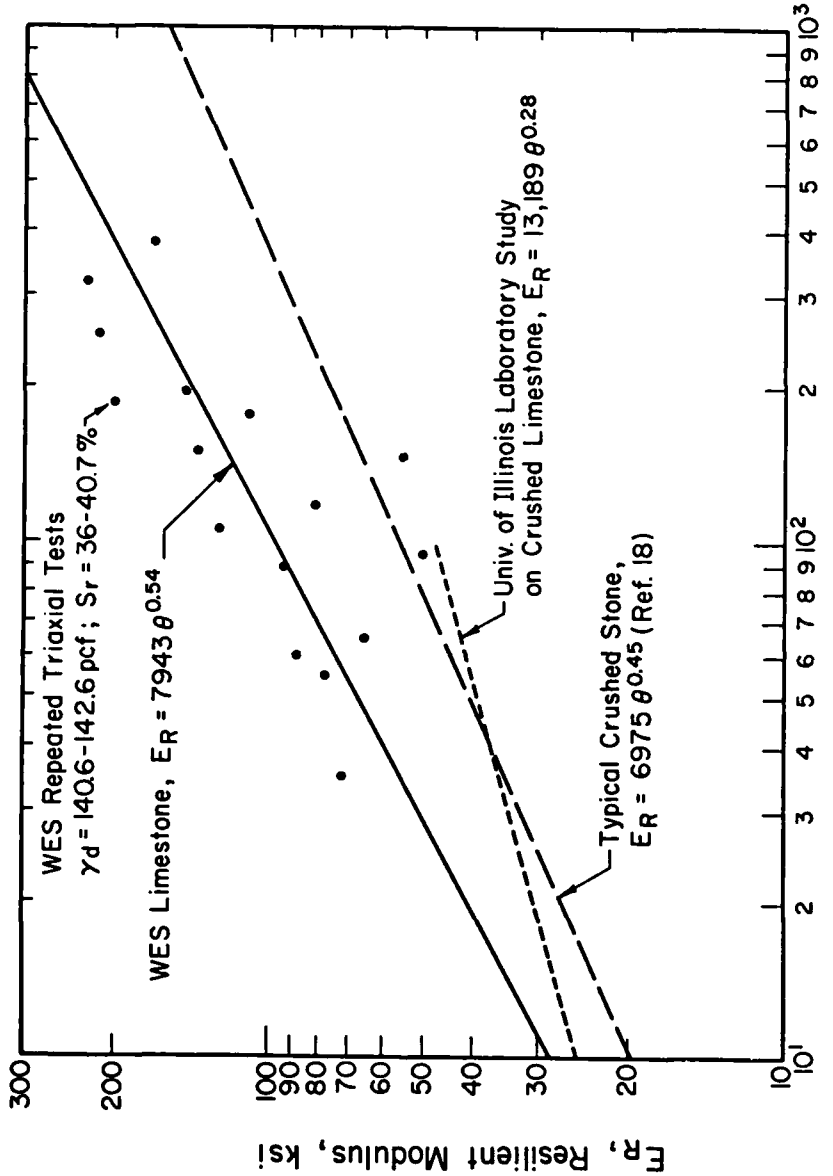

Figure 3-15. Resilient Modulus Behavior of Crushed Limestone

modulus behavior of a typical crushed stone (Reference 18) is also shown.

2. Strength

Quick drained triaxial tests were also performed by WES and the results are shown in the p-q diagram of Figure 3-16. The K_f-line through these points is curved. Since ILLI-PAVE cannot model a curved failure envelope a best fit line is drawn passing through the origin. The result is an alpha angle, α, of 39.3 degrees and a friction angle, ϕ, of 54 degrees. For comparison, a typical crushed stone (Reference 19) ϕ of 45 degrees is also shown.

E. CEMENT AGGREGATE MIXTURE

1. Modulus

The modulus of the CAM layers was estimated using the back-calculation procedure. The FWD test in each item best representing an interior load condition was used. Item 4 had extensive block cracking in the traffic lane after construction and these greatly influenced the FWD deflection measurements. The ILLI-PAVE structural models used in the back-calculation procedure are shown in Figure 3-17. Figures 3-18 through 3-26 show the ILLI-PAVE predicted and actual FWD deflection basins for items 1 through 8 and 11.

A 15 kip, 5.9 inch radius load was used in the ILLI-PAVE solutions. The actual FWD loads were less than 15 kips. The FWD deflections shown in the figures were increased to reflect a full 15 kips. Figure 3-27 shows a linear relationship between FWD load and D0 deflection for the CAP test items. Therefore, the FWD D0 deflection was

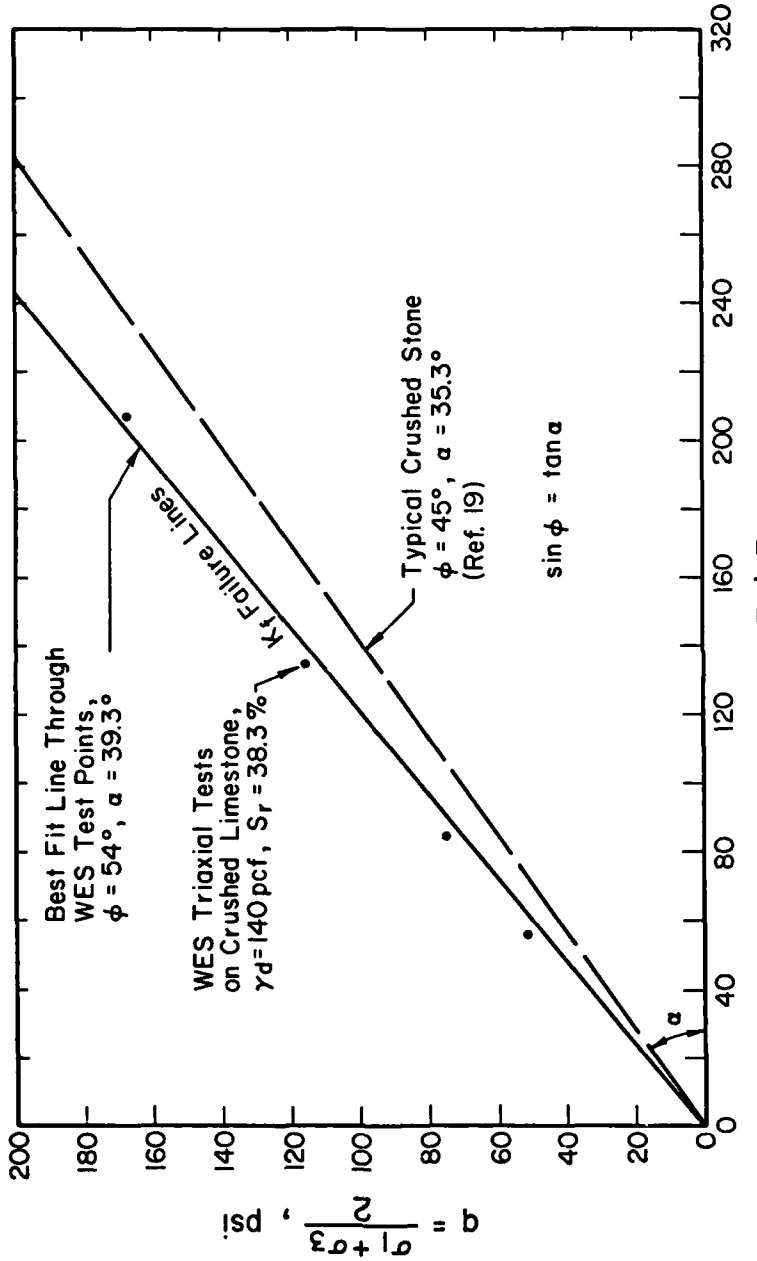

Figure 3-16. Shear Failure Envelope of Crushed Limestone

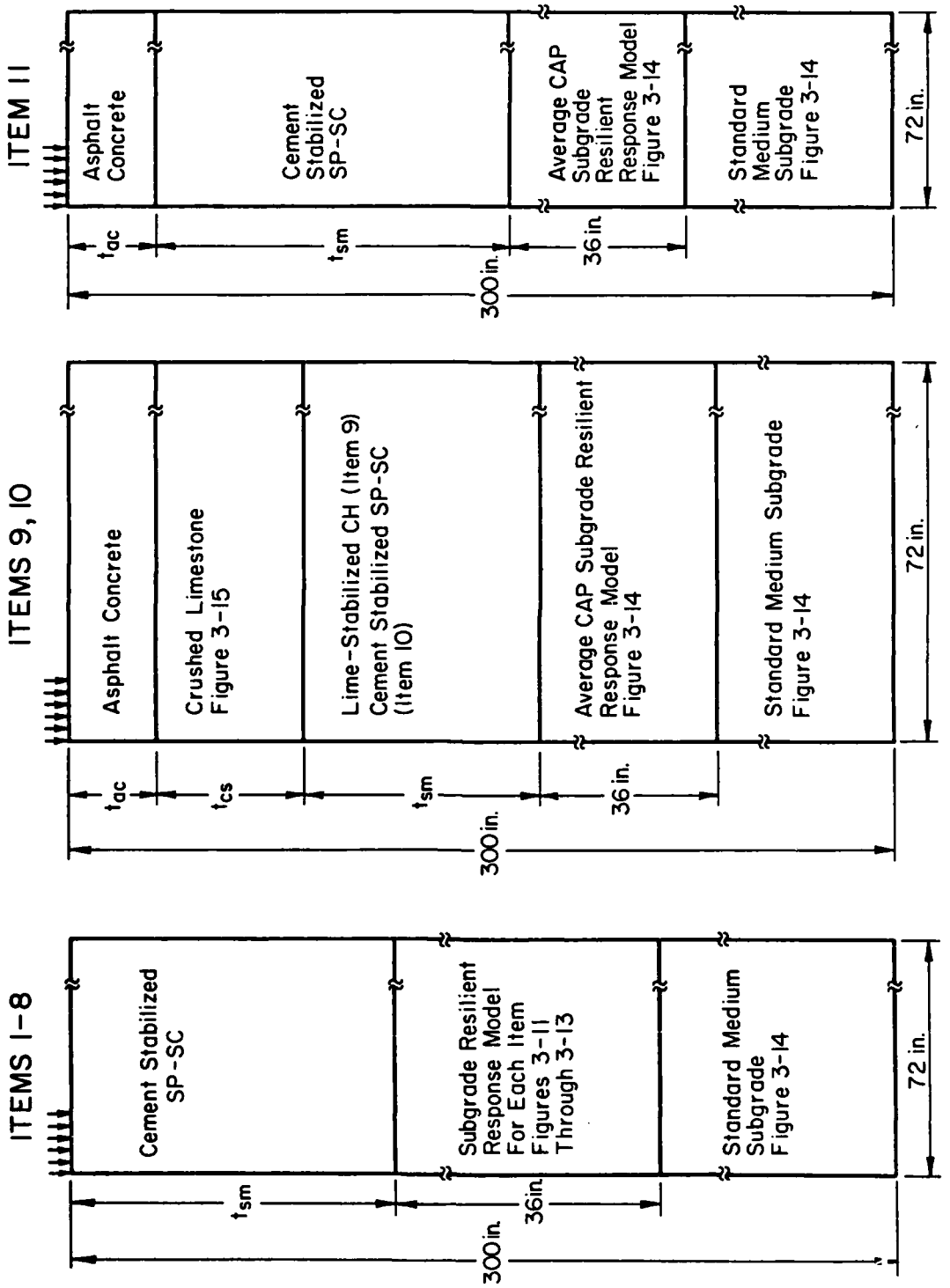

Figure 3-17. FWD ILLI-PAVE Models, 27 kip, 265 psi Load

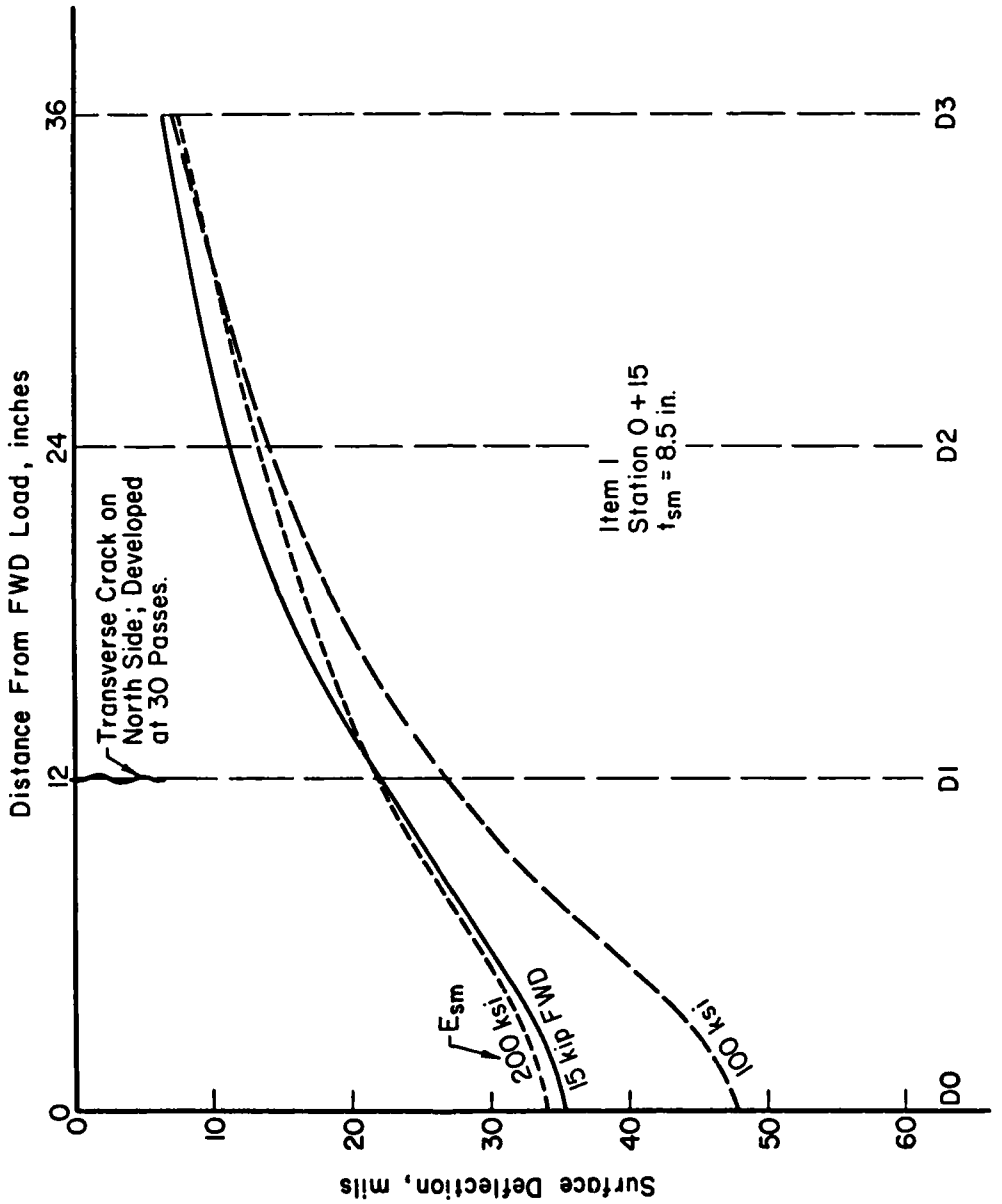

Figure 3-18. ILLI-PAVE and FWD Deflection Basins, Item 1

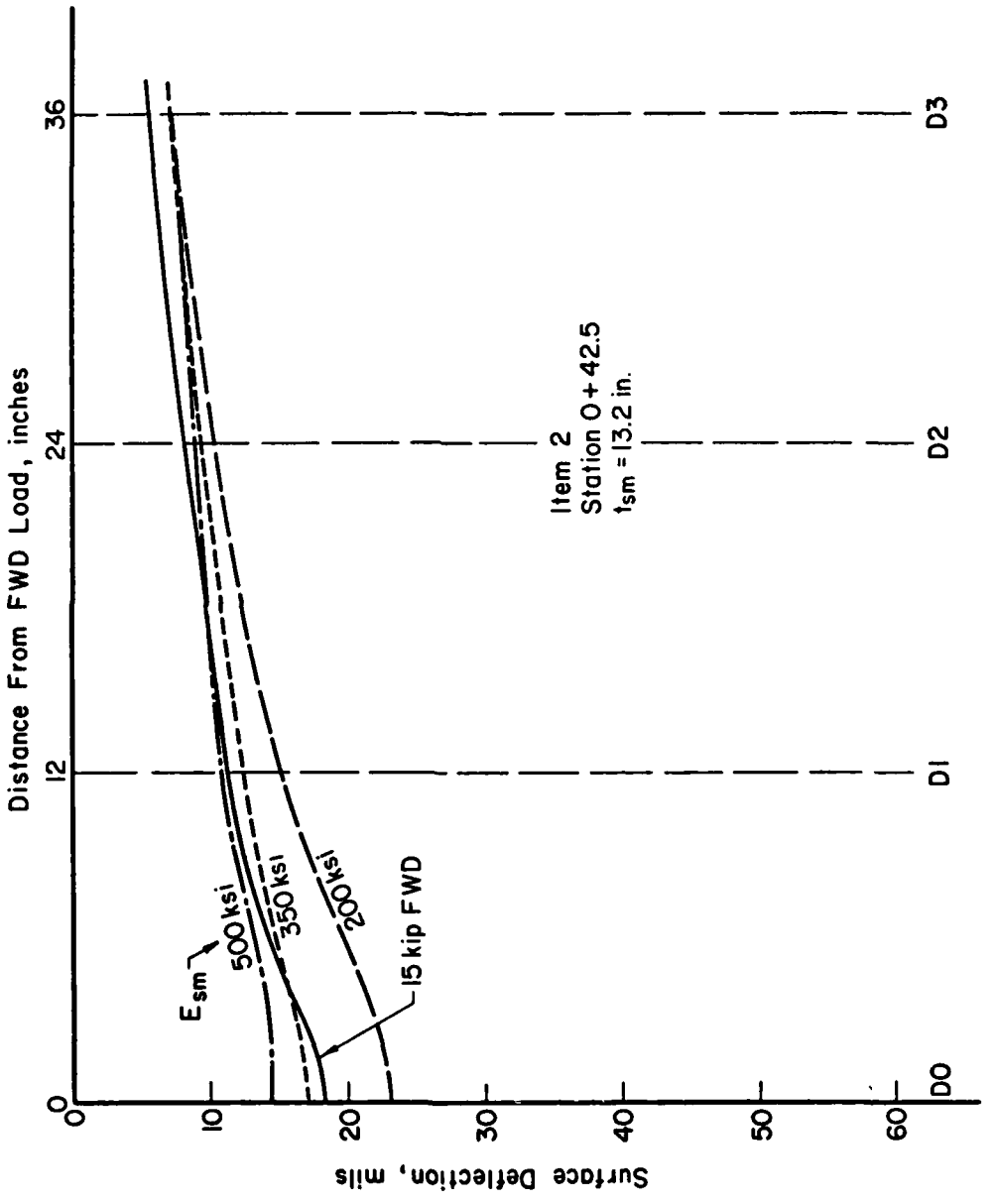

Figure 3-19. ILLI-PAVE and FWD Deflection Basins, Item 2

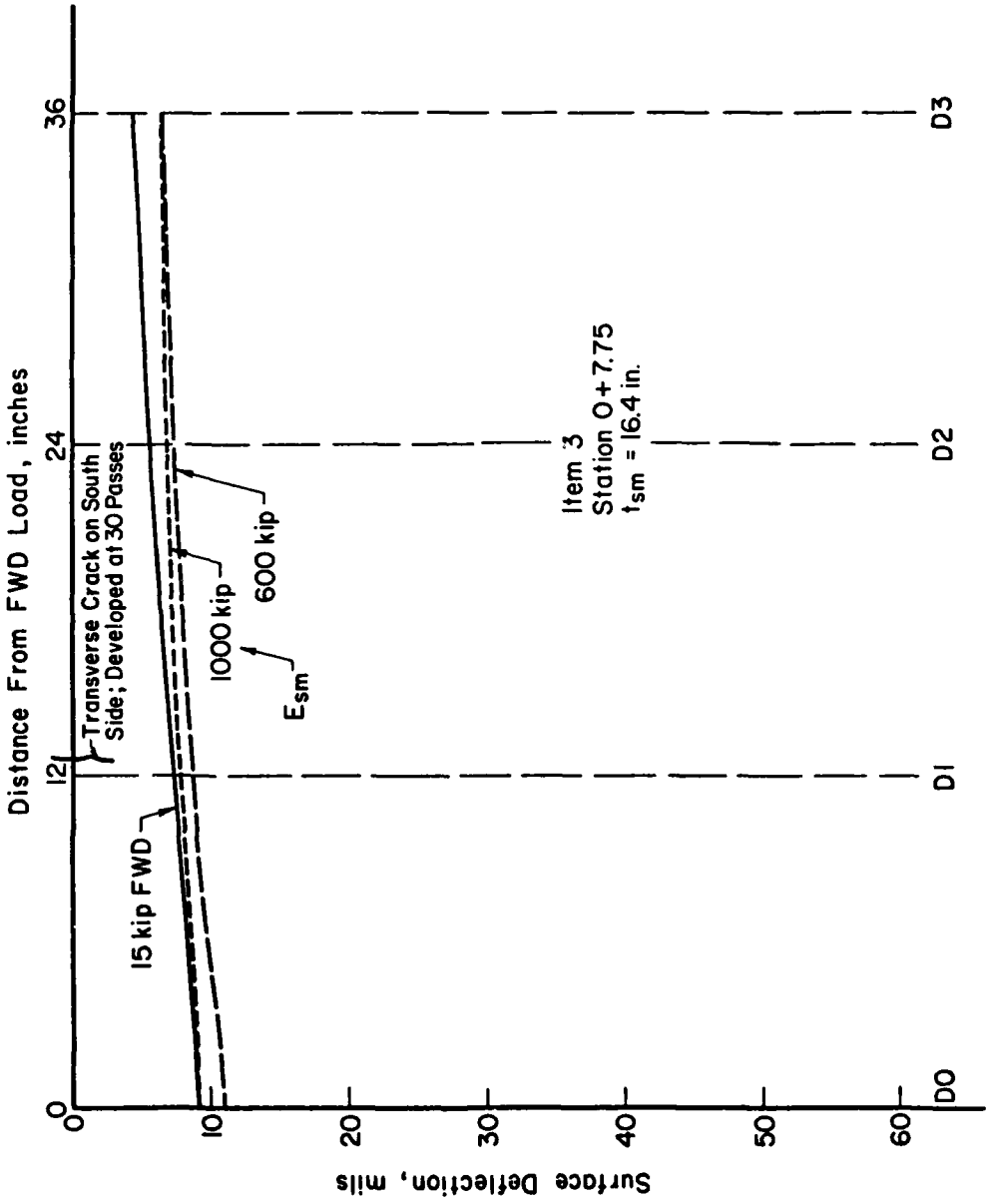

Figure 3-20. ILLI-PAVE and FWD Deflection Basins, Item 3

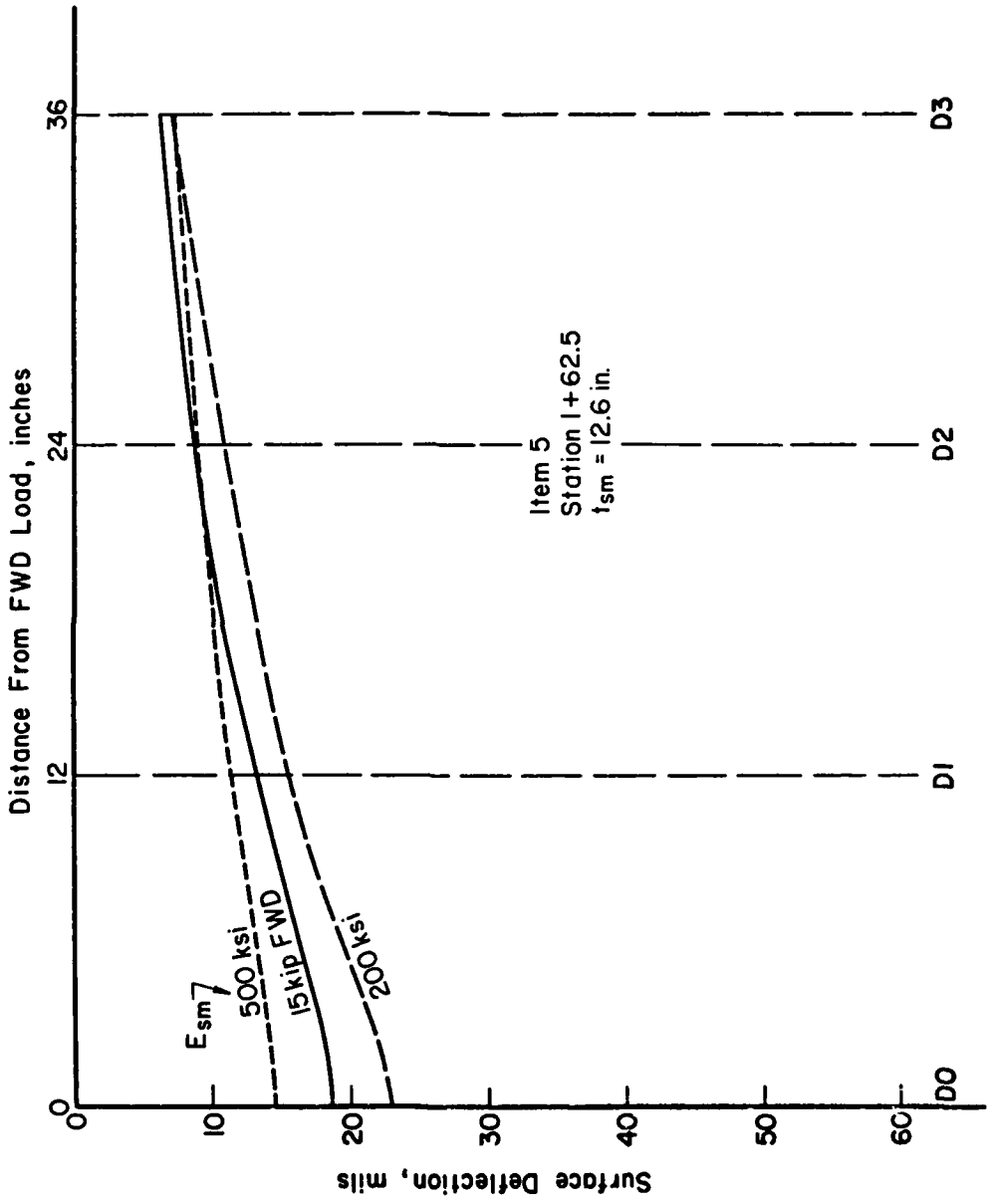

Figure 3-21. ILLI-PAVE and FWD Deflection Basins, Item 5

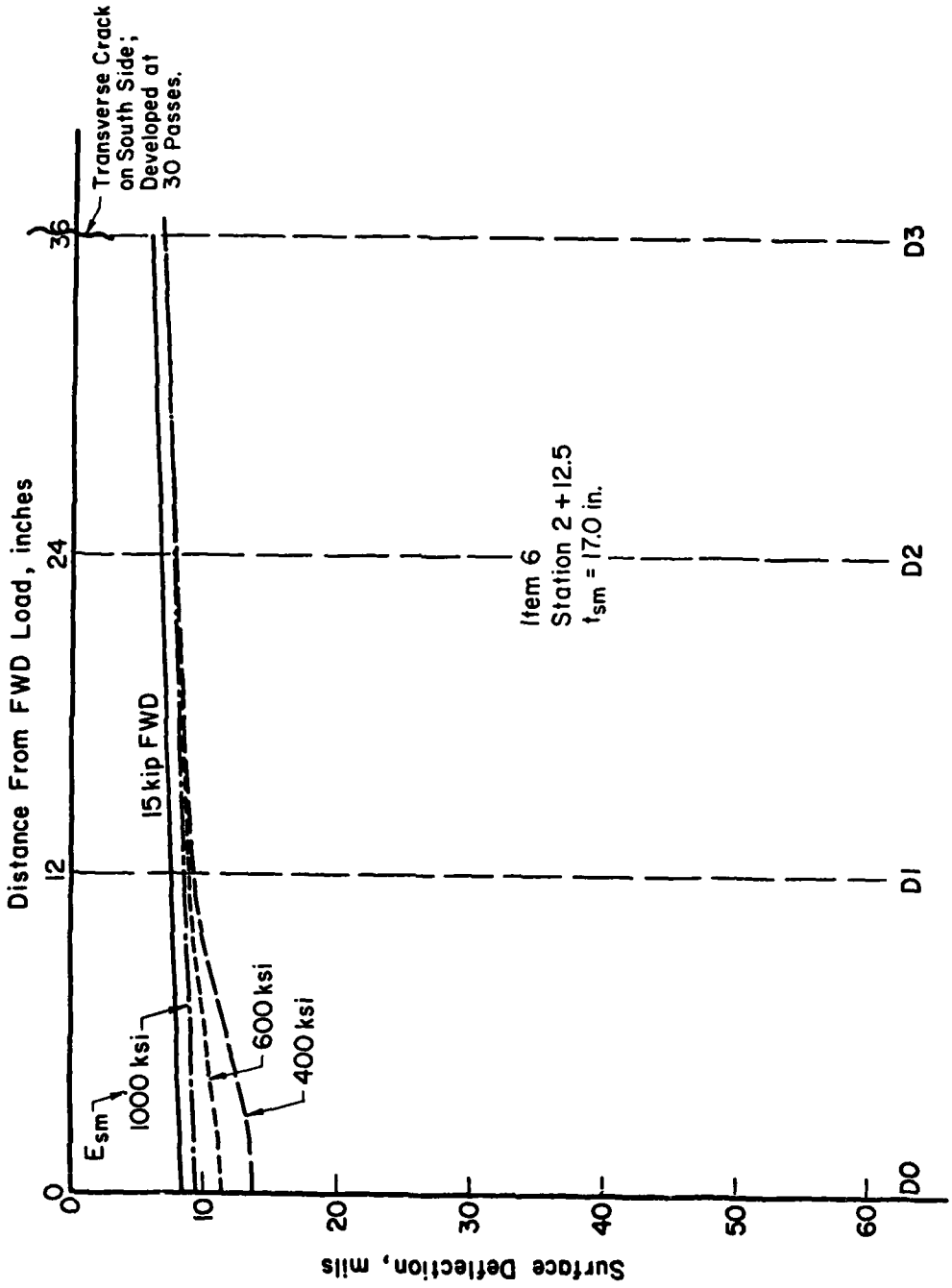

Figure 3-22. ILLI-PAVE and FWD Deflection Basins, Item 6

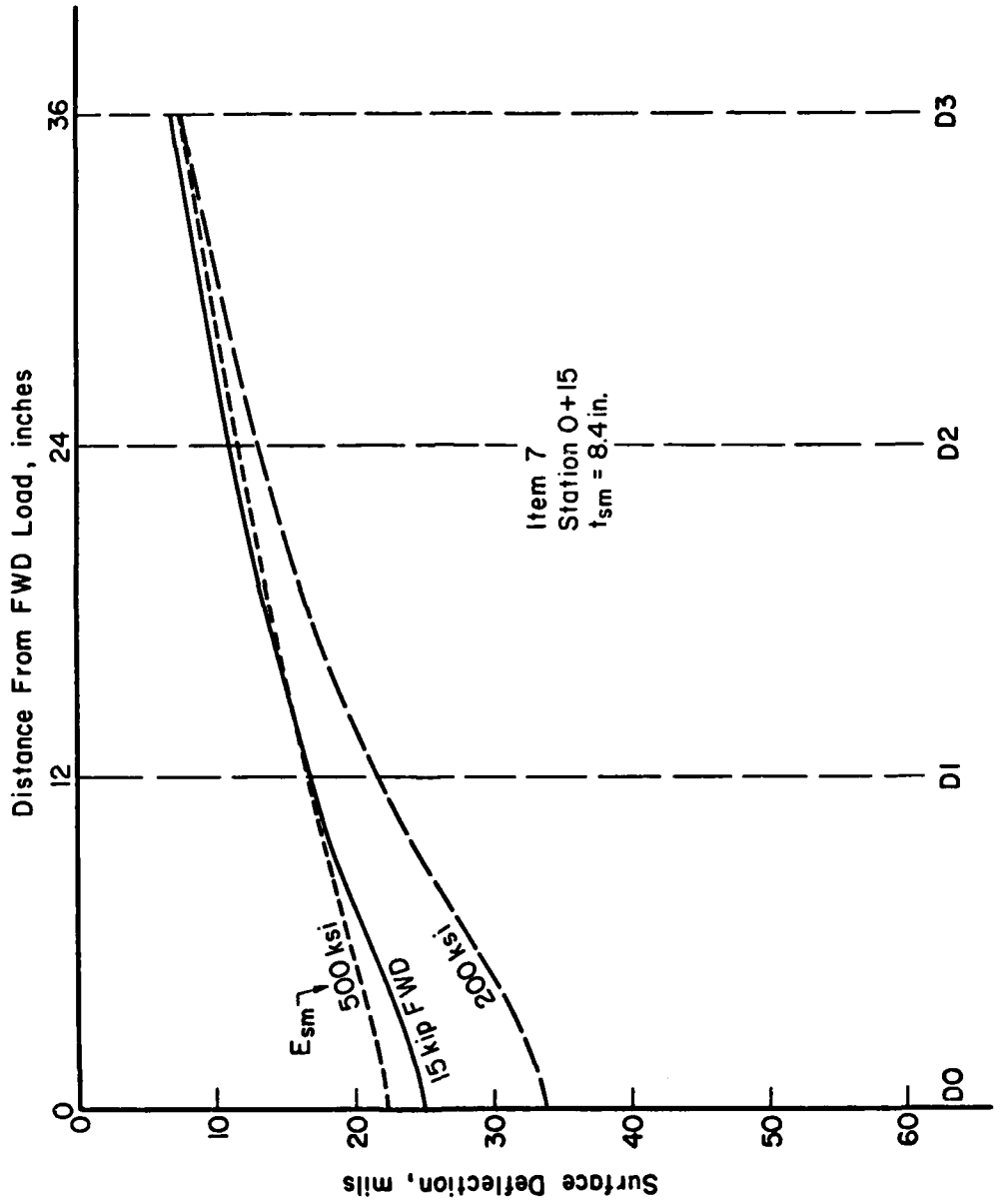

Figure 3-23. ILLI-PAVE and FWD Deflection Basins, Item 7

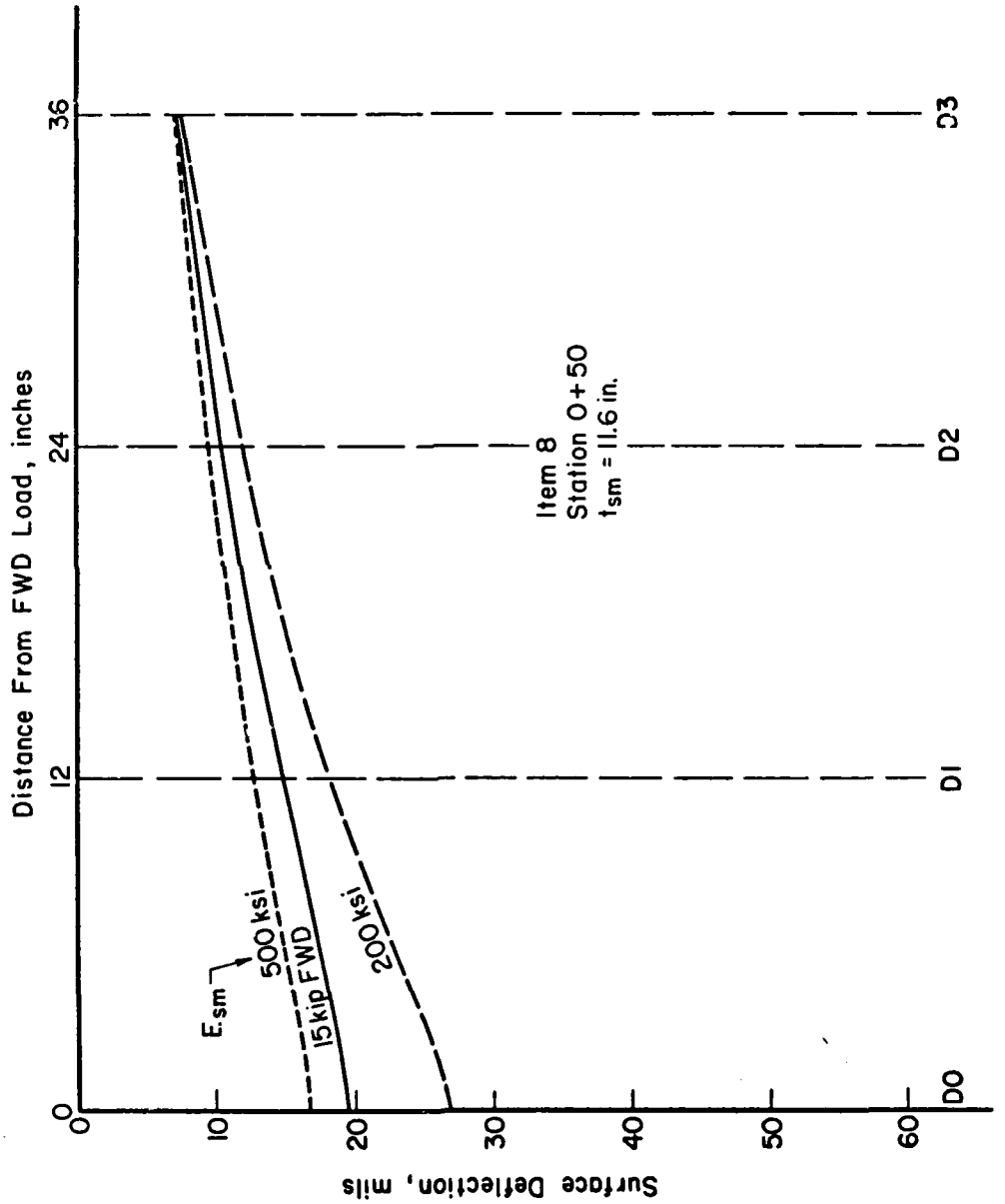

Figure 3-24. ILLI-PAVE and FWD Deflection Basins, Item 8

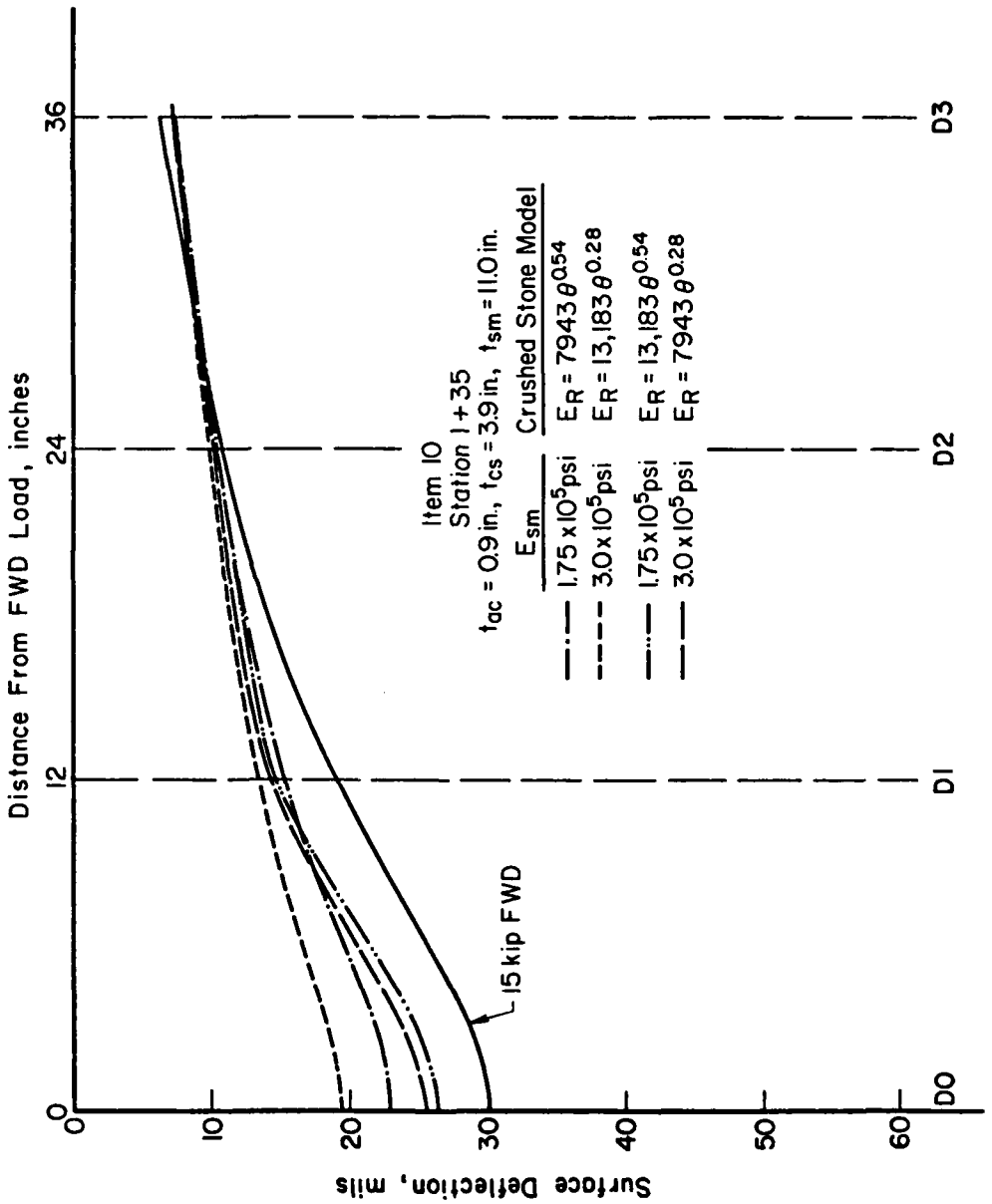

Figure 3-25. ILLI-PAVE and FWD Deflection Basins, Item 10

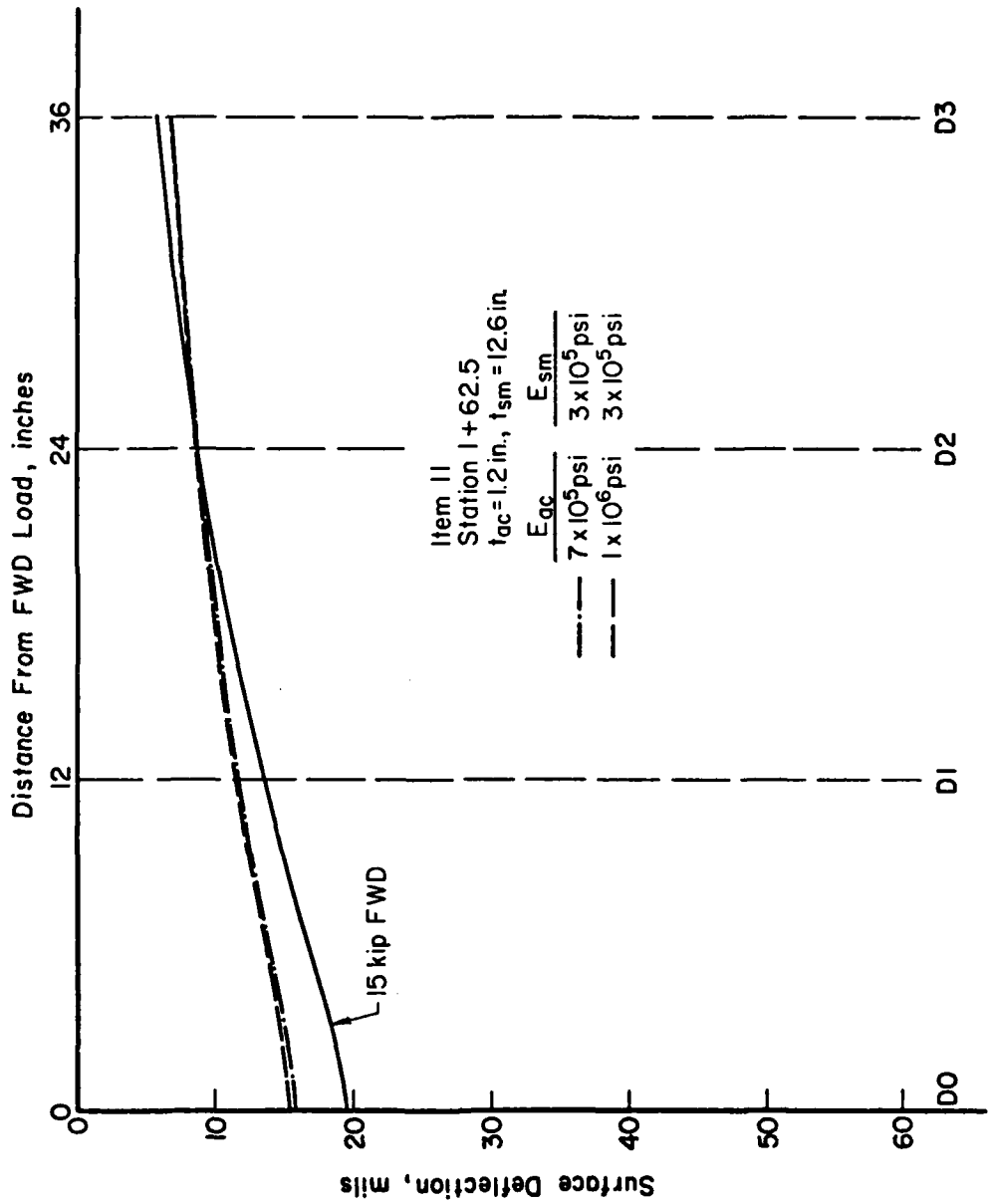

Figure 3-26. ILLI-PAVE and FWD Deflection Basins, Item 11

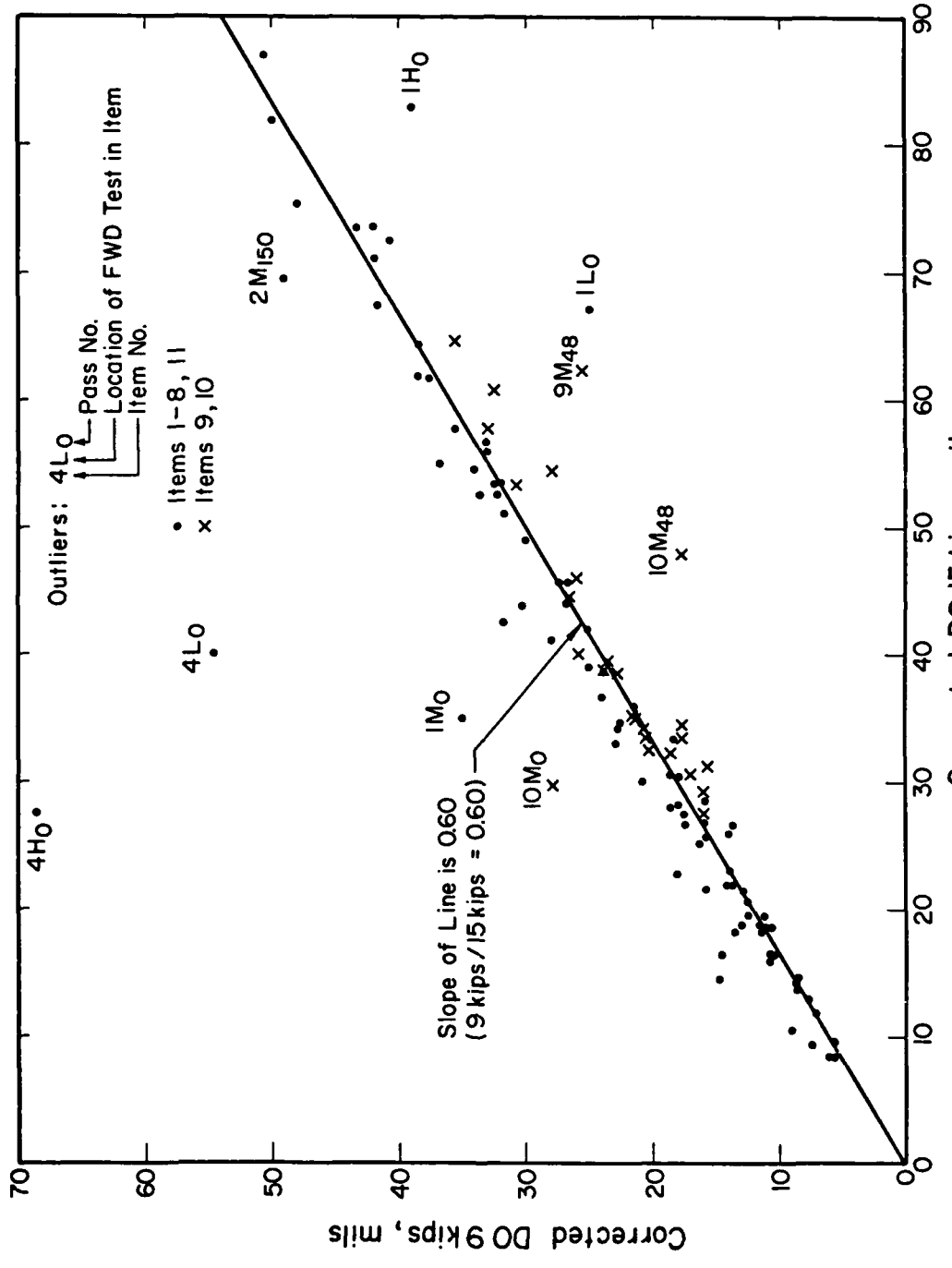

Figure 3-27. FWD DO Deflection at 9 and 15 kips (FWD Deflection Data, Appendix A)

increased by the ratio 15 kips/actual FWD load. The D1, D2, and D3 deflections were then increased using the new D0 deflection and the ratios D1/D0, D2/D1, and D3/D2 determined from the actual FWD load-deflection data.

The resilient modulus behavior of the subgrade tube samples in item 11 was much softer than any other item. ILLI-PAVE solutions using this soft modulus predicted much larger D3 deflections than were obtained with the FWD. When the average CAP subgrade model was used in item 11, the predicted and actual D3 deflections closely matched. Table 3-3 lists the back-calculated modulus of the various CAM layers in the test items.

2. Strength

Accurate assessment of the effects of strength and thickness on performance requires a good measure of the field strength of the CAM. CAM strength is affected by soil properties, mixing efficiency, cement content, moisture, curing conditions, and density.

The WES strength tests results on the field mixed CAM samples (Reference 9) are inconsistent with expected results. For instance, strength decreases with increasing cement content. Preliminary nuclear density measurements of the compacted CAM material were 112 pcf. The field mixed, laboratory compacted samples made during construction were compacted to this density. However, later density measurements (Table 2-3) determined the actual field densities were greater than 112 pcf. Compaction of the samples to 115-117 pcf would have resulted in cement content-strength relationships as expected.

TABLE 3-3. BACK-CALCULATED CAM LAYER MODULUS
(MATCHING OF PREDICTED AND ACTUAL FWD SURFACE DEFLECTION BASIN)

Item	CAM Layer Modulus (ksi)	Comments
1	200	Transverse crack developed 12 inches north of FWD load at 30 passes.
2	400	
3	1,000	Transverse crack developed 12.5 inches south of FWD load at 30 passes.
4	25	Extensive block cracking in traffic lane after construction.
5	350	
6	1,200	Transverse crack developed 36 inches south of FWD load at 30 passes.
7	400	
8	400	
10	175	Crushed stone model $E_r = 13{,}183\theta^{0.28}$
10	100	Crushed stone model $E_r = 7943\theta^{0.54}$
11	300	FWD deflection basin distorted indicating a crack in the vicinity of the FWD load; location of crack unknown due to asphalt concrete wearing course.

A laboratory strength study was conducted at the University of Illinois in 1983 on the CAM to determine the effects of density, cement content, and curing on strength (Table 3-4). Unconfined compression tests (ASTM-D-1633) were conducted on laboratory prepared standard Proctor size specimens (4.0 inches in diameter and 4.6 inches high). A partial factorial design was used with the following factor levels:

Dry Density: 3 levels obtained by varying the number of layers and number of blows per layer.
High density - 3 layers, 25 blows per layer
Medium density - 3 layers, 12 blows per layer
Low density - 2 layers, 6 blows per layer

Cement Content: 5, 7, and 9 percent

Moist Curing: 7 and 28 days at 72 degrees F.

The WES test items received approximately 1150 degree days of curing (40 degree F base temperature) based upon the mean air temperature. The laboratory 28 day moist cure (896 degree days) results were used as an estimate of the field curing. Least squares regression equations were developed for the 28 day moist cured laboratory unconfined compressive strengths (Table 3-5). These equations are shown in graphical form in Figure 3-28.

A review of this figure explains why the WES strength results were inconsistent with expected results. At 112 pcf dry density, the density effect masked the expected strength gain from increased cement content.

TABLE 3-4. RESULTS OF UNIVERSITY OF ILLINOIS CAM STRENGTH STUDY

Percent Cement	Curing[1] Degree Days	Dry Density (pcf)	Unconf. Comp. Strength (psi)	Percent Cement	Curing[1] Degree Days	Dry Density (pcf)	Unconf. Comp. Strength (psi)
5	224	131.0	414	7	896	132.5	890
5	224	131.0	480	7	896	131.9	830
5	224	131.0	529	7	896	132.9	760
5	224	131.0	503	7	896	127.5	1190
5	224	127.1	460	7	896	124.1	910
5	224	126.7	460	7	896	115.9	430
5	224	126.2	470	7	896	115.1	420
5	224	115.0	200	7	896	112.6	390
5	224	116.7	260				
5	224	115.0	200	9	224	132.0	783
				9	224	132.0	849
5	896	131.3	540	9	224	132.0	766
5	896	131.1	530	9	224	132.0	812
5	896	132.5	560	9	224	125.9	770
5	896	126.4	580	9	224	125.3	690
5	896	127.7	660	9	224	125.3	650
5	896	124.9	560	9	224	115.0	320
5	896	118.9	450	9	224	115.6	400
5	896	115.8	380	9	224	115.6	490
5	896	115.4	370				
				9	896	130.6	1080
7	224	132.0	774	9	896	132.0	1060
7	224	132.0	683	9	896	131.4	1160
7	224	132.0	762	9	896	128.3	1270
7	224	132.0	751	9	896	128.6	1420
7	224	126.0	540	9	896	127.3	1310
7	224	125.5	700	9	896	116.5	700
7	224	113.6	320	9	896	116.0	600
7	224	115.0	300	9	896	116.5	750
7	224	113.5	280				

(1) Degree days based on 40 degrees F in a moist cure room.

TABLE 3-5. CAM STRENGTH REGRESSION EQUATIONS

Cement Content (percent)	Regression Equation(1)	R^2 Adjusted	Standard Deviation (psi)
5	$UCS = -17{,}738.5 + 216.12DD - .00445DD^3$	0.85	36.88
7	$UCS = -40{,}851.1 + 495.74DD - .01039DD^3$	0.78	136.23
9	$UCS = -3{,}363.9 + 35.1536DD$	0.64	175.64

(1) UCS is unconfined compressive strength in psi.
DD is dry density in pcf.

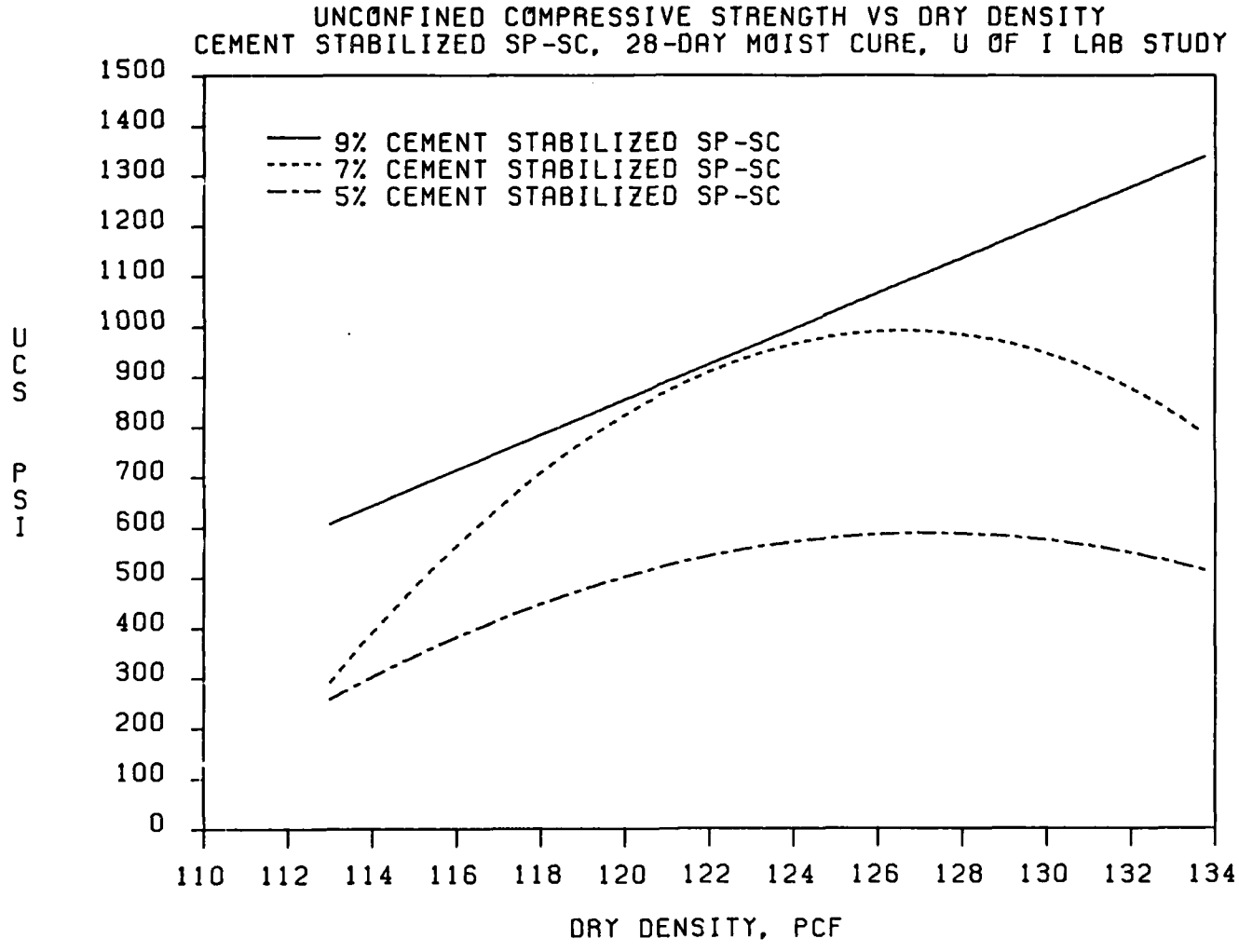

Figure 3-28. CAM Strength Regression Equations, University of Illinois Study

F. LIME STABILIZED CH SOIL

The addition of hydrated lime to fine-grained soils improves plasticity, workability, volume change, and strength characteristics (Reference 20). The CH soil was stabilized with 5 percent hydrated lime and used as a subbase course in item 9.

1. Resilient Modulus

a. Standard Relationship

The resilient modulus of the lime stabilized material in the subbase course of item 9 was estimated using the relationship (Reference 20):

$$E_R = 9.98 + .124q_u \qquad (3\text{-}2)$$

where:

E_R = compressive modulus of elasticity, ksi

q_u = unconfined compressive strength, psi.

Unconfined triaxial tests were conducted by WES and the q_u was 20 psi. Using the above relationship, the modulus is estimated to be 12.5 ksi. A typical modulus for this type of stabilized soil is 30 to 60 ksi. Since the 12.5 ksi modulus is unrealistically low, FWD deflections were used to back calculate the modulus of the lime stabilized subbase course in item 9.

b. Back-Calculation Procedure

The back-calculation procedure was used to estimate the modulus of the lime stabilized CH soil subbase course in item 9 (Figure 3-29). Figure 3-17 shows the ILLI-PAVE model used. Both crushed stone models (Figure 3-15) were used for the base course in the ILLI-PAVE solutions. A modulus for the lime stabilized CH soil subbase course in

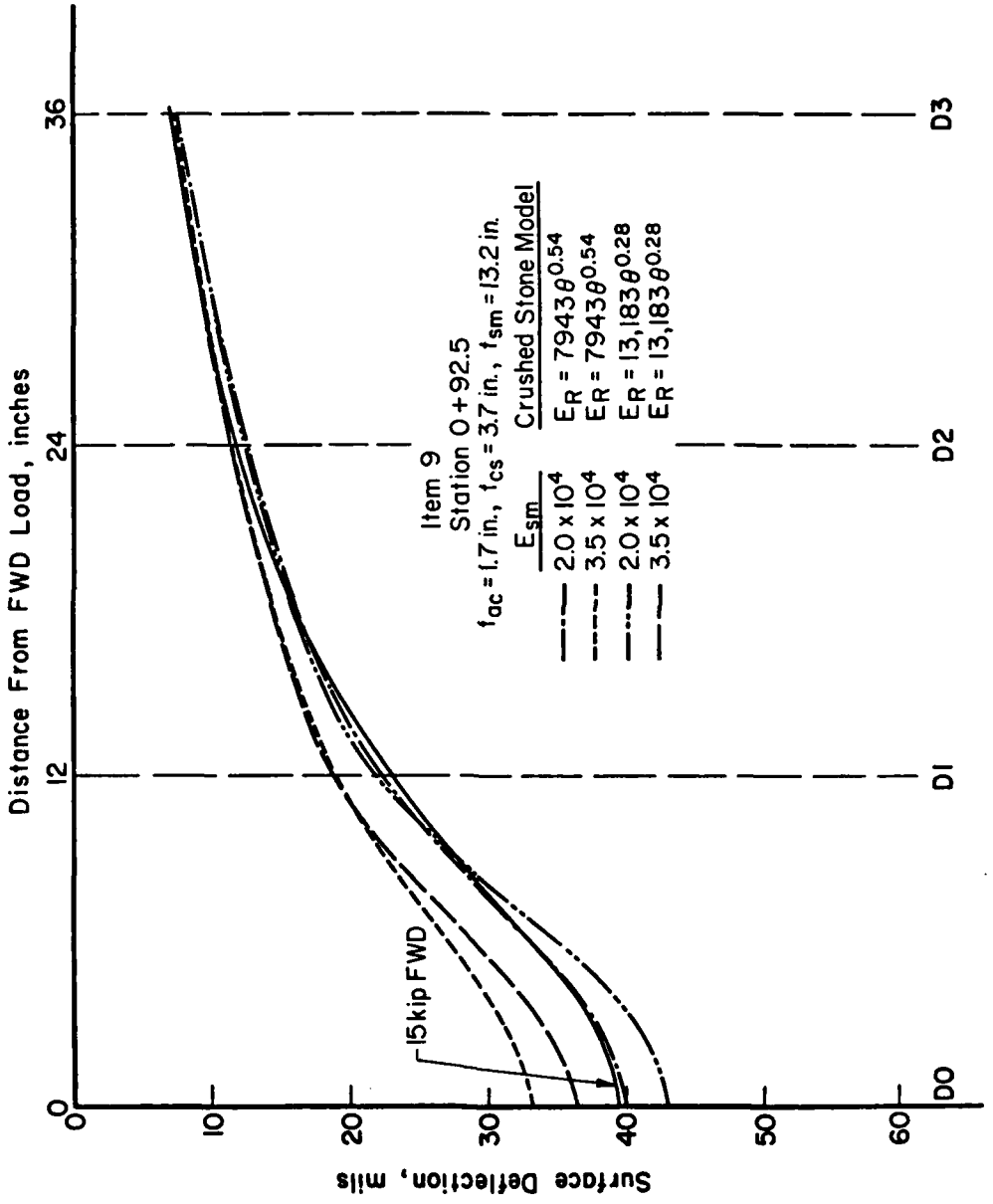

Figure 3-29. ILLI-PAVE and FWD Deflection Basins, Item 9

item 9 of approximately 20 ksi was obtained using either stress dependent stone model.

2. Flexural Strength

The lime stabilized CH soil subbase was constructed to a dry density of 88 pcf and 27 percent moisture. Although the density was low, it was consistent with the maximum dry density obtained in the laboratory for CE 12 compaction effort (Figure 2-7). Field mixed and laboratory compacted samples were made during construction. The samples were compacted to 88 pcf dry density and field cured in a sand pit adjacent to the test items. During the initial stages of traffic, part of the samples were tested in flexure (ASTM D1635-63) with a resulting flexural strength of approximately 14 psi (Reference 9). This value is consistent with other lime stabilized clay soils of low density (Reference 20).

G. MATERIAL CHARACTERISTICS FOR F-4 LOAD STRUCTURAL MODELING

Selection of the material characteristics used as inputs to the ILLI-PAVE program for determining predicted first pass structural response (Chapters 5 and 6) is discussed in the following sections.

1. Subgrade

a. Resilient Modulus

Predicted item structural response to the F-4 load is essentially the same using either the individual item or average CAP subgrade stress dependent resilient models. Deflections, flexural stress, and subgrade deviator stress do not vary by more than 4 percent and usually by less than 2 percent. Therefore, the average CAP subgrade resilient modulus

model was used to represent the top 36 inches of the subgrade in the ILLI-PAVE models and the standard medium subgrade was used for the remainder of the subgrade (Figure 3-14).

b. Strength

The average unconfined compressive strength for the tube samples in each item was used to determine the cohesion for the top 36 inches of the subgrade (Table 3-2).

2. Asphalt Concrete

The modulus of the nominal 1 inch thick asphalt concrete was estimated at 700 ksi.

3. Crushed Stone

a. Resilient Modulus

There is no significant difference in structural response of items 9 and 10 using either the WES or University of Illinois stress dependent resilient modulus stone model. The University of Illinois model ($E_R = 13{,}183\theta^{0.23}$) will be used since it agrees with expected values for this type of granular material.

b. Strength

The friction angle of the crushed stone is 54 degrees with no cohesion.

4. Cement Aggregate Mixture

a. Modulus

The back-calculated CAM layer modulus used in the F-4 ILLI-PAVE analyses is listed in Table 3-6.

b. Strength

CAM field flexural (tensile) strength was estimated from

TABLE 3-6. CAM MODULUS USED IN F-4 ILLI-PAVE ANALYSIS

Item	CAM Layer Modulus (ksi)	Comments
1	300	
2	400	
3	1,000	
4	25	Estimated due to extensive block cracking.
5	400	
6	1,200	
7	400	
8	400	
10	175	Stone model, $E_r = 13.183\theta^{0.28}$
11	300	

the University of Illinois laboratory strength study. In order to account for inefficiencies in field mixing compared to laboratory mixing, adjustment of laboratory strengths was required. Several studies (Reference 21, 22, 23) have shown the mixing efficiency for mixed-in-place operations ranges from 0.6 to 0.8 for the same dry density, moisture content, and curing conditions. Mixing efficiency is defined as:

mixing efficiency = field strength/laboratory strength.

A field mixing efficiency of 0.65 was selected for the CAP field test.

Flexural strength is approximately 20 to 30 percent of unconfined compressive strength (UCS) (Reference 8). For the CAM material, flexural strength was estimated at 22 percent of the UCS.

The CAM field flexural strength (at a specific dry density and cement content) was estimated by:

$$f_b = UCS_{lab} \times 0.65 \times 0.22 \qquad (3\text{-}3)$$

where:

f_b = field flexural strength, psi

UCS_{lab} = laboratory unconfined compressive strength determined from Figure 3-28, psi.

0.65 = field mixing efficiency

0.22 = relationship of f_b to UCS.

The estimated field flexural strength for the various CAM layers is listed in Table 3-7.

TABLE 3-7. ESTIMATED CAM FIELD FLEXURAL STRENGTH

Item	Percent Cement	Dry Density (pcf)	Predicted Lab.[1] Unconf. Comp. Strength (psi)	Estimated Field[2] Flexural Strength (psi)
1	5	112.6[3]	241	35
2	5	118.2[3]	455	65
3	5	118.9[3]	475	68
4	7	-----	----	---
5	7	120.7[3]	857	123
6	7	125.8[3]	990	142
7	9	113.2[3]	615	88
8	9	127.3[3]	1111	159
10	5	120.0[4]	500	72
11	5	118.2[4]	455	65

(1) Mean value from Figure 3-28.

(2) $f_b = UCS_{lab} \times 0.65 \times 0.22$.

(3) Average of 2 tests in lower portion of CAM layer.

(4) Estimated from nuclear density tests.

5. Lime Stabilized CH Soil

a. Resilient Modulus

The back-calculated modulus of the lime stabilized CH soil subbase course in item 9, using either of the stone models, is 20 ksi. This modulus is much lower than expected and not representative of a typical lime reactive CH soil. Preliminary laboratory tests conducted by WES on the CH soil showed it was reactive to the lime and produced modulus values over 100 ksi. The reason for the apparent non-reaction of the CH soil with the lime is unknown.

b. Strength

The flexural strength of the lime stabilized CH soil subbase course in item 9 was 14.0 psi (as determined by the WES tests).

6. Summary of Material Characteristics for F-4 Analysis

Table 3-8 gives a summary of the material characteristics used in the F-4 ILLI-PAVE analysis of the CAP test items.

TABLE 3-8. SUMMARY OF MATERIAL CHARACTERISTICS FOR F-4 ANALYSIS

Material	Modulus	Strength
Asphalt Concrete	700 ksi	Not required
Crushed Limestone	$E_r = 13{,}183\theta^{0.28}$	$\phi = 54$ degrees, c = 0 psi
Cement Aggregate Mixture (CAM)	Modulus for each layer listed in Table 3-6.	Flexural strength listed in Table 3-7.
Lime Stabilized CH soil	20 ksi	Unconfined compressive strength 14.0 psi.
CH Subgrade	Top 36 inches average CAP subgrade model. Remainder standard medium subgrade. See Figure 3-13.	Top 36 inches, undrained shear strength Table 3-2. Remainder is standard medium subgrade.

CHAPTER 4

INTRODUCTION TO RESPONSE AND PERFORMANCE

A. STRUCTURAL AND FUNCTIONAL FAILURE

Performance is the measure of how well a pavement fulfills its intended purpose. The general purpose of airfield pavements is to provide a surface for the safe, comfortable, and convenient operation of aircraft during takeoff, landing, and taxi for a designated period of time and/or traffic levels. Functional failure of the pavement is reached when it can no longer meet the requirements of the user, i.e. when the pavement causes handling problems for the pilot or causes damage to the aircraft. Structural failure is defined as the collapse of the pavement structure or the breakdown of one or more of the pavement components to the extent that the pavement is not capable of carrying the imposed loads. Although both failures can occur at the same time, functional failure usually occurs before structural failure.

Performance is directly related to the type and severity of distress that develops in a pavement. Pavement distress can be either load related, environment related, or a combination of both. Load related distress (those considered in this study) includes cracking, faulting, and rutting. Since the CAP field test was conducted over several months and under an enclosure, no environment related distress occurred. Only load related distress contributed to item performance decline.

Surface roughness accumulation is a function of traffic induced distress when no environmentally related distress occurs. As long as

the rigid stabilized material layer is intact, pavement deflections are stable and the degree of surface roughness is acceptable. Major surface roughness occurs when the slab type behavior of the intact stabilized material layer breaks down due to severe cracking.

B. CRACK STRUCTURAL RESPONSE

1. Stress

A high strength and high modulus stabilized material layer displays a "slab type" behavior. Most rational analyses of pavement behavior concerning cementitious materials have shown flexural (tensile) stresses are the most critical factor affecting initiation and early propagation of load related cracks (Reference 24).

The maximum flexural (tensile) stress occurs when the load is adjacent to a crack (References 21, 25, 26). This stress is at the bottom of the stabilized material layer and acts parallel to the crack. Researchers have reported this "crack" stress is 40 to 50 percent greater than the interior load flexural (tensile) stress (Reference 8). This increased stress may be characterized as a "load placement effect factor (LPEF)" and defined as:

$$LPEF = \sigma_{crack}/\sigma_{interior} \qquad (4\text{-}1)$$

where:

σ_{crack} = flexural stress in the stabilized layer when the load is at a crack for a specific LTE

$\sigma_{interior}$ = flexural stress in the stabilized layer for an interior load condition.

The maximum value for the LPEF occurs when the load is at a free edge, LTE = 0 percent. Using Westergaard's new formulas for stresses in concrete airfield pavements (Reference 27), the LPEF approaches 1.8 for 8 inch thick slabs and 2.0 for 16 inch slabs. Large variations in subgrade support and slab modulus have little effect on the LPEF (Figure 4-1).

To determine the effect of LTE on the LPEF, a study was conducted using the ILLI-SLAB program (References 12, 28). The study results (Figure 4-2) show LPEF is a function of thickness and LTE. Note the upper limit for LPEF approaches that calculated by Westergaard's equations. The flexural (tensile) stress in the stabilized layer at a crack, σ_{crack}, with partial load transfer is estimated by the equation:

$$\sigma_{crack} = \sigma_{interior} \times LPEF \qquad (4-2)$$

where:

$\sigma_{interior}$ = interior flexural stress calculated by ILLI-PAVE

LPEF = load placement effects factor for a specific LTE determined from Figure 4-2.

2. Strain

The maximum crack flexural (tensile) strain acting parallel to the crack at the bottom of the stabilized material layer is larger than for an interior load condition. Maree and Freeme of South Africa (Reference 29) have conducted studies on the strain at a crack relative to the maximum tensile strain under an interior load. Their method to estimate the maximum tensile strain at a crack is to increase the

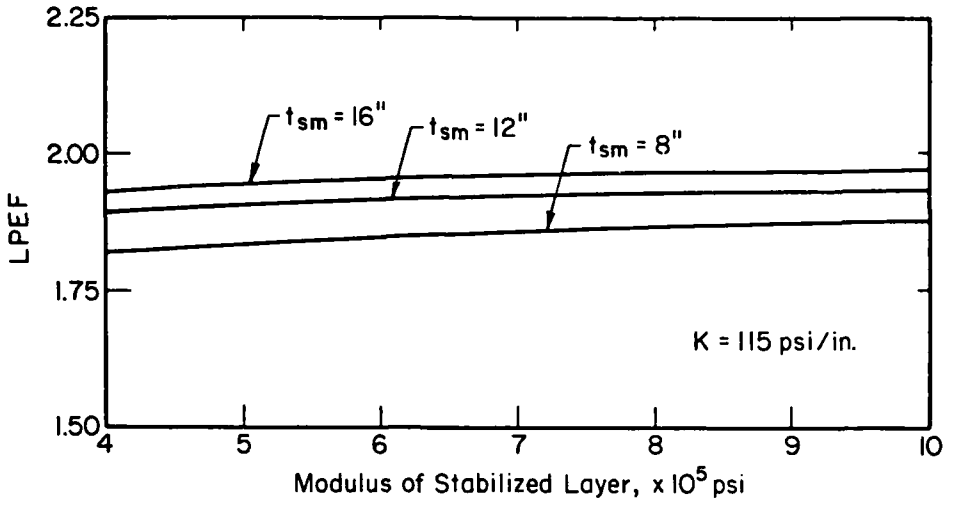

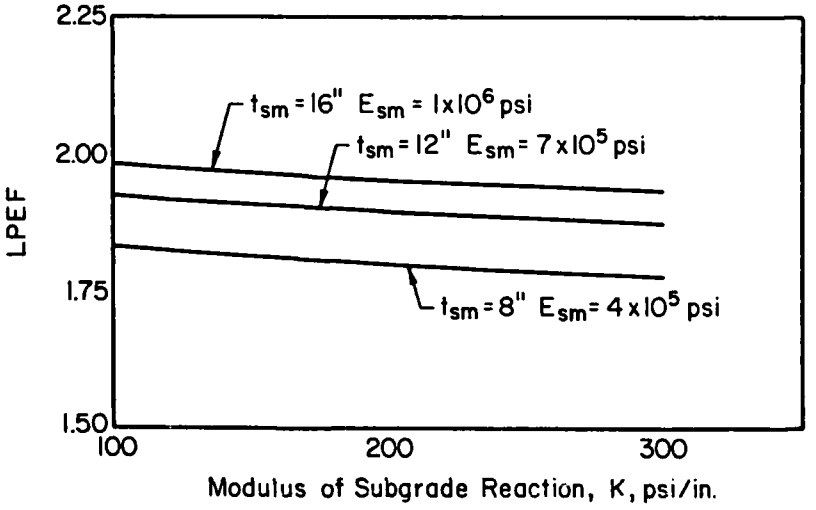

Figure 4-1. Effect of Slab Modulus, Thickness and Subgrade Support on the Load Placement Effect Factor (LPEF), 27 kips, 265 psi (Westergaard's 1947 Equations)

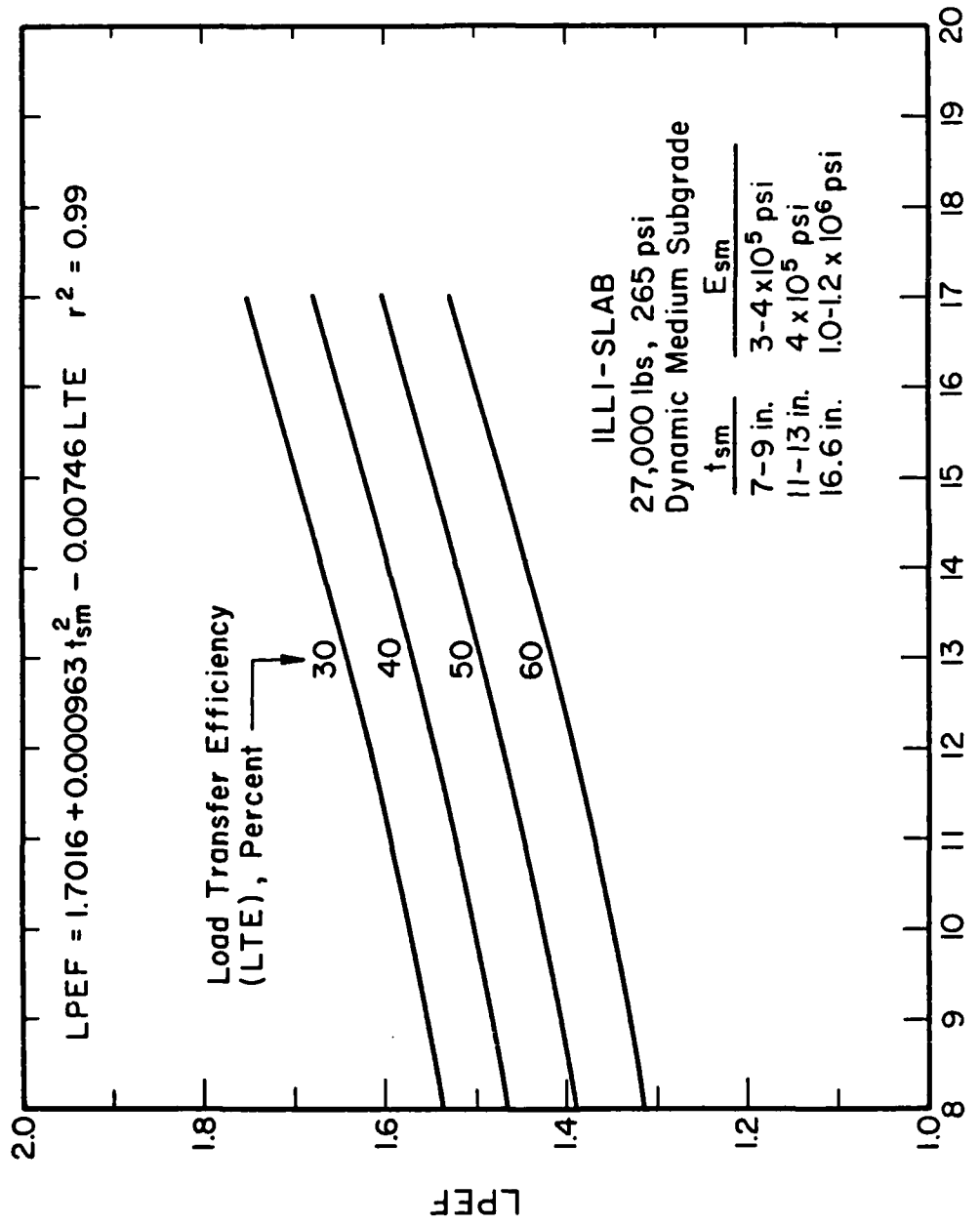

Figure 4-2. Load Placement Effect Factor (LPEF)

interior load tensile strain by a factor, c, which depends upon the type of cracking, material strength and material thickness. The factor c ranges from 1.1 for cracks less than 2mm wide in cemented natural gravel less than 7.82 inches thick to 1.4 for cracks greater than 2mm wide in cemented granular materials over 7.82 inches thick.

C. TRANSFER FUNCTIONS

1. Stress Ratio and Performance

For high strength and modulus stabilized material layers, a "fatigue approach" is frequently used relating stress ratio to number of repeated load applications to failure. Fatigue behavior is generally described by some functional relationship between repeated tensile stress, repeated tensile strain, or the ratio of repeated stress-to-strength and the number of load applications to failure (Reference 8).

The stress ratio concept has been used in the fatigue analysis of cement and lime stabilized materials (References 8, 30, 31, 32). Stress ratio (SR) is defined by:

$$SR = \sigma_{flex}/f_b \qquad (4\text{-}3)$$

where:

σ_{flex} = maximum flexural (tensile) stress at the bottom of the stabilized layer, psi

f_b = flexural strength determined from flexural beam tests or estimated from unconfined compressive strength-flexural strength relationships, psi.

The relationship between stress ratio and performance is often expressed in log-log or semi-log form since the distribution of performance at a specific stress ratio is log normal (Reference 33). When the log-log relationship is used the equation takes the form:

$$SR = AN^b \qquad (4\text{-}4)$$

where:

SR = stress ratio

N = number of load repetitions to failure

A, b = laboratory or field determined constants.

Typical laboratory determined values of A and b for beams made of cement stabilized materials subjected to third point loading and stress ratios less than one are 0.8-1.0 for A and 0.025-0.037 for b (Reference 32). Figure 4-3 shows several laboratory semi-log transfer functions for stabilized materials for stress ratios less than one.

It is generally accepted that the fatigue concept relates to crack initiation in the stabilized material and additional load repetitions are required to propagate the crack to the surface. Laboratory behavior of simply supported beams does not reflect the number of load repetitions required in the field to propagate cracks once they have initiated in the stabilized layer (Reference 21). There is considerable useful life remaining in a pavement after crack initiation in the stabilized layer at traffic levels of 1000 passes or less. Conservative designs will result if laboratory derived transfer functions are used directly to design low volume CAPs.

Relating the number of load repetitions at functional failure to the number required for crack initiation in the laboratory has been

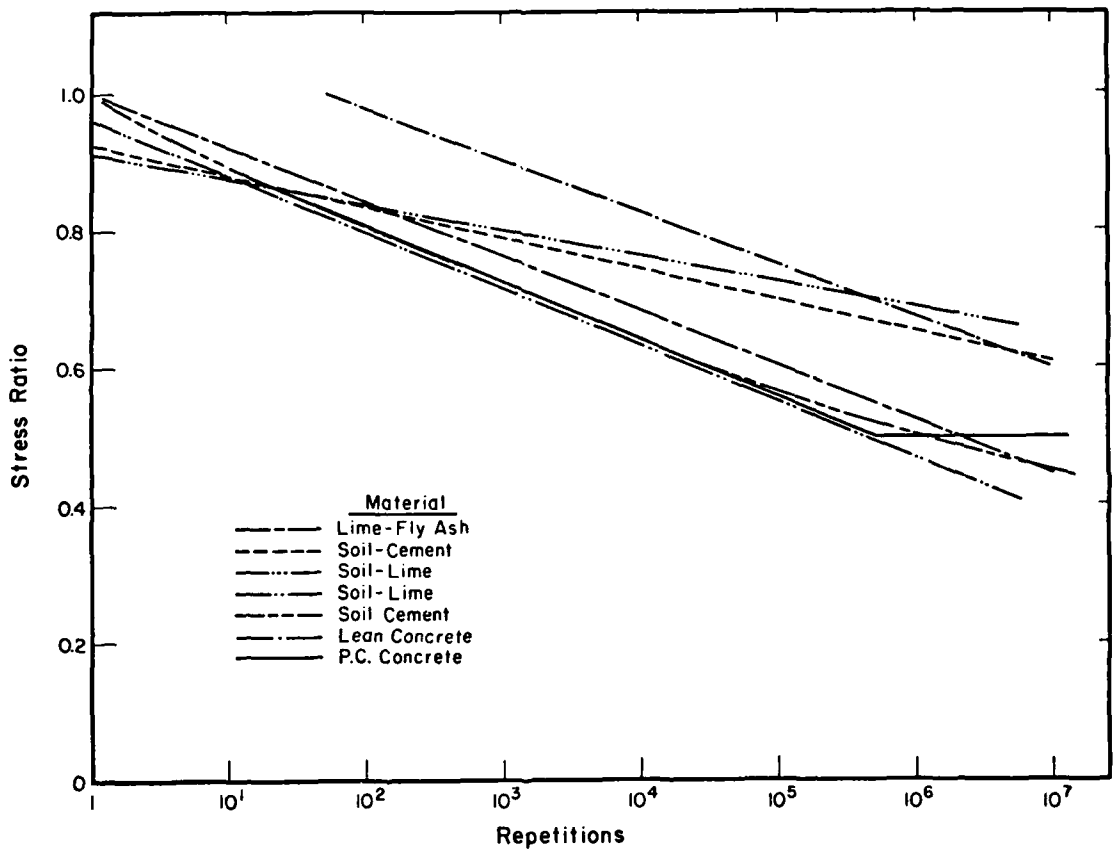

Figure 4-3. Reported Stress Ratio-Fatigue Relations for Cemented Materials (Reference 8)

handled by "shift factors." Investigations indicate the shift factor is variable and ranges from 1.07 to 4.6 (Reference 34). The proposed shift factors are for high pass levels to functional failure, i.e. 10^5 to 10^7 passes. No research has been conducted on shift factors for pass levels to functional failure of 1000 or less. What is needed is to determine the level of performance that constitutes functional failure for low traffic volume pavements and relate this to the predicted first pass stress ratio in the stabilized material layer.

2. Strain Ratio and Performance

Maree and Freeme (Reference 29) have proposed a tensile strain criterion for initiation of fatigue cracking in cemented pavement layers under repeated flexure. The interior load tensile strain is increased by a factor, c, to estimate the maximum tensile strain at a transverse crack, ϵ_s (3.B.2). A crack strain ratio, ϵ_{sr}, is then calculated by:

$$\epsilon_{sr} = \epsilon_s/\epsilon_b \tag{4-5}$$

where:

ϵ_s = crack tensile strain

ϵ_b = tensile strain at break measured in static beam flexure.

The strain at break varies from 120 to 145 microstrain depending upon the strength of the cemented material. The fatigue life to crack initiation is represented by the following proposed transfer function:

$$N_f = 10^{9.1(1-\epsilon_{sr})} \tag{4-6}$$

where N_f is the number of repetitions at strain ϵ_s to crack initiation. This transfer function is plotted in Figure 4-4.

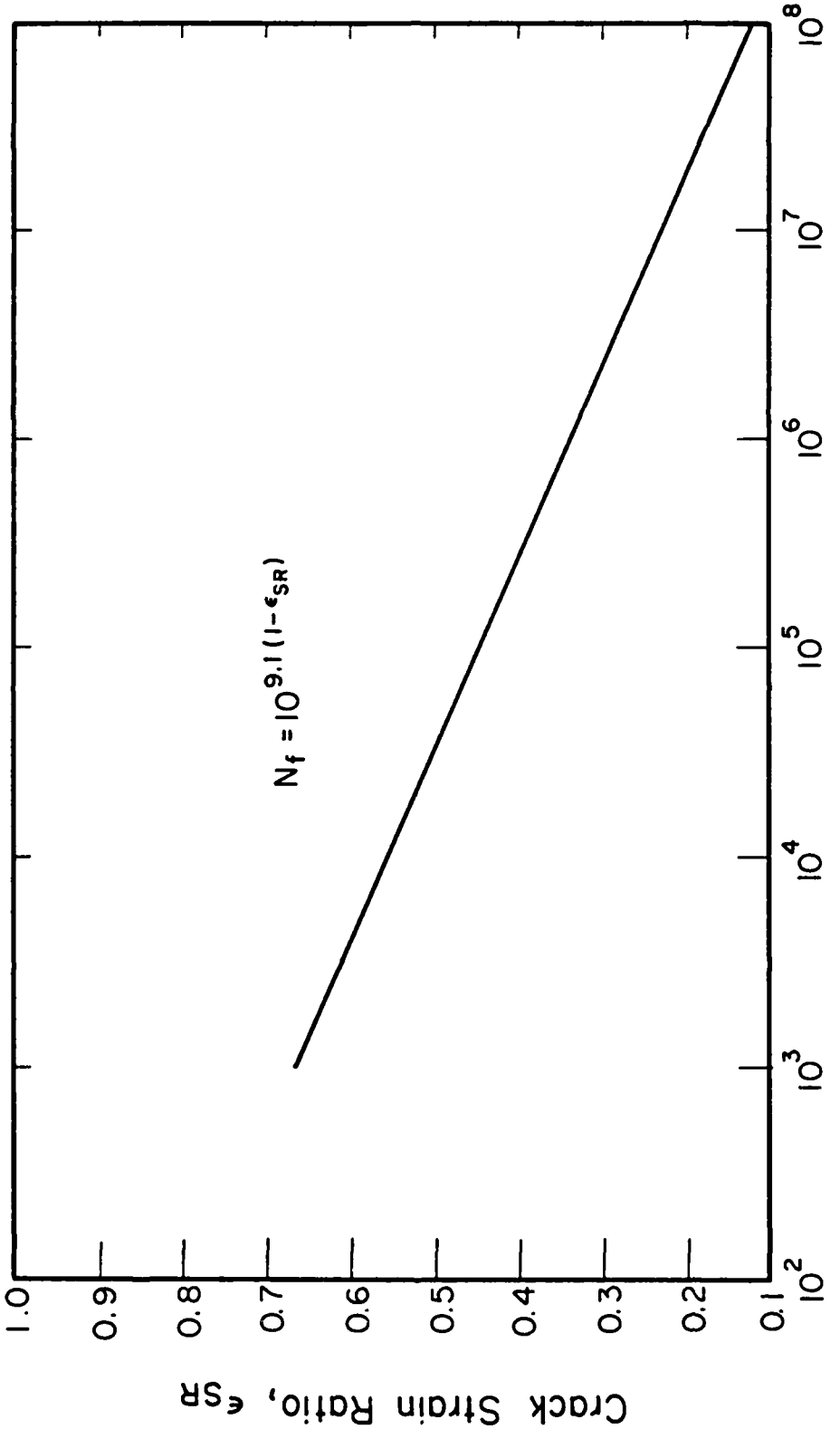

Figure 4-4. Transfer Function Relating Crack Tensile Strain to Initiation of Fatigue Cracking in Cemented Layers (Reference 29)

Crack propagation for strain based transfer functions is also handled by applying shift factors to N_f. The shift factor is a function of thickness and traffic levels and varies from 1.2 to 7.5.

D. COLLAPSE LOAD AND PERFORMANCE

The ultimate load carrying capacity or collapse load of a rigid two-layer pavement for interior, edge, and corner load conditions can be predicted using Meyerhof's equations (Reference 35). These equations are shown in Figure D-1 of Appendix D. A graphical solution of these equations is shown in Figure 4-5.

Three studies have been conducted on the ultimate collapse load of rigid two-layer pavements constructed with pozzolanic mixtures, cement stabilized soils, and lime stabilized soils (References 36, 37, 38). A summary of the test results is presented in Table D-1 of Appendix D and constitutes the ultimate load data base used in the following analysis. A review of the data base shows the collapse load predicted by the Meyerhof equations is conservative; the field collapse load is greater than the predicted collapse load. The ratio of field collapse load to predicted collapse load for the test sections in the ultimate load data base is shown in Figure 4-6. The field collapse load is 150 to 400 percent of the predicted collapse load. A typical value is 200 percent.

The load-deflection curve for each test section in the data base was analyzed to determine the following ratios:

load ratio = applied load/field collapse load

deflection ratio = applied load deflection/field collapse load deflection.

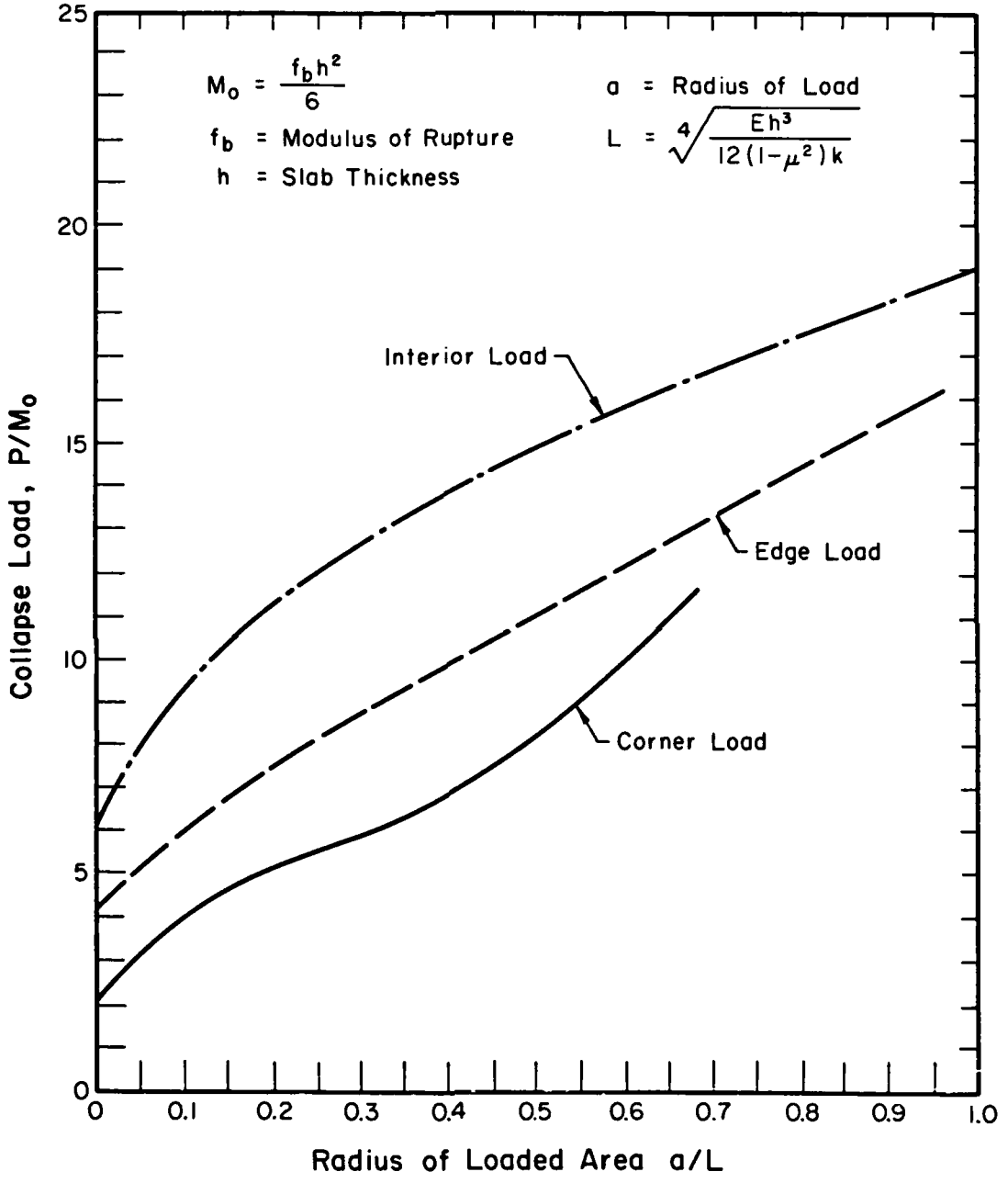

Figure 4-5. Graphic Solution of Meyerhof's Ultimate Load Equations

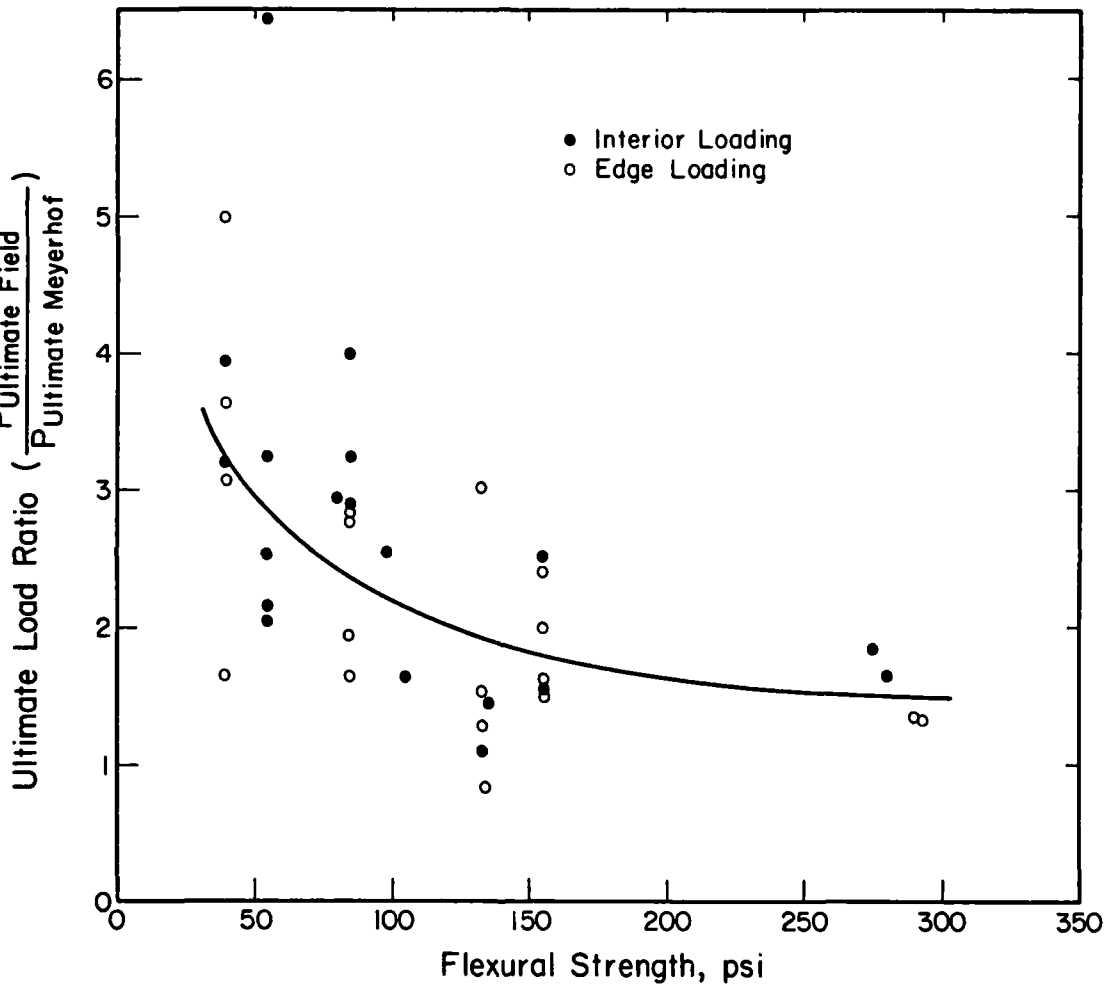

Figure 4-6. Comparison of Meyerhof Collapse Loads to Field Collapse Loads

These ratios were plotted and analyzed. The results showed the curves could be grouped according to the a/l ratio where a is the load radius and l is the radius of relative stiffness. Figures 4-7 through 4-10 are plots of the least squares regression equations of the load ratio versus deflection ratio for various ranges of a/l. Approximately 60 percent of the collapse load is developed at only 33 percent of the maximum deflection. Suddath and Thompson (Reference 38) reported an average of 73 percent of the ultimate load carrying capacity was developed at a deflection equal to one-third of the deflection required to develop the ultimate load-carrying capacity. This is expected since large deflections do not occur until the stabilized material layer is severely cracked.

Of primary interest for low traffic volume airfields is the relationship between the field collapse load and the predicted load required to produce a SR of one in the stabilized material layer. The test sections in the ultimate load data base were analyzed using Westergaard's equations and ILLI-PAVE to predict the load at a SR of one. First, a comparison was made between the flexural stress calculated by Westergaard's equations and ILLI-PAVE for similar conditions (Table 4-1). The flexural stress in the stabilized layer calculated by the Westergaard equations is an average 42 percent greater than calculated by ILLI-PAVE. Therefore, the interior load producing a predicted SR of one, as determined by the Westergaard equations (Table 4-2), must be increased 42 percent to be comparable with the ILLI-PAVE predictions. Edge load values are not corrected since a 3-dimensional

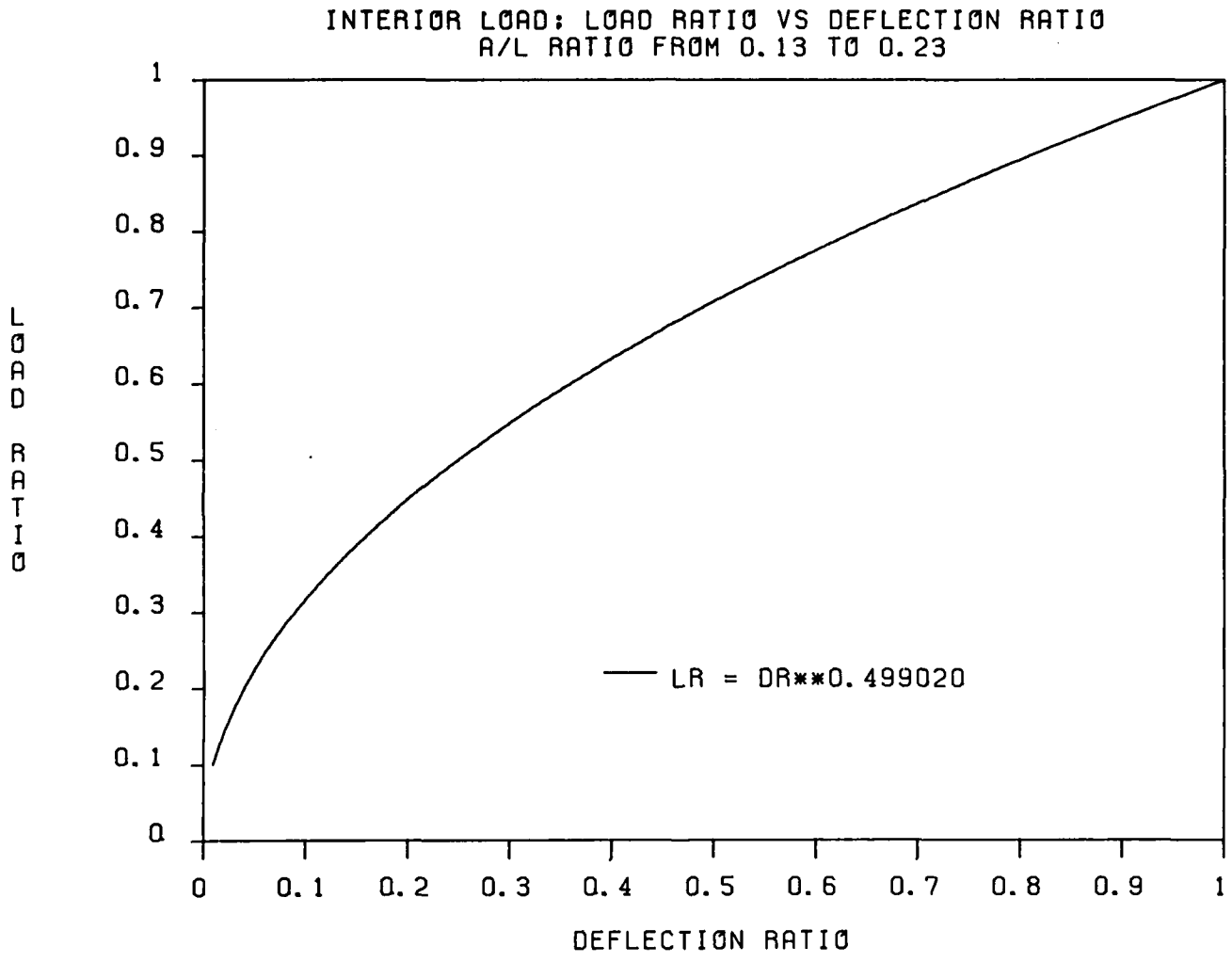

Figure 4-7. Normalized Ultimate Interior Load-Deflection Curve, a/1 0.13 to 0.23 (Ultimate Load Data Base, Appendix D)

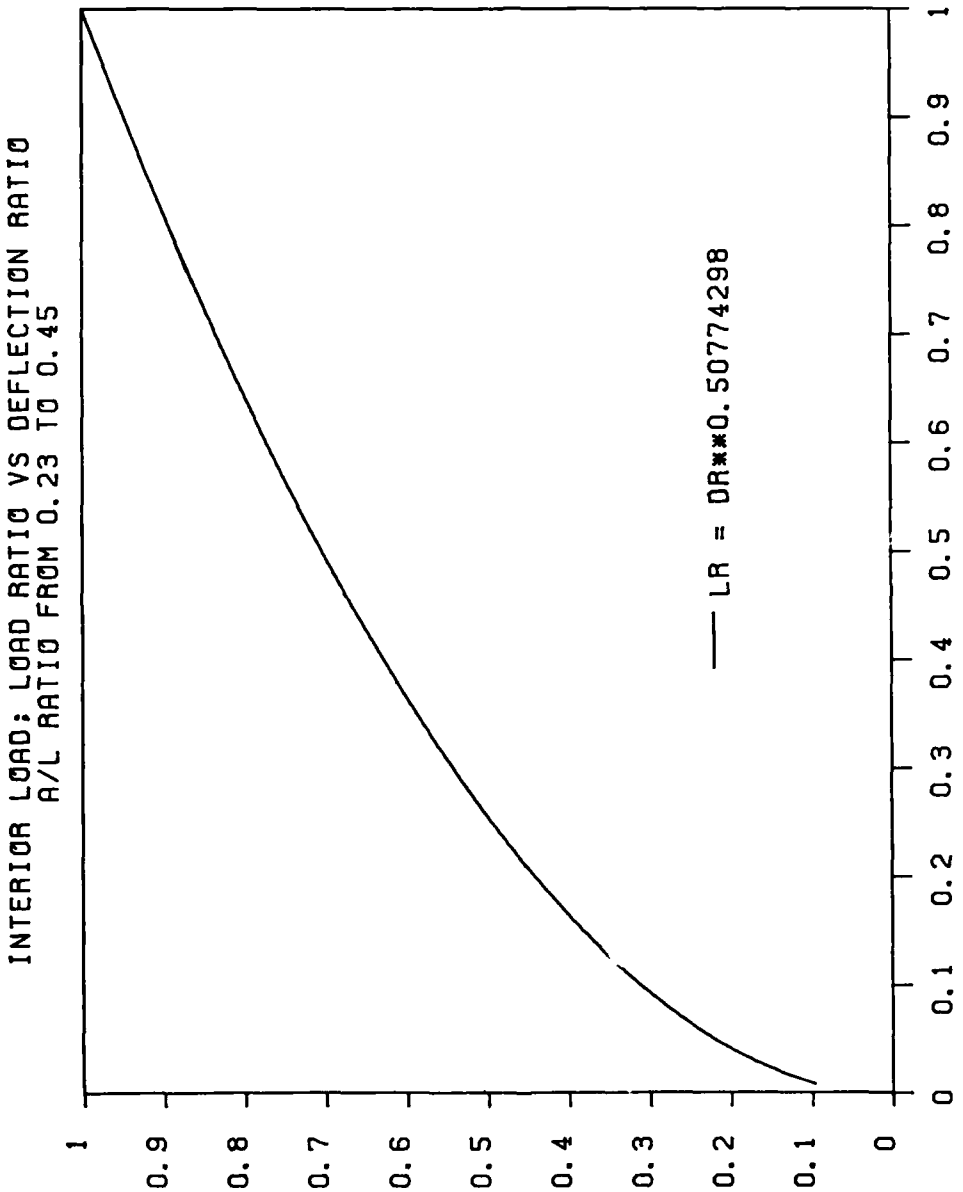

Figure 4-8. Normalized Ultimate Interior Load-Deflection Curve, a/l 0.23 to 0.45 (Ultimate Load Data Base, Appendix D)

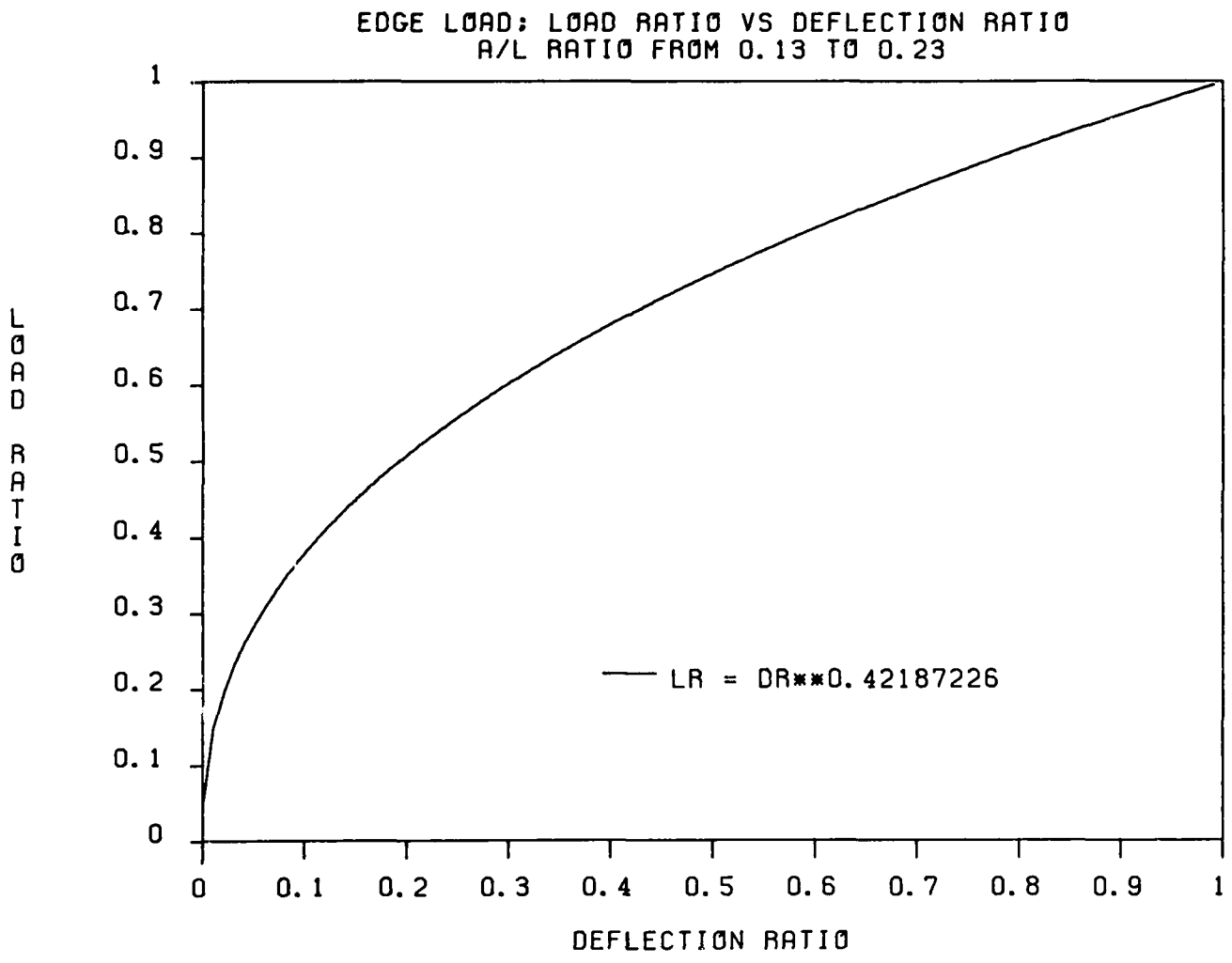

Figure 4-9. Normalized Ultimate Edge Load-Deflection Curve, a/l 0.13 to 0.23 (Ultimate Load Data Base, Appendix D)

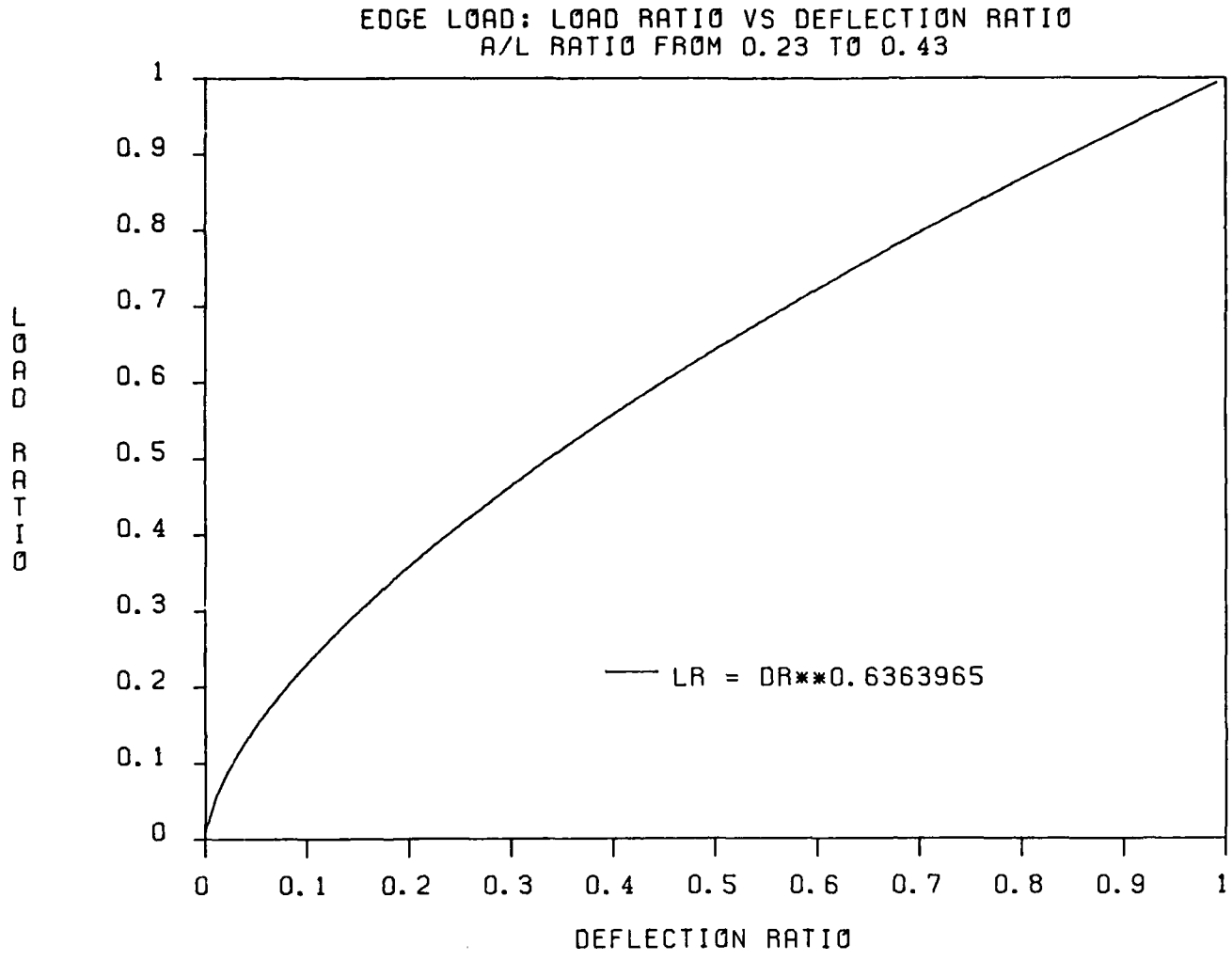

Figure 4-10. Normalized Ultimate Edge Load-Deflection Curve, a/l 0.25 to 0.43 (Ultimate Load Data Base, Appendix D)

TABLE 4-1. COMPARISON OF STRESS COMPUTED BY WESTERGAARD'S EQUATIONS AND ILLI-PAVE FOR F-4 LOAD (27 KIPS, 265 PSI)

t_{sm} (in.)	E_{sm} (ksi)	E_{ri}[1] (ksi)	k (psi/in.)	Interior Flexural Stress Bottom of Slab		Ratio of Stress West. / ILLI-PAVE
				ILLI-PAVE (psi)	West. (psi)	
9	200	3.02	100	250	331	1.33
9	500	3.02	100	281	373	1.33
9	1,000	3.02	100	305	405	1.32
9	2,000	3.02	100	324	436	1.35
9	200	7.68	150	214	313	1.46
9	500	7.68	150	258	355	1.38
9	1,000	7.68	150	287	386	1.35
9	2,000	7.68	150	311	418	1.35
15	200	3.02	100	97	144	1.48
15	500	3.02	100	108	160	1.48
15	1,000	3.02	100	115	171	1.49
15	2,000	3.02	100	119	182	1.53
15	200	7.68	150	87	138	1.58
15	500	7.68	150	102	153	1.50
15	1,000	7.68	150	111	165	1.48
15	2,000	7.68	150	116	176	1.52

Mean of 9 and 15 inch t_{sm} at k = 100 psi/in. is 1.41.

Mean of 9 and 15 inch t_{sm} at k = 150 psi/in. is 1.45.

(1) Standard subgrade models.

TABLE 4-2. LOAD AT PREDICTED STRESS RATIO OF 1.0 USING WESTERGAARD'S EQUATIONS (APPENDIX D)

Reference	Test Number	Ratios: $P_{SR=1.0}$ / $P_{ult\ load}$	Ratios: $\Delta_{SR=1.0}$ / $\Delta_{ult\ load}$
		Interior Load	
k = 50 to 150 psi/in, a = 3.5 in, h = 4.5 to 12 in.			
1	1	0.13	0.01
1	2	0.20	0.06
1	3	0.17	0.03
1	4	0.20	0.03
1	7	0.11	0.03
1	8	0.10	0.03
2	I-1	0.14	0.03
2	I-2	0.26	0.09
2	I-3	0.22	0.08
2	I-4	0.31	0.13
2	II-1	0.12	0.09
2	II-2	0.14	0.07
2	II-3	0.11	0.05
2	II-4	0.13	0.06
3	1	0.10	0.02
3	3	0.15	0.02
3	5	0.16	0.03
		Interior Load	
k = 450 psi/in, a = 3.5 in, h = 6 to 12 in.			
3	2	0.05	0.02
3	4	0.12	0.02
3	6	0.15	0.04
	Mean =	0.154	0.061
	Standard Deviation =	0.060	0.035
	Coef. of Variation =	39%	57%

TABLE 4-2. (CONTINUED)

Reference	Test Number	Ratios: $P_{SR=1.0}$ / $P_{ult\ load}$	Ratios: $\Delta_{SR=1.0}$ / $\Delta_{ult\ load}$
		Edge Load	
k = 126 to 140 psi/in, a = 3.5 in, h = 4 and 5.5 in.			
2	I-5	0.16	0.095
2	I-6	0.13	0.044
2	I-7A	0.18	0.046
2	I-7B	0.19	0.047
2	I-9	0.36	0.238
2	I-10	0.23	0.036
2	I-11	0.22	0.075
2	I-12	0.11	0.027
2	II-6	0.12	0.054
2	II-7	0.08	0.030
2	II-8A	0.14	0.090
2	II-9	0.12	0.283
2	II-10	0.19	0.103
2	II-11	0.13	0.057
2	II-12	0.20	0.126
	Mean =	0.171	0.090
	Standard Deviation =	0.068	0.075
	Coef. of Varoation =	40%	84%

References:

1. Barenberg and Alhberg, Pozzolanic Pavements, Bulletin 473, EES, University of Illinois, 1975.

2. Barenberg, Evaluating Stabilized Materials, NCHRP No. 63-45-1, EES, University of Illinois, 1967.

3. Suddath and Thompson, Load-Deflection Behavior of Lime-Stabilized Layers, TR-M-118, CERL, 1975.

stress dependent model is not currently available. The results of this analysis are:

> For an interior load condition, the load that produces a predicted SR = 1.0 is approximately 22 percent of the field collapse load.
>
> For free edge load condition, the load that produces a predicted SR = 1.0 is approximately 17 percent of the field collapse load.

If the collapse load is applied to a pavement, structural and functional failure occur on the first pass. The predicted stress ratio at the ultimate interior collapse load is estimated to be 4.54 (1.0/0.22). Loads less than the collapse load will require more than one pass to produce functional and structural failure. The ability of the stabilized material layer to sustain a limited number of load passes that produce a first pass predicted SR of one or greater is termed "reserve performance capability." This reserve performance capability enables highly overstressed pavements to provide acceptable performance for a limited number of passes.

Barenberg (References 36, 39) found good correlation between predicted and actual number ot load applications to failure using Meyerhof's theory for the failure load and fatigue properties of pozzolanic materials. A transfer function was developed using the ultimate load ratio defined by:

ultimate load ratio = applied load/static load to failure. (4-7)

Static load to failure is estimated using Meyerhof's ultimate edge collapse load. Barenberg states that if the predicted ultimate edge load of the stabilized base layer is from 1.5 to 2.0 times the applied wheel load, the pozzolanic pavements are likely to give good performance. Although good correlation was obtained for pozzolanic pavements, Barenberg felt the ultimate load approach was even more applicable for use with materials which attain a major portion of their strength at an early age such as soil-cement and lean concretes (Reference 39).

CHAPTER 5

RESPONSE AND PERFORMANCE OF TWO-LAYER PAVEMENT ITEMS

A. PERFORMANCE

1. General Item Performance

Items 1 through 8 and 11 are two-layer pavements with a rigid CAM surface layer providing slab type load carrying capability. The nominal one inch asphalt concrete wearing course on item 11 is too thin to provide any significant added structural capability so item 11 is also considered a two-layer pavement. A brief summary of the performance of the two-layer pavement items during F-4 load cart trafficking is presented below. Appendix A contains the LVDT pass deflection and permanent deformation data at the item center. The LVDT gage was installed at the surface of the subgrade in items 1 through 8 and at the surface of the asphalt concrete in item 11. Transverse and longitudinal cracks in the vicinity of the item center affect the magnitude of the LVDT deflections. FWD deflection data and longitudinal surface profiles are also included in Appendix A. Appendix B contains the crack survey data.

Item 1 (nominal 12 inches of 5 percent cement stabilized SP-SC, item center at station 0+15). Two transverse cracks, one at station 0+16 (only 1 foot from the item center) and the other at station 0+20.5, were noted at 30 passes. Item center LVDT pass deflection began at over 100 mils and increased rapidly after 30 passes. Item center permanent deformation

accumulated rapidly with 700 mils recorded at only 40 passes. Structural failure occurred at 48 passes by the load cart punching through the CAM layer into the subgrade at the transverse crack at station 0+16. The shoulders of the rut were much higher than the surrounding slab surface indicating subgrade shear failure.

Item 2 (nominal 12 inches of 5 percent cement stabilized SP-SC, item center at station 0+50). A transverse shrinkage crack was noted prior to traffic at station 0+47 (3 feet from the item center). Longitudinal cracks at the edge of the traffic lane for the full length of the item were noted at 30 passes. A transverse crack at station 0+59.5 was noted at 60 passes. Extensive ladder cracking the entire length of the item in the traffic lane was noted at 500 passes. Structural failure occurred at 663 passes by the load cart punching through the CAM layer into the subgrade. Failure occurred at the transverse crack, station 0+59.5. The shoulders of the ruts were much higher than the surrounding slab indicating a subgrade shear failure. Item center LVDT pass deflection increased steadily from an initial 40 mils to 130 mils at 500 passes and increased to 180 mils at 650 passes. Item center permanent deformation accumulated steadily to 140 mils at 500 passes and then increased sharply to 232 mils at 649 passes. FWD 15 kip DO deflections at station 0+57.5 increased from

22.3 mils before traffic to 93 mils at 500 passes. The FWD 15 kip deflection basin area decreased from 20.0 inches to 14.0 inches for the same period.

Item 3 (nominal 16 inches of 5 percent cement stabilized SP-SC, item center at station 0+85). A transverse shrinkage crack was noted prior to traffic at station 0+84 (1 foot from the item center). Two additional transverse cracks at stations 0+76.3 and 0+92 were noted at 30 passes. Longitudinal cracks along the edge of the traffic lane at the south end of the item were noted at 500 passes and by 750 passes these extended the entire length of the item. Minor spalling of the transverse crack at station 0+84 was noted at 1000 passes. Structural failure did not occur prior to the 1000 pass test limit. Ruts approximately 1 inch deep were noted in the traffic lane and in the load cart drive wheel lanes at 1000 passes. The ruts appeared to be caused by tire abrasion of the surface material. Item center LVDT pass deflection increased slightly throughout the traffic period from an initial 26 mils to 54 mils. Item center permanent deformation accumulated quickly to 25 mils at 175 passes and then increased at an average rate of only 2.5 mils per 100 passes. FWD 15 kip D0 deflection at the item center increased slowly from 18 mils prior to traffic to 39 mils at 1000 passes. The FWD 15 kip deflection basin area decreased from an initial 24.7 inches to 18.0 inches at 1000 passes.

Item 4 (nominal 8 inches of 7 percent cement stabilized SP-SC, item center at station 1+35). Extensive block cracking 2 feet each side of the item centerline greatly affected item performance. The FWD 15 kip D0 deflection at the item center prior to traffic was over 100 mils. The first pass item center LVDT pass deflection was over 750 mils. Over 900 mils of item center permanent deformation was recorded by the LVDT gauge at only 5 passes. Structural failure occurred at 6 passes near the item center by the load cart punching through the CAM layer into the subgrade. The shoulders of the ruts were much higher than the surrounding slab indicating a subgrade shear failure.

Item 5 (nominal 12 inches of 7 percent cement stabilized SP-SC, item center at station 1+70). A transverse shrinkage crack was noted prior to traffic at the extreme north edge of the item, station 1+85. Longitudinal cracks along the centerline of the item were also noted prior to traffic. Extensive ladder cracking in the traffic lane at the northern end of the item was noted at 30 passes. Structural failure occurred at 127 passes at station 1+79 by the load cart punching through the CAM layer into the subgrade. The shoulders of the ruts were much higher than the surrounding slab indicating a subgrade shear failure. Item center LVDT pass deflection increased slowly from an initial 60 mils to 110 mils at 100 passes then increased rapidly to 170 mils at

126 passes. Item center permanent deformation increased steadily to 154 mils at 99 passes then rapidly increased to 249 mils at 129 passes. FWD 15 kip D0 deflection at station 1+77.5 increased from 27.9 mils prior to traffic to 71 mils at 48 passes. The FWD 15 kip deflection basin area decreased from an initial 19.2 inches to 15.4 inches over the same period.

Item 6 (nominal 16 inches of 7 percent cement stabilized SP-SC, item center at station 2+05). A transverse shrinkage crack was noted prior to traffic at station 2+09.5 (4.5 feet from the item center). An additional transverse crack was noted at station 1+96 at 30 passes. A crescent shaped crack was noted near the centerline at station 2+12 at 150 passes. No additional major cracks occurred in the test item. Structural failure did not occur prior to the 1000 pass test limit. Ruts approximately one-quarter to one-eight of an inch deep in the traffic lane were noted at 1000 passes. The ruts appeared to be caused by tire abrasion of the surface material. Item center LVDT pass deflection increased slowly from an initial 14 mils to 27 mils at 1000 passes. Item center permanent deformation accumulated steadily to 34 mils at 1000 passes. FWD 15 kip D0 deflection at station 2+12.5 increased from 8 mils prior to traffic to 23 mils at 1000 passes. FWD 15 kip deflection basin area decreased from 30.7 to 25.4 inches over the traffic period. FWD 15 kip D0

deflection at 1000 passes for the three test locations ranged from 16.7 to 23.0 mils.

Item 7 (nominal 8 inches of 9 percent cement stabilized SP-SC, item center at station 0+15). Two transverse shrinkage cracks were noted prior to traffic at stations 0+6.8 and 0+27.5. Longitudinal cracks along the edges of the traffic lane were also noted prior to traffic. Extensive block cracking in the traffic lane for the entire length of the item was noted at 30 passes. Structural failure occurred at 82 passes at the transverse crack at station 0+6.8 by the load cart punching through the CAM layer into the subgrade. The shoulders of the ruts were higher than the surrounding slab indicating a subgrade shear failure. Item center LVDT pass deflection increased steadily from an initial 77 mils to 155 mils at 66 passes then increased rapidly to 235 mils at 76 passes. Item center permanent deformation increased steadily to 156 mils at 65 passes then rapidly increased to 337 mils at 80 passes. The FWD 15 kip D0 deflection at station 0+7.5 increased from 33 mils prior to traffic to 74 mils at 48 passes. The FWD 15 kip deflection basin area decreased from 17.3 to 12.9 inches over the same period.

Item 8 (nominal 12 inches of 9 percent cement stabilized SP-SC, item center at station 0+50). Longitudinal cracks along the item centerline were noted prior to traffic but no

transverse shrinkage cracks were noted. Additional longitudinal cracks at the edge of the traffic lane were noted at 48, 150, and 500 passes. Ladder cracking in the traffic lane near station 0+40 was noted at 500 passes. Structural failure occurred at 550 passes near station 0+42 by the load cart punching through the CAM layer into the subgrade. The shoulder of the ruts were much higher than the surrounding slab indicating a subgrade shear failure. Item center LVDT pass deflection increased steadily from 45 mils to 120 mils at 550 passes. Item center permanent deformation accumulated steadily to 129 mils at 540 passes. FWD 15 kip D0 deflection at station 0+42.5 increased from 21 mils prior to traffic to 87 mils at 500 passes. The FWD deflection basin area decreased from 23.3 to 10.1 inches over the same period.

Item 11 (nominal 12 inches of 5 percent cement stabilized SP-SC with a nominal 1 inch asphalt concrete wearing course, item center at station 1+70). Longitudinal cracks in the asphalt concrete 2 feet west of the item centerline were noted prior to traffic. At 341 passes longitudinal cracks at the edges of the traffic lane at the north end of the item, station 1+85, were noted. At 500 passes these longitudinal cracks had extended down the traffic lane to station 1+77.5. A one-quarter to one-half inch deep rut in the traffic lane was also noted at 500 passes. The rut had deepened to 2.5 inches at station 1+77.5 at 663 passes with extensive ladder

cracking in the traffic lane extending from the item center to the north edge of the item. Traffic was stopped at 636 passes to prevent the load cart from punching through into the subgrade. The shoulder of the ruts was much higher than the surrounding slab indicating a subgrade shear failure. Item center LVDT pass deflection taken at the surface of the item was steady at approximately 180 mils over the 636 passes. Item center permanent deformation accumulated steadily to 583 mils at 209 passes then increased rapidly to 874 mils at 249 passes when the gauge failed. FWD 15 kip D0 deflection at station 1+77.5 increased from 27 mils prior to traffic to 67 mils at 500 passes. FWD 15 kip deflection basin area decreased from 20.6 inches to 14.5 inches over the same period.

2. Phases of Item Performance

Test item cracking and deflection measurements indicate performance of the two-layer items can be divided into three general phases (Figure 5-1).

Phase I begins with the initial condition of the pavement and ends with the development of load related longitudinal cracking along the edges of the traffic lane. These cracks usually started at a transverse crack and propagated away from the transverse crack. Some of the items exhibited

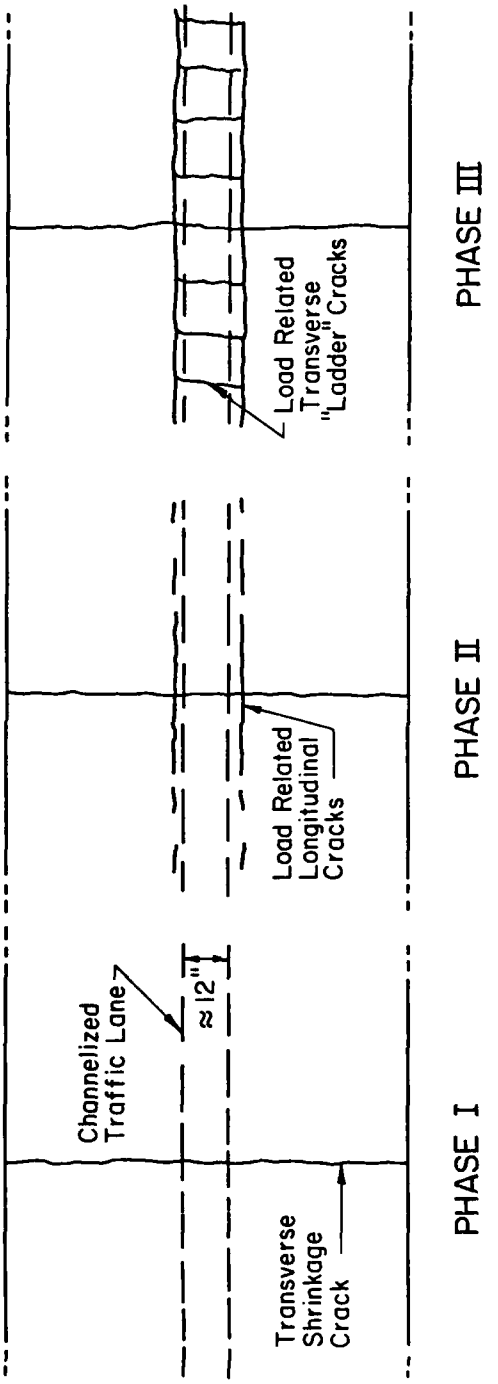

Figure 5-1. Phases of Performance, Two-Layer Pavement Items

longitudinal construction cracks associated with compacting the CAM layers on the soft subgrade.

Phase II includes continued lengthening and "working" of the load related longitudinal cracks.

Phase III begins with the development of transverse ladder cracks in the traffic lane and ends with the load cart punching through the CAM layer into the subgrade.

The type of cracking observed in the CAP field test was also noted in cement stabilized pavements subjected to channelized traffic described in Reference 40.

The type and severity of cracking influences traffic lane surface deflections (Figure 5-2). During Phase I, pass deflection is relatively constant and permanent deformation accumulates slowly. During Phase II pass deflection begins to slowly increase with each pass but in Phase III it increases dramatically until failure occurs. Cumulative permanent deformation continues to increase during Phase II and large increases occur during Phase III.

The number of passes in each phase for the two-layer pavement test items is shown in Figure 5-3. Pass levels denoting the division between phases are subjective. There was no abrupt change between phases, but rather a transition. The pass levels were selected as convenient dividing points after carefully considering the cracking and

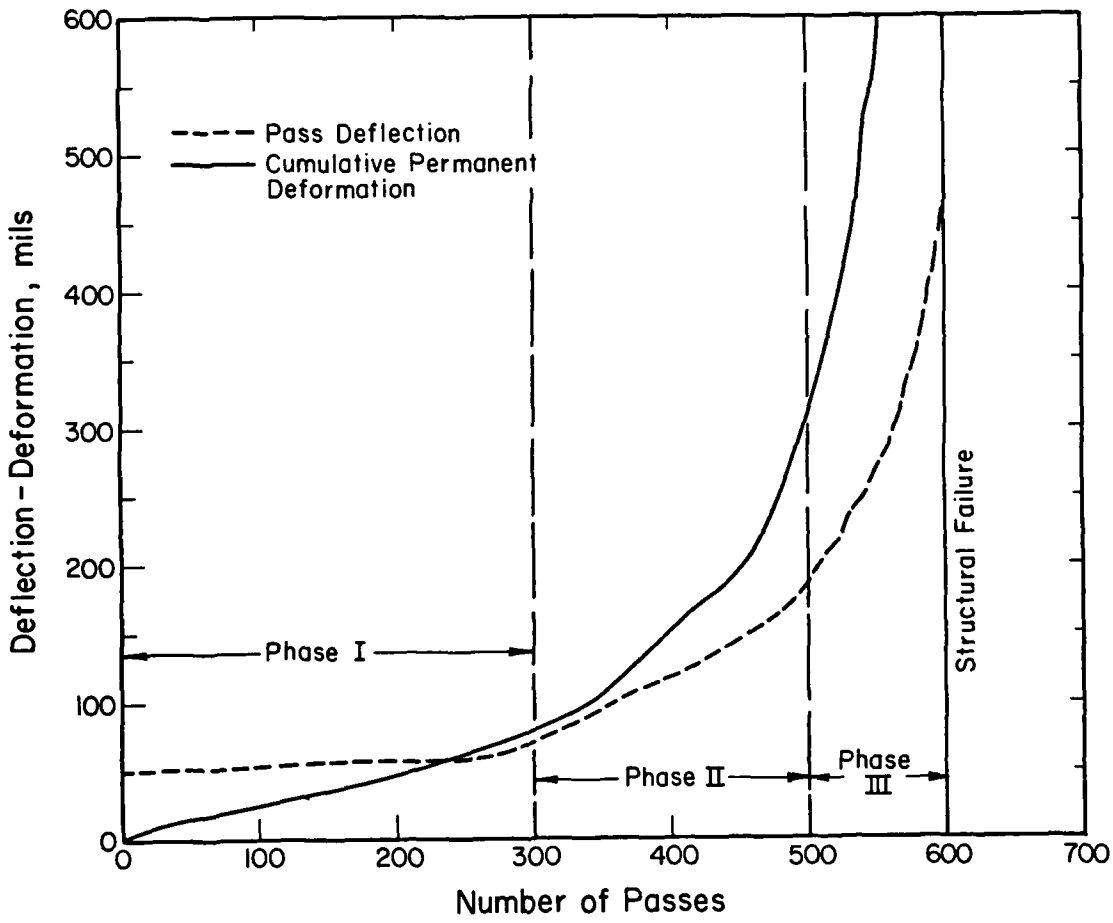

Figure 5-2. Typical Pass Deflection and Cumulative Permanent Deformation, Two-Layer Pavement Items

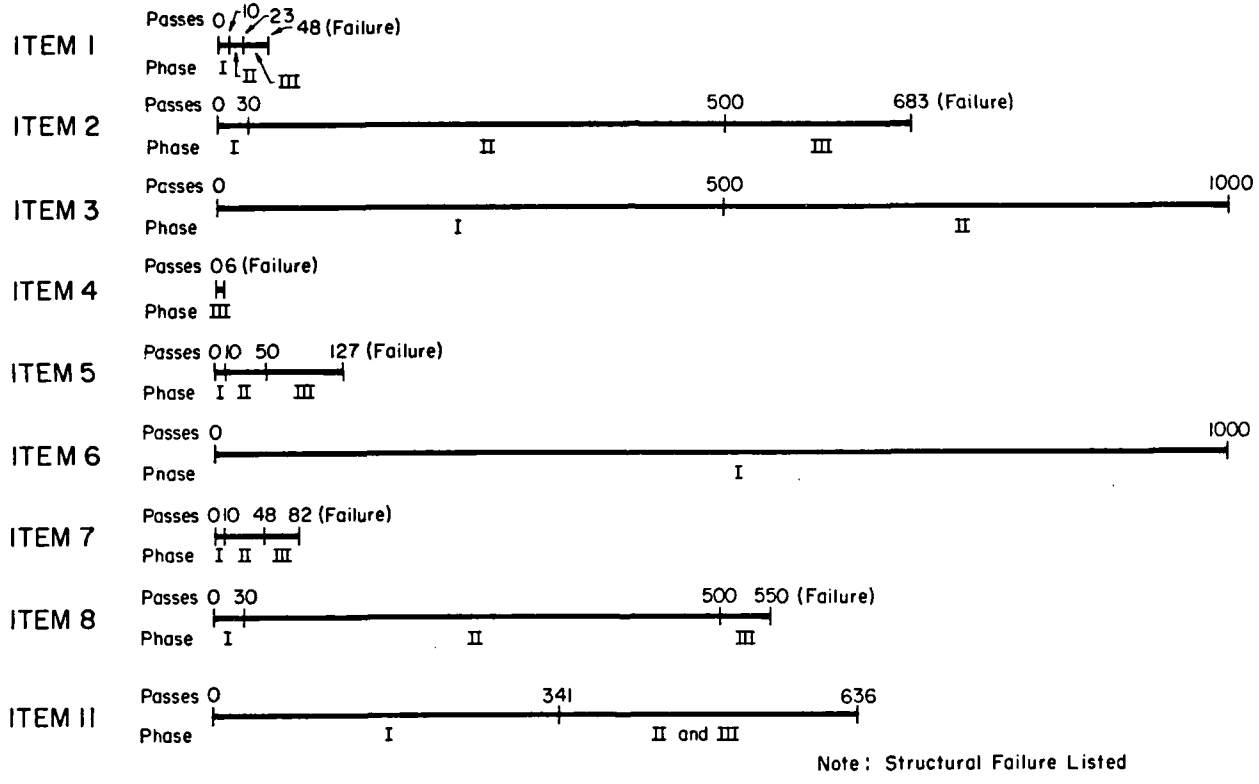

Figure 5-3. Pass Levels Denoting Divisions Between Phases of Performance, Two-Layer Pavement Items

deflection data. Detailed discussion of crack development and deflections is presented in Chapter 7.

3. Passes to Functional Failure

Extensive research has been conducted (References 41, 42, 43, 44) on aircraft-pavement interaction. Attempts have been made to characterize and define the limits of surface roughness producing functional failure in various aircraft. It is beyond the scope of this study to determine when the item surface roughness reached the F-4 functional failure level. Recent field and model studies on the response of the F-4 to various forms of surface roughness indicate the need for a relatively smooth surface (Reference 45). This "general smoothness criteria" served as a guideline in estimating the passes to functional failure.

Pass levels to functional failure for the two-layer test items are listed in Table 5-1. These were determined from an intensive review of the LVDT deflection data, longitudinal and transverse profiles, and surface cracking data.

B. FIRST PASS INTERIOR LOAD STRUCTURAL RESPONSE

The ILLI-PAVE program was used to determine the predicted first pass structural response for an F-4 interior load of 27 kips and 265 psi tire pressure (Table 5-2). Figure 5-4 shows the ILLI-PAVE structural model used in the analysis of items 1 through 8 and 11. The material characteristics for each layer are listed in Table 3-8.

TABLE 5-1. F-4 PASSES TO FUNCTIONAL FAILURE AND STRUCTURAL FAILURE, TWO-LAYER PAVEMENT ITEMS

Item	Description	Failure Location	Passes To: Functional Failure	Passes To: Structural Failure
1	8.4 in. CAM (5% cement)	0+16	30	48
2	12.4 in. CAM (5% cement)	0+59	500	650
3	16.6 in. CAM (5% cement)	0+84(1)	1000	1000+
4	7.6 in. CAM (7% cement)	1+35	1	6
5	10.9 in. CAM (7% cement)	1+77.5	110	127
6	16.6 in. CAM (7% cement)	2+09.5(1)	1000+	1000+
7	8.0 in. CAM (9% cement)	0+06.8	65	82
8	10.7 in. CAM (9% cement)	0+42.5	520	550
11	1.5 in. Asphalt Concrete 10.0 in. CAM (5% cement)	1+77.5	500	636

(1) Probable failure location if trafficked beyond 1000 passes.

TABLE 5-2. ILLI-PAVE STRUCTURAL RESPONSE TO INTERIOR F-4 LOAD (27 KIPS, 265 PSI), ITEMS 1 THROUGH 8 AND 11

Information and Structural Response	Item 1	2	3	4	5	6	7	8	11
Station	0+16	0+59	0+84	1+35	1+77	2+09	0+07	0+42	1+77
Stabilized Material									
Thickness, inches	8.4	12.4	16.6	7.6	10.9	16.6	8.0	10.7	10.0
Modulus, ksi	300	400	1000	25	400	1200	400	400	300
Surface Deflection Basin									
D0 at R = 0 inches, mils	52.05	30.97	16.91	202	34.95	15.99	47.44	35.58	33.19
D1 at R = 12 inches, mils	35.77	22.88	14.27	67.8	25.72	13.78	33.79	26.16	24.45
D2 at R = 24 inches, mils	22.89	17.30	12.81	24.6	18.69	12.55	22.21	18.89	18.02
D3 at R = 36 inches, mils	13.95	12.92	11.62	9.8	13.27	11.54	13.94	13.32	13.11
Area, inches	21.13	24.06	29.34	11.78	23.52	30.09	21.93	23.44	23.73
Stabilized Material (Bottom of Layer)									
Radial Tensile Stress, psi	258	148	95	130	184	97	295	190	140
Radial Tensile Strain, microstrain	752	336	86	5255	422	72	689	436	427
Subgrade (Top of Layer)									
Normal Stress, psi	17.6	9.3	4.6	59.7	10.9	4.3	16.3	11.2	10.3
Shear Stress, psi	5.67	2.92	1.08	13.80	3.50	0.96	5.14	3.59	3.46
Deviator Stress, psi	11.38	5.84	2.17	27.60	6.98	1.91	10.24	7.20	6.93
Shear Stress Ratio (τ/c)	0.37	0.20	0.07	1.00	0.30	0.07	0.36	0.30	0.32

Note: Item 11 has 1.5 inch asphalt concrete wearing course at the surface (modulus of 700 ksi).

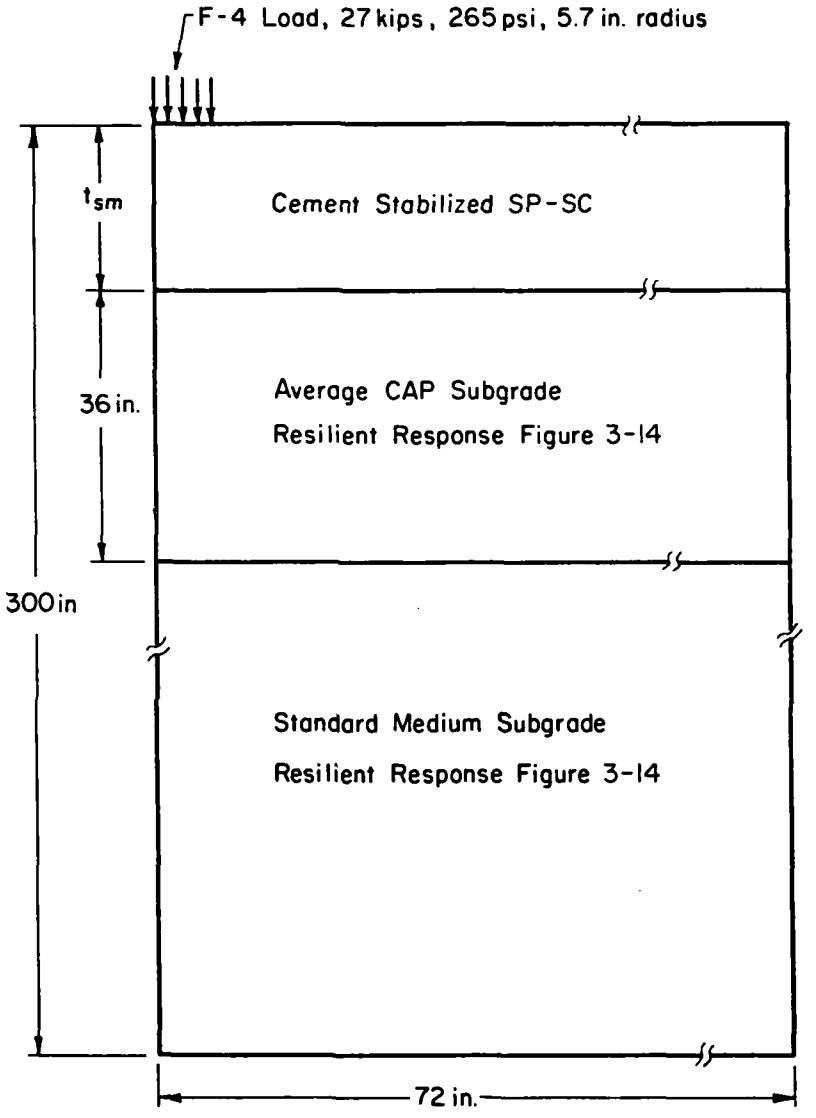

Note: Item 11 has a 1.5 inch asphalt concrete wearing course

Figure 5-4. ILLI-PAVE Model for F-4 Analysis, Two-Layer Pavement Items

C. CAM LAYER FLEXURAL (TENSILE) STRESS AND PERFORMANCE

1. Sensitivity of Stress to CAM Modulus

For a given thickness and a subgrade support condition similar to that of the two-layer CAP test items, the flexural (tensile) stress at the bottom of the CAM layer is fairly insensitive to variations in the back-calculated CAM modulus (Figure 5-5). For a medium standard subgrade, a 25 percent variation in the back-calculated CAM modulus over a thickness range of 9-15 inches only results in an average 4 percent tensile stress variation in the CAM layer.

2. CAM Stress at Transverse Crack

As discussed in Chapter 4, transverse cracks significantly increased the CAM flexural (tensile) stress. The flexural stress at a crack compared to the interior flexural stress is related to the thickness of the CAM layer and the LTE of the crack by the load placement effect factor (LPEF) in Figure 4-2. Table 5-3 lists the predicted first pass crack flexural (tensile) stress at the bottom of the CAM layer.

3. First Pass Stress Ratio and Performance

The predicted transverse crack stress ratio (tensile stress divided by flexural strength) in the CAM layer for the first pass of the F-4 is listed in Table 5-4. No transverse cracks were noted in item 8 so the interior flexural (tensile) stress was used for this item. The field flexural strength was estimated using the results of the University of Illinois strength study and field density data (Table 3-7).

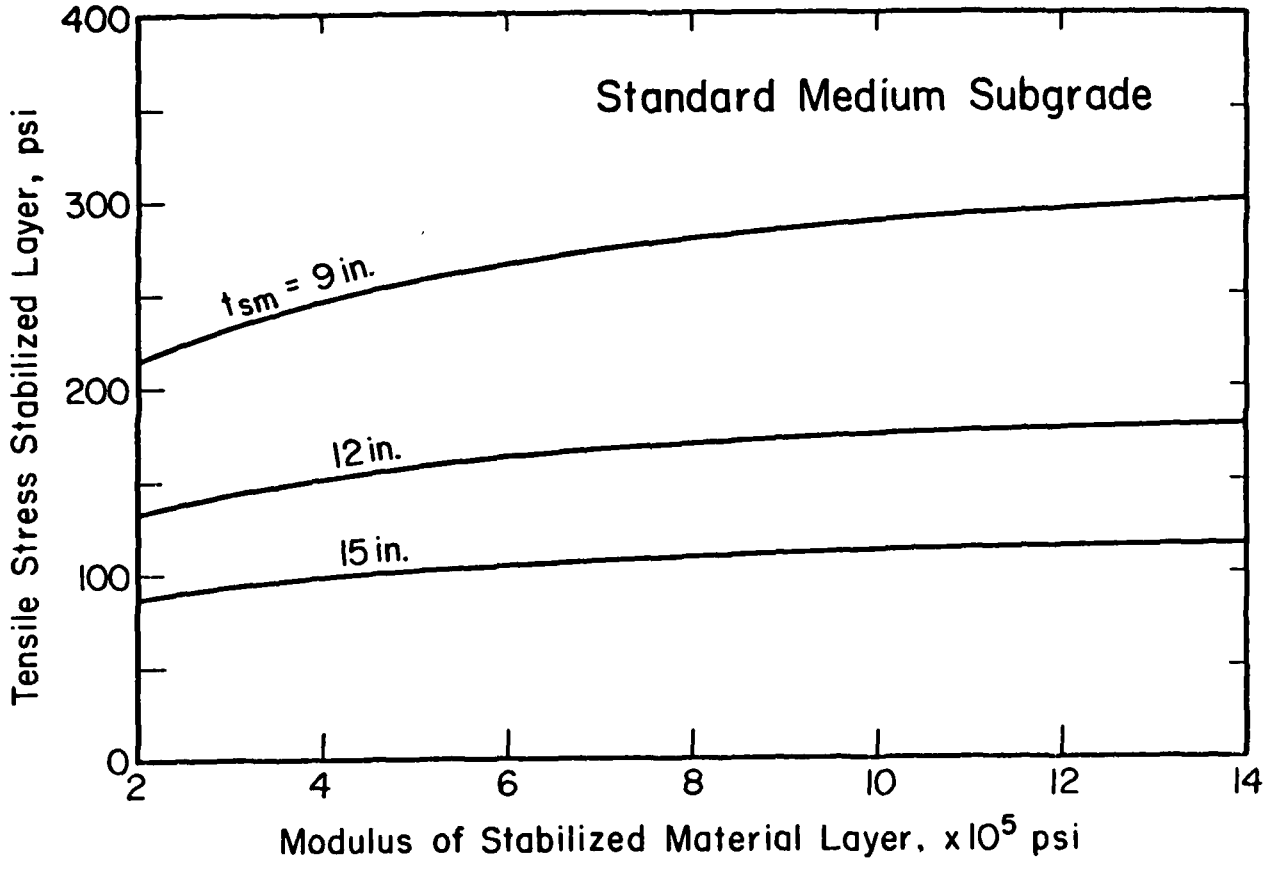

Figure 5-5. Effect of Modulus and Thickness of the Stabilized Layer on Maximum Flexural (Tensile) Stress in Stabilized Layer, Two-Layer Pavements (F-4 ILLI-PAVE Data Base, Appendix C)

TABLE 5-3. PREDICTED F-4 FIRST PASS FLEXURAL (TENSILE) STRESS BOTTOM OF STABILIZED LAYER, TWO-LAYER PAVEMENT ITEMS

Item	Thickness (in.)	ILLI-PAVE Tensile Stress Bottom of CAM Layer (psi)	First Pass[1] Crack LTE (percent)	Load Placement[2] Effect Factor	Predicted Crack Tensile Stress Bottom of Stabilized Layer (psi)
1	8.4	258	77	1.19	307
2	12.4	148	45	1.50	222
3	16.6	95	38	1.68	160
4	7.6	Subgrade Shear Failure First Pass of F-4 Load Cart			
5	10.9	184	50[3]	1.50	276
6	16.6	97	45	1.64	158
7	8.0	295	62	1.32	389
8	10.7	190	(4)	1.00	190
11	10.0	140	90[5]	1.10	154

(1) Table B-1.
(2) Figure 4-2.
(3) Estimated LTE for crack at north end of item.
(4) No transverse shrinkage crack; interior loading condition used.
(5) Estimated; no LTE FWD test conducted on item 11.

TABLE 5-4. PREDICTED F-4 FIRST PASS CRACK STRESS RATIO BOTTOM OF STABILIZED MATERIAL LAYER, TWO-LAYER PAVEMENT ITEMS

Item	Station	Predicted Crack[1] Flexural Stress Stabilized layer (psi)	Estimated Mean Flexural Strength (psi)	Predicted First Pass Stress Ratio
1	0+16	307	35	8.77
2	0+59	222	65	3.42
3	0+84	160	68	2.35
4	1+35	---	---	----
5	1+77.5	276	123	2.24
6	2+09.5	158	142	1.11
7	0+06.8	389	88	4.42
8	0+42.6	190	159	1.20
11	1+77.5	154	65	2.37

(1) Table 5-3.
(2) Table 3-7.

Nussbaum and Larsen (Reference 46) noted a 26 percent coefficient of variation (standard deviation/mean) for the flexural strength of cemented materials. Predicted stress ratios should reflect this variability. Figure 5-6 shows the range of the predicted first pass crack stress ratio in the CAM layer using a 25 percent strength variability. The passes to functional failure for the two-layer items are also shown in Figure 5-6.

D. CAM LAYER (TENSILE) STRAIN AND PERFORMANCE

1. Sensitivity of CAM Flexural (Tensile) Strain to CAM Modulus

For a given subgrade condition similar to the CAP subgrade, the flexural (tensile) strain at the bottom of the CAM layer, ϵ_{sm}, is sensitive to the back-calculated CAM modulus for the range of thickness and modulus in the CAP test items (Figure 5-7). A 25 percent variation in the back-calculated CAM modulus results in an average 20 percent variation in CAM tensile strain. This sensitivity of strain to modulus should be considered in reporting strain ratios using back-calculated CAM modulus values.

2. CAM Strain at Transverse Crack

The flexural (tensile) strain at the bottom of the CAM layer at a transverse crack is greater than for an interior load condition. Researchers have reported the increase to be from 40 percent (Reference 26) to 50 percent (Reference 47). Maree and Freeme (Reference 29) recommend a 40 percent increase for cemented materials over 200 mm (7.83 inches) thick and unconfined compressive strength greater than 326 psi.

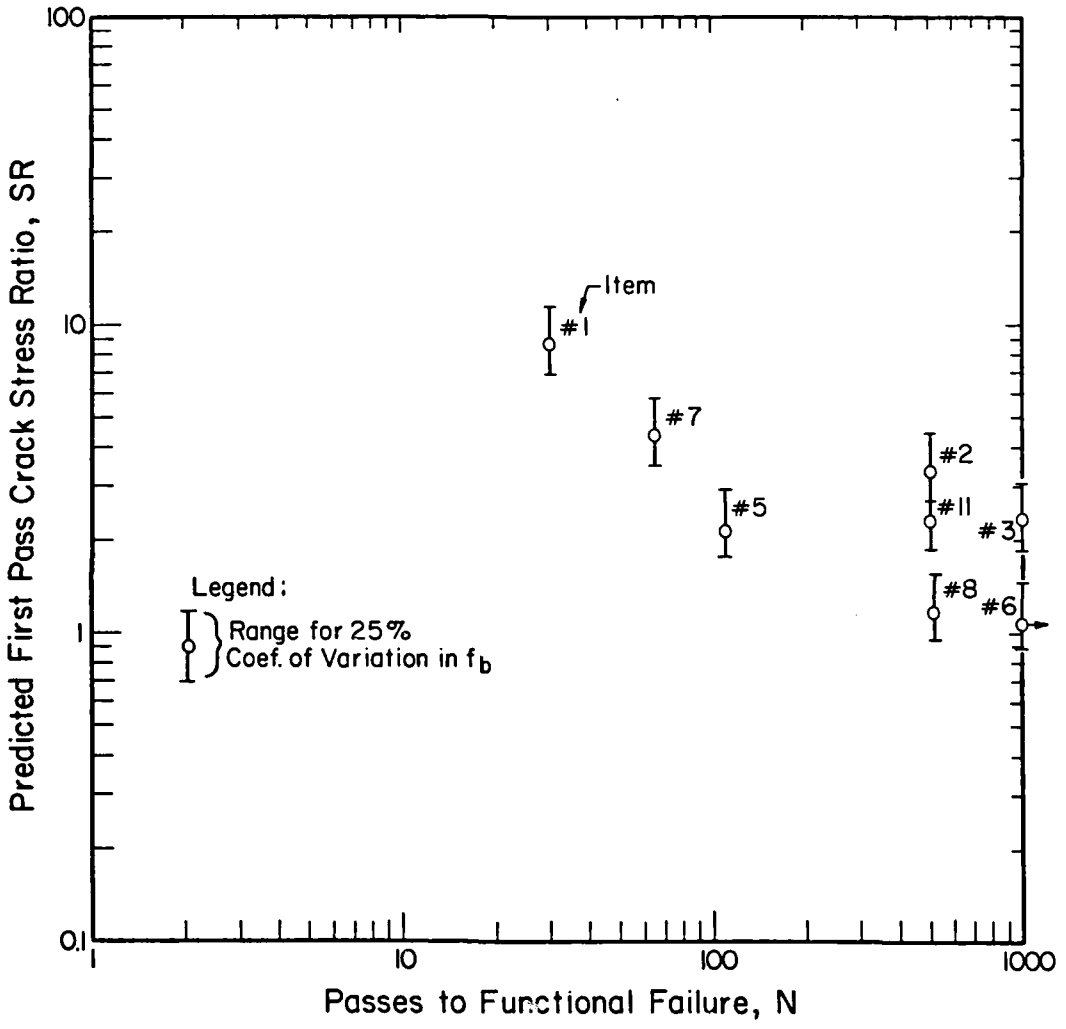

Figure 5-6. Item Performance and Predicted First Pass Crack Stress Ratio in CAM Layer, Two-Layer Pavement Items

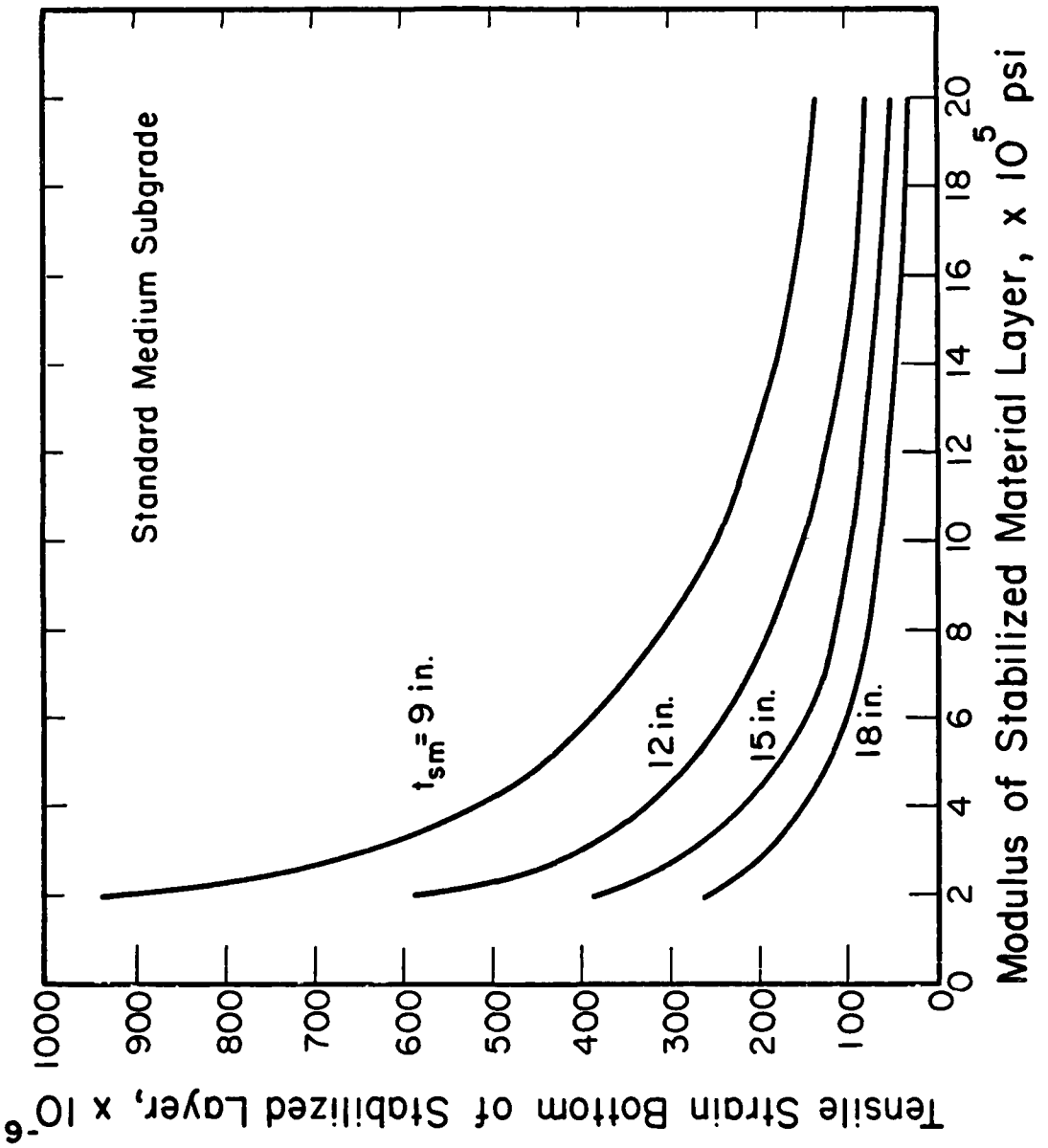

Figure 5-7. Effect of Stabilized Material Layer Modulus and Thickness on Tensile Strain in Stabilized Layer, Two-Layer Pavements (F-4 ILLI-PAVE Data Base, Appendix C)

The cement stabilized SP-SC meets this criteria so a 40 percent increase was used for the CAP test items.

3. CAM Strain Ratio and Performance

Crack strain ratio, ϵ_{sr}, is the ratio of flexural (tensile) strain at the bottom of the stabilized material layer acting parallel to the crack, ϵ_s, divided by the strain at break, ϵ_b. The strain at break was estimated at 120 microstrain using the laboratory flexural beam data developed by Maree and Freeme (Reference 29). Predicted first pass crack strain ratios in the CAM layer are shown in Figure 5-8 along with passes to functional failure. The strain used for item 8 is the interior load condition strain as no transverse cracks were noted. A 20 percent variation in strain was used to reflect the sensitivity of strain to back-calculated CAM modulus.

E. ULTIMATE LOAD AND PERFORMANCE

1. Field Ultimate Loads

The load-deflection data for the ultimate load tests on items 1, 2, 3, 5, 6, and 7 are shown in Figures 2-9 and 2-11. The presence of longitudinal and transverse cracks near the plate load invalidates the assumptions for interior or edge loads. The load-deflection data were affected by these cracks. The resulting field ultimate loads are less than interior ultimate loads and probably slightly greater than edge ultimate loads. Only items 1 and 7 failed at less than the 50 kip test limit. Item 1 had a ultimate load of 38 kips and item 7 had a ultimate load of 45 kips. A review of the load-deflection data for items 2, 3, 5, and 6 does not allow for determination of field ultimate load. The

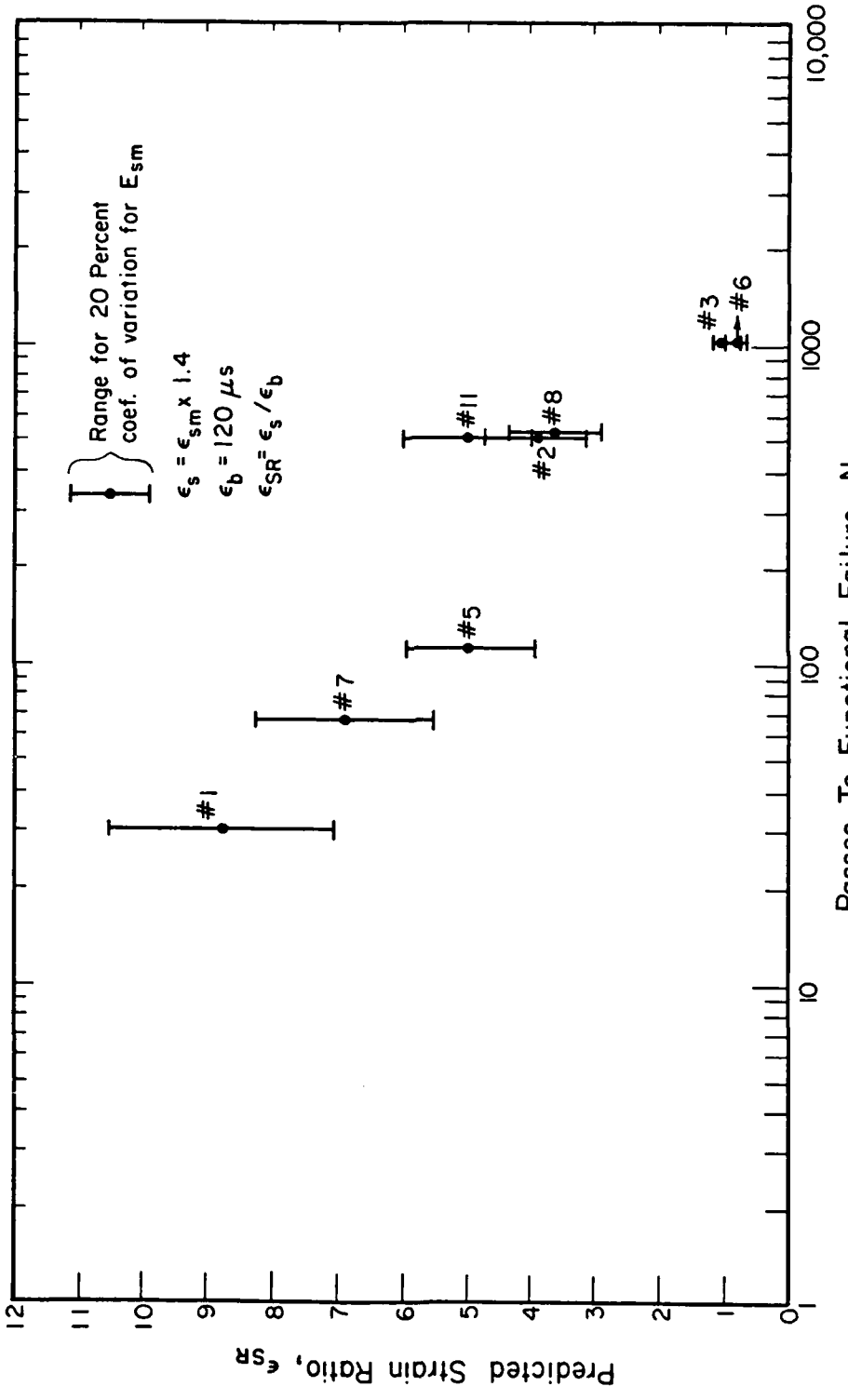

Figure 5-8. Item Performance and Predicted First Pass Stress Ratio in the CAM Layer, Two-Layer Pavement Items

only valid conclusion is that the field ultimate load for these items is greater than 50 kips.

2. Predicted Ultimate Edge Load

For a given subgrade and load radius, the Meyerhof predicted edge collapse load is sensitive to CAM layer thickness and flexural strength (Figure 5-9). A 25 percent variation in flexural strength results in a 25 percent variation in predicted edge collapse load. Figure 5-10 shows the Meyerhof predicted edge collapse load with the 25 percent variation and the passes to functional failure for the two-layer items.

F. DEFLECTION AND PERFORMANCE

1. Deflection at a Transverse Crack

When the load is tangent to a transverse crack, the maximum crack deflection occurs on the loaded slab next to the load. For a given load, the maximum crack deflection is a function of subgrade support, CAM modulus and thickness, and crack load transfer efficiency (LTE) and can be related to the interior load deflection. Figure 5-11 shows this relationship for the two-layer items. The deflection factor plotted in Figure 5-11 is defined by:

$$\text{Deflection Factor} = \Delta_{\text{loaded slab}}/\Delta_{\text{interior}} \qquad (5\text{-}1)$$

where:

$\Delta_{\text{loaded slab}}$ = maximum crack deflection for a specific LTE when the load is tangent to the crack

Δ_{interior} = maximum interior load deflection.

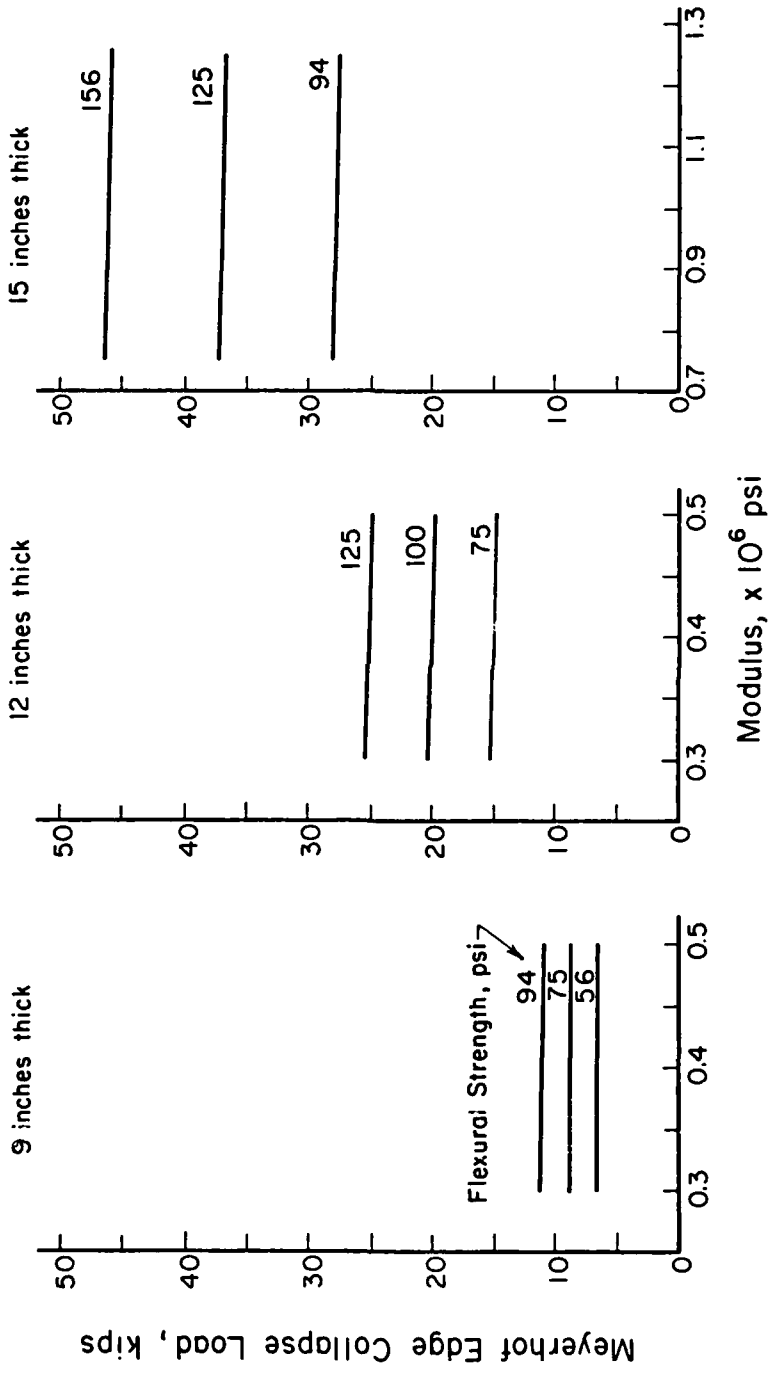

Figure 5-9. Effect of Thickness, Modulus and Strength on Meyerhof Predicted Edge Collapse Load (k = 115 psi, μ = 0.15, a = 5.7 in.)

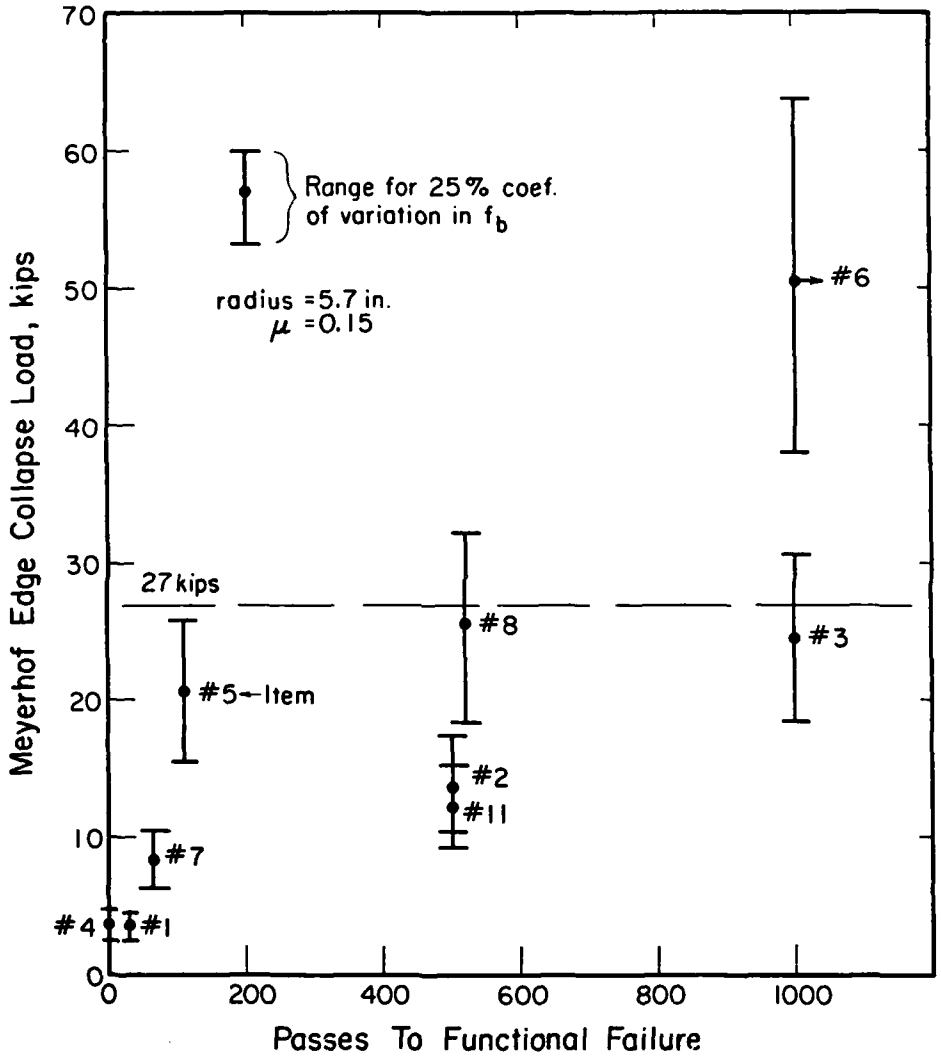

Figure 5-10. Item Performance and Meyerhof Predicted Edge Collapse Load, Two-Layer Pavement Items

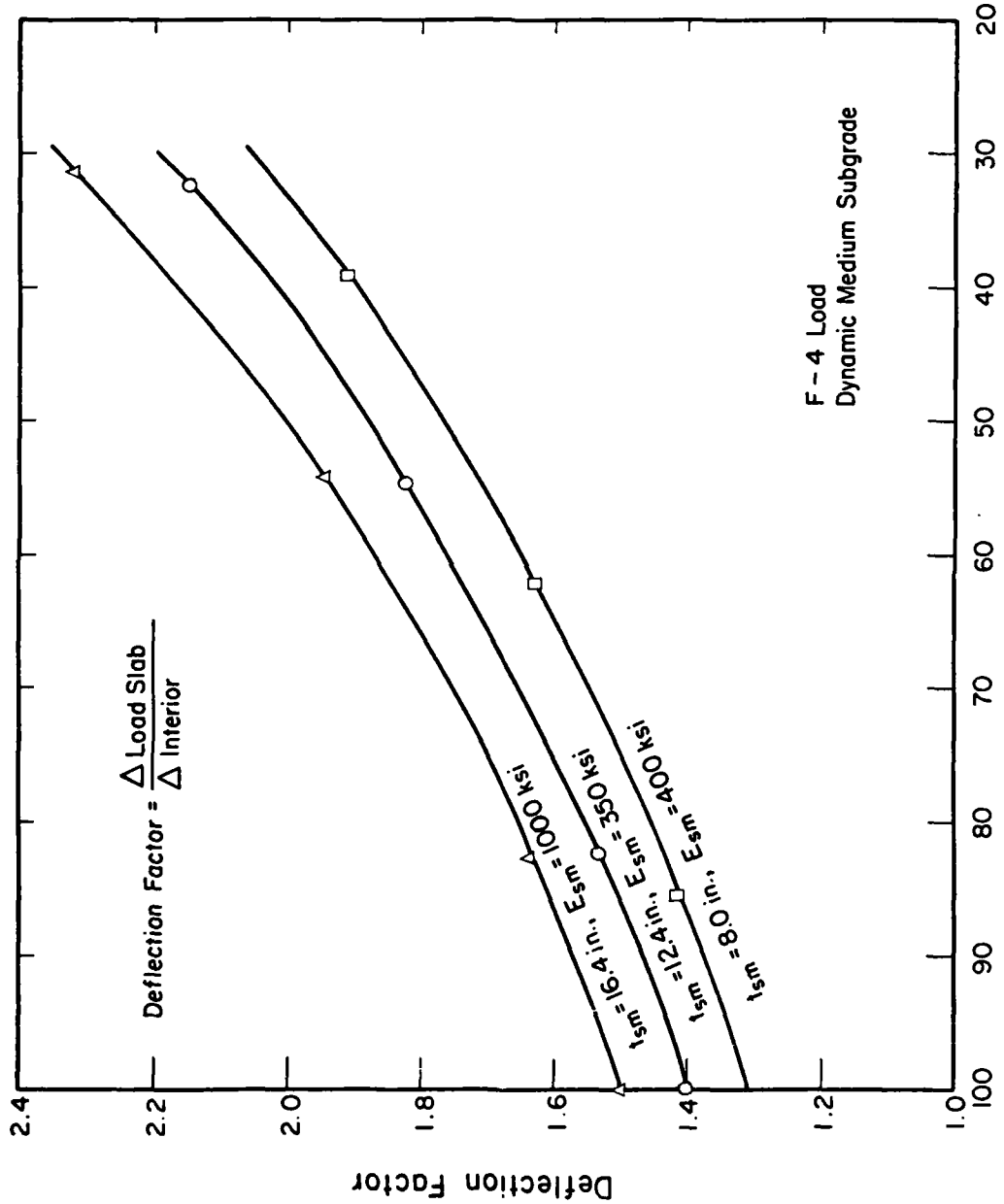

Figure 5-11. Deflection Factor for Two-Layer Pavement Items

Figure 5-11 is based on ILLI-SLAB solutions for the thickness and modulus ranges of the CAP test items and the F-4 load. This figure is only applicable for an F-4 load. Predicted first pass crack deflection can be estimated from the interior load deflection determined by ILLI-PAVE and then increased by the deflection factor in Figure 5-11 for the appropriate LTE and CAM layer thickness. Figure 5-12 shows the predicted first pass crack deflection and the passes to functional failure for the two-layer items.

2. Measured Deflections and Performance

The LVDT pass deflection and cumulative permanent deformation were measured at the item center. Transverse and longitudinal cracks near the item center affect the LVDT deflection measurements. Since the cracking was not the same in each item, quantitative comparison of these deflections as a function of pass levels cannot be made. However, comparison of these deflections for items of the same relative strength does show the qualitative effect of thickness on pass deflection and permanent deformation (Figures 5-13 through 5-18).

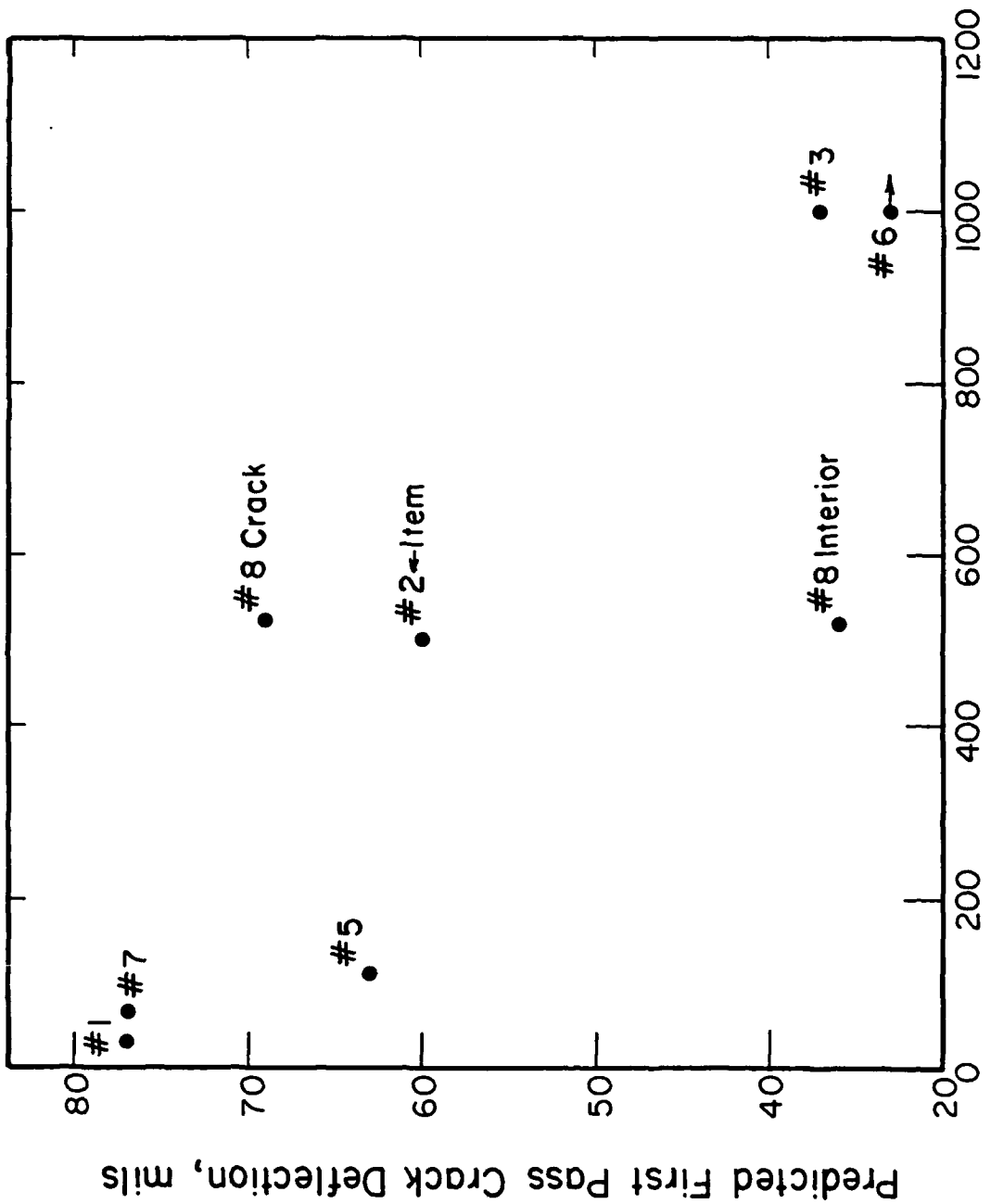

Figure 5-12. Item Performance and Predicted First Pass Crack Deflection, Two-Layer Pavement Items

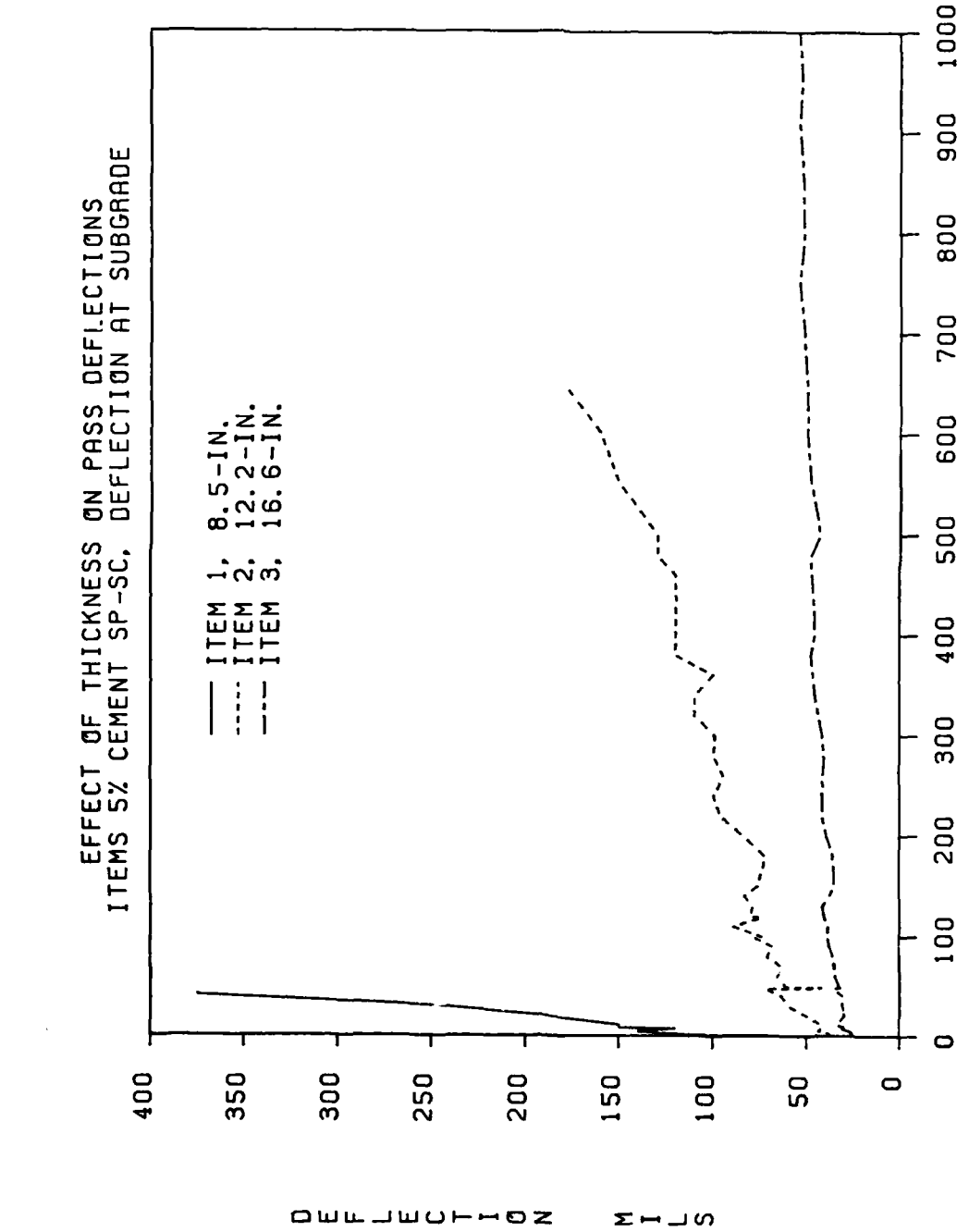

Figure 5-13. Comparison of LVDT Pass Deflection at Item Center, Items 1, 2 and 3

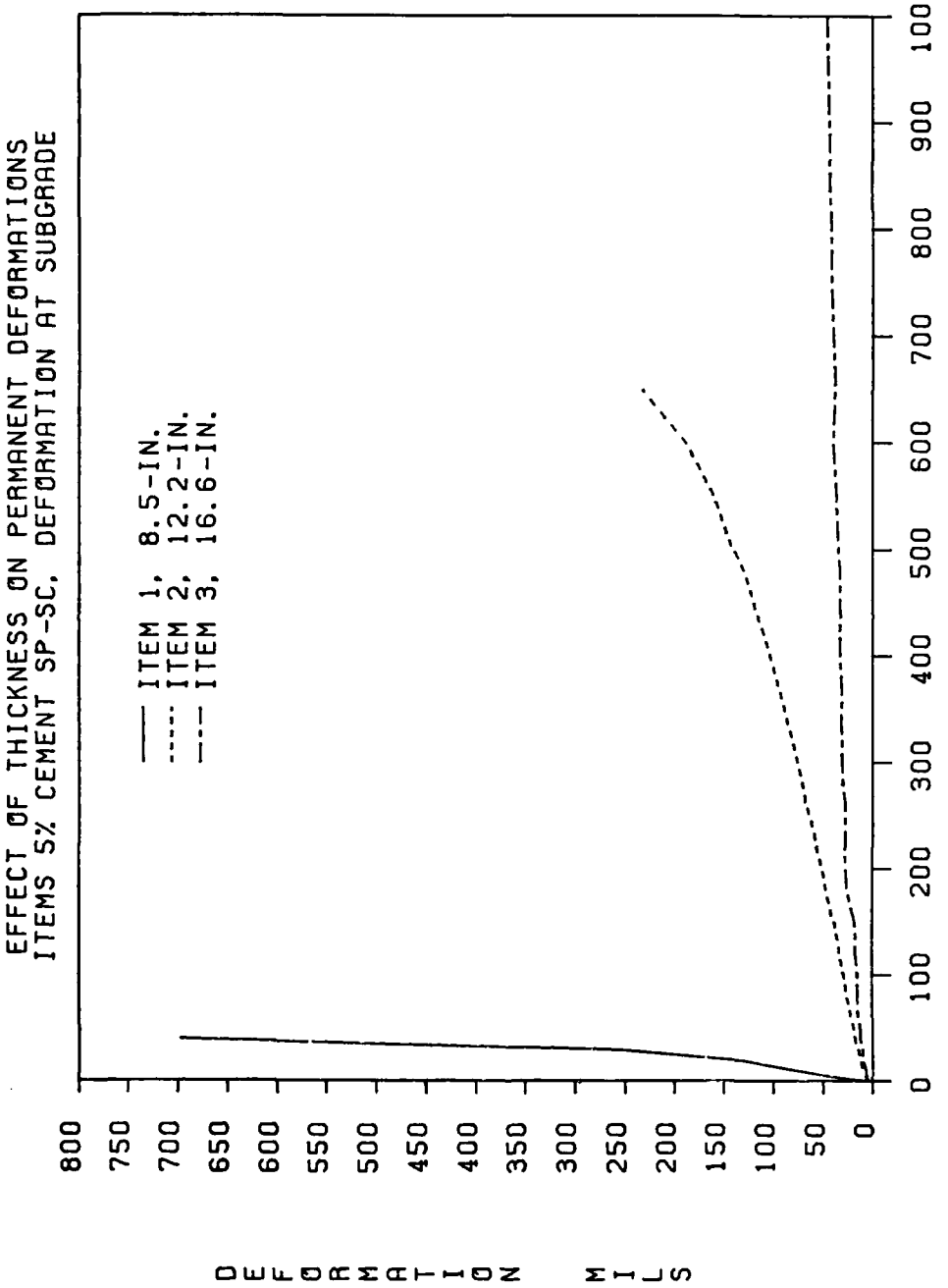

Figure 5-14. Comparison of Cumulative Permanent Deformation at Item Center, Items 1, 2 and 3

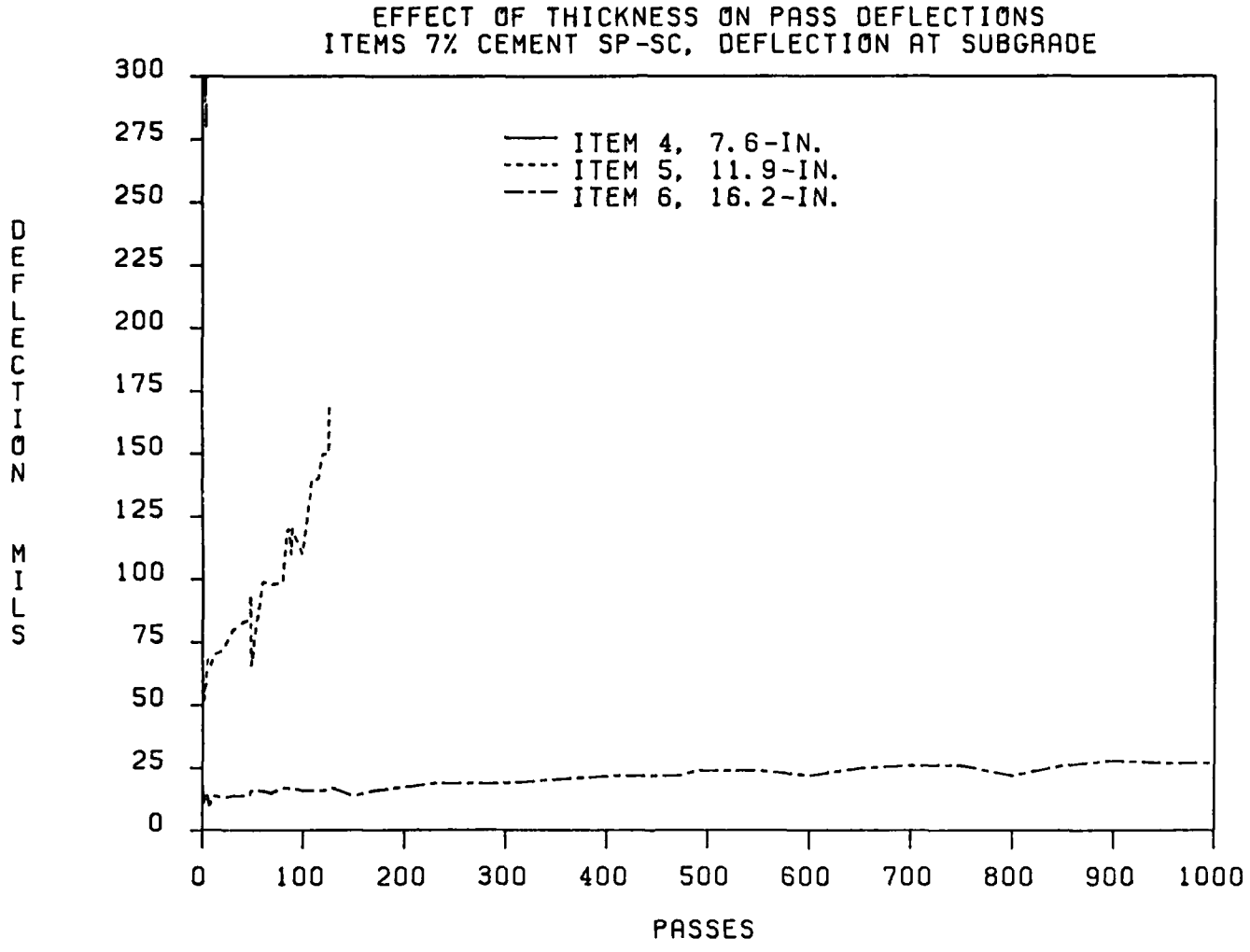

Figure 5-15. Comparison of LVDT Pass Deflection at Item Center, Items 4, 5 and 6

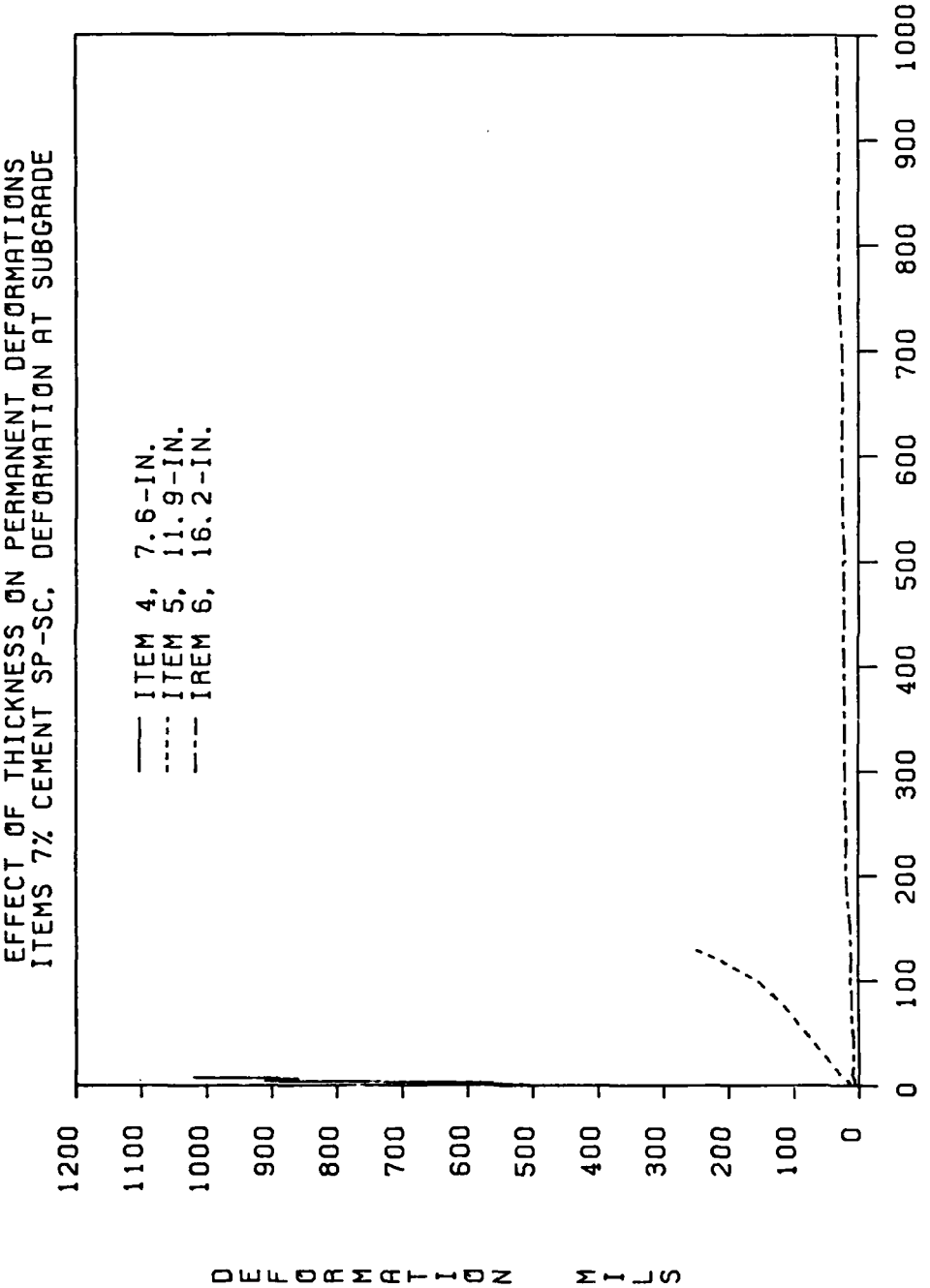

Figure 5-16. Comparison of Cumulative Permanent Deformation at Item Center, Items 4, 5 and 6

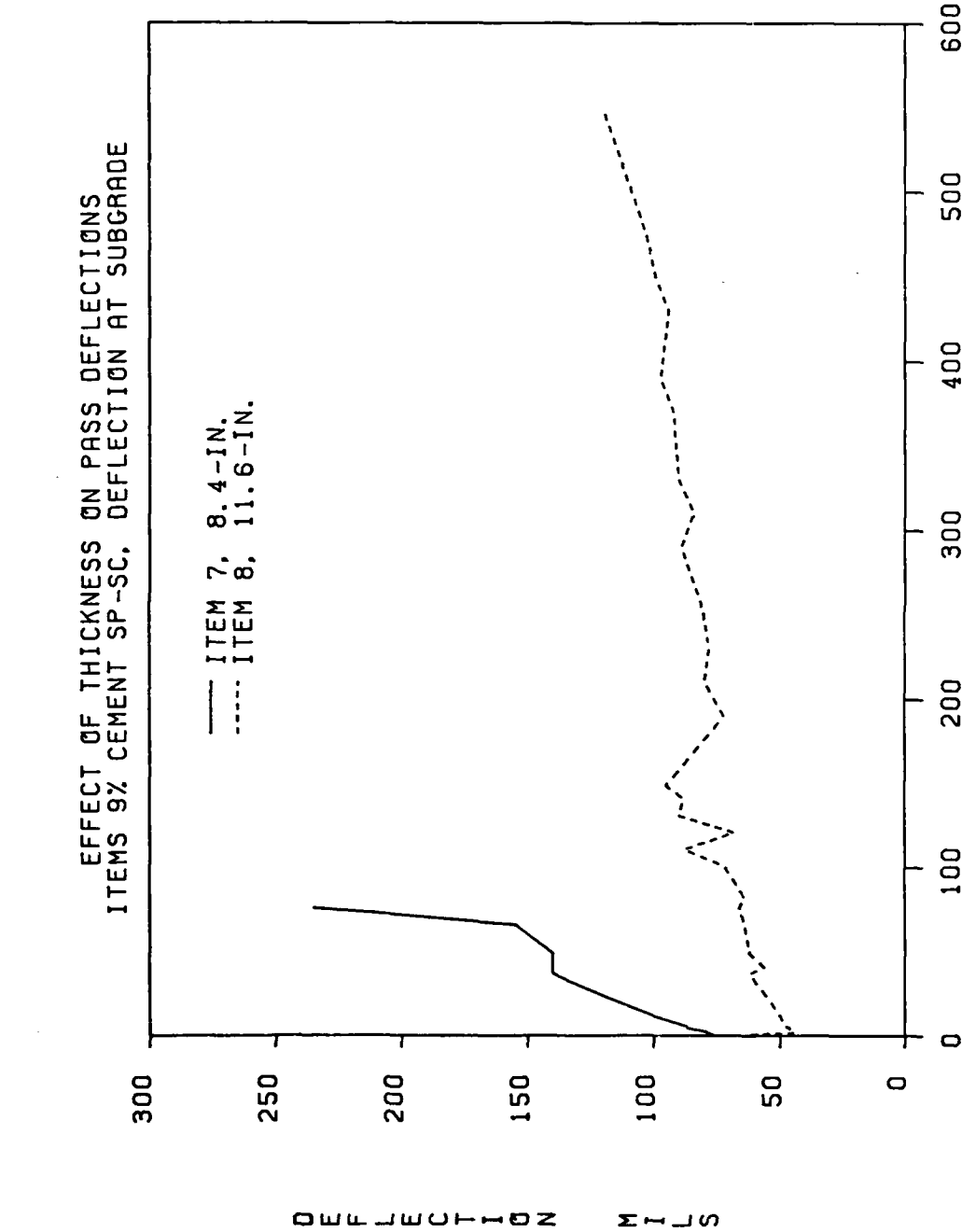

Figure 5-17. Comparison of LVDT Pass Deflection at Item Center, Items 7 and 8

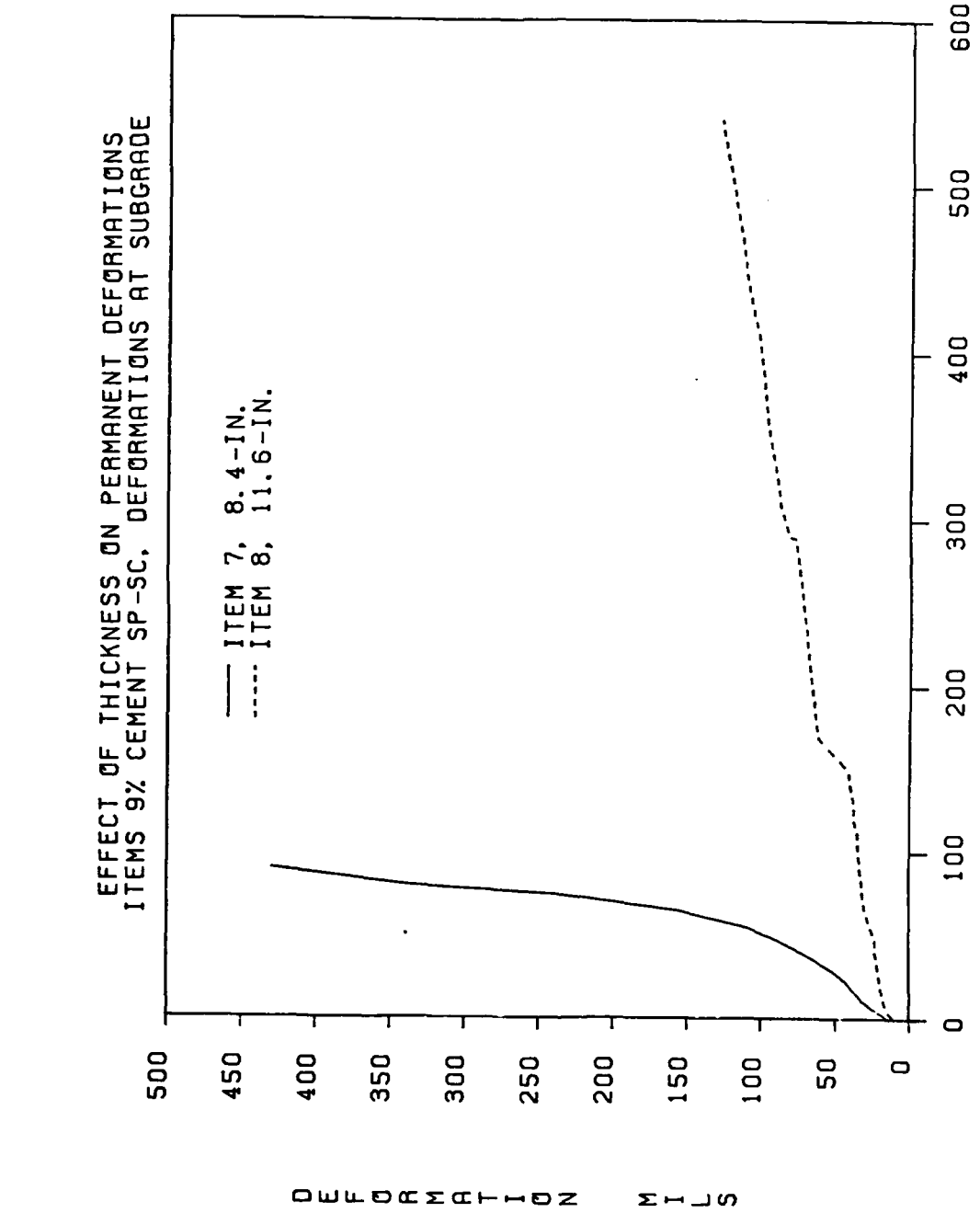

Figure 5-18. Comparison of Cumulative Permanent Deformation at Item Center, Items 7 and 8

CHAPTER 6

RESPONSE AND PERFORMANCE OF INVERTED PAVEMENT ITEMS 9 AND 10

In conventional pavements, the modulus of the various pavement layers decreases with depth. In an inverted pavement, the modulus of the subbase course is greater than the modulus of the base course. Item 9 and 10 were designed as inverted pavements. The lime stabilized subbase material in item 9 did not achieve a modulus greater than the modulus of the crushed limestone base course and item 9 is not an inverted pavement.

A. PERFORMANCE

1. General Item Performance

Items 9 and 10 have a nominal 1 inch asphalt concrete wearing course, 4 inches of crushed limestone base course, 12 inches of stabilized material subbase course and approximately 30 inches of processed CH subgrade. The stabilized material in items 9 and 10 is 5 percent lime stabilized CH soil and 5 percent cement stabilized SP-SC respectively.

A brief summary of item performance during F-4 load cart trafficking is presented below. Appendix A contains the item center LVDT deflection data. The LVDT gage for these items was installed at the surface of the asphalt concrete. FWD load-deflection data and longitudinal surface profiles are also presented in Appendix A. Cracking data is presented in the figures of Appendix B.

Item 9 (item center at station 1+00). At 48 passes of the F-4 load cart, longitudinal cracks were noted at the edges of the traffic lane extending from station 0+92.5 to the north edge of the item. Traffic lane rut depths at station 1+07.5 for 48 passes were 1 inch deep and 1.5 inches deep at stations 1+00 and 0+92.5. The shoulders of the ruts were higher than the surface of the surrounding pavement indicating a shear failure in the crushed stone base course. At 150 passes the longitudinal cracks increased in severity and rut depths deepened to approximately 2 inches at station 1+07.5. The shoulders of the ruts at 150 passes were higher than at 48 passes. Continued traffic resulted in ruts almost 3 inches deep at 419 passes at station 1+07.5. The shoulders of the ruts at station 1+07.5 were 0.75 inches higher than the surrounding pavement surface indicating continued shear failure and displacement of the stone base course. Additional longitudinal cracks along the traffic lane were noted at 419 passes. Structural failure occurred at 419 passes at station 1+09 when the ruts exceeded 3 inches. Item center LVDT pass deflection at the surface of the asphalt concrete was relatively constant at 260 mils up to 60 passes. Item center permanent deformation was 1339 mils at 150 passes when the rut depth exceeded the gage limits. FWD 15 kip D0 deflection at station 1+07.5 increased from 40 mils prior to traffic to 58 mils at 150 passes. FWD deflection basin area was relatively constant at approximately 16 inches for the first 150 passes.

FWD tests were not performed past 150 passes because of the deep ruts.

Item 10 (item center at station 1+35). No surface cracking was noted during the 1000 F-4 load cart passes. Traffic lane rut depths were approximately one-half of an inch at 1000 passes. The shoulders of the ruts were not higher than the surrounding pavement surface indicating some densification of the crushed limestone base course. The centerline profile at 1000 passes indicated very little surface roughness buildup. Item center LVDT pass deflection at the surface increased from an initial 100 mils to 180 mils at 1000 passes. Item center permanent deformation accumulated rapidly to 247 mils at 169 passes then at a rate of approximately 46 mils per 100 passes up to 1000 passes. The FWD 15 kip D0 deflection at the three item quarter points was approximately 29 mils and increased to approximately 41 mils at 1000 passes. The FWD 15 kip deflection basin area was relatively constant at approximately 18 inches over the 1000 passes. The erratic FWD deflection measurements at the item center were most likely caused by the presence of the LVDT gage.

2. Phases of Item Performance

Test item cracking, ruts, and deflection measurements indicate the performance of items 9 and 10 can be divided into three general phases (Figure 6-1).

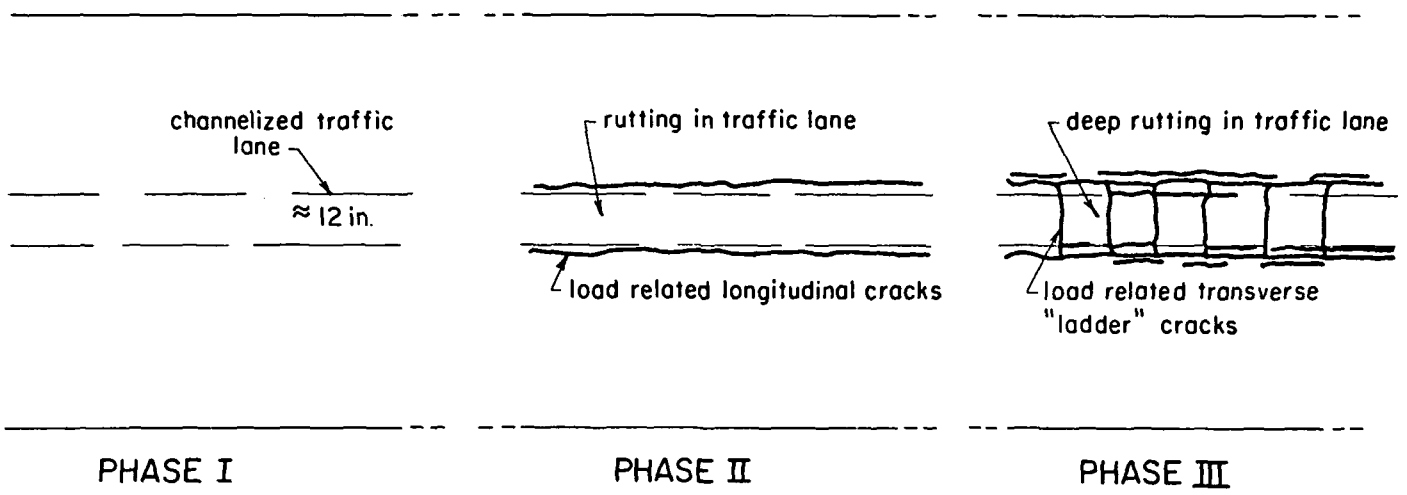

Figure 6-1. Phases of Item Performance, Inverted Pavement Items

Phase I begins with the initial condition of the pavement. Traffic causes only minor rutting in the traffic lane during this phase.

Phase II begins with a deepening of the ruts and development of longitudinal cracks at the edges of the traffic lane. High stress levels in the crushed stone base course resulted in large initial permanent deformation and rapid accumulation. Low stress levels in the crushed stone base course results in small initial permanent deformation and slow accumulation.

Phase III begins with the development of additional longitudinal cracks at the edges of the traffic lane. Transverse "ladder" cracks in the traffic lane develop just prior to failure. Structural failure occurs when the rut depth exceeds 3 inches.

The first 48 passes on item 9 were in Phase I. Phase II started at approximately 48 passes with Phase III ending at 419 passes. The division between Phases II and III for item 9 could not be precisely determined. The performance of item 10 was classified Phase I for all 1000 passes of the load cart.

3. Passes to Functional Failure

The "general smoothness criteria" for the F-4 aircraft (Chapter 4) served as a guideline in estimating the passes to functional failure for items 9 and 10. Surface roughness accumulated in item 10

was minimal and functional failure did not occur before the 1000 pass test limit. Although the load cart applied 419 passes to item 9, functional failure was estimated at 150 passes due to large pass deflections, deep rutting and extensive surface roughness.

B. FIRST PASS INTERIOR LOAD STRUCTURAL RESPONSE

The ILLI-PAVE program was used to determine the predicted first pass structural response for an interior load condition of 27 kips at 265 psi (Table 6-1). Figure 6-2 shows the ILLI-PAVE model used in the analysis. Layer material characteristics are listed in Figure 3-8. A summary of the predicted F-4 first pass interior load stress ratios in the crushed stone base course, stabilized material subbase course and the subgrade along with the passes to functional failure are listed in Table 6-2. The stress ratio in the crushed stone base course is calculated by:

$$\text{stone stress ratio} = q/q_f \qquad (6\text{-}1)$$

where:

$q = (\sigma_1 - \sigma_3)/2$, psi

$q_f = (\tan \alpha)p$, psi

$p = (\sigma_1 + \sigma_3)/2$, psi

ϕ = friction angle.

$\alpha = \tan^{-1}(\sin \phi)$

In item 10, tensile stress in the stabilized material subbase is fairly insensitive to the back-calculated modulus of the CAM subbase (Figure 6-3). The estimated field strength for the stabilized material used to calculate the stress ratio is listed in Figure 3-7. Stress

TABLE 6-1. ILLI-PAVE STRUCTURAL RESPONSE TO F-4 INTERIOR LOAD (27 KIPS, 265 PSI), ITEMS 9 AND 10

Information and Response	Item Number 9	10
Station	1+07.5	1+35
Material Characteristics		
Thickness, inches		
Asphalt Concrete	1.1	0.9
Crushed Limestone	3.4	3.9
Lime Stabilized CH Soil	12.8	N/A
Cement Stabilized SP-SC	N/A	11.0
Modulus, ksi		
Asphalt Concrete	700	700
Crushed Limestone	(1)	(1)
Stabilized Material	20	175
Surface Deflection Basin		
D0 at R = 0 inches, mils	89.8	46.6
D1 at R = 12 inches, mils	41.9	26.5
D2 at R = 24 inches, mils	23.2	18.6
D3 at R = 36 inches, mils	13.3	13.0
Area, inches	15.59	19.30
Radial Strain Bottom of Asphalt Concrete, microstrain	508	206
Crushed Stone Shear Stress Ratio, q/q_f (2)	1.22 (3)	0.52 (4)
Stabilized Material		
Radial Tensile Stress, psi	19.8	91.5
Radial Tensile Strain, microstrain	1005	480
Subgrade		
Normal Stress, psi	16.2	11.6
Deviator Stress, psi	12.5	7.7
Shear Stress Ratio, τ/c	0.62	0.34

(1) $E_{cs} = 13{,}183\theta^{0.28}$

(2) $q_f = p(\tan 39.3 \text{ degrees})$

(3) At 0.5 in. radius and 1.80 in. stone depth.

(4) At 0.5 in. radius and 1.95 in. stone depth.

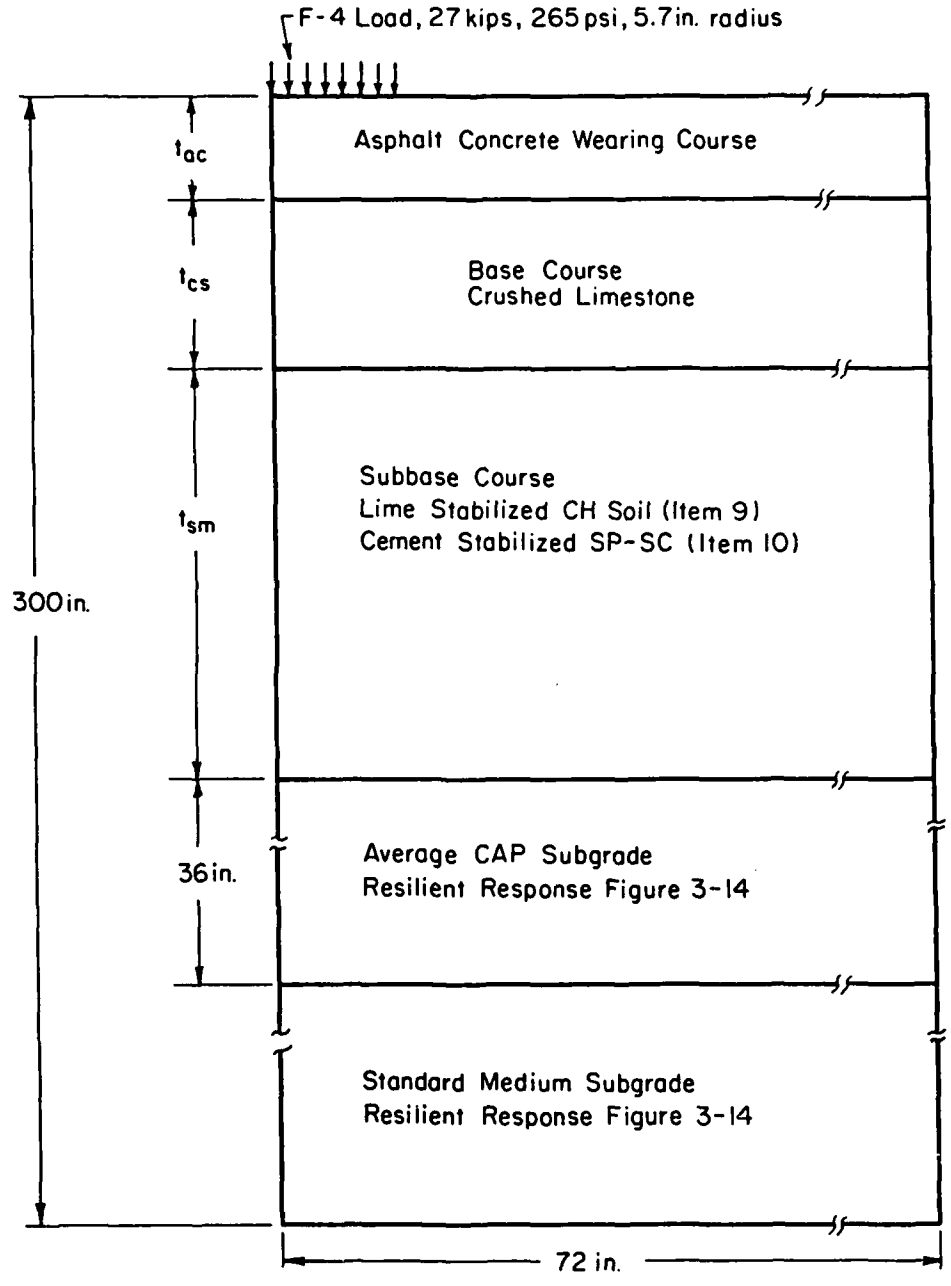

Figure 6.2. ILLI-PAVE Models for F-4 Analysis, Inverted Pavements

TABLE 6-2. SUMMARY OF PREDICTED F-4 FIRST PASS INTERIOR LOAD STRUCTURAL RESPONSE RATIOS AND PERFORMANCE, ITEMS 9 AND 10

Interior Load Ratios	Item 9	Item 10
Stress Ratio Middle of Crushed Stone Base	1.22	0.52
Stress Ratio Bottom of Stabilized Subbase(1)	1.42	1.27
Shear Stress Ratio Top of Subgrade	0.62	0.34
Passes to Functional Failure	150	1000+
Passes to Structural Failure	419	1000+

(1) Plus and minus 26 percent variation.

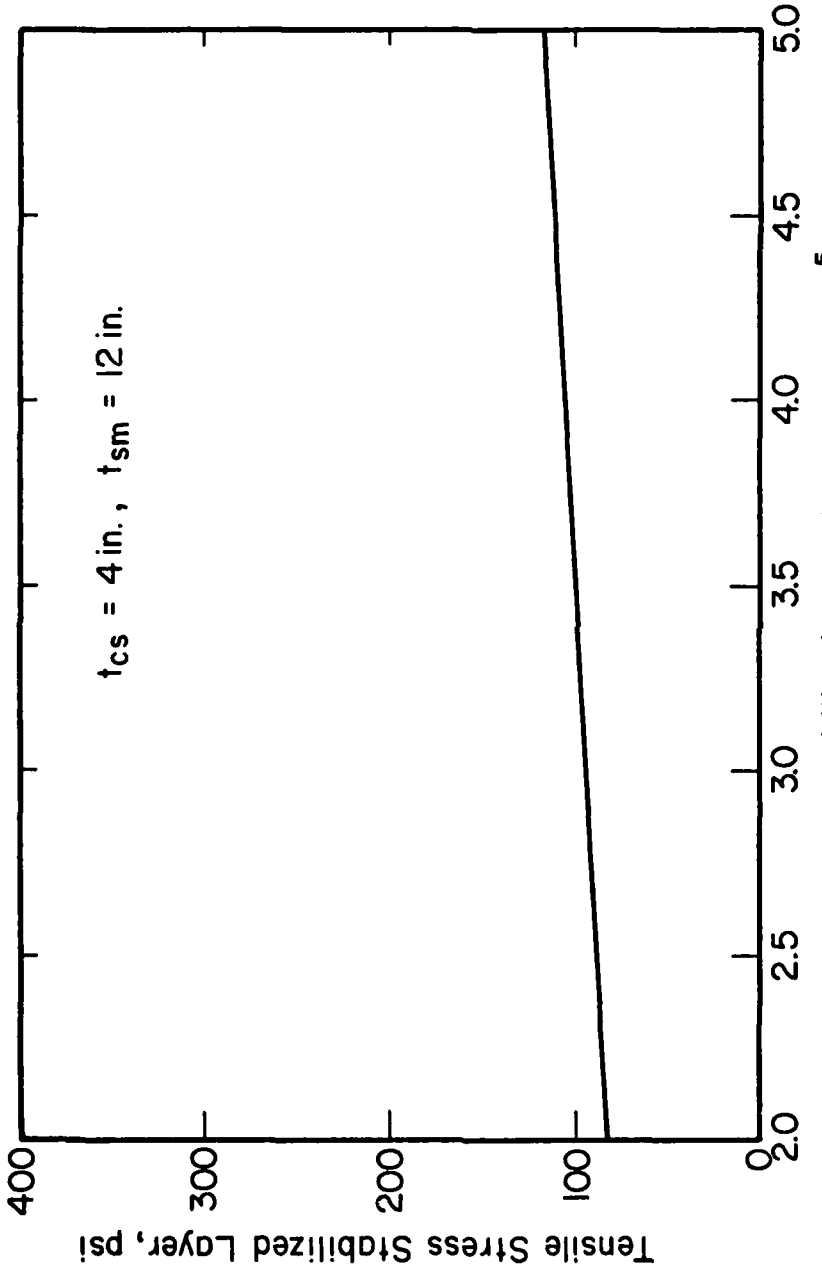

Figure 6-3. Interior Load Maximum Flexural (Tensile) Stress Bottom of Stabilized Material Subbase Course (F-4 ILLI-PAVE Inverted Pavement Data Base, Appendix E)

ratio in the stabilized material subbase has the same coefficient of variation as flexural strength, 25 percent (Reference 46).

C. F-4 ILLI-PAVE INVERTED PAVEMENT DATA BASE

A comprehensive ILLI-PAVE study was conducted for F-4 interior loading (27 kips, 265 psi tire pressure) on inverted pavements with a 1 inch asphalt concrete wearing course, crushed stone base course, stabilized material subbase course and a stress dependent subgrade. The purpose of the study was to determine the effects of stone base course thickness, stabilized material subbase course thickness and modulus on structural response. The ILLI-PAVE model used was similar to that shown in Figure 6-2 except all of the subgrade was the same type (standard medium subgrade). The material characteristics used in the ILLI-PAVE structural model are listed in Table E-1 of Appendix E. The parameters considered were:

Crushed stone base course thickness, t_{cs}: 4, 6 and 8 inches.
Stabilized material subbase modulus, E_{sm}: 200, 500, and 1000 ksi.
Stabilized material subbase thickness, t_{sm}: 6, 9 and 12 inches.

Maximum pavement response data for the 27 ILLI-PAVE runs are presented in Table E-2 of Appendix E. The effect of the parameters (for the ranges considered) on structural response is discussed below.

1. Tensile Strain Bottom of the Asphalt Concrete

The resilient modulus of the asphalt concrete was assumed to be 700 ksi. The effect of the parameters on radial (tensile) strain at

the bottom of the asphalt concrete wearing course, ϵ_{ac}, is shown in Figure 6-4. The ϵ_{ac} is sensitive to t_{cs} with ϵ_{ac} increasing with increasing t_{cs}. The sensitivity of ϵ_{ac} to t_{cs} can be explained by the sensitivity of surface deflections to t_{cs} (Figures 6-5 and 6-6). The thicker the stone base course the larger the D0 deflection and the sharper the radius of curvature in the asphalt concrete. The ϵ_{ac} is fairly insensitive to t_{sm} and E_{sm} over a reasonable range.

2. Stress Ratio in the Stone Base Course

A ϕ of 45 degrees was assumed to represent a typical crushed stone. The effect of the parameters on the stone stress ratio, q/q_f, is shown in Figure 6-7. Maximum stone stress ratios occur in the middle of the stone layer where the confining stress is the lowest. Therefore, stress in the stone base course was calculated at approximately the mid-depth of the stone layer under the center of the wheel load. The stone stress ratio is fairly insensitive to t_{sm} and E_{sm} but is very sensitive to t_{cs}. The thicker the t_{cs} the larger the stone stress ratio.

3. Tensile Stress Bottom of Stabilized Subbase

The effect of the parameters on the radial (tensile) stress at the bottom of the stabilized material subbase, σ_{sm}, is shown in Figure 6-8. Increasing t_{cs} from 4 to 8 inches has little effect on σ_{sm}. The effect of E_{sm} on σ_{sm} is expected.

The effect of the parameters on the stress ratio (σ_{sm}/f_b) at the bottom of the stabilized material subbase is also shown in Figure 6-8. The flexural strength, f_b, of the stabilized material is

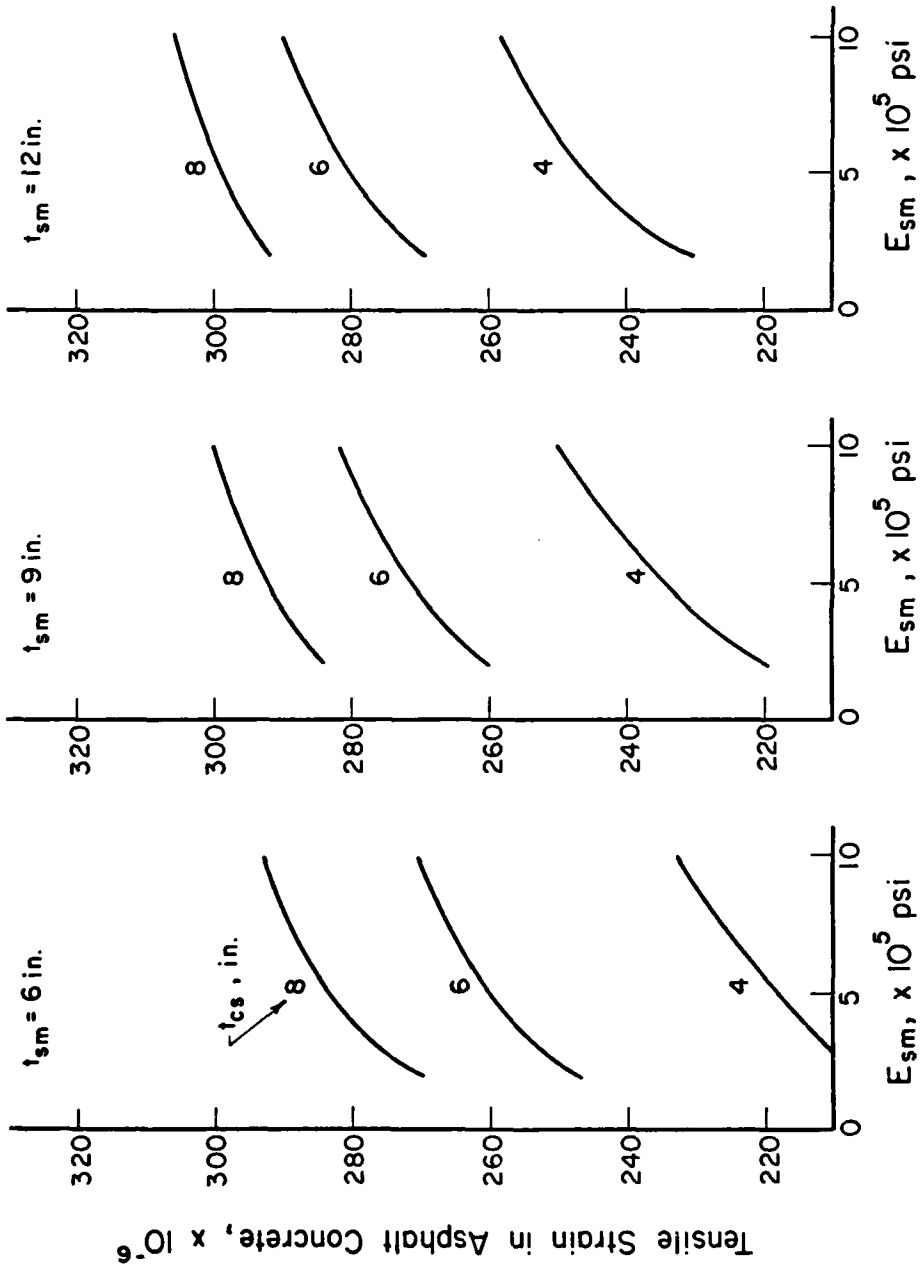

Figure 6-4. Interior Load Maximum Radial (Tensile) Strain in One Inch Asphalt Concrete Wearing Course (F-4 ILLI-PAVE Inverted Pavement Data Base, Appendix E)

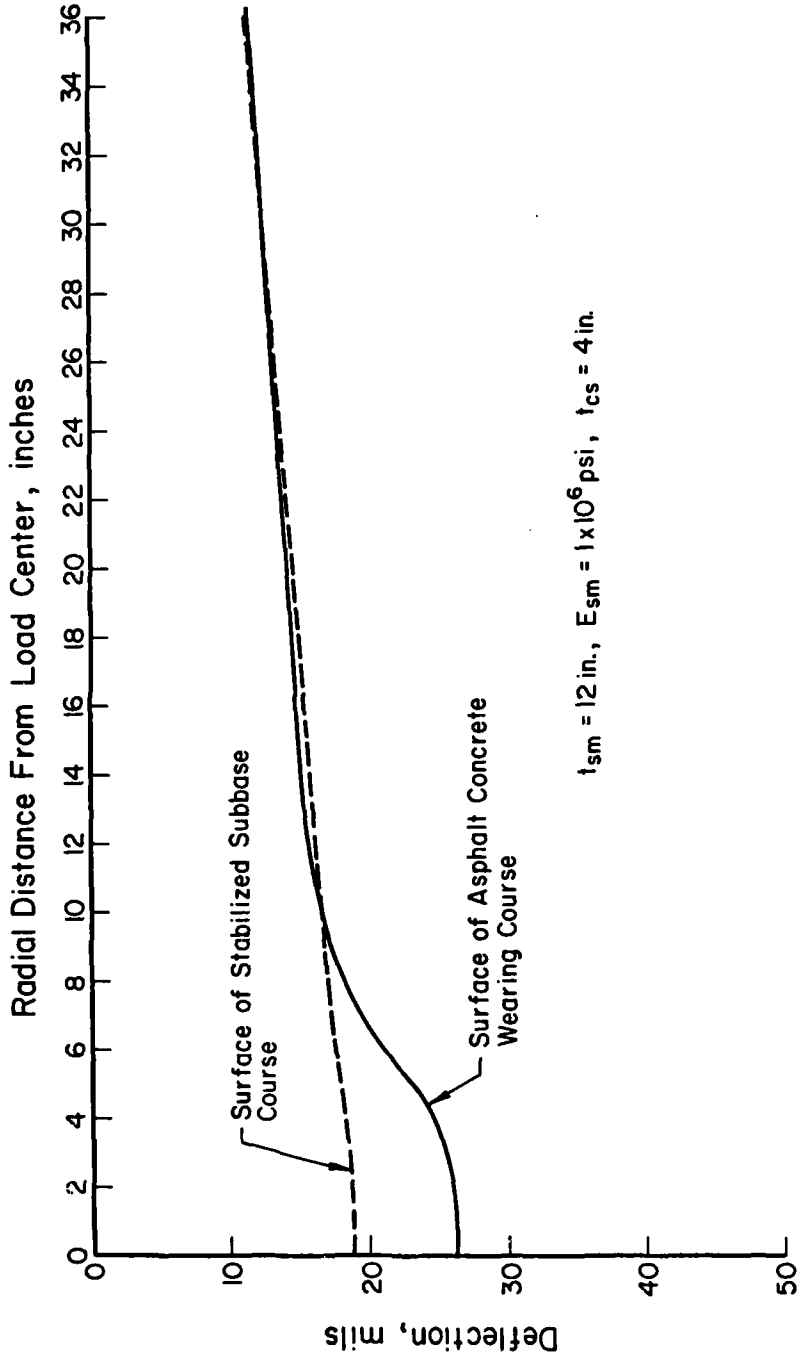

Figure 6-5. Deflection Basin at Surface of Asphalt Concrete Wearing Course and Stabilized Material Subbase Course, t_{cs} = 4 inches

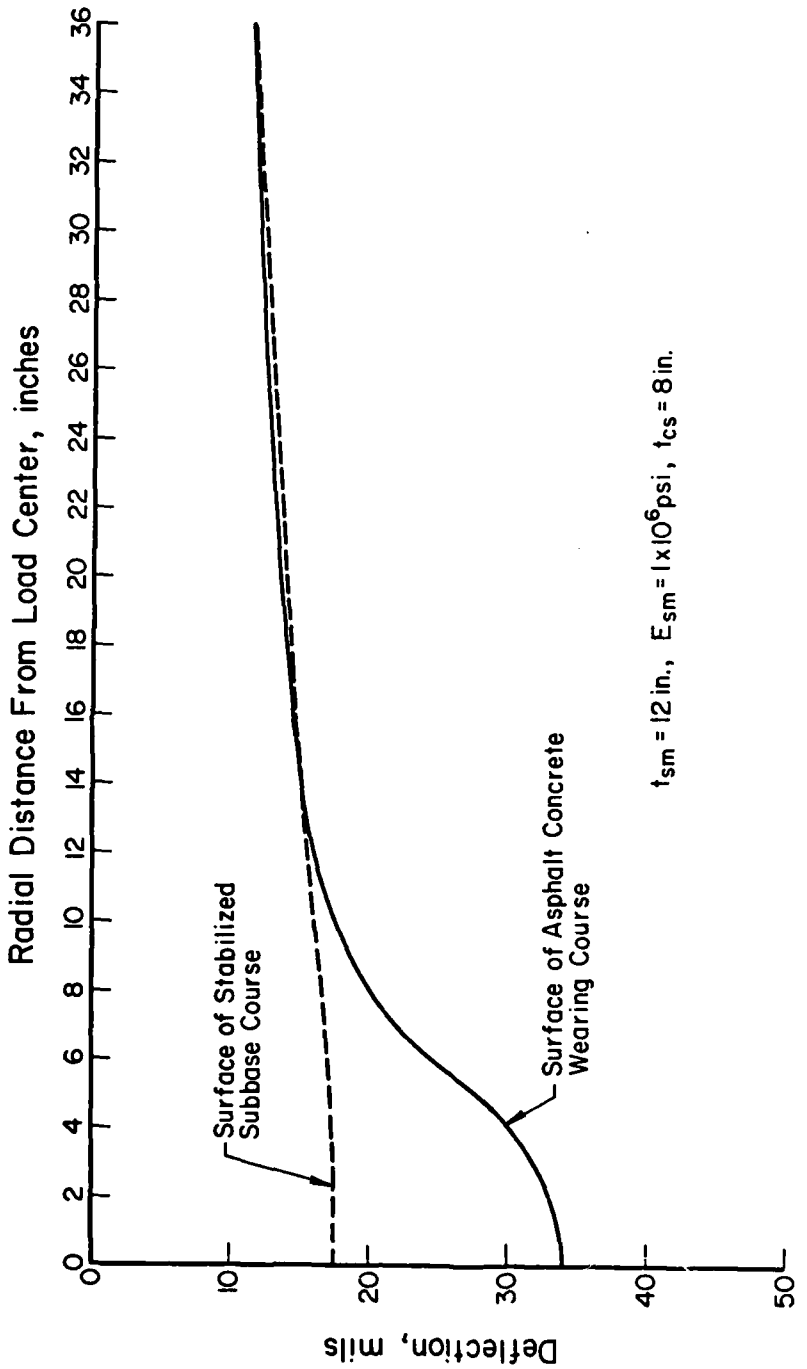

Figure 6-6. Deflection Basin at Surface of Asphalt Concrete Wearing Course and Stabilized Material Subbase Course, t_{cs} = 8 inches

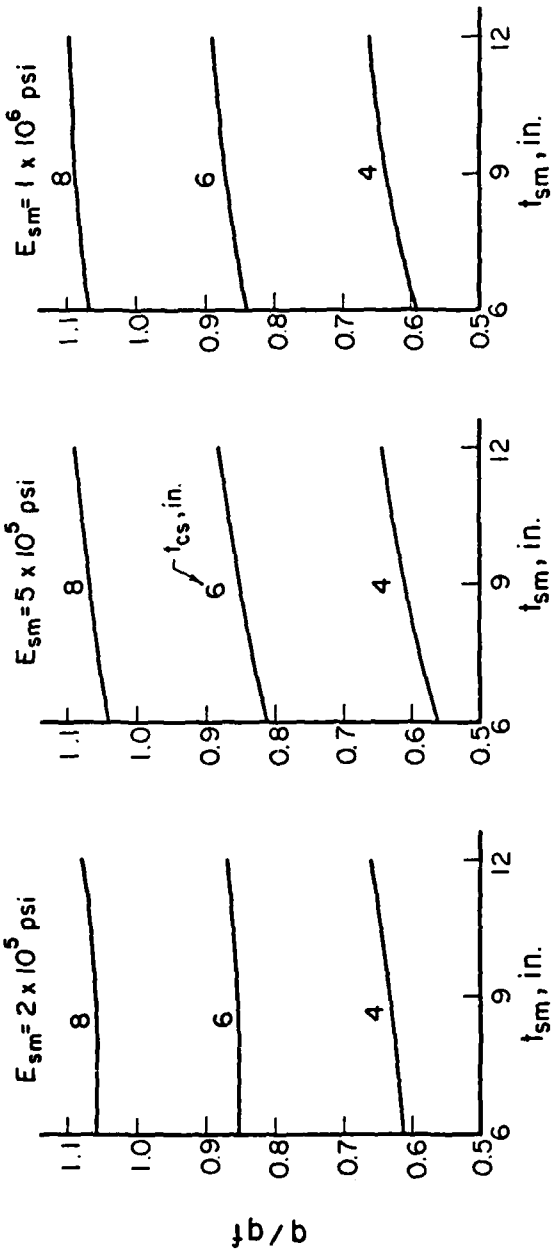

Figure 6-7. Maximum Interior Load Stress Ratio in Stone Base Course Near Mid-depth Under Center of Load (F-4 ILLI-PAVE Inverted Pavement Data Base, Appendix E)

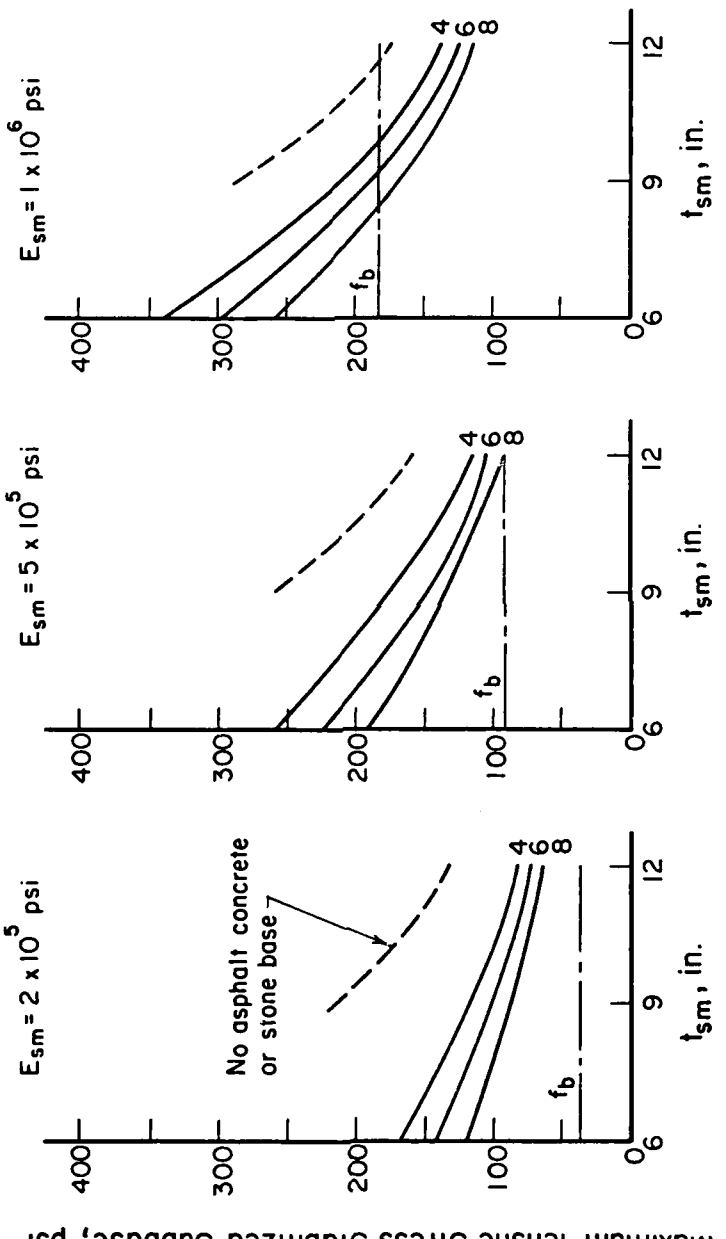

Figure 6-8. Maximum Flexural (Tensile) Stress in Stabilized Material Subbase Course (F-4 ILLI-PAVE Inverted Pavement Data Base, Appendix E)

approximately 20 to 25 percent of the unconfined compressive strength, q_u (Reference 8). For the CAM material in the CAP test items, $f_b = .22q_u$ was selected. In general, the q_u of cement stabilized sandy and low quality granular material can be related to the modulus of elasticity by the relationship $q_u = E_{sm}/1200$ where E_{sm} and q_u are in psi (Reference 8). A general relationship between q_u and E_{sm} is obtained by combining these two relationships and is expressed by;

$$f_b = .22(E_{sm}/1200) \qquad (6-2)$$

where:

f_b = flexural strength, psi

E_{sm} = modulus of elasticity, psi.

For a given E_{sm} used to calculate σ_{sm}, this equation was used to estimate f_b for calculating the stress ratio shown in Figure 6-8.

For 9 inches or greater of stabilized subbase, increasing t_{cs} from 4 to 8 inches has a minor effect on the stress ratio in the stabilized material subbase. For high quality stabilized material, a greater reduction in the stress ratio is obtained by increasing the thickness of the stabilized material subbase than by increasing the thickness of the stone base course. For example, at t_{sm} of 12 inches and E_{sm} of $1x10^6$ psi, increasing the t_{sm} by 3 inches reduces the stress ratio from 0.95 to 0.60. Adding 4 inches of stone base and 1 inch of asphalt concrete wearing course reduces the stress ratio to 0.75.

4. Tensile Strain Bottom of Stabilized Subbase

The effect of the parameters on the radial (tensile) strain at the bottom of the stabilized material subbase, ϵ_{sm}, is shown in Figure

6-9 and is very similar to the effects on the stress ratio shown in Figure 6-8. Increasing t_{cs} from 4 to 8 inches has only a minor effect on reducing ϵ_{sm}. For high quality stabilized subbase materials, the effect of the 1 inch asphalt concrete wearing course and the stone base course is minor on reducing ϵ_{sm} for t_{sm} of 9 inches and greater. The ϵ_{sm} is very sensitive to both t_{sm} and E_{sm}.

5. Load Pressure Distribution on Surface of Stabilized Subbase

The 1 inch asphalt concrete wearing course and the stone base course distribute the surface load over a larger area than the wheel radius as is illustrated in Figure 6-10. Notice the maximum pressure at the surface of the subbase is sensitive to t_{cs}.

6. Deviator Stress in the Subgrade

The effect of the parameters on the maximum deviator stress in the subgrade, σ_{dsg}, is shown in Figure 6-11. For high quality stabilized material, t_{cs}, t_{sm}, and E_{sm} have a small effect on σ_{dsg}. For low quality stabilized material, both t_{cs} and t_{sm} affect σ_{dsg}.

D. RESPONSE OF CRACKED STABILIZED SUBBASE

The structural response of a stabilized material subbase with a transverse shrinkage crack can be approximated using the ILLI-SLAB program and the surface pressure distributions at the surface of the subbase determined by ILLI-PAVE (C.2. above). The circular pressure distribution was converted to a square pressure distribution having the same load and relative pressures over the same areas.

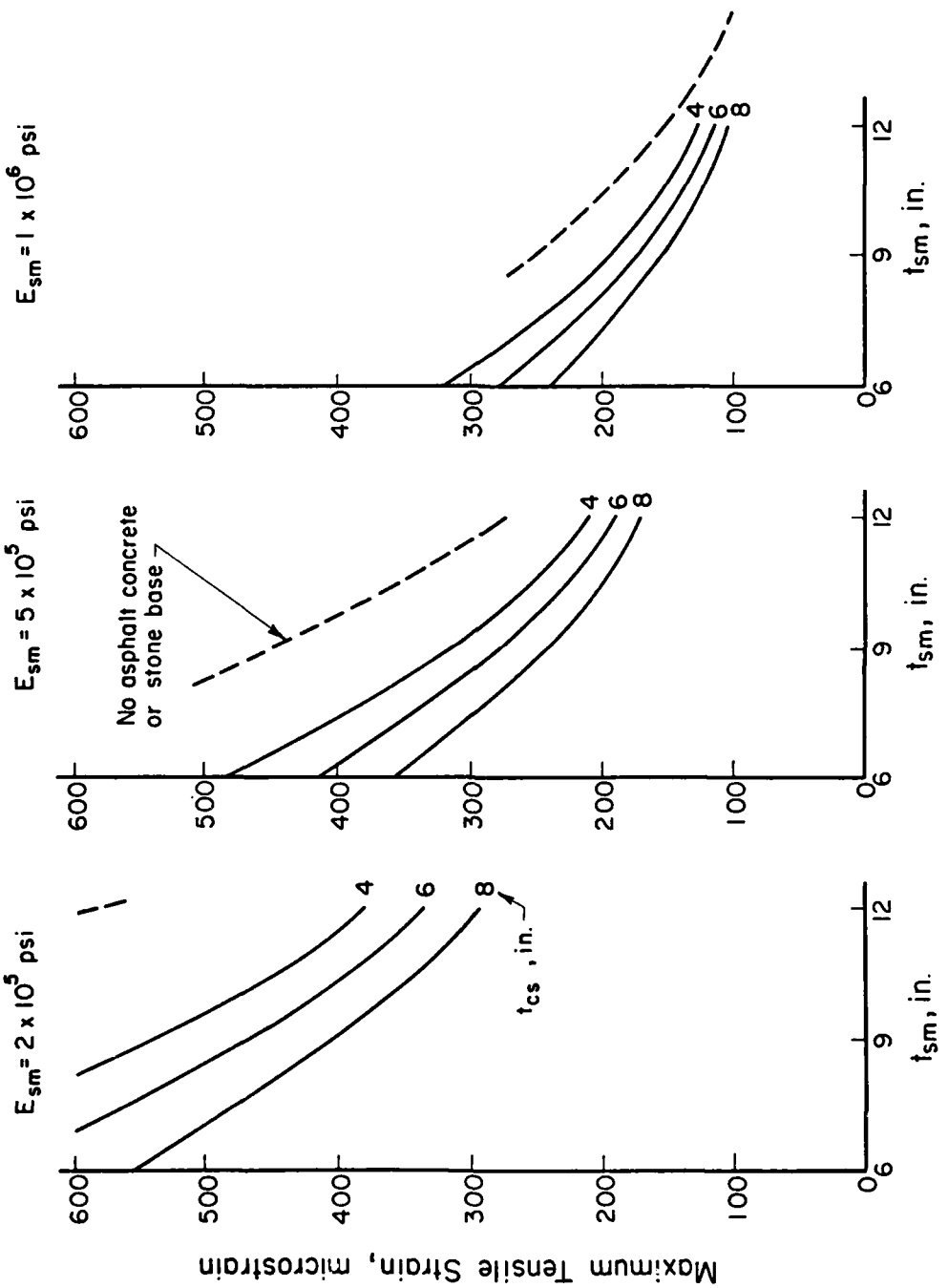

Figure 6-9. Maximum Flexural (Tensile) Strain in Stabilized Material Subbase Course (F-4 ILLI-PAVE Inverted Pavement Data Base, Appendix E)

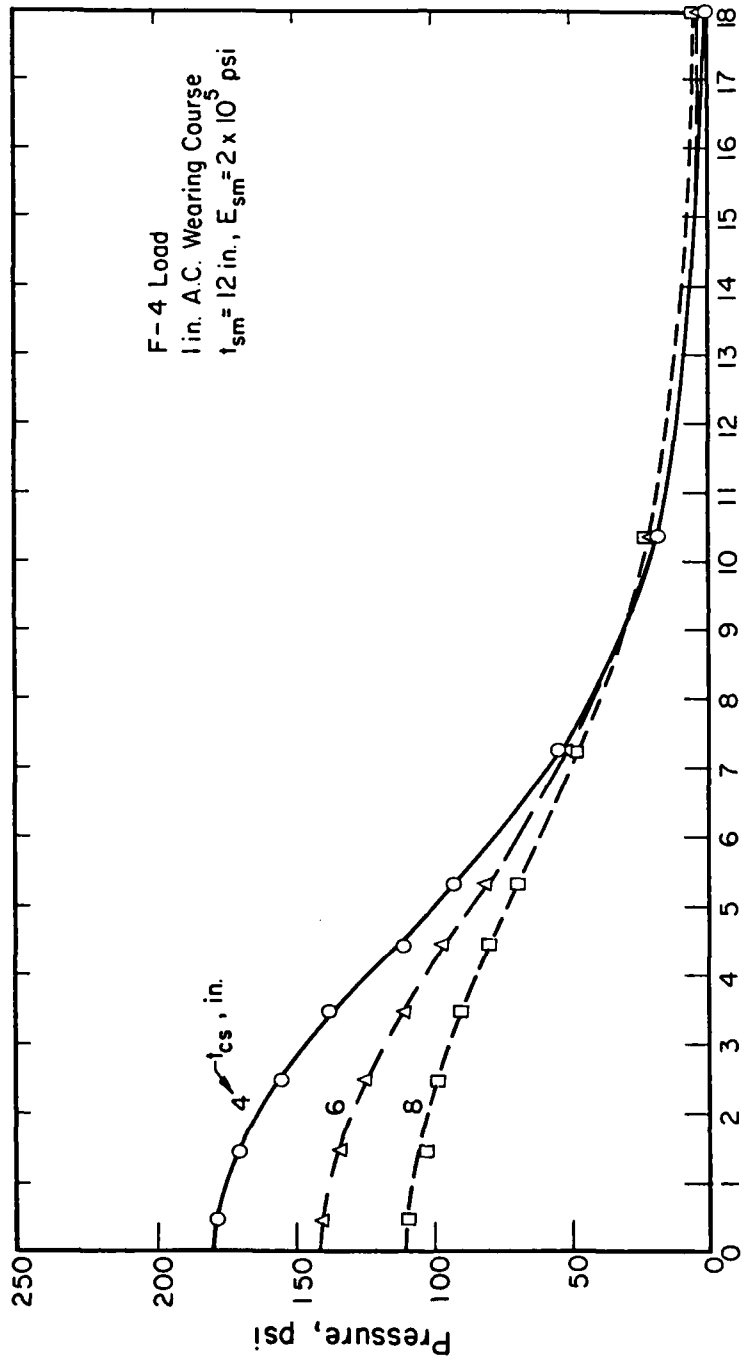

Figure 6-10. Load Pressure Distribution on Surface of Stabilized Material Subbase Course (F-4 ILLI-PAVE Inverted Pavement Data Base, Appendix E)

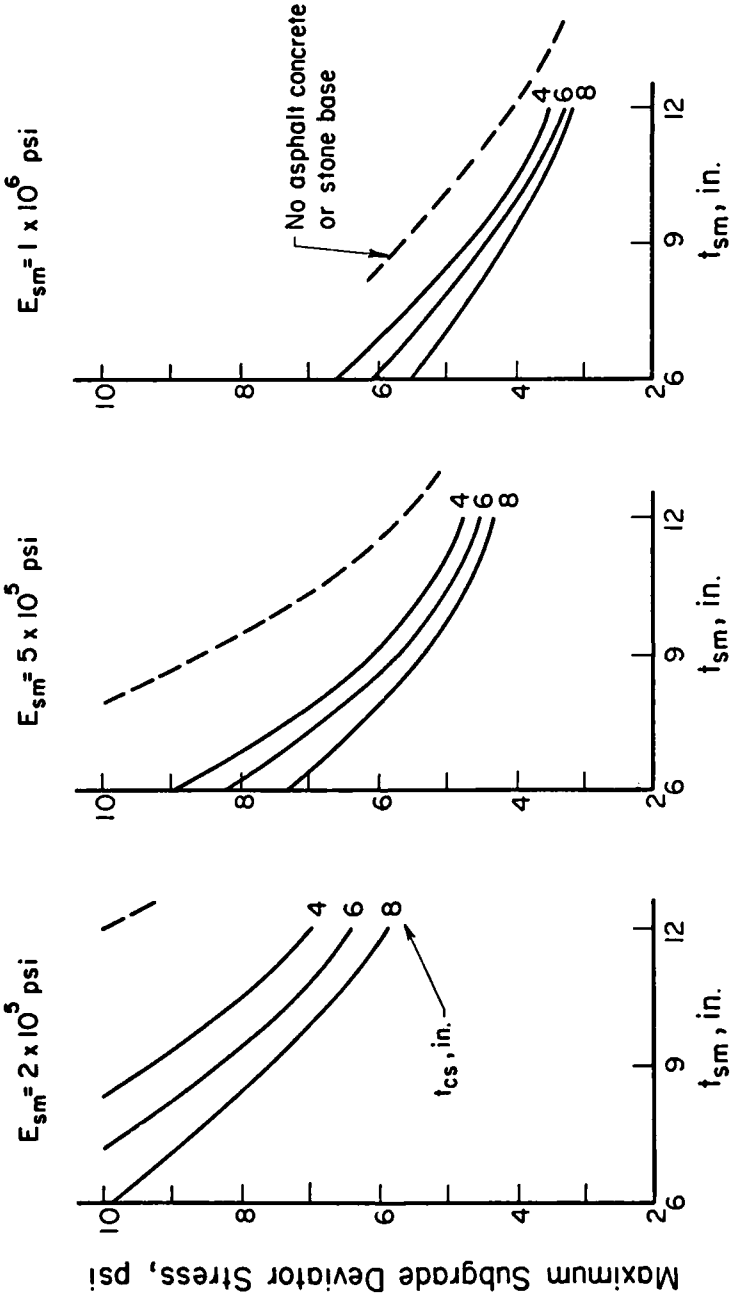

Figure 6-11. Maximum Subgrade Deviator Stress (F-4 ILLI-PAVE Inverted Pavement Data Base, Appendix E)

An ILLI-SLAB study was conducted to determine the location of the square pressure distribution in relation to the crack to produce the maximum crack flexural (tensile) stress in the subbase. The result of the study (Figure 6-12) shows for a 4 to 8 inch thickness of stone base course, the maximum crack tensile stress occurs when approximately 80 percent of the load is on the approach slab. A crack LTE of 30 percent was selected as represenative of field conditions.

The effect of the asphalt concrete and stone subbase on reducing the crack flexural (tensile) stress in the stabilized material subbase is shown in Figure 6-13. The beneficial effect of the asphalt concrete and stone base course is more evident for thin subbases. For a given t_{sm} and E_{sm}, increasing the thickness of the stone base course from 4 to 8 inches results in an additional 18 percent reduction in crack stress.

The effect of t_{cs} on crack stress and crack stress ratio in the stabilized material subbase is shown in Figure 6-14. The interior flexural stress, σ_{sm}, was determined using ILLI-PAVE (standard medium subgrade) without the asphalt concrete wearing surface and stone base course. To calculate the crack tensile stress, σ_{sm} was increased by the LPEF (Figure 4-2) for a 30 percent LTE. The crack tensile stress was then reduced by the factor in Figure 6-13 for the appropriate stone base course thickness. Flexural strength, f_b, was estimated using Equation 6-2.

The benefit of the 1 inch asphalt concrete wearing course and the stone base course in reducing the crack flexural (tensile) stress is

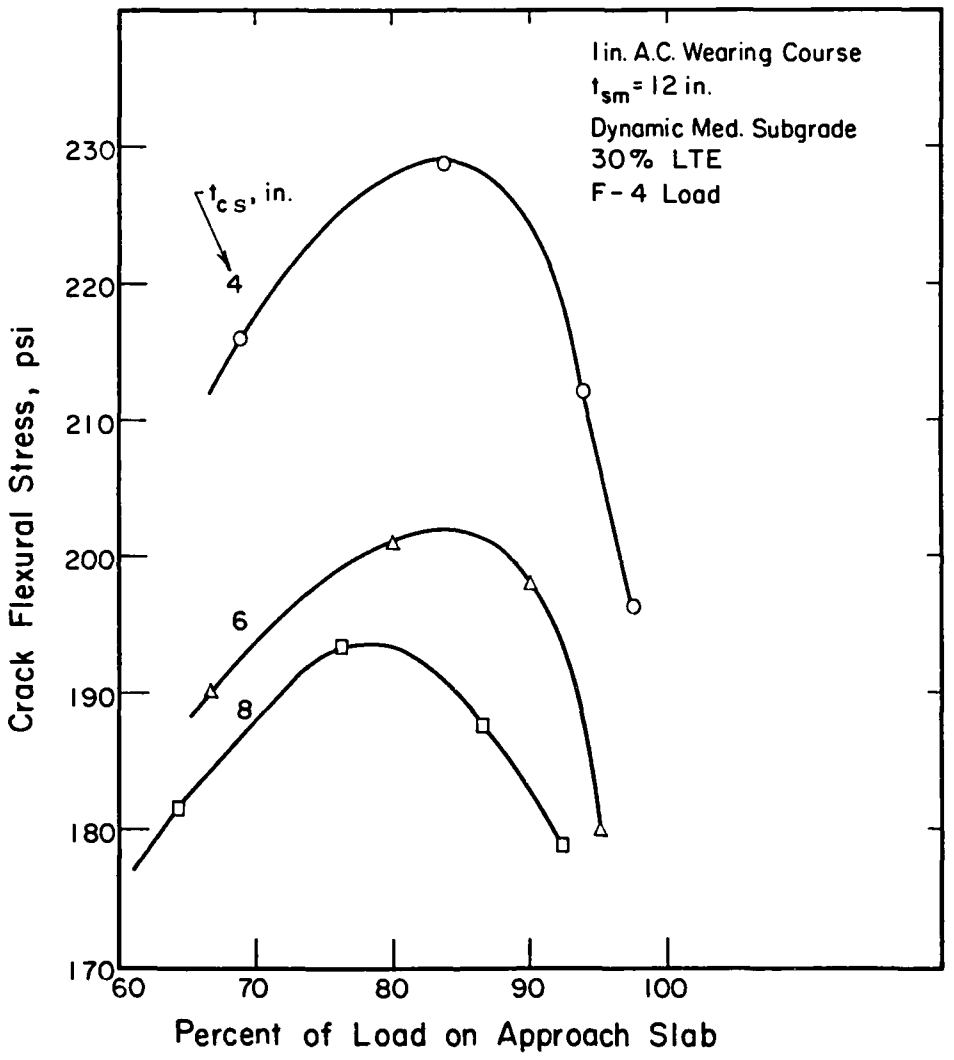

Figure 6-12. Effect of Percent of Total Load on Approach Slab on Crack Flexural (Tensile) Stress in Stabilized Material Subbase Course

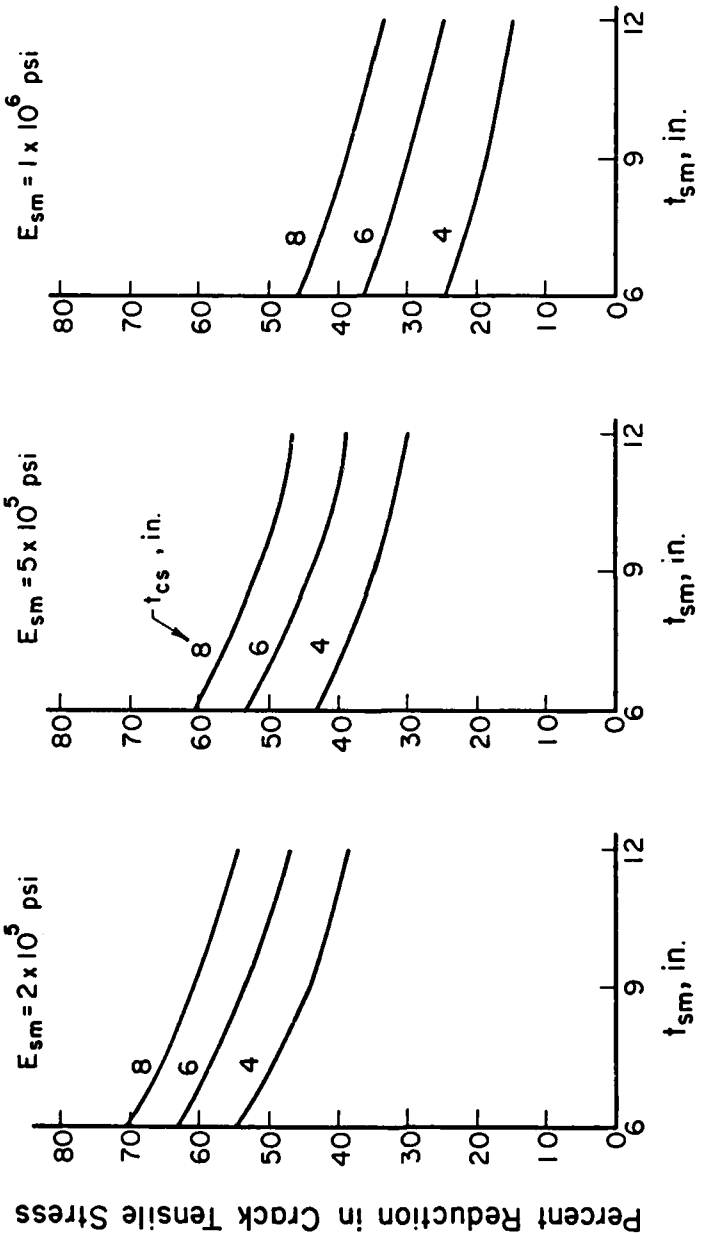

Figure 6-13. Effect of Thickness of Stone Base Course on Reducing Flexural (Tensile) Stress in Stabilized Material Subbase Course, F-4 Load, 30 Percent LTE

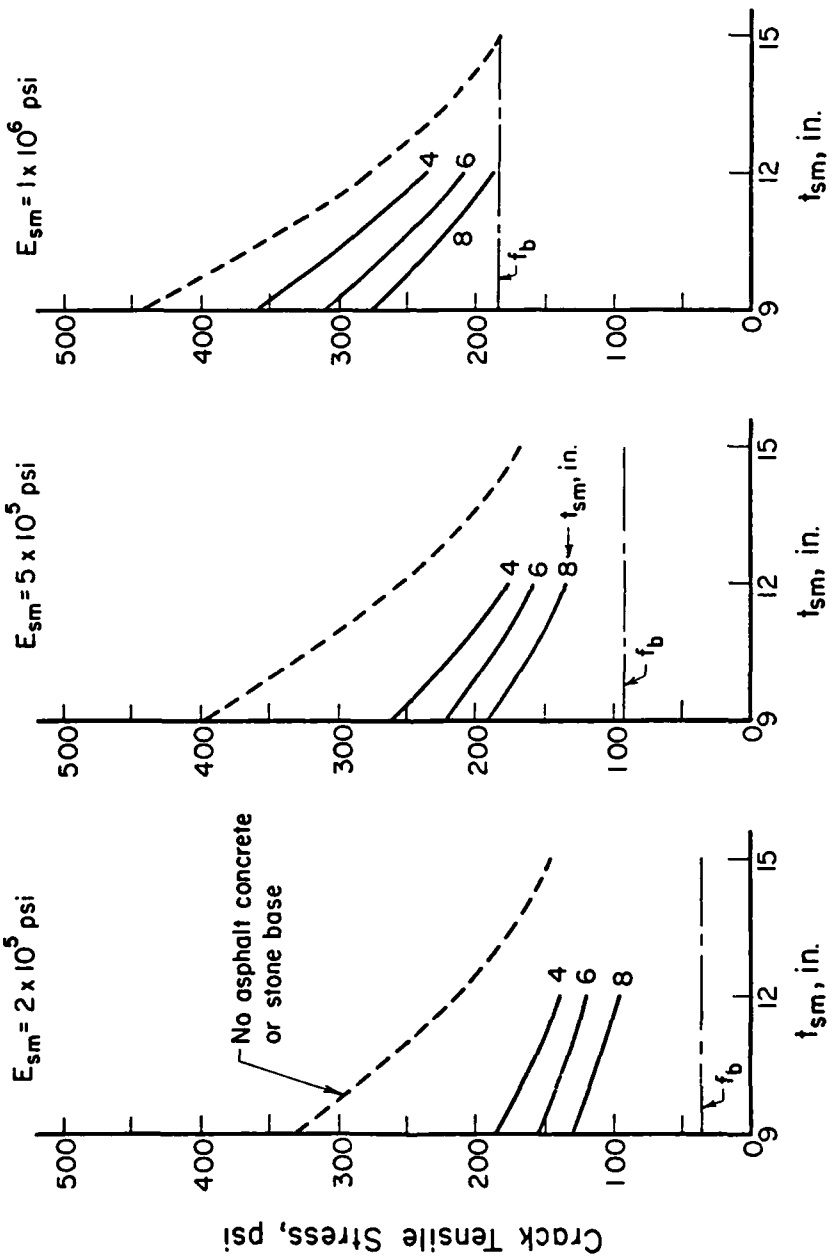

Figure 6-14. Effect of Thickness of Stone Base Course on Flexural (Tensile) Stress in Stabilized Material Subbase Course, 30 Percent LTE (F-4 ILLI-PAVE Inverted Pavement Data Base, Appendix E)

more pronounced for thin subbases of low quality. For thicker subbases of higher quality, the effect of t_{sm} is larger than t_{cs} on reducing the flexural stress and stress ratio in the stabilized subbase course.

The effect of t_{cs} on reducing the strain ratio in the stabilized material subbase is similar to the effect on the stress ratio discussed above.

CHAPTER 7

DISCUSSION OF THE RESPONSE AND PERFORMANCE OF THE CAP TEST ITEMS

A. EXPLANATION OF PHASES OF ITEM PERFORMANCE

1. Two-Layer Pavement Test Items

a. Overview

Understanding why cracks developed in the CAM layer and the relationship between pass deflection, permanent deformation and cracking is necessary to determine the significant factors affecting item response and performance. Pavement response and CAM strength are related since higher CAM strength generally means higher layer modulus.

b. Phase I

The predicted F-4 first pass crack flexural (tensile) stress (acting parallel to the transverse shrinkage crack) at the bottom of the CAM layer exceeded the estimated field flexural strength in all CAP two-layer items. Therefore, a longitudinal crack on the underside of the CAM layer at the center of the traffic lane formed on the first pass of the F-4 load cart (Figure 7-1). Continued traffic caused the crack to propagate up into the CAM layer and away from the transverse crack. This longitudinal crack reduced the stiffness of the CAM layer in the traffic lane and resulted in increased pass deflections and subgrade permanent deformations.

c. Phase II

Continued traffic further propagated the longitudinal crack on the underside of the CAM layer. Increased pass deflection caused a decrease in the radius of curvature and an increase in the

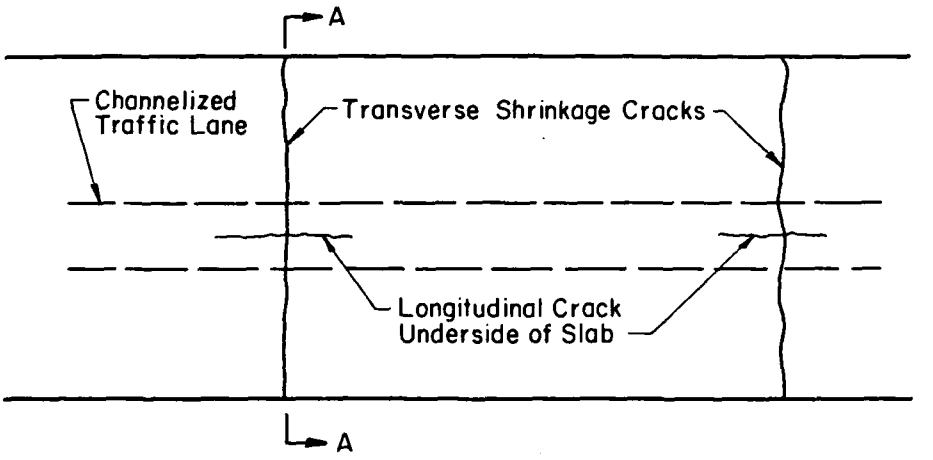

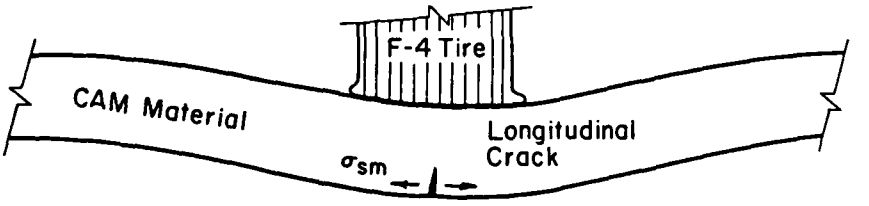

Section A-A

Figure 7-1. Cracking in Phase I of Item Performance, Two-Layer Items

tensile stress on the surface of the CAM layer at the edges of the traffic lane causing longitudinal cracks to develop (Figure 7-2). As the surface longitudinal cracks propagated down into the CAM layer, the flexural stress at the bottom of the CAM layer acting parallel to the transverse shrinkage crack is reduced. This is because the transverse distance between the longitudinal surface cracks at the edges of the traffic lane is too short to produce large flexural action in this direction. The area within the traffic lane begins to act as a long thin slab bounded on the ends by the transverse shrinkage cracks and on the sides by the longitudinal surface cracks at the traffic lane edges. The continued propagation of the longitudinal surface cracks further reduces the stiffness of the CAM layer in the traffic lane.

d. Phase III

With the development of the surface longitudinal cracks, subgrade deviator stress greatly increases causing increased subgrade permanent deformation. The LTE across the longitudinal surface cracks decreases with continued traffic further increasing the subgrade deviator stress. The critical stress in the CAM layer now shifts from parallel to the transverse shrinkage crack to parallel to the traffic lane. The flexural (tensile) stress parallel to the short axis is now very small in comparison to the long axis. The stress levels at the bottom and top of the CAM layer parallel to the long axis in the traffic lane are very large and equal the flexural strength causing transverse ladder cracks to form in the traffic lane (Figure 7-3). The effective "slab " size is now only slightly larger than the area of the wheel load. Critical pavement stress now shifts from the rigid stabilized

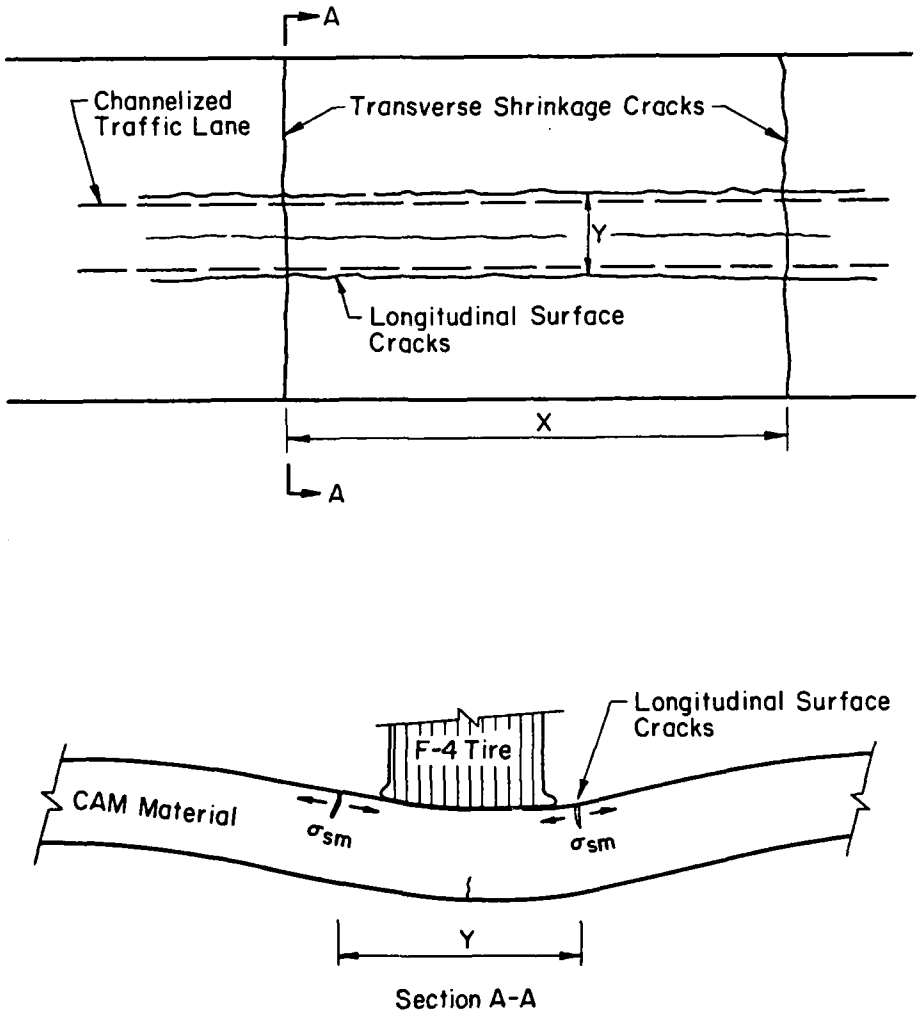

Figure 7-2. Cracking in Phase II of Item Performance, Two-Layer Items

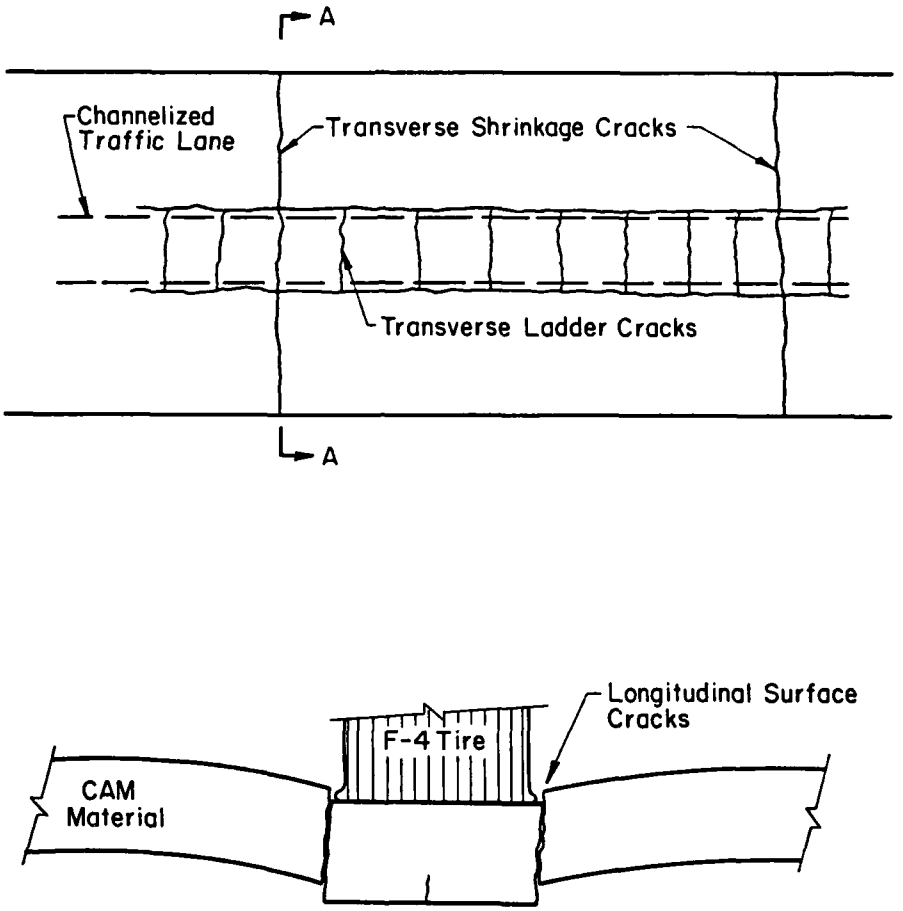

Figure 7-3. Cracking in Phase III of Item Performance, Two-Layer Items

material layer to the subgrade. When the subgrade shear stress equals the shear strength, large subgrade displacements occur and the wheel load punches through the CAM layer into the subgrade.

e. Summary

The longitudinal cracks on the underside of the CAM layer developed on the first pass because the stress ratio at the transverse shrinkage crack exceeded one. The rate of crack propagation in the CAM layer is primarily a function of the resilient and permanent behavior of the subgrade. Softer subgrades with larger resilient deflections and permanent deformations for the same CAM stress ratio have faster crack propagation and earlier functional failure.

Design traffic levels should occur during Phase I of item performance for low volume traffic CAPs. Crack propagation and subgrade permanent deformation in rigid two-layer pavements with a stress ratio greater than one is a very complex relationship between t_{sm}, E_{sm}, strength of the CAM, crack LTE, and the response and strength of the subgrade. Once the longitudinal crack on the underside of the CAM layer forms, the pavement structure cannot be accurately modeled. To use a mechanistic approach, an intact slab without the longitudinal cracks must be analyzed.

2. Inverted Pavement Items

The following discussion concerns the inverted pavement item 10 (nominal 12 inches of 5 percent cement stabilized SP-SC subbase). Item 9 (nominal 12 inches of 5 percent lime stabilized CH soil subbase) as constructed was not an inverted pavement item because of the low modulus and strength of the stabilized material subbase. Consequently,

this item failed very early and behaved as a highly overstressed conventional flexible pavement.

Transverse shrinkage cracks in the stabilized material subbase course produced larger crack stresses than interior stresses. However, the crushed stone base course had a bridging effect across the crack that reduced the rate of crack propagation, surface differential deflection at the crack, and rate of surface roughness accumulation. Longitudinal surface roughness resulted from several sources. Permanent deformation in the crushed stone base course, cracking in the stabilized material subbase course, permanent deformation in the subgrade and horizontal pavement structure variability all influenced the accumulation of surface roughness.

The rate of rut development and the depth of the rut are related to the stress ratio in the crushed limestone base course. For small stone stress ratios, minor rutting occurs due to the densification of the stone. However, if the stone stress ratio is high, large permanent deformations occur and accumulate quickly. Very large deformations in the stone base course occur if the stress ratio equals one. In this case stone shear failure occurs and the shoulders of the rut are higher than the surrounding pavement surface.

The rate of crack propagation in the stabilized material subbase course of an inverted pavement is difficult to define. Available structural models cannot accurately analyze an inverted pavement with a cracked subbase. The effect of differential movement of the subbase at a crack on the stresses in the stone base course is unknown.

As a result of the complex relationships between the factors influencing the rate of crack propagation in an inverted pavement, design traffic levels should occur during Phase I of item performance for low traffic volume CAPs. Stress levels in the stone base and stabilized subbase courses in this phase should be kept less than one so a mechanistic approach can be used.

B. SIGNIFICANCE OF STRESS AND STRAIN RATIOS GREATER THAN ONE

All the predicted F-4 first pass stress ratios in the CAM layers of the CAP test items exceeded one. By definition, stress ratio cannot exceed one since the limiting stress is the strength of the material. A stress ratio less than one is a realistic measure of the stress level in a material compared to its strength and is useful in fatigue analysis.

Stress ratios greater than one are still useful but only as "quantitative indicators of performance" and not as absolute values. These quantitative indicators of performance are useful in comparing performance among items with stress ratios greater than one. Transfer functions developed for stress ratios greater than one reflect crack propagation rates after crack initiation while those for stress ratios less than one relate to crack initiation. These "crack propagation" stress ratio transfer functions are more relevant for analysis than design.

C. TWO-LAYER PAVEMENT ITEMS

1. Predicted F-4 First Pass Crack Response

CAM layer thickness had the largest effect on the structural response of the two-layer items. The thicker items had smaller surface

deflections, larger deflection basin areas, smaller CAM flexural stress and stress ratios, smaller CAM flexural strain and strain ratios, smaller subgrade deviator stress and shear stress ratios. When the variability of the back-calculated E_{sm} and CAM strength are considered, both 16 inch items had predicted first pass crack CAM stress and strain ratios near one.

The 16 inch items also had predicted first pass interior flexural (tensile) strains, ϵ_{sm}, less than 100 microstrain. Since strain is inversely proportional to E_{sm} and the 16 inch items had large E_{sm}, the strains were much less than for the other items. However, even at large E_{sm}, t_{sm} still has a pronounced effect on ϵ_{sm} (Figure 5-7).

The subgrade shear stress ratio is largely affected by t_{sm}. The 16 inch items had predicted first pass interior subgrade shear stress ratios less than 0.10. The exact relationship between the subgrade deviator stress at a crack and the interior stress is unknown so crack subgrade shear stress ratios were not determined. However, the deviator stress for the 16 inch items are still very low even when increased for the crack effect.

2. Effect of Thickness, Modulus and Strength on Stress Ratio

A study was conducted using the F-4 ILLI-PAVE data base of Appendix C to determine the combination of slab thickness, slab modulus and slab strength for a predicted crack stress ratio in the stabilized material layer larger than one. A standard medium subgrade was selected with a 30 percent LTE across the transverse shrinkage cracks. The flexural strength was estimated using Equation 6-2. Crack tensile

stress was estimated by increasing the interior load stress by the LPEF in Figure 4-2.

The results of the study are shown in Figure 7-4. One combination that produces a stress ratio of one is:

f_b = 137 psi

$E_{sm} = 7.5 \times 10^5$ psi

t_{sm} = 16.6 inches.

This combination is very close to item 6 which had a predicted first pass crack stress ratio of 1.1. Although the unconfined compressive strength of cement stabilized granular materials can be greater than 2,000 psi, a typical value is approximately 1000 psi. This equates to an estimated flexural strength of 220 psi and an estimated modulus of elasticity of 1.2×10^6 psi (Equation 6-2). From Figure 7-4 a minimum of 13.6 inches of stabilized material would be required for a first pass predicted crack stress of one or less.

3. Transfer Functions for Two-Layer Items

Many factors influence the rate of crack propagation in the CAM layer for stress ratios greater than one and large variability in performance at a given stress ratio should be expected. A transfer function based upon the results of the CAP field test should be conservative to reflect this variability.

a. Stress Ratio

Figure 7-5 shows a recommended transfer function relating passes to functional failure and the predicted first pass crack stress ratio in the stabilized material layer for two-layer items. The form of the transfer function is:

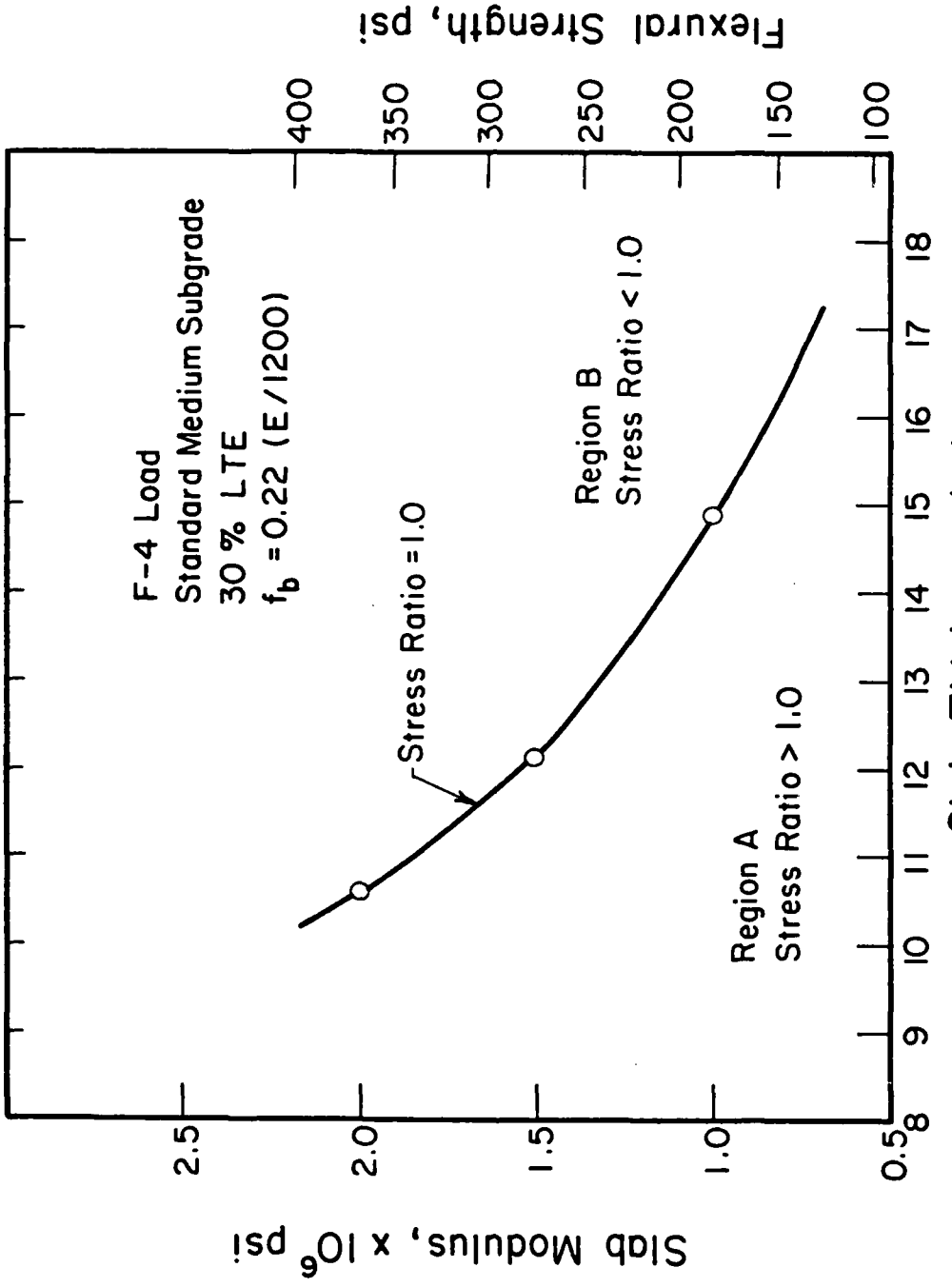

Figure 7-4. Combinations of Slab Modulus, Strength and Thickness for Crack Stress Ratio of One

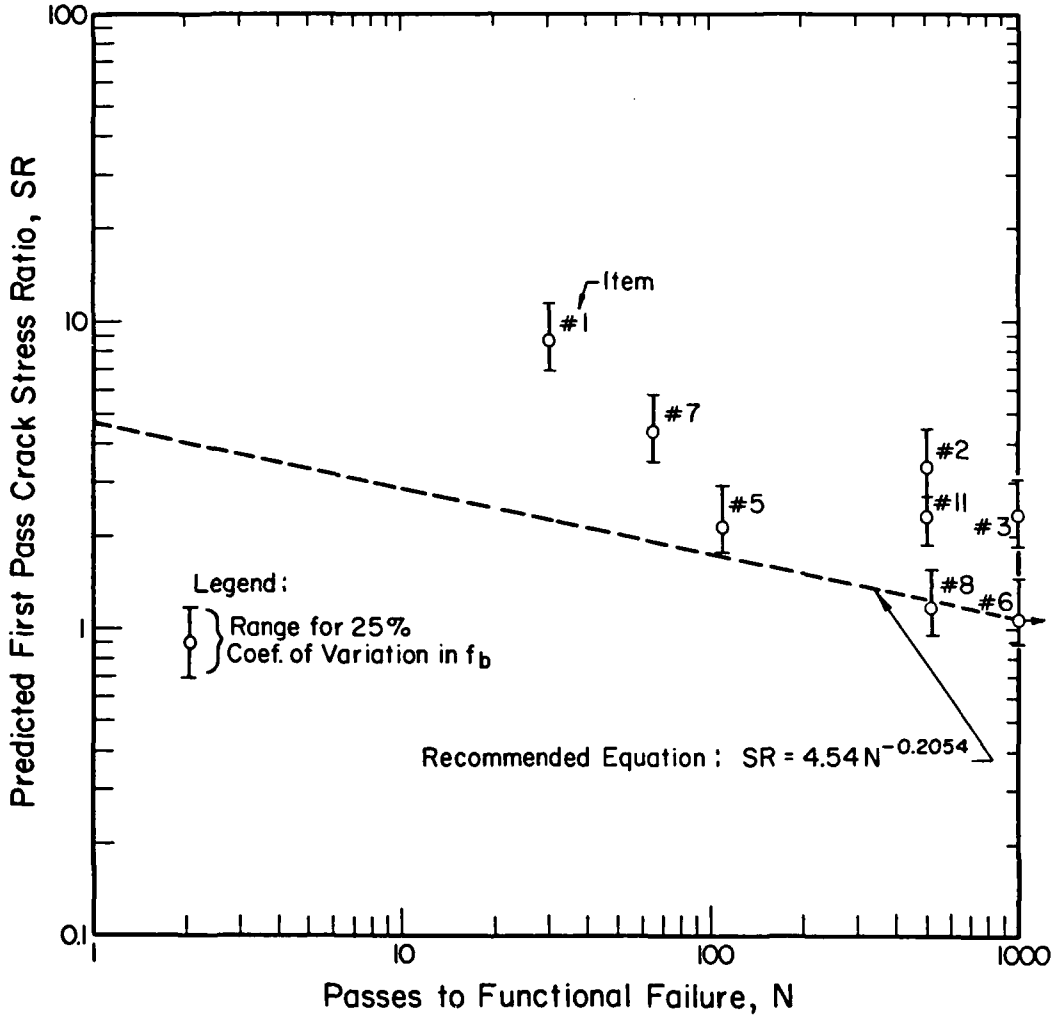

Figure 7-5. Transfer Function Relating Performance and Predicted First Pass Crack Stress Ratio in CAM Layer, Two-Layer Pavement Items

$$SR = 4.54N^{-0.2054} \quad (7\text{-}1)$$

where:

SR = crack stress ratio in the stabilized material layer

N = passes to functional failure.

The upper bound of the stress ratio for one pass is approximately 4.54 (Chapter 4). The performance of the two-layer CAP test items fall above this transfer function as shown in Figure 7-5. Notice the 16 inch items have stress ratios near one at 1000 passes.

b. Strain Ratio

Figure 7-6 shows a recommended transfer function relating passes to functional failure and the predicted first pass crack strain ratio in the stabilized material layer for two-layer items. The transfer function may be stated in either of the following forms:

$$N = 1800(10^{-0.2532\varepsilon_{SR}}) \quad (7\text{-}2)$$

$$\log N = 3.2553 - 0.2532\varepsilon_{SR} \quad (7\text{-}3)$$

where:

N = passes to functional failure

$\varepsilon_{SR} = \varepsilon_s/\varepsilon_b$

ε_s = crack strain (interior strain x 40 percent)

ε_b = strain at break estimated at 120 microstrain.

Notice the 16 inch items have a predicted crack strain ratio near one at 1000 passes. CAM strain at break used in the strain ratio was estimated at 120 microstrain (Reference 29).

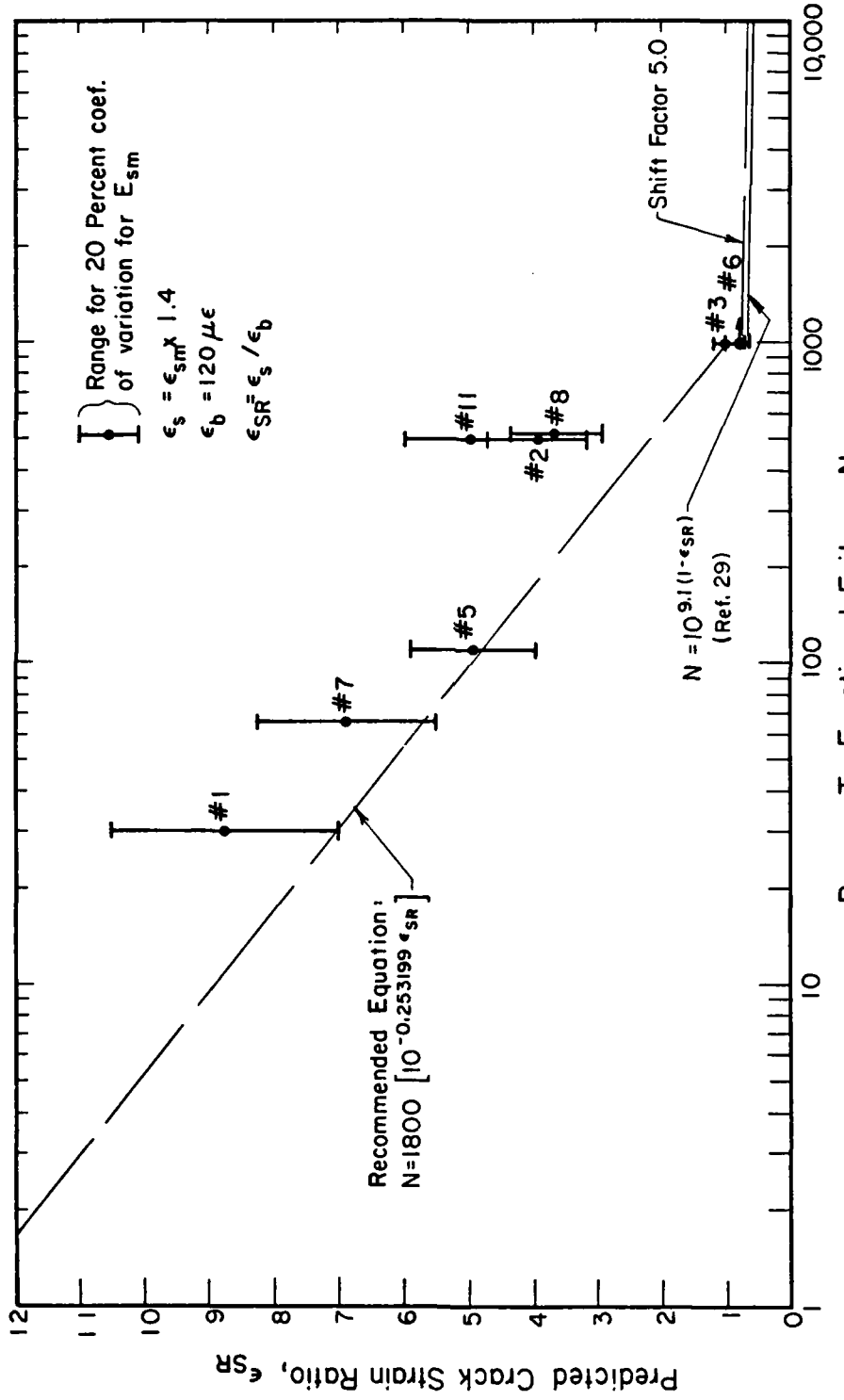

Figure 7-6. Transfer Function Relating Performance and Predicted First Pass Crack Strain Ratio in CAM Layer, Two-Layer Pavement Items

c. Deflection

Figure 7-7 shows the relationship between F-4 interior load DO deflection and radial tensile strain at the bottom of the stabilized material layer in a two-layer item. For a given thickness, the relationship is linear. Therefore, a transfer function relating deflection and performance will give the same results as strain and performance.

d. Comments on Transfer Functions

The transfer functions for stress ratios and strain ratios greater than one are largely influenced by subgrade suppo. . The slope of the transfer function will vary depending on the subgrade resilient behavior and strength. The transfer functions developed above are for a stress dependent cohesive clay subgrade of a CBR 5-6. A transfer function for a soft subgrade, CBR 3-4, will have a steeper slope. A stiff subgrade will have a more shallow slope. The exact relationship between subgrade support and the slope of the transfer function cannot be determined from available data.

4. Ultimate Load and Performance

Barenberg (Reference 39) indicated that if the predicted Meyerhof edge collapse load of a pavement is from 1.5 to 2.0 times the applied wheel load, good pavement performance will result. Of the two-layer items, only item 6 had a predicted Meyerhof edge collapse load twice the applied F-4 wheel load of 27 kips. Item 6 had excellent performance and did not experience functional failure during the 1000 passes of the F-4 load cart.

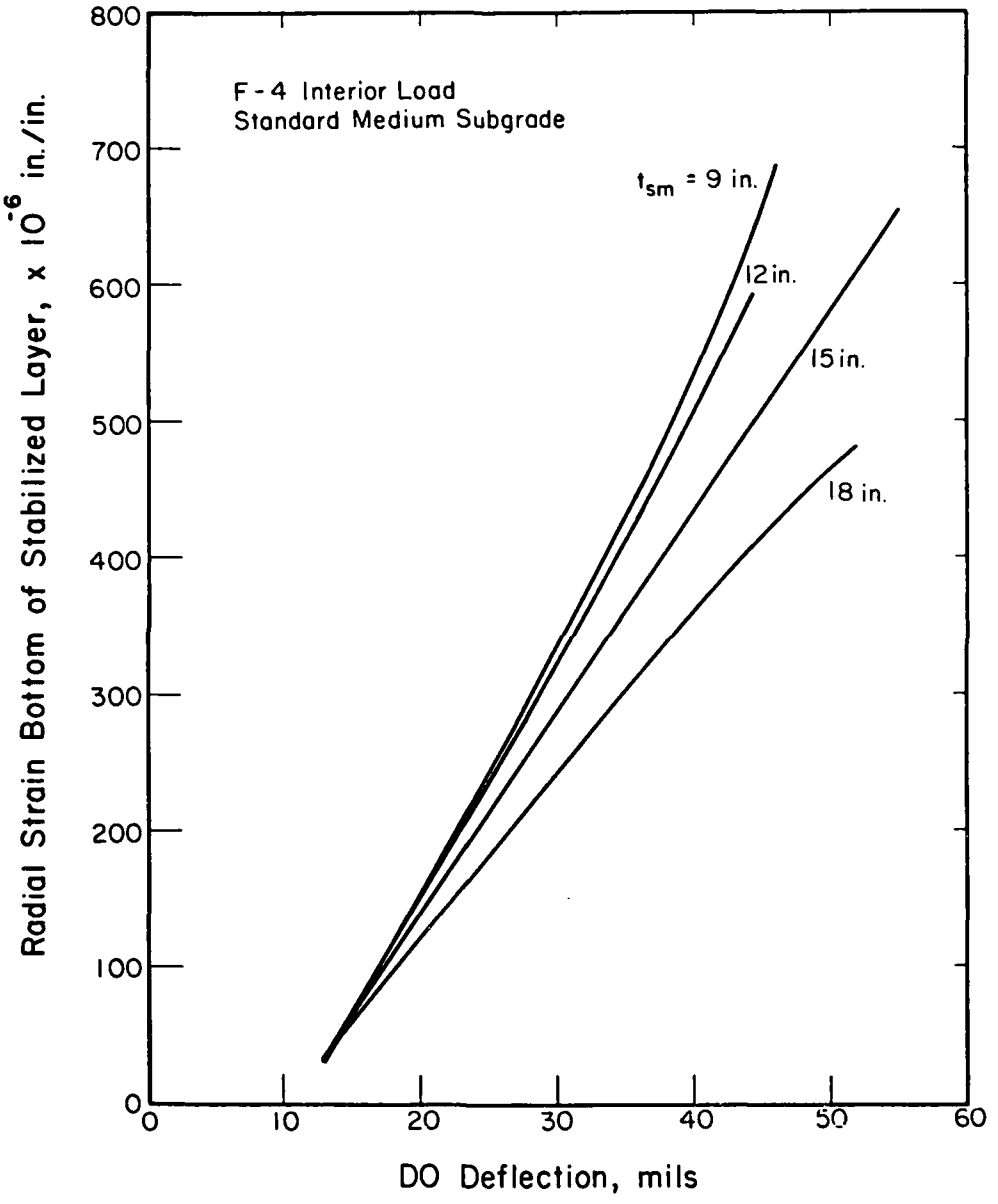

Figure 7-7. Relation of Strain in Stabilized Material Layer and DO Deflection, Two-Layer Pavements (F-4 ILLI-PAVE Data Base, Appendix C)

A study was conducted to determine the relationship between slab thickness, modulus, and strength for a predicted edge collapse load twice the 27 kip F-4 load. A standard medium subgrade (k = 150 psi/in.) was selected and a circular load radius of 5.7 inches was used to reflect radius of the F-4 load. Flexural strength was estimated from the slab modulus using equation 6-1.

The results of the study are presented in Figure 7-8. Comparison of this figure with Figure 7-4 shows an almost identical relationship between thickness, strength and modulus for a stress ratio of one and a predicted edge collapse load twice the 27 kip F-4 load. This explains why good performance can be expected from pavements that have a predicted Meyerhof edge collapse load twice the applied wheel load since the stress ratio for such a pavement structure is one or less.

D. INVERTED PAVEMENT ITEMS

1. Response

The predicted first pass stress ratios in the various layers of item 9 were greater than one. As explained earlier, although item 9 was designed as an inverted pavement, the modulus of the lime stabilized subbase course was considerably less than the crushed stone base course modulus. Analysis of the response of item 9, although beneficial for the study of overstressed low volume flexible pavements, is not meaningful for the study of inverted pavements and will not be included herein. The remainder of the discussion will concern item 10.

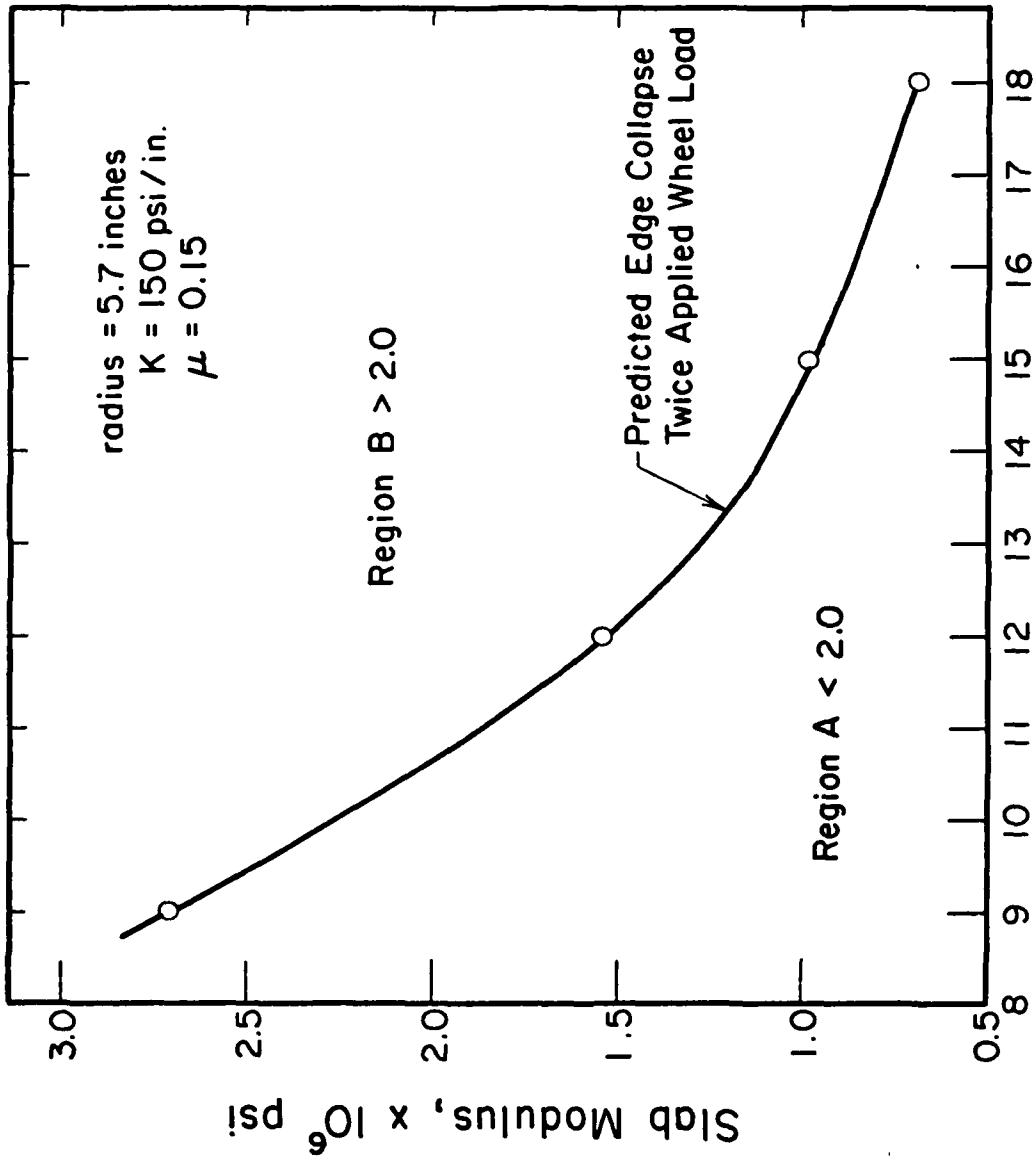

Figure 7-8. Combinations of Slab Modulus and Thickness for Predicted Edge Collapse Load Twice the 27 kip F-4 Wheel Load

The predicted first pass interior load flexural (tensile) strain at the bottom of the 1 inch asphalt concrete wearing course was 206 microstrain. Fatigue cracking of the asphalt concrete before 1000 passes will not occur at this strain level.

The predicted first pass interior load stress ratio at the mid-depth of the stone base course under the center of the load was 0.52. A stone base course stress ratio in this range will result in only minor densification over 1000 passes.

The predicted first pass interior load stress ratio in the CAM subbase course was 1.27. Cracking of the subbase occurred on the first pass of the F-4 load cart.

The effects of transverse shrinkage cracks in the CAM subbase course on structural response of the asphalt concrete, crushed stone base course, and subgrade cannot be accurately determined using structural models currently available (1984). Since too many assumptions must be made to determine crack response using the models currently available, interior load structural response parameters are used.

The effects of layer thickness, subgrade resilient modulus behavior and subgrade strength on interior load structural response is important since the presence of a crack in the stabilized material subbase only magnifies these effects. The F-4 ILLI-PAVE inverted pavement data base of Appendix E was used to determine the effects of stone base thickness, subbase thickness and subbase modulus on the structural response of inverted pavements with a 1 inch asphalt concrete wearing course (Chapter 6).

The thickness of the stabilized subbase course has a larger effect on the stress ratio in the subbase than does the thickness of the stone base course (Figure 6-10). For example, increasing the thickness of the stabilized subbase from 12 to 15 inches reduces the interior load stress ratio in the stabilized subbase from 0.95 to 0.62. By comparison, adding 1 inch of asphalt concrete wearing course and 8 inches of crushed stone base course reduces the stress ratio from 0.95 to 0.62. An inch of stabilized subbase is much more effective in reducing the stress ratio in the subbase than an inch of crushed stone base course. The stress ratio in the subbase should be controlled by the stabilized subbase thickness and not by the stone base course thickness.

Increasing the thickness of the stone base course from 4 to 8 inches has two detrimental effects. The modulus of the stone is a function of the confining pressure. The confining pressure at the mid-depth of the stone base course is reduced with increased thickness but the principal stress is not significantly reduced. Therefore, the stress ratio in the stone layer at mid-depth increases with increasing stone base thickness (Figure 6-7). The combination of reduced modulus and increased thickness of the stone base course results in increased surface deflection in the vicinity of the load. This reduces the radius of curvature in the asphalt concrete wearing course and increases flexural (tensile) strain (Figures 6-4, 6-5 and 6-6).

2. Performance

Item 9 experienced functional failure after only 150 passes of the F-4 load cart. The stone base course experienced shear failure

under the wheel load on the first pass and deep ruts developed rapidly as would be expected for stone stress ratios of one.

Item 10 experienced only minor rutting in the traffic lane after 1000 passes of the F-4 load cart. The predicted first pass interior load stress ratio in the stone base course was 0.52 and only minor plastic deformation would occur in 1000 passes at this stress ratio.

The effect of the 4 inch stone base course and 1 inch asphalt concrete wearing course was to inhibit the propagation of cracks in the stabilized subbase to the surface. The stone had a bridging effect at the cracks and reduced the rate of surface roughness accumulation. The effect of the 4 inch stone base course was significant for the CAP test since only 1000 passes were applied.

CHAPTER 8

REPORT FINDINGS AND IMPLICATIONS FOR CAP DESIGN AND ANALYSIS

The findings of this report are pertinent to both the design and evaluation of contingency airfield pavements (CAPs) containing stabilized material layers for fighter aircraft with single tire main gears. Although the CAP field test was conducted under restrictive conditions, the use of the mechanistic approach during analysis allowed the extrapolation of the findings beyond the test conditions. The primary emphasis of this report is the validation of the mechanistic design approach. However, the design and evaluation processes are similar and the validated concepts of this report can be used in both processes.

A. TEST CONDITIONS

The report findings contained herein are based on observations and analyses of 11 CAP items tested under the following conditions:

1. Test items were rigid type pavements containing stabilized material layers. The items were thin by conventional design standards and over stressed (initial pass crack stress ratio greater than one).
2. Subgrade was a stress dependent (stress softening) cohesive soil of CBR 5-6.
3. Item distress that developed after formation of the transverse shrinkage cracks was load related. There was no long term environmental related distress.

4. The F-4 aircraft has two main gears, each with one tire. The two main gear on the F-4 are spaced far enough apart so the pavement response under one is not affected by the other. One F-4 main gear tire was used in trafficking the items. The wheel load was 27 kips with a tire pressure of 265 psi.
5. Traffic was applied at a steady moving speed of approximately 15 mph. Dynamic response (bouncing) of the wheel load was minimal. Traffic was channelized and located at least 4 feet from a longitudinal construction joint.
6. Item functional failure was defined by the "general smoothness criteria" of the F-4 aircraft (Chapter 4). Item functional failure occurred in 9 of the 11 test items at 1000 passes or less.

B. REPORT FINDINGS

The following report findings apply to both two-layer and inverted contingency airfield pavements (CAPs) containing a stabilized material layer as the primary load carrying pavement course.

1. The mechanistic approach to the design and analysis of CAPs containing stabilized material layers is validated. Important pavement section parameters affecting response and performance can be identified and performance predicted using appropriate transfer functions.
2. Critical pavement response occurred at a transverse shrinkage crack. A crack load transfer efficiency (LTE) of 30 percent is typical of field conditions. Increasing the interior

flexural (tensile) stress in the stabilized material layer by 50 percent is a good estimate of the crack tensile stress for a 30 percent LTE.

3. Performance is dominated by the thickness of the stabilized material layer. Strength of the stabilized material for pavements with a stress ratio greater than one does not have a major effect on performance.

4. The design of CAPs for passes to functional failure of 1000 or less should be based upon an intact slab analysis where the predicted first pass crack stress ratio is less than one. The relationship between thickness, modulus, strength, LTE and subgrade strength in partially cracked stabilized material layers is too complex to model.

The following report findings apply to two-layer CAP pavements containing a rigid stabilized material layer:

1. CAPs with an applied wheel load induced predicted crack stress ratio greater than one, but the load being less than twice the predicted Meyerhof edge collapse load, have "reserve performance capability" and will give acceptable performance for a limited number of passes. The lower the predicted stress ratio the better the performance.

2. Conservative transfer functions were developed relating predicted first pass crack stress or strain ratios to pavement performance.

   a. The transfer functions were developed for stress and strain ratios greater than one, F-4 aircraft loading and cohesive soil subgrades of CBR 5-6.

b. Transfer functions developed using stress and strain ratios greater than one do not give the same strength, modulus, thickness and performance relationships. This is not unexpected since the relationship between the parameters affecting crack propagation and performance in a cracked pavement is very complex. However, both transfer functions predict 1000 passes to functional failure for first pass crack stress or strain ratios near one.

c. The transfer functions developed are more applicable for the analysis of CAPs than for design. Design of new CAPs should use a mechanistic approach and transfer functions based on stress ratios less than one and appropriate shift factors.

3. Distributed traffic will initiate many small cracks at the bottom of the stabilized layer in pavements with a predicted first pass crack stress ratio greater than one. The effect of these numerous cracks at the bottom of the stabilized material layer on structural response and performance cannot be determined. Therefore, for pavements with a predicted first pass crack stress ratio in the stabilized material layer greater than one, all traffic should be considered channelized in a single traffic lane.

4. The relationship of thickness, modulus and strength of the stabilized material layer for a predicted Meyerhof edge collapse load twice the applied wheel load of the F-4 is nearly identical to that required to produce a predicted first

pass crack stress ratio of one. Test items with a predicted Meyerhof edge collapse load twice the 27 kip F-4 load had good performance.

5. CAPs containing cement stabilized materials require a wearing course on the surface of the stabilized material to prevent tire abrasion. The wearing course need not provide additional load carrying capability.

The following report findings apply to inverted pavement CAPs containing a rigid stabilized material subbase course.

1. The thickness of the stone base course should be approximately 4 inches for thin asphalt concrete wearing courses (less than 1.5 inches). The maximum stress ratio in the stone base course occurs at mid-depth in the stone layer where the confining stress is the lowest. Increasing the stone base course thickness reduces confining stress at mid-depth producing a softer stone response, increased surface deflection, increased asphalt concrete strain, and increased permanent deformation in the stone layer.
2. The stress ratio in the stabilized material subbase course is affected more by the thickness of the subbase than by the thickness of the stone base course. An inch of subbase has a much greater effect on the subbase stress ratio than does an inch of stone base.
3. The crushed stone base course had a bridging effect across the cracks in the stabilized material subbase course. This bridging effect reduced the rate of crack propagation to the

surface of the item and resulted in better item performance for the same stabilized material stress ratio.

C. IMPLICATIONS FOR DESIGN AND EVALUATION OF CAPS

The findings in this report are applicable to both the design of new CAPs and the evaluation of existing pavements containing stabilized material layers as potential CAPs. The processes of design and evaluation are similar and include many of the same steps. In design, the strength, thickness and modulus of the stabilized material layer are not fixed but can be varied over a broad range to determine the most economical pavement structure. In evaluation, the strength, thickness and modulus of the stabilized material layers are determined/assumed based on existing conditions. In both, a mechanistic analysis of the resulting pavement structure is performed to determine the response parameters of interest (stress, strain and deflection). These are then used to predict performance through appropriate transfer functions.

The implications of the report findings for the design and evaluation of CAPs with stabilized material layers for low traffic volume single wheel main gear fighter aircraft are:

1. Base the analysis on an intact slab condition with only transverse shrinkage cracks and longitudinal construction joints. Locate longitudinal construction joints during design so the center of the main gear traffic pattern is at least 3-4 feet from a longitudinal joint.
2. Increase the ILLI-PAVE maximum predicted interior flexural (tensile) stress at the bottom of the stabilized layer

obtained in the analysis by 50 percent to estimate the maximum crack flexural (tensile) stress acting parallel to the transverse shrinkage crack.

3. Predict performance using available transfer functions for stabilized materials. In design, keep the crack stress ratio less than one, use the available transfer functions in Reference 8, and apply appropriate shift factors to estimate field performance. In evaluation, for calculated stress ratios greater than one, use the transfer functions developed in this report as a guide in predicting potential CAP field performance.
4. Check the mechanistically designed pavement section against the ultimate load criteria. Good performance is obtained for pavements with a Meyerhof predicted edge collapse load twice the applied wheel load. Adjust the pavement section properties so both the stress ratio and ultimate load criteria are met.
5. Select a design strength for the stabilized material that is economical and easy to obtain with conventional quality control procedures. Control the stress ratio in the stabilized material layer by varying the thickness of the stabilized material layer.
6. Design for a minimum of 1000 passes. The variability in performance is large for functional failures at less than 1000 passes.

An example of the application of these concepts for the design or evaluation of CAPs with stabilized material layers is shown in Figure 8-1. The F-4 ILLI-PAVE Data Base was used to determine the maximum interior flexural (tensile) stress at the bottom of the stabilized layer for a wide range of two-layer pavement sections. This stress was increased by 50 percent to estimate the crack flexural (tensile) stress. Equation 6-2 was used to estimate the flexural strength from the modulus of the stabilized material layer used in the ILLI-PAVE analysis. Performance was predicted using the transfer functions developed in Chapter 7 (Equation 7-1). Figure 8-1 relates slab thickness, stabilized material modulus and strength, and predicted performance.

D. CONCLUSIONS

The following conclusions summarize the major report findings and their implications for the design and evaluation of CAPs containing stabilized material layers.

1. The mechanistic approach to the design and evaluation of CAPs is valid. The response and performance of all 11 CAP field test items are explained using this concept.
2. Pavement structural response at transverse shrinkage cracks is the critical response and controls performance. The intact slab concept should be used for the design and evaluation of CAPs.
3. Subgrade behavior and strength controls performance in overstressed (stress ratio greater than one) CAPs containing stabilized material layers as the primary load carrying layer.

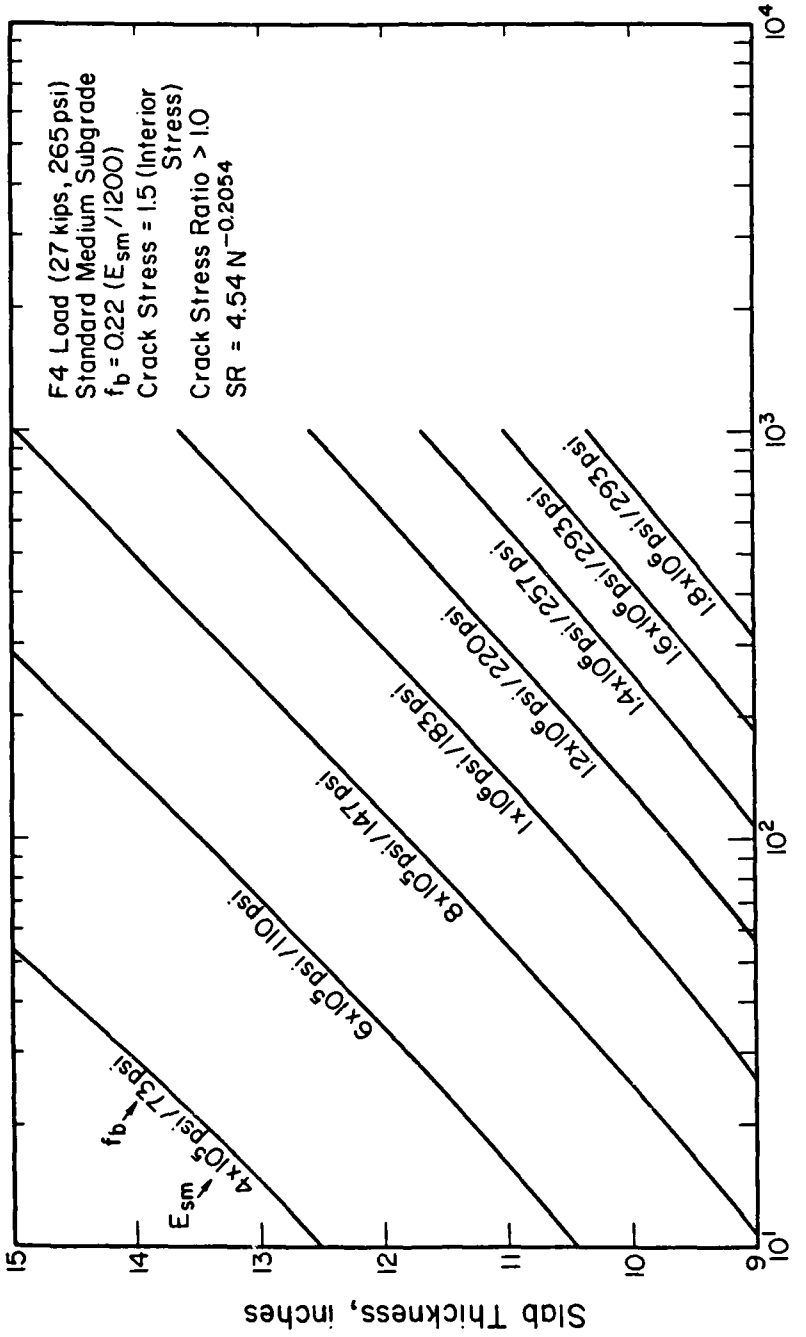

Figure 8-1. Performance as a Function of Slab Thickness, Modulus and Strength Using Stress Ratio Transfer Function (F-4 ILLI-PAVE Data Base, Appendix C)

4. The thickness effect is dominant and controls the performance of low volume CAPs.
5. CAPs should be designed for a crack stress ratio or strain ratio of less than one to ensure good performance for at least 1000 passes.
6. If thin asphalt wearing courses are used, the thickness of the crushed stone subbase course in an inverted pavement should be approximately 4 inches to keep deflections and asphalt tensile strains low. The thickness of the stabilized material subbase controls the stress in the stabilized material subbase course. The thickness of the crushed stone base course has little effect on the stress in the stabilized material subbase course.

APPENDIX A

DEFLECTION MEASUREMENTS

TABLE A-1. LVDT DEFLECTION AND DEFORMATION DATA, ITEMS 1, 2 AND 3

ITEM 1
TWO-LAYER CAM PAVEMENT

DEF. TOP OF SUBGRADE

PASS DEFLECTION		PERMANENT DEFORMATION	
PASS NO	DEF. (MILS)	PASS NO	DEF. (MILS)
1	30	1	10
2	110	3	28
3	120	4	35
4	130	6	49
5	140	11	80
6	140	20	132
8	120	30	257
9	150	40	698
12	150		
21	190		
31	250		
41	375		

ITEM 2
TWO-LAYER CAM PAVEMENT

DEF. TOP OF SUBGRADE

PASS DEFLECTION		PERMANENT DEFORMATION	
PASS NO	DEF. (MILS)	PASS NO	DEF. (MILS)
1	37	1	5
2	38	3	6
3	38	4	6
4	39	5	6
5	40	6	7
6	44	11	10
8	42	20	13
9	42	30	15
12	42	40	18
21	50	48	19
31	60	59	22
41	64	69	23
48	72	79	26
49	42	89	27
50	61	99	29
60	66	109	31
70	63	119	33
80	71	129	34
90	68	139	37
99	78	149	38
100	74	150	40
110	89	179	47
119	74	199	51
120	80	219	56
130	79	239	61
140	83	259	67
150	76	279	71
170	73	299	76
180	72	319	81
200	84	339	87
220	96	359	92
240	100	379	98
260	94	399	104
280	100	419	110
300	99	439	118
320	110	459	123
340	110	479	130
360	100	499	140
380	120	500	142
400	120	549	160
420	120	599	188
440	120	649	232
460	120		
480	130		
500	130		
550	150		
600	160		
650	180		

ITEM 3
TWO-LAYER CAM PAVEMENT

DEF. TOP OF SUBGRADE

PASS DEFLECTION		PERMANENT DEFORMATION	
PASS NO	DEF. (MILS)	PASS NO	DEF. (MILS)
1	26	1	4
2	25	3	5
3	26	4	6
4	26	5	5
5	26	6	7
6	27	11	7
8	31	20	10
9	28	30	10
12	34	40	13
21	30	48	13
31	31	59	14
41	31	69	15
48	36	79	15
49	32	89	15
50	33	99	15
60	35	109	16
70	35	119	17
80	36	129	17
90	38	139	17
100	39	149	18
110	39	179	26
120	41	199	27
130	42	219	29
140	38	239	28
150	35	259	28
180	36	279	30
200	40	299	31
220	42	319	31
240	42	339	32
280	41	359	31
300	42	379	32
340	46	399	33
380	48	419	33
400	46	439	33
420	46	459	33
480	48	479	33
500	43	499	35
550	48	549	37
600	50	599	40
650	50	649	38
700	52	699	40
750	54	749	42
800	52	799	42
850	52	849	43
900	54	899	44
950	53	949	45
1000	54	999	46

TABLE A-2. LVDT DEFLECTION AND DEFORMATION DATA, ITEMS 4, 5 AND 6

ITEM 4
TWO-LAYER CAM PAVEMENT

DEF. TOP OF SUBGRADE

PASS DEFLECTION		PERMANENT DEFORMATION	
PASS NO	DEF. (MILS)	PASS NO	DEF. (MILS)
1	802	1	505
4	260	3	600
		5	912
		6	860
		7	860
		8	1020

ITEM 5
TWO-LAYER CAM PAVEMENT

DEF. TOP OF SUBGRADE

PASS DEFLECTION		PERMANENT DEFORMATION	
PASS NO	DEF. (MILS)	PASS NO	DEF. (MILS)
1	62	1	12
2	52	3	15
3	57	4	16
4	58	5	16
5	64	6	21
6	68	11	29
8	68	20	41
9	66	30	55
12	70	40	68
21	72	48	78
31	80	59	93
41	83	69	105
47	84	79	120
48	94	89	137
49	66	99	154
50	70	109	182
60	99	119	212
70	98	129	249
80	99		
81	107		
84	120		
86	120		
88	110		
89	120		
99	110		
109	140		
115	140		
119	150		
125	150		
126	170		

ITEM 6
TWO-LAYER CAM PAVEMENT

DEF. TOP OF SUBGRADE

PASS DEFLECTION		PERMANENT DEFORMATION	
PASS NO	DEF. (MILS)	PASS NO	DEF. (MILS)
1	18	1	3
2	10	3	8
3	14	4	6
4	12	5	6
5	14	6	6
6	14	11	11
8	10	20	9
12	14	30	9
21	13	40	9
31	14	48	9
48	14	59	11
49	16	69	11
60	16	79	11
69	15	89	11
80	17	99	13
90	17	109	12
100	16	119	12
120	16	129	13
130	17	149	13
150	14	189	19
170	16	209	20
230	19	229	20
270	19	249	20
290	19	269	21
330	20	289	21
370	21	309	21
410	22	329	22
470	22	349	22
490	24	369	22
550	24	389	22
600	22	409	22
650	25	429	23
700	26	449	23
750	26	469	23
800	22	489	23
850	26	499	24
900	28	500	21
950	27	549	25
1000	27	599	25
		649	25
		699	25
		749	30
		799	31
		849	31
		899	31
		949	32
		999	34

TABLE A-3. LVDT DEFLECTION AND DEFORMATION DATA, ITEMS 7 AND 8

ITEM 7
TWO-LAYER CAM PAVEMENT

DEF. TOP OF SUBGRADE

PASS DEFLECTION		PERMANENT DEFORMATION	
PASS NO	DEF. (MILS)	PASS NO	DEF. (MILS)
1	77	1	15
3	80	6	24
4	84	11	32
5	87	23	43
6	87	29	52
12	100	36	65
24	120	40	73
37	140	48	90
49	140	55	110
66	155	65	156
76	235	75	240
		80	337
		90	430

ITEM 8
TWO-LAYER CAM PAVEMENT

DEF. TOP OF SUBGRADE

PASS DEFLECTION		PERMANENT DEFORMATION	
PASS NO	DEF. (MILS)	PASS NO	DEF. (MILS)
1	61	1	11
2	44	6	16
3	45	11	18
4	46	23	20
5	46	29	21
6	48	36	22
12	50	40	23
23	55	48	23
37	62	55	27
41	56	65	30
49	62	75	32
66	64	80	32
76	66	100	35
82	64	110	35
92	68	120	38
101	72	130	38
111	88	140	40
121	68	150	42
131	90	169	62
141	88	189	65
149	95	209	68
190	72	229	70
210	80	249	73
230	78	269	75
250	80	289	78
290	89	290	82
310	84	309	88
330	90	329	91
370	92	349	95
390	97	369	98
430	94	389	100
450	99	409	103
470	102	429	108
490	106	449	112
550	120	469	115
		489	119
		500	121
		540	129

TABLE A-4. LVDT DEFLECTION AND DEFORMATION DATA, ITEMS 9, 10 AND 11

ITEM 9
INVERTED PAVEMENT

DEFLECTION AT SURFACE

PASS DEFLECTION		PERMANENT DEFORMATION	
PASS NO	DEF. (MILS)	PASS NO	DEF. (MILS)
1	466	1	208
2	240	6	309
3	260	11	374
4	260	23	491
5	260	29	561
6	260	36	632
12	200	40	676
24	260	48	717
37	270	55	794
41	280	65	866
49	220	75	889
66	200	80	959
		90	1019
		100	1059
		110	1099
		120	1159
		130	1239
		140	1299
		150	1339

ITEM 10
INVERTED PAVEMENT

DEFLECTION AT SURFACE

PASS DEFLECTION		PERMANENT DEFORMATION	
PASS NO	DEF. (MILS)	PASS NO	DEF. (MILS)
1	167	1	39
2	105	6	68
3	100	11	83
4	75	23	100
5	80	29	114
6	90	36	120
12	110	40	115
24	110	48	135
37	120	55	144
41	120	65	153
66	120	75	166
81	130	80	160
101	140	90	173
111	110	100	118
131	90	110	186
141	80	120	192
150	140	130	188
170	120	140	207
189	130	150	212
230	140	169	247
290	140	189	252
330	120	209	258
390	140	229	267
430	160	249	275
600	160	269	283
650	140	289	291
700	150	290	306
750	160	329	314
800	160	349	322
850	160	369	326
900	150	389	334
950	160	409	342
1000	180	429	354
		449	362
		469	370
		489	380
		499	385
		500	382
		549	404
		599	430
		649	450
		699	483
		749	512
		799	536
		849	560
		899	580
		949	619
		999	679

ITEM 11
TWO-LAYER CAM PAVEMENT

DEFLECTION AT SURFACE

PASS DEFLECTION		PERMANENT DEFORMATION	
PASS NO	DEF. (MILS)	PASS NO	DEF. (MILS)
1	212	1	57
2	100	6	68
3	90	11	78
4	60	23	100
5	85	29	113
6	145	36	129
12	160	40	133
24	140	48	157
37	170	55	166
41	170	65	201
66	200	75	222
76	220	80	230
82	220	90	253
92	240	100	283
101	150	110	303
111	210	120	324
121	140	130	342
131	110	140	383
141	180	150	403
149	240	169	481
170	210	189	535
190	220	209	583
210	210	229	721
230	230	249	874

TABLE A-5. FWD LOAD-DEFLECTION DATA, ITEM 1

NON-DESTRUCTIVE TESTING DATA
FALLING WEIGHT DEFLECTOMETER

ITEM NO. 1

PASS NO	FWD LOAD LEVEL	STATION: 7.5 — 8.8" STABILIZED LAYER							STATION: 15.0 — 8.5" STABILIZED LAYER							STATION: 22.5 — 8.8" STABILIZED LAYER						
		(COR) D0	ACT. LOAD LEVEL	D0	D1	D2	D3	AREA	(COR) D0	ACT. LOAD LEVEL	D0	D1	D2	D3	AREA	(COR) D0	ACT. LOAD LEVEL	D0	D1	D2	D3	AREA
0	9	24.7	8.6	23.5	16.7	7.8	4.1	19.6	35.4	8.8	34.5	17.4	6.3	3.5	14.9	39.1	8.5	36.9	22.1	10.2	4.4	17.2
0	15	67.1	14.3	64.0	39.2	15.2	7.2	16.9	35.3	13.7	32.3	20.4	10.4	6.0	18.6	83.4	14.2	79.1	35.0	22.2	7.2	15.2
48	9	57.4	8.1	51.6	23.6	5.6	3.4	13.2	0.0	0.0	0.0	0.0	0.0	0.0	0.0	72.8	8.1	65.2	24.2	5.4	3.5	11.8
48	15	104.1	13.2	91.3	41.3	10.4	5.8	13.2	0.0	0.0	0.0	0.0	0.0	0.0	0.0	108.3	13.1	94.3	44.9	9.4	5.8	13.3

NOTES: LOAD IN KIPS, DEFL IN MILS, AREA IN INCHES

IF D0 EQUALS 0 0, FWD NOT CONDUCTED.

CORRECTED D0 IS ACTUAL D0 CORRECTED TO FWD LOAD LEVEL OF 9 OR 15 KIPS.

AREA=6*(1+2(D1/D0)+2(D2/D0)+(D3/D0)),

TABLE A-6. FWD LOAD-DEFLECTION DATA, ITEM 2

NON-DESTRUCTIVE TESTING DATA
FALLING WEIGHT DEFLECTOMETER

ITEM NO. 2

PASS NO	FWD LOAD LEVEL	STATION: 42.5 — 13.2" STABILIZED LAYER (COR) DO	ACT. LOAD LEVEL	DO	D1	D2	D3	AREA	STATION: 50.0 — 12.2" STABILIZED LAYER (COR) DO	ACT. LOAD LEVEL	DO	D1	D2	D3	AREA	STATION: 57.5 — 12.4" STABILIZED LAYER (COR) DO	ACT. LOAD LEVEL	DO	D1	D2	D3	AREA
0	9	13.6	8.8	13.4	8.8	4.9	3.5	19.8	14.7	8.9	14.5	7.6	5.5	2.9	18.0	17.9	9.1	18.0	11.2	5.8	3.7	18.6
0	15	18.1	14.4	17.4	10.7	7.8	5.7	20.7	14.5	14.0	13.5	10.1	7.5	5.8	24.2	22.3	14.4	21.4	14.1	8.0	5.8	20.0
48	9	26.6	8.2	24.3	14.0	5.7	3.2	16.5	24.0	8.4	22.4	13.1	5.8	3.5	17.1	32.2	8.2	29.4	17.4	6.7	3.5	16.6
48	15	45.6	13.5	41.3	23.7	10.1	5.4	16.6	36.7	13.9	34.0	19.3	9.5	5.8	17.2	52.4	13.4	46.9	29.9	11.7	6.5	17.5
150	9	36.8	8.9	36.3	28.5	6.7	2.8	18.1	33.6	8.8	32.9	13.1	6.3	3.6	13.7	49.0	8.8	48.0	19.8	8.9	3.9	13.7
150	15	55.0	14.5	53.2	26.1	11.5	5.6	15.1	52.4	14.6	51.2	22.8	10.5	6.3	14.5	69.6	14.4	66.9	33.2	14.9	7.0	15.3
500	9	50.0	8.5	47.2	19.6	6.4	3.6	13.1	45.8	8.6	43.7	18.9	5.4	3.6	13.2	59.9	8.6	57.1	24.9	6.6	4.5	13.1
500	15	82.1	14.0	76.4	37.2	11.0	5.7	14.0	75.1	14.1	70.5	31.0	9.0	5.7	13.3	92.5	13.9	85.4	41.3	12.0	6.6	14.0

NOTES: LOAD IN KIPS, DEFL IN MILS, AREA IN INCHES

IF DO EQUALS 0.0, FWD NOT CONDUCTED.

CORRECTED DO IS ACTUAL DO CORRECTED TO FWD LOAD LEVEL OF 9 OR 15 KIPS.

AREA=6*(1+2(D1/D0)+2(D2/D0)+(D3/D0)),

TABLE A-7. FWD LOAD-DEFLECTION DATA, ITEM 3

NON-DESTRUCTIVE TESTING DATA
FALLING WEIGHT DEFLECTOMETER

ITEM NO. 3

PASS NO	FWD LOAD LEVEL	STATION: 77.5 16.4" STABILIZED LAYER (COR) DO	ACT LOAD LEVEL	DO	D1	D2	D3	AREA	STATION: 85.0 16.6" STABILIZED LAYER (COR) DO	ACT. LOAD LEVEL	DO	D1	D2	D3	AREA	STATION: 92.5 16.1" STABILIZED LAYER (COR) DO	ACT. LOAD LEVEL	DO	D1	D2	D3	AREA
0	9	7.4	9.1	7.5	5.6	3.8	2.7	23.2	11.2	9.2	11.4	10.2	2.6	2.3	20.7	9.0	9.2	9.2	5.5	3.8	2.8	20.0
0	15	9.2	14.8	9.1	7.1	5.7	4.4	25.8	18.1	15.1	18.2	16.2	10.2	3.9	24.7	10.5	14.8	10.4	8.0	6.1	4.7	25.0
48	9	11.0	8.3	10.2	8.1	4.1	2.6	21.9	15.9	8.4	14.8	11.5	3.5	2.6	19.2	10.7	8.3	9.9	5.7	3.7	2.7	19.0
48	15	18.5	13.9	17.1	13.4	7.1	4.3	21.9	28.4	14.0	26.4	21.0	5.9	4.2	19.2	18.4	14.0	17.1	10.3	6.5	4.5	19.4
150	9	13.8	9.0	13.8	8.7	4.6	2.6	18.7	20.9	9.3	21.5	4.5	3.6	2.4	11.2	14.1	9.1	14.2	6.6	4.1	2.5	16.1
150	15	21.9	15.1	22.1	14.5	8.1	4.3	19.4	30.1	15.2	30.6	9.0	6.1	4.3	12.8	25.9	15.4	26.6	10.2	7.4	4.8	15.0
500	9	18.3	8.7	17.6	12.1	4.6	2.8	18.3	21.3	8.8	20.9	15.8	4.2	3.1	18.4	17.9	8.8	17.5	8.4	4.7	3.0	16.0
500	15	30.2	14.4	28.9	20.6	9.0	4.8	19.3	35.9	14.5	34.8	25.8	7.6	5.1	18.4	28.1	14.7	27.6	16.2	8.3	5.3	17.8
750	9	0.0	0.0	0.0	0.0	0.0	0.0	0.0	25.1	8.7	24.2	14.6	5.3	3.2	16.7	22.7	8.9	22.4	9.6	4.8	3.2	14.6
750	15	0.0	0.0	0.0	0.0	0.0	0.0	0.0	39.1	14.3	37.3	24.7	10.0	5.2	18.0	34.1	14.4	32.8	18.2	8.2	5.7	16.7

NOTES: LOAD IN KIPS, DEFL IN MILS, AREA IN INCHES

IF DO EQUALS 0.0, FWD NOT CONDUCTED.

CORRECTED DO IS ACTUAL DO CORRECTED TO FWD LOAD LEVEL OF 9 OR 15 KIPS.

AREA=6*(1+2(D1/D0)+2(D2/D0)+(D3/D0)),

TABLE A-8. FWD LOAD-DEFLECTION DATA, ITEM 4

NON-DESTRUCTIVE TESTING DATA
FALLING WEIGHT DEFLECTOMETER

ITEM NO. 4

		STATION: 127.5							STATION: 135.0							STATION: 142.5						
		8.3" STABILIZED LAYER							7.6" STABILIZED LAYER							7.8" STABILIZED LAYER						
PASS NO	FWD LOAD LEVEL	(COR) D0	ACT. LOAD LEVEL	D0	D1	D2	D3	AREA	(COR) D0	ACT. LOAD LEVEL	D0	D1	D2	D3	AREA	(COR) D0	ACT. LOAD LEVEL	D0	D1	D2	D3	AREA
0	9	54.4	8.2	49.4	20.0	7.1	3.9	13.1	40.8	8.5	38.4	18.5	8.0	4.2	14.9	68.7	4.6	35.2	13.4	3.9	2.0	12.2
0	15	39.8	14.5	38.5	25.0	14.3	7.2	19.4	106.4	12.8	90.9	34.4	6.3	5.5	11.7	27.5	14.3	26.2	16.9	9.2	5.4	19.2

NOTES: LOAD IN KIPS, DEFL IN MILS, AREA IN INCHES

IF D0 EQUALS 0.0, FWD NOT CONDUCTED.

CORRECTED D0 IS ACTUAL D0 CORRECTED TO FWD LOAD LEVEL OF 9 OR 15 KIPS.

AREA=6*(1+2(D1/D0)+2(D2/D0)+(D3/D0)),

TABLE A-9. FWD LOAD-DEFLECTION DATA, ITEM 5

NON-DESTRUCTIVE TESTING DATA
FALLING WEIGHT DEFLECTOMETER

ITEM NO. 5

		STATION: 162.5							STATION: 170.0							STATION: 177.5						
		12.6" STABILIZED LAYER							11.9" STABILIZED LAYER							10.9" STABILIZED LAYER						
PASS NO	FWD LOAD LEVEL	(COR) D0	ACT. LOAD LEVEL	D0	D1	D2	D3	AREA	(COR) D0	ACT. LOAD LEVEL	D0	D1	D2	D3	AREA	(COR) D0	ACT. LOAD LEVEL	D0	D1	D2	D3	AREA
0	9	12.9	8.3	12.0	8.4	5.4	3.6	21.6	14.5	8.2	13.3	9.5	5.0	3.3	20.6	18.5	8.4	17.2	11.1	6.0	3.2	19.0
0	15	18.7	15.0	18.7	13.4	8.9	6.3	22.3	16.2	14.0	15.1	10.9	7.9	5.5	23.1	27.9	13.7	25.4	15.7	9.2	6.2	19.2
48	9	33.1	8.3	30.4	16.3	6.9	3.8	15.9	31.8	8.3	29.3	16.6	5.8	3.4	15.9	41.9	8.3	38.6	20.9	7.0	3.4	15.2
48	15	56.7	13.6	51.6	28.1	12.2	6.5	16.1	42.8	14.2	40.4	25.6	10.3	5.6	17.5	71.0	13.6	64.1	34.8	12.4	6.5	15.4
127	9	48.5	9.3	50.0	13.1	6.2	3.7	11.1	63.9	9.0	64.2	18.8	6.7	3.7	11.1	0.0	0.0	0.0	0.0	0.0	0.0	0.0
127	15	0.0	0.0	0.0	0.0	0.0	0.0	0.0	0.0	0.0	0.0	0.0	0.0	0.0	0.0	0.0	0.0	0.0	0.0	0.0	0.0	0.0

NOTES: LOAD IN KIPS, DEFL IN MILS, AREA IN INCHES

IF D0 EQUALS 0.0, FWD NOT CONDUCTED.

CORRECTED D0 IS ACTUAL D0 CORRECTED TO FWD LOAD LEVEL OF 9 OR 15 KIPS.

AREA=6*(1+2(D1/D0)+2(D2/D0)+(D3/D0)),

TABLE A-10. FWD LOAD-DEFLECTION DATA, ITEM 6

NON-DESTRUCTIVE TESTING DATA
FALLING WEIGHT DEFLECTOMETER

ITEM NO. 6

		STATION: 197.5							STATION: 205.0							STATION: 212.5						
		16.7" STABILIZED LAYER							16.2" STABILIZED LAYER							17.0" STABILIZED LAYER						
PASS NO	FWD LOAD LEVEL	(COR) DO	ACT. LOAD LEVEL	D0	D1	D2	D3	AREA	(COR) DO	ACT. LOAD LEVEL	D0	D1	D2	D3	AREA	(COR) DO	ACT. LOAD LEVEL	D0	D1	D2	D3	AREA
0	9	5.7	8.3	5.3	4.6	3.7	2.9	28.1	5.3	8.4	5.0	4.8	3.8	2.8	30.0	5.8	8.5	5.4	4.8	4.3	3.8	30.4
0	15	9.8	14.0	9.1	6.7	5.4	4.3	24.8	8.3	14.0	7.8	6.7	5.6	4.5	28.4	8.2	14.0	7.7	6.8	6.3	5.5	30.7
48	9	8.5	8.5	8.0	6.0	4.4	3.5	24.2	6.9	8.5	6.5	5.2	4.7	3.5	27.5	8.5	8.7	8.2	7.4	4.9	4.1	27.0
48	15	14.5	14.1	13.7	9.8	7.5	5.4	23.5	11.8	14.3	11.2	8.9	7.0	5.4	25.9	14.2	14.4	13.6	11.8	8.4	7.5	27.1
150	9	8.4	8.5	7.9	5.6	4.5	2.8	23.5	7.7	8.7	7.4	5.3	4.4	3.0	24.2	10.3	8.5	9.7	6.7	5.6	3.7	23.5
150	15	13.8	14.1	13.0	9.2	7.6	4.9	23.8	12.9	14.2	12.2	9.1	7.4	5.3	24.8	16.3	14.2	15.4	12.8	9.3	7.3	26.1
500	9	11.4	8.8	11.2	7.1	5.0	3.4	20.8	10.5	8.9	10.3	7.1	5.0	3.5	22.1	12.8	9.2	13.1	9.7	5.8	4.5	22.3
500	15	18.8	14.7	18.5	12.3	8.4	5.6	21.2	16.4	14.9	16.3	12.1	8.4	6.1	23.3	21.3	15.1	21.5	16.1	10.2	8.1	22.9
750	9	18.3	8.9	18.1	8.9	5.6	3.1	16.6	17.3	8.8	17.0	8.7	5.6	3.5	17.3	17.6	8.9	17.4	11.3	7.7	6.7	21.4
750	15	0.0	0.0	0.0	0.0	0.0	0.0	0.0	26.7	14.6	25.9	14.6	9.5	5.8	18.5	27.5	14.6	26.9	20.5	13.6	10.3	23.5
1000	9	12.4	8.5	11.7	7.5	4.9	3.7	20.6	13.5	8.6	12.8	8.1	5.4	3.7	20.3	13.9	8.6	13.3	10.8	6.0	3.5	22.7
1000	15	20.4	14.1	19.2	12.5	8.2	5.3	20.6	16.7	14.4	16.0	13.1	8.9	5.8	24.7	23.0	14.5	22.2	17.6	14.4	7.8	25.4

NOTES: LOAD IN KIPS, DEFL IN MILS, AREA IN INCHES

IF DO EQUALS 0.0, FWD NOT CONDUCTED.

CORRECTED DO IS ACTUAL DO CORRECTED TO FWD LOAD LEVEL OF 9 OR 15 KIPS.

AREA=6*(1+2(D1/D0)+2(D2/D0)+(D3/D0)),

TABLE A-11. FWD LOAD-DEFLECTION DATA, ITEM 7

NON-DESTRUCTIVE TESTING DATA
FALLING WEIGHT DEFLECTOMETER

ITEM NO. 7

PASS NO	FWD LOAD LEVEL	STATION: 7.5 — 8.0" STABILIZED LAYER								STATION: 15.0 — 8.4" STABILIZED LAYER								STATION: 22.5 — 9.1" STABILIZED LAYER							
		(COR) D0	ACT. LOAD LEVEL	D0	D1	D2	D3	AREA		(COR) D0	ACT. LOAD LEVEL	D0	D1	D2	D3	AREA		(COR) D0	ACT. LOAD LEVEL	D0	D1	D2	D3	AREA	
0	9	18.2	8.3	16.8	8.9	5.3	3.6	17.4		16.3	8.3	15.1	9.8	6.0	4.0	20.1		13.9	8.3	12.9	9.6	6.3	4.2	22.7	
0	15	33.2	13.8	30.6	16.2	9.5	6.3	17.3		25.1	13.9	23.2	15.6	10.1	6.7	21.0		21.9	14.2	20.7	15.0	10.8	7.3	23.1	
48	9	41.9	8.6	40.2	14.2	5.9	4.0	12.6		35.4	8.8	34.7	18.5	7.8	4.3	15.8		43.2	8.7	41.7	20.7	7.9	4.5	14.9	
48	15	73.5	14.1	68.9	26.7	9.9	6.3	12.9		57.8	14.3	55.1	20.5	12.2	7.0	13.9		73.5	14.1	69.3	36.0	14.1	8.4	15.4	

NOTES: LOAD IN KIPS, DEFL IN MILS, AREA IN INCHES

IF D0 EQUALS 0.0, FWD NOT CONDUCTED.

CORRECTED D0 IS ACTUAL D0 CORRECTED TO FWD LOAD LEVEL OF 9 OR 15 KIPS.

AREA=6*(1+2(D1/D0)+2(D2/D0)+(D3/D0)),

TABLE A-12. FWD LOAD-DEFLECTION DATA, ITEM 8

NON-DESTRUCTIVE TESTING DATA
FALLING WEIGHT DEFLECTOMETER

ITEM NO. 8

		STATION: 42.5							STATION: 50.0							STATION: 57.5						
		10.7" STABILIZED LAYER							11.6" STABILIZED LAYER							12.7" STABILIZED LAYER						
PASS NO	FWD LOAD LEVEL	(COR) D0	ACT. LOAD LEVEL	D0	D1	D2	D3	AREA	(COR) D0	ACT. LOAD LEVEL	D0	D1	D2	D3	AREA	(COR) D0	ACT. LOAD LEVEL	D0	D1	D2	D3	AREA
0	9	15.7	8.5	14.8	9.1	6.3	4.2	20.2	11.1	8.7	10.7	8.6	6.2	4.1	24.9	10.5	8.6	10.0	8.2	5.4	3.9	24.7
0	15	21.3	14.1	20.0	15.0	10.3	6.9	23 3	19.4	13.9	18.0	13.8	9.7	6.8	23.9	15.9	14.4	15.2	12.5	9.3	6.6	25.8
48	9	27.2	8.9	27.0	17.2	8.9	4.9	18.7	22.6	9.1	22.8	15.6	8.0	5.0	19.7	18.7	9.0	18.8	12.8	7.8	5.1	20.8
48	15	45.6	14.5	44.1	29.5	15.0	8.6	19.3	34.4	14.6	33.5	10.6	13.7	9.8	16.5	30.6	14.9	30.5	21.1	13.6	8.5	21.3
150	9	38.5	8.0	34.3	13.7	7.7	3.8	14.2	28.0	8.1	25.1	13.3	7.7	4.0	17.0	30.2	8.1	27.2	11.1	7.4	4.1	15.1
150	15	61.9	13.3	55.1	24.9	21.8	6.6	16.9	41.1	13.8	37.7	25.2	13.7	7.8	19.6	43.8	13.5	39.4	20.8	12.9	7.4	17.4
500	9	50.6	8.1	45.7	16.4	6.0	4.6	12.5	37.8	8.4	35.4	18.7	0.0	4.4	13.1	34.0	8.3	31.3	16.7	8.4	4.8	16.5
500	15	86.9	13.3	76.8	12.4	10.6	7.1	10.1	61.7	13.6	55.9	33.1	13.3	7.4	16.8	54.5	13.7	49.6	28.8	13.1	8.2	17.1
550	9	0.0	0.0	0.0	0.0	0.0	0.0	0.0	38.7	8.2	35.1	19.3	4.9	4.5	15.0	31.9	8.2	29.1	15.4	7.4	4.4	16.3
550	15	0.0	0.0	0.0	0.0	0.0	0.0	0.0	64.2	13.5	57.9	34.7	14.6	7.7	17.0	53.6	13.7	48.8	28.2	12.8	7.6	17.0

NOTES: LOAD IN KIPS, DEFL IN MILS, AREA IN INCHES

IF D0 EQUALS 0.0, FWD NOT CONDUCTED.

CORRECTED D0 IS ACTUAL D0 CORRECTED TO FWD LOAD LEVEL OF 9 OR 15 KIPS.

AREA=6*(1+2(D1/D0)+2(D2/D0)+(D3/D0)),

TABLE A-13. FWD LOAD-DEFLECTION DATA, ITEM 9

NON-DESTRUCTIVE TESTING DATA
FALLING WEIGHT DEFLECTOMETER

ITEM NO. 9

PASS NO	FWD LOAD LEVEL	STATION: 92.5 (COR) D0	ACT. LOAD LEVEL	D0	D1	D2	D3	AREA	STATION: 100.0 (COR) D0	ACT. LOAD LEVEL	D0	D1	D2	D3	AREA	STATION: 107.5 (COR) D0	ACT. LOAD LEVEL	D0	D1	D2	D3	AREA
		1.7" AC, 3.7" STONE, 13.2" STAB. LAYER							1.4" AC, 3.7" STONE, 12.9" STAB. LAYER							1.1" AC, 3.4" STONE, 12.8" STAB. LAYER						
0	9	23.5	8.6	22.4	12.5	6.3	3.7	17.1	26.0	8.4	24.3	12.7	6.4	3.9	16.4	25.9	8.5	24.3	12.7	6.2	4.2	16.4
0	15	39.3	13.8	36.2	21.2	10.8	6.6	17.7	46.1	15.0	46.1	23.4	11.2	6.9	15.9	40.0	14.1	37.5	20.1	10.0	6.7	16.7
48	9	27.9	8.2	25.5	14.7	6.9	4.3	17.2	25.6	8.1	23.0	14.7	7.8	4.8	19.0	35.5	8.2	32.5	15.8	8.9	5.0	16.0
48	15	54.5	13.4	48.8	26.4	12.4	7.3	16.4	62.1	14.4	59.5	28.2	14.3	8.2	15.4	64.8	13.5	58.3	28.9	15.3	8.7	16.0
150	9	30.8	9.1	27.7	9.3	7.4	3.7	14.0	32.2	8.1	28.9	12.6	8.5	4.0	15.6	32.7	8.1	29.5	14.2	9.0	4.5	16.4
150	15	53.2	13.4	47.6	22.7	13.1	6.7	15.9	60.9	13.3	53.9	25.4	15.1	7.3	15.8	57.8	13.3	51.2	26.4	16.1	7.9	16.9

NOTES: LOAD IN KIPS, DEFL IN MILS, AREA IN INCHES

IF D0 EQUALS 0.0, FWD NOT CONDUCTED.

CORRECTED D0 IS ACTUAL D0 CORRECTED TO FWD LOAD LEVEL OF 9 OR 15 KIPS.

AREA=6*(1+2(D1/D0)+2(D2/D0)+(D3/D0)),

TABLE A-14. FWD LOAD-DEFLECTION DATA, ITEM 10

NON-DESTRUCTIVE TESTING DATA
FALLING WEIGHT DEFLECTOMETER

ITEM NO. 10

PASS NO	FWD LOAD LEVEL	STATION: 127.5 .8" AC, 4.0" STONE, 11.2" STAB. LAYER (COR) DO	ACT. LOAD LEVEL	DO	D1	D2	D3	AREA	STATION: 135.0 .9" AC, 3.9" STONE, 11.0" STAB. LAYER (COR) DO	ACT. LOAD LEVEL	DO	D1	D2	D3	AREA	STATION: 142.5 1.3" AC, 3.4" STONE, 11.0" STAB. LAYER (COR) DO	ACT. LOAD LEVEL	DO	D1	D2	D3	AREA
0	9	16.0	8.6	15.4	9.5	5.2	3.3	18.7	27.8	9.2	28.4	10.9	6.9	3.5	14.3	15.8	8.7	15.3	9.6	5.1	3.1	18.7
0	15	29.1	14.1	27.3	17.5	9.5	5.7	19.1	29.8	14.2	28.2	18.1	10.0	5.8	19.2	27.4	14.3	26.1	16.9	9.2	5.4	19.2
48	9	17.5	9.6	18.7	10.9	5.7	3.4	17.7	17.7	9.8	19.3	10.3	5.9	3.5	17.2	17.7	9.8	19.2	10.8	5.6	3.4	17.3
48	15	33.4	13.7	30.6	17.8	9.7	5.9	17.9	47.9	14.9	47.4	20.1	11.1	6.2	14.7	34.5	13.9	31.9	19.4	9.5	5.6	17.9
150	9	20.2	8.2	18.4	8.8	5.6	2.9	16.3	21.5	8.2	19.5	9.6	6.1	3.1	16.6	21.2	8.2	19.3	9.3	5.6	2.9	16.2
150	15	32.5	13.6	29.4	16.1	9.7	5.2	17.6	35.2	13.6	31.9	16.6	10.9	5.3	17.3	34.9	13.6	31.6	17.4	9.9	5.2	17.4
500	9	20.5	8.3	19.0	11.6	5.4	3.5	17.8	18.4	8.2	16.8	11.8	5.8	3.3	19.8	23.8	8.4	22.1	13.2	5.6	3.3	17.1
500	15	33.6	13.9	31.0	20.0	9.8	5.9	18.7	32.2	13.8	29.7	21.1	10.4	5.8	19.9	39.2	13.8	36.1	22.7	10.4	5.8	18.0
750	9	20.7	8.4	19.3	12.4	5.4	3.4	18.1	16.9	8.3	15.7	12.4	5.7	3.4	21.1	23.6	8.5	22.2	13.4	5.7	3.5	17.3
750	15	34.2	13.8	31.5	21.1	9.8	5.6	18.8	30.6	13.9	28.3	21.9	10.1	5.6	20.8	38.8	13.9	36.0	23.0	10.5	5.9	18.2
1000	9	22.7	8.2	20.8	12.9	6.0	3.7	18.0	15.6	8.3	14.3	13.8	6.7	3.8	24.8	26.5	8.5	24.9	16.0	6.7	3.7	17.8
1000	15	38.5	13.7	35.2	22.7	11.1	6.4	18.6	31.1	13.8	28.7	24.4	13.1	6.7	23.1	44.7	13.7	41.0	26.8	12.2	6.6	18.4

NOTES: LOAD IN KIPS, DEFL IN MILS, AREA IN INCHES

IF DO EQUALS 0.0, FWD NOT CONDUCTED.

CORRECTED DO IS ACTUAL DO CORRECTED TO FWD LOAD LEVEL OF 9 OR 15 KIPS.

AREA=6*(1+2(D1/D0)+2(D2/D0)+(D3/D0)),

TABLE A-15. FWD LOAD-DEFLECTION DATA, ITEM 11

NON-DESTRUCTIVE TESTING DATA
FALLING WEIGHT DEFLECTOMETER

ITEM NO. 11

		STATION: 162.5							STATION: 170.0							STATION: 177.5						
		1.2" AC, 12.6" STAB. LAYER							1.3" AC, 11.4" STAB. LAYER							1.5" AC, 10.0" STAB. LAYER						
PASS NO	FWD LOAD LEVEL	(COR) D0	ACT. LOAD LEVEL	D0	D1	D2	D3	AREA	(COR) D0	ACT. LOAD LEVEL	D0	D1	D2	D3	AREA	(COR) D0	ACT. LOAD LEVEL	D0	D1	D2	D3	AREA
0	9	12.4	8.8	12.1	7.7	5.0	3.2	20.2	15.8	9.2	16.2	10.7	6.8	4.1	20.5	15.8	9.4	16.5	11.5	6 9	4.1	20.9
0	15	19.4	14.7	19.0	13.3	8.6	5.9	21.7	25.7	14.6	25.0	16.0	10.6	6.7	20.4	26.7	14.7	26.1	17.8	10.6	6.6	20.6
48	9	22.9	8.3	21.2	17.9	5.2	2.2	19.7	25.1	8.4	23.3	13.0	6.2	2.1	16.4	31.7	8.5	29.8	15.8	7.2	2.5	15.8
48	15	32.9	13.9	30.6	18.5	9.5	5.8	18.1	41.9	14.7	41.0	19.0	11.4	6.8	15.9	51.1	14.0	47.6	28.4	12.5	6.9	17.2
150	9	23.7	8.2	21.6	9.7	5.5	2.8	15.2	32.3	8.3	29.7	12.2	6.4	3.0	14.1	33.9	8.2	31.0	17.8	6.2	3.5	16.0
150	15	38.6	13.7	35.2	16.9	9.5	5.0	15.9	53.3	13.6	48.4	28.2	11.0	6.1	16.5	56.0	13.6	50.8	29.7	11.4	6.0	16.4
500	9	26.8	8.3	24.7	13.6	5.3	3.1	15.9	40.6	8.4	37.8	18.6	6.8	3.7	14.7	41.4	8.3	38.2	18.2	5.4	3.4	13.9
500	15	44.0	13.9	40.6	22.7	9.5	5.5	16.3	72.3	13.5	65.0	24.9	11.8	6.3	13.4	67.3	13.6	61.0	30.9	9.4	5.5	14.5
636	9	30.0	8.4	28.1	14.5	5.4	3.3	15.2	0.0	0.0	0.0	0.0	0.0	0.0	0.0	0.0	0.0	0.0	0.0	0.0	0.0	0.0
636	15	49.0	13.9	45.3	24.6	9.7	5.6	15.8	0.0	0.0	0.0	0.0	0.0	0.0	0.0	0.0	0.0	0.0	0.0	0.0	0.0	0.0

NOTES: LOAD IN KI. , DEFL IN MILS, AREA IN INCHES

IF DO EQUALS 0.0, FWD NOT CONDUCTED.

CORRECTED DO IS ACTUAL DO CORRECTED TO FWD LOAD LEVEL OF 9 OR 15 KIPS.

AREA=6*(1+2(D1/D0)+2(D2/D0)+(D3/D0)),

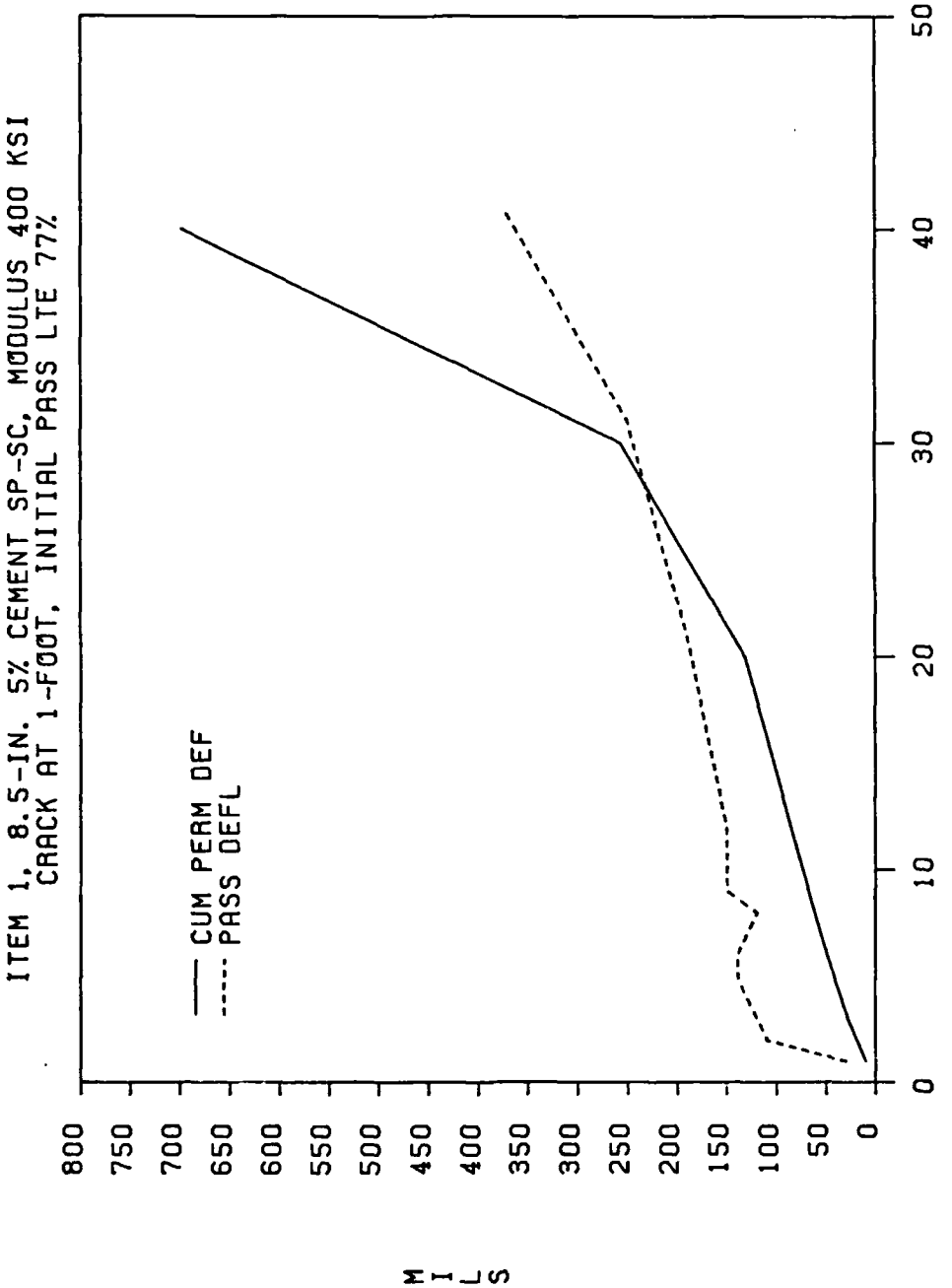

Figure A-1. LVDT Deflection and Deformation Data, Item 1

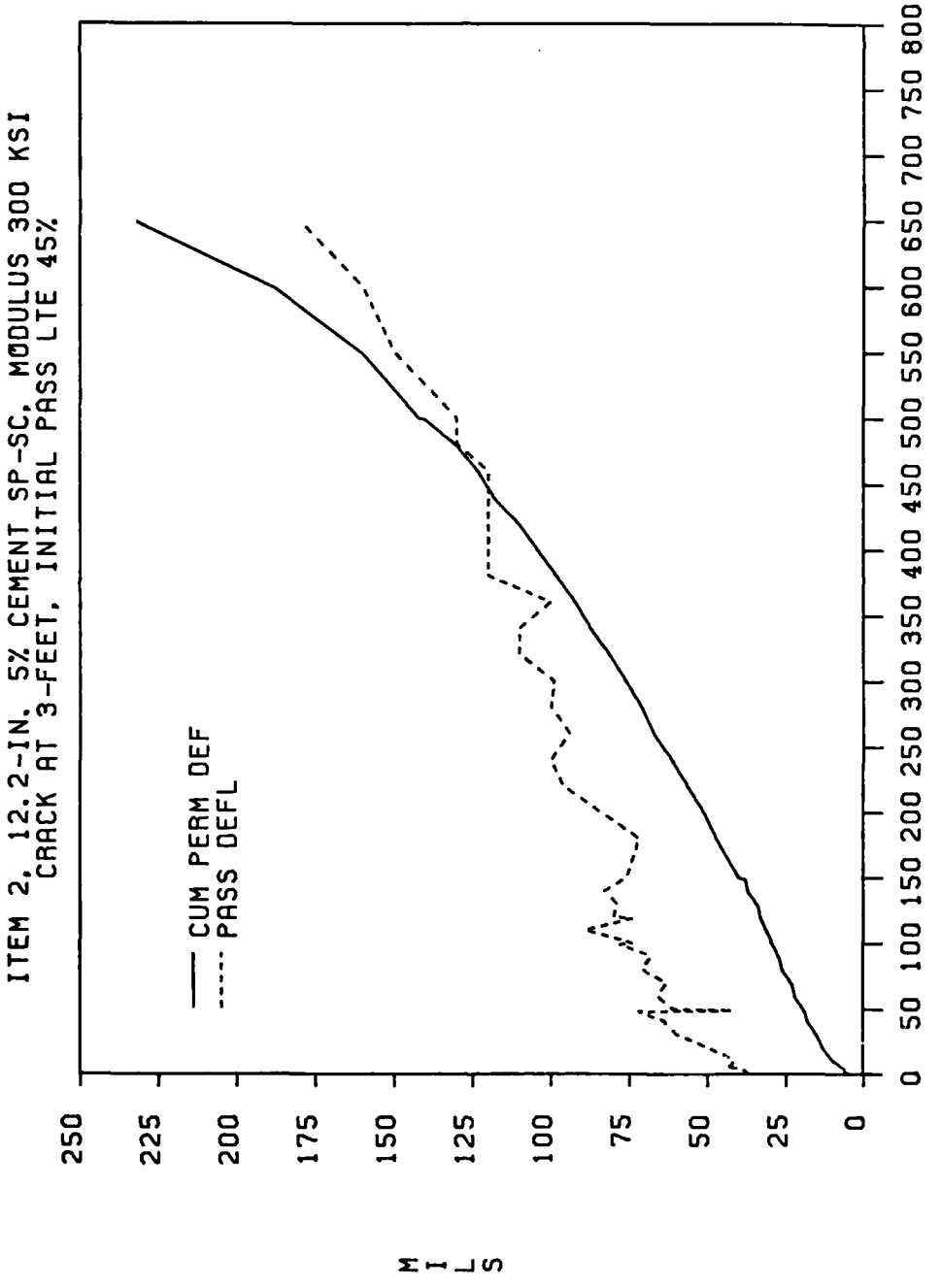

Figure A-2. LVDT Deflection and Deformation Data, Item 2

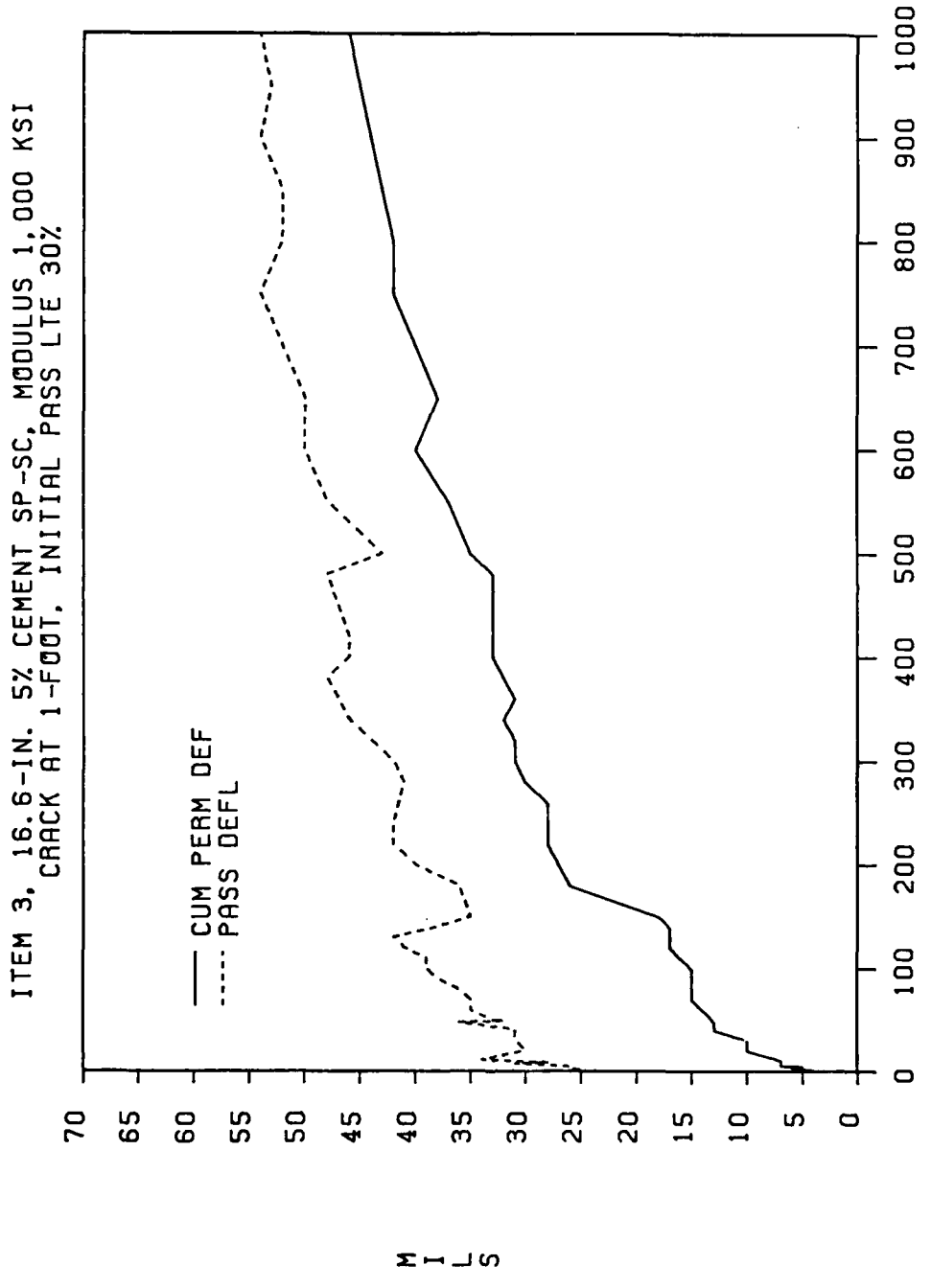

Figure A-3. LVDT Deflection and Deformation Data, Item 3

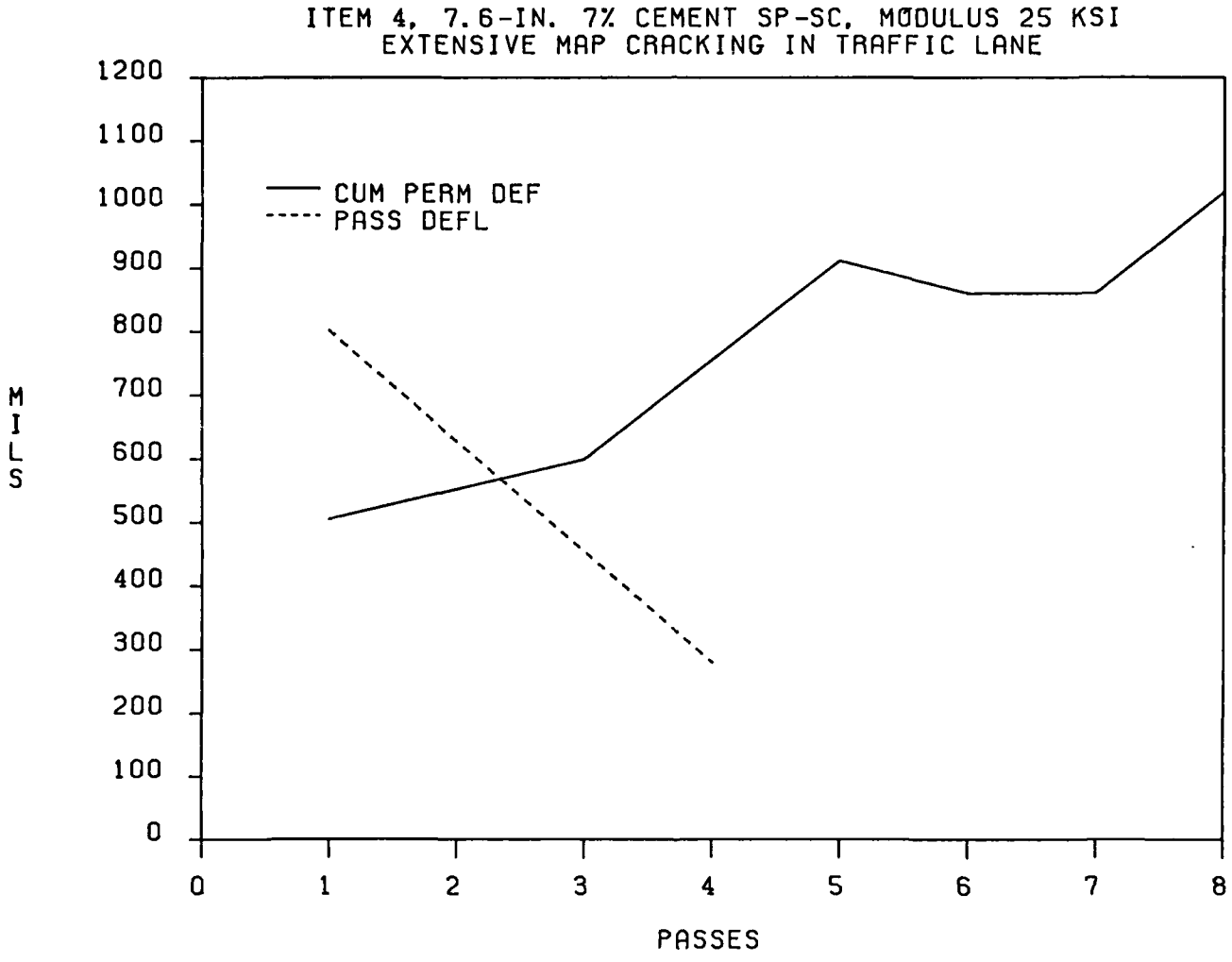

Figure A-4. LVDT Deflection and Deformation Data, Item 4

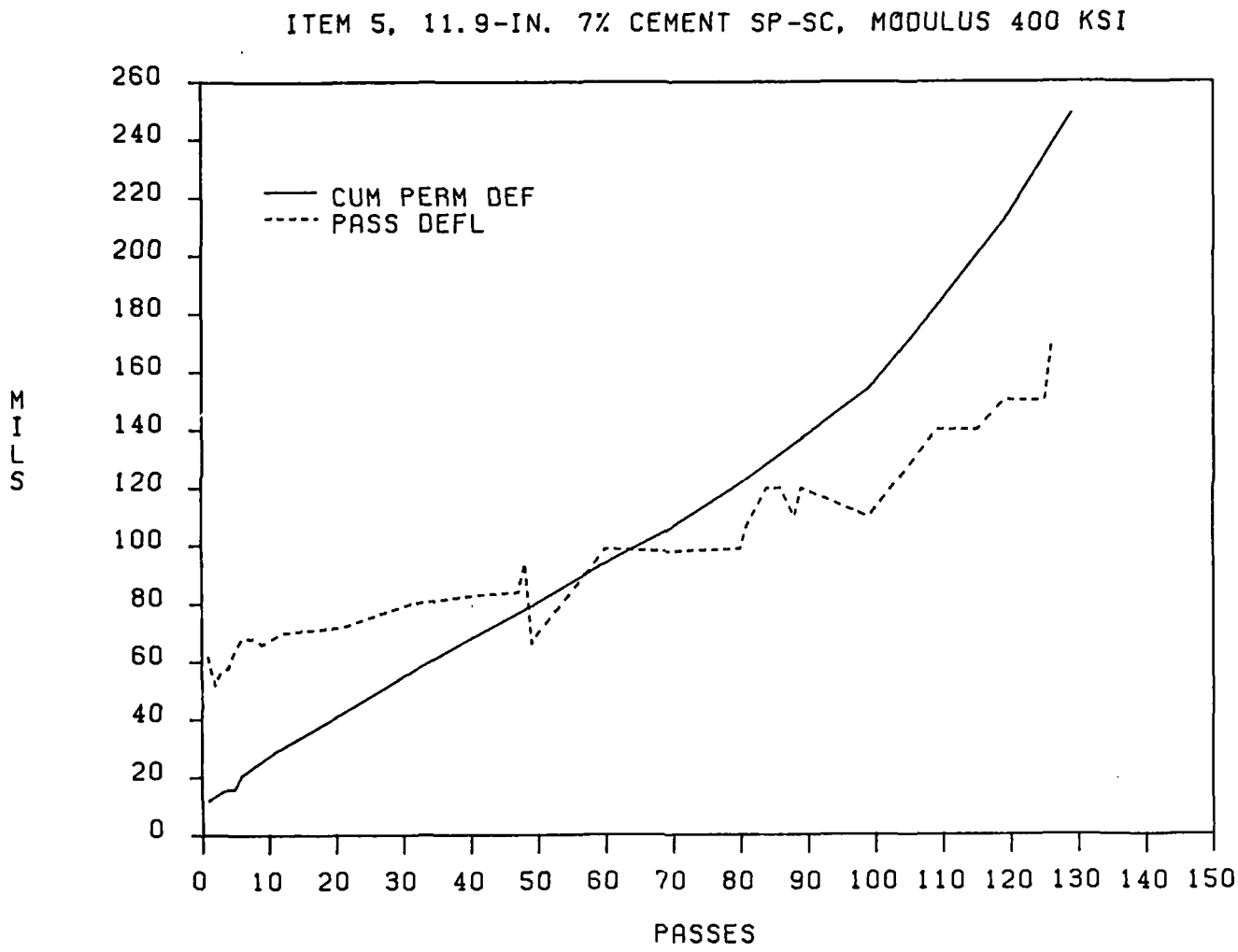

Figure A-5. LVDT Deflection and Deformation Data, Item 5

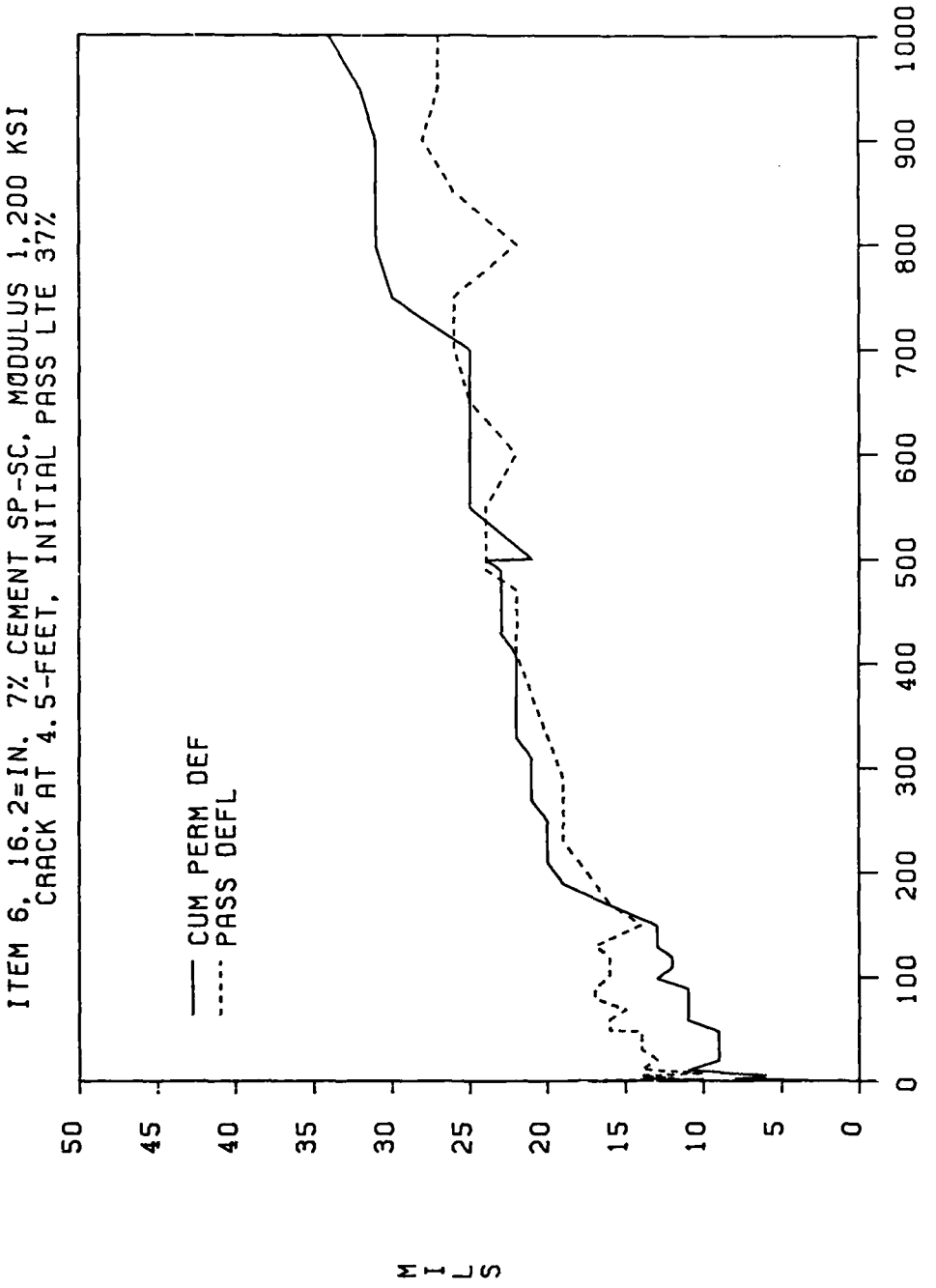

Figure A-6. LVDT Deflection and Deformation Data, Item 6

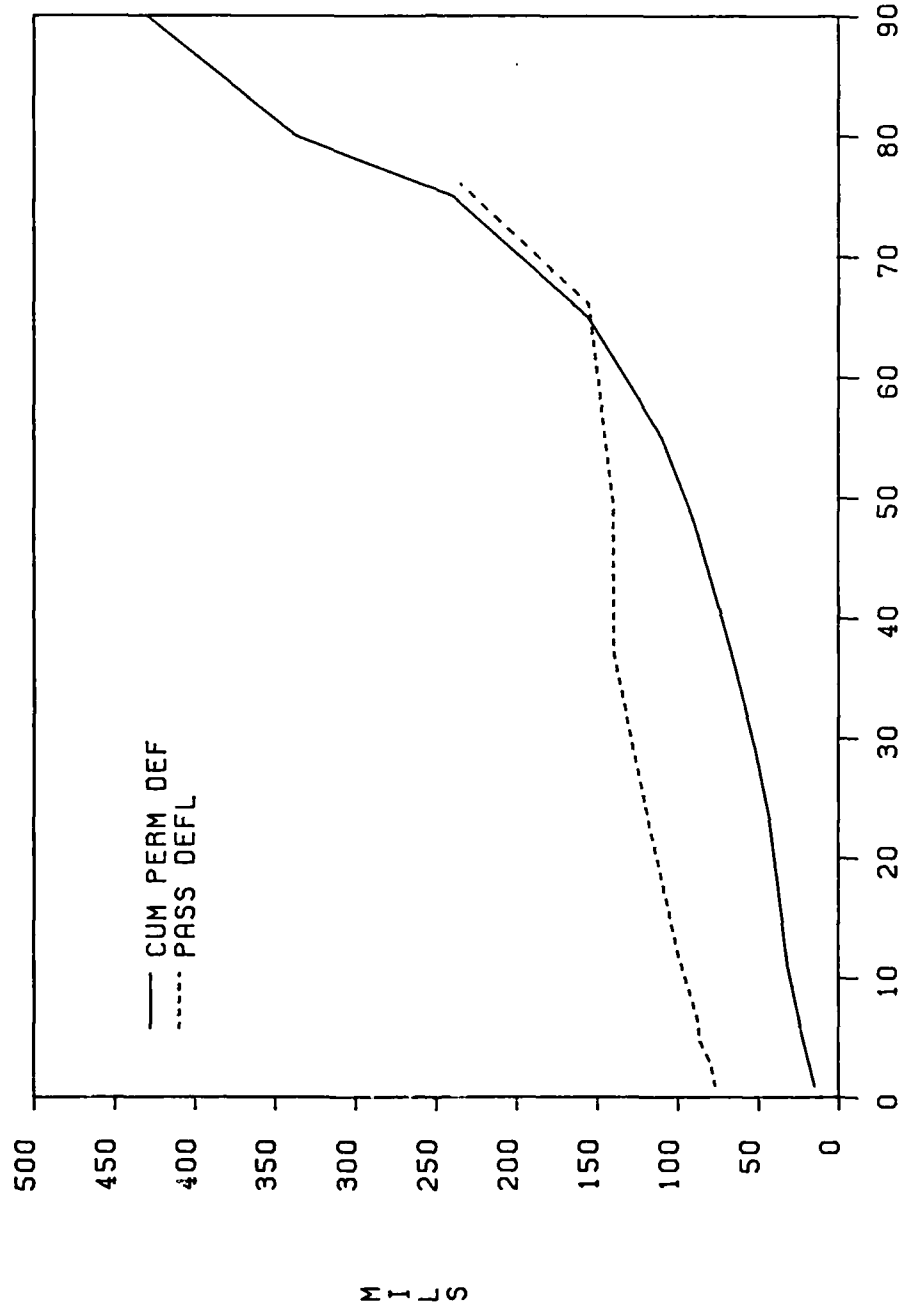

Figure A-7. LVDT Deflection and Deformation Data, Item 7

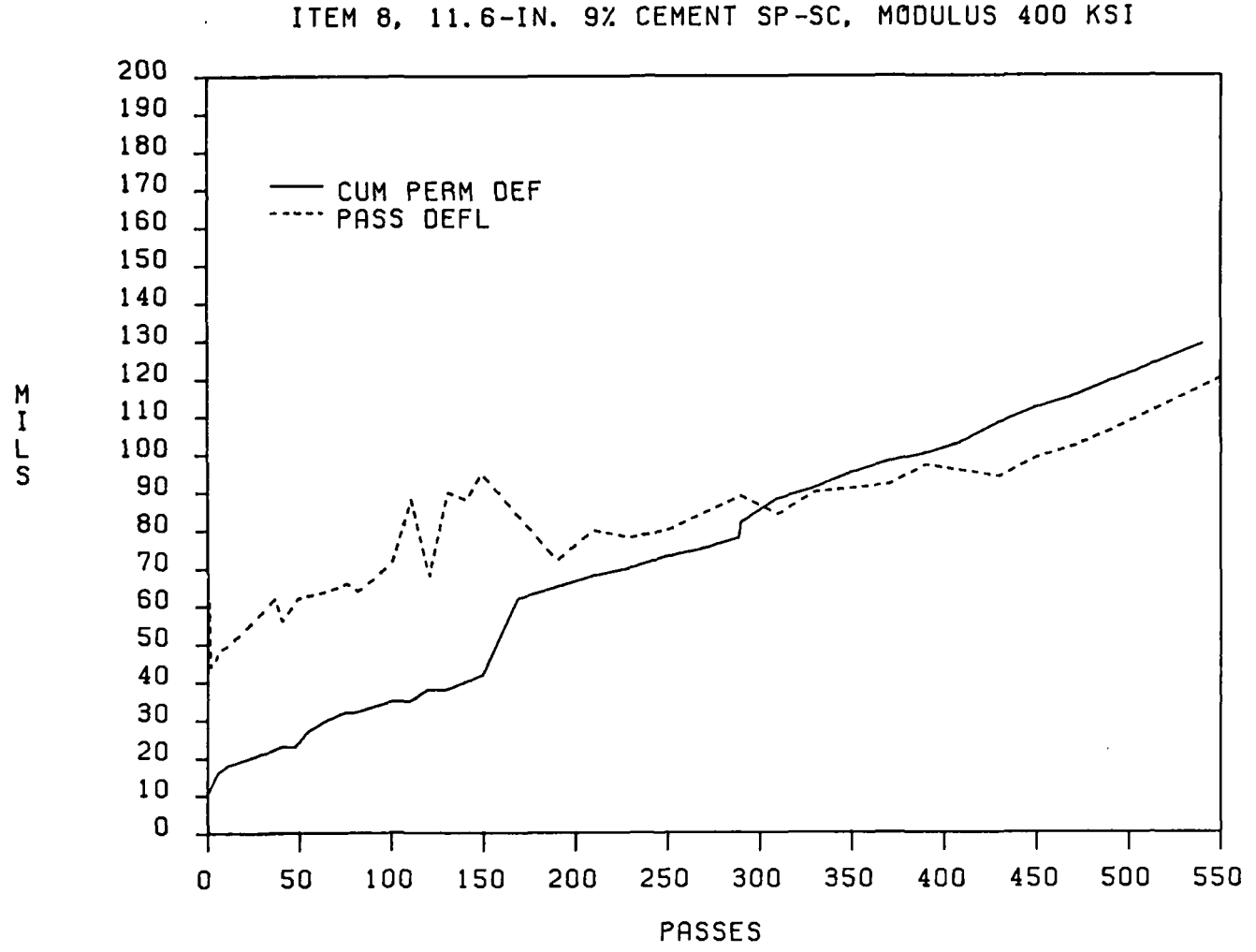

Figure A-8. LVDT Deflection and Deformation Data, Item 8

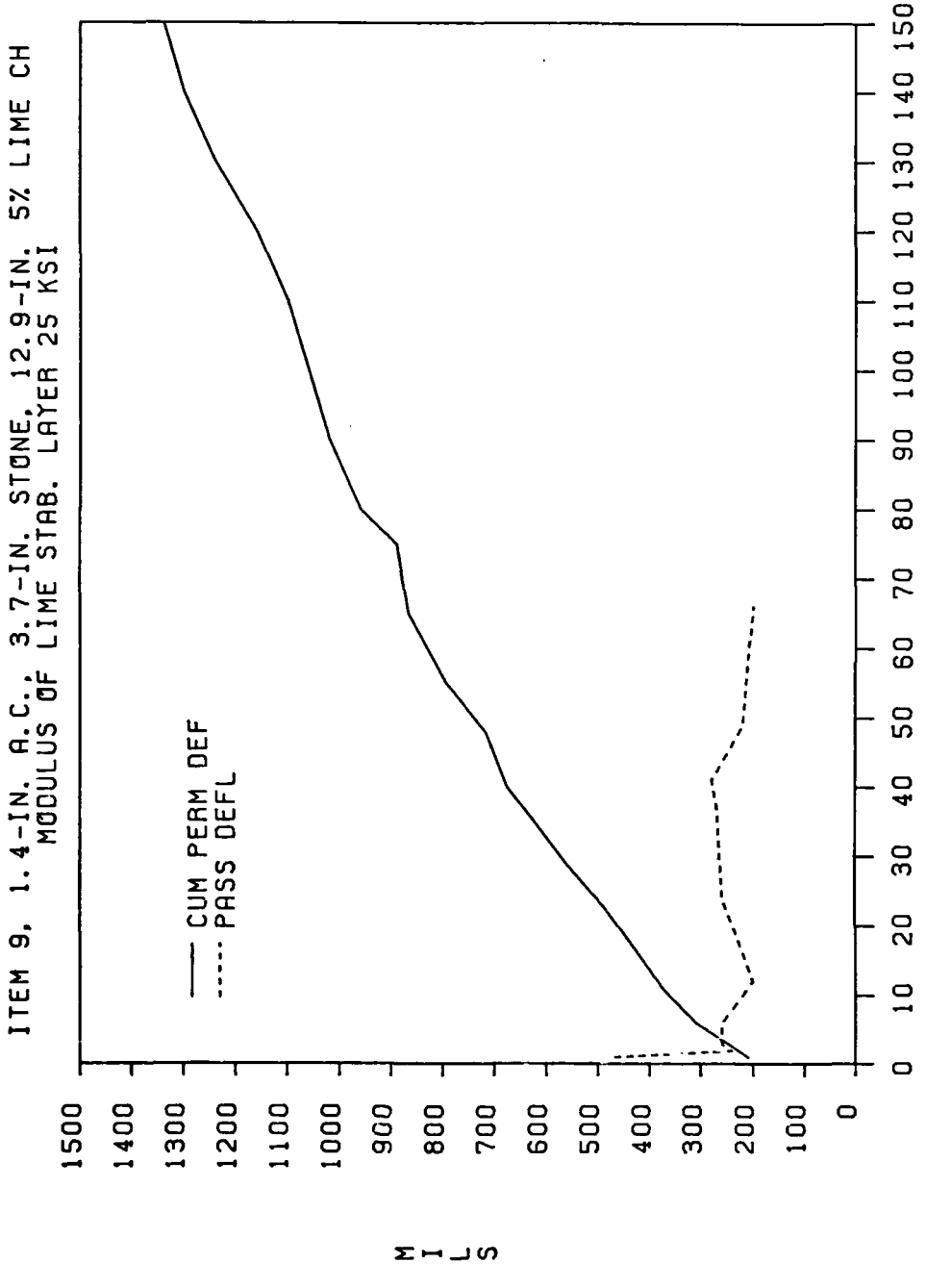

Figure A-9. LVDT Deflection and Deformation Data, Item 9

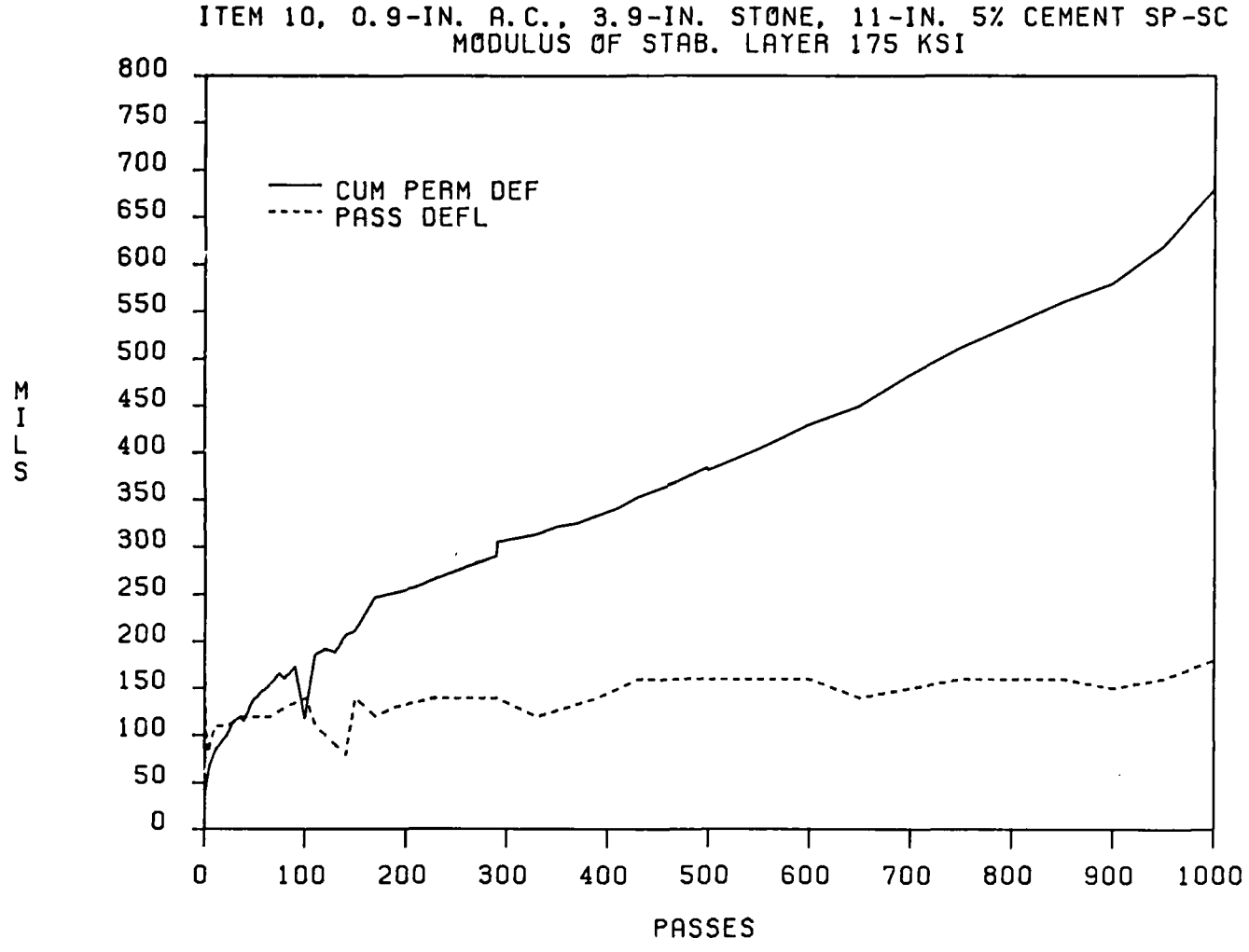

Figure A-10. LVDT Deflection and Deformation Data, Item 10

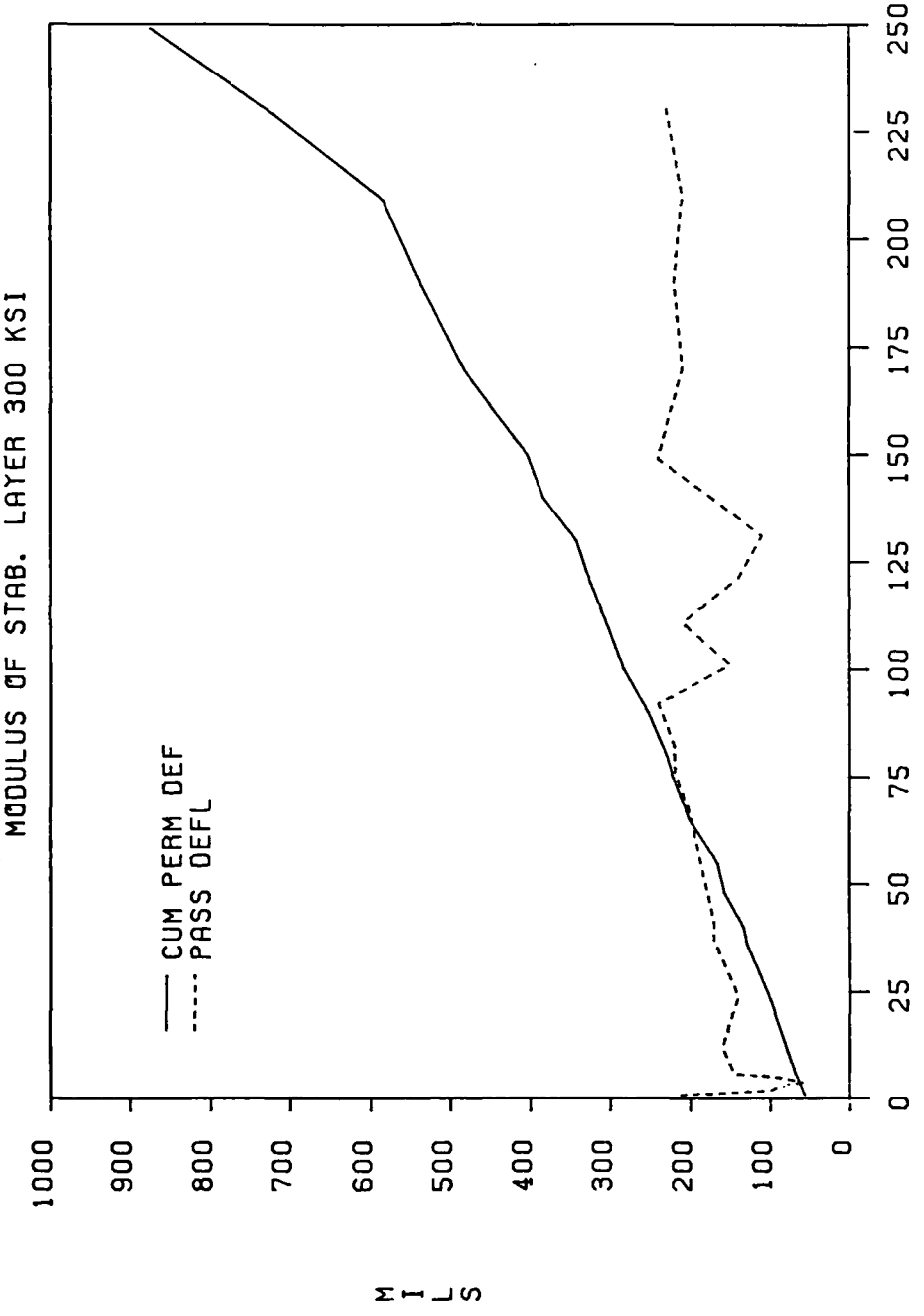

Figure A-11. LVDT Deflection and Deformation Data, Item 11

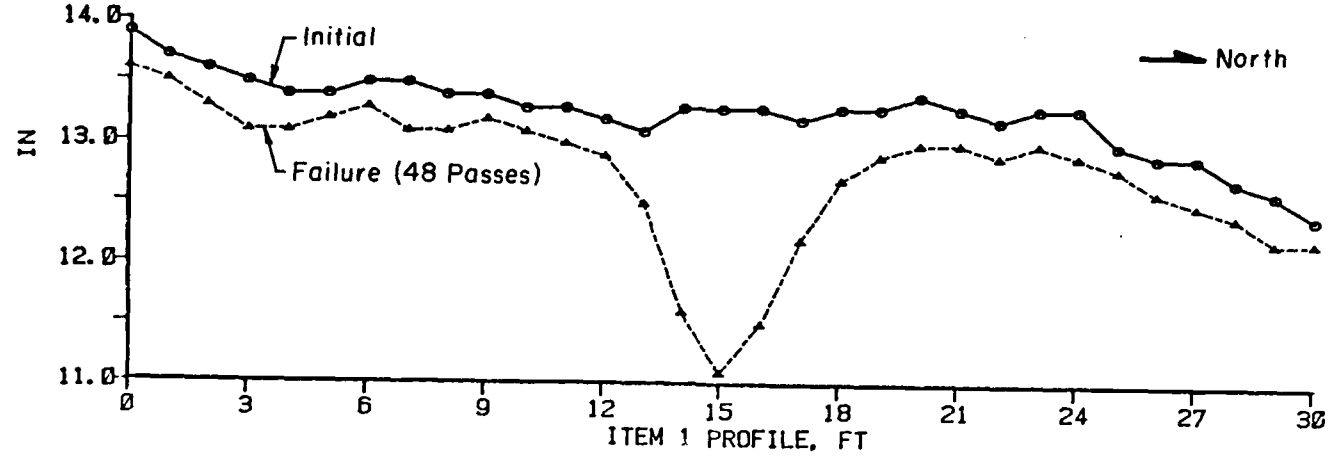

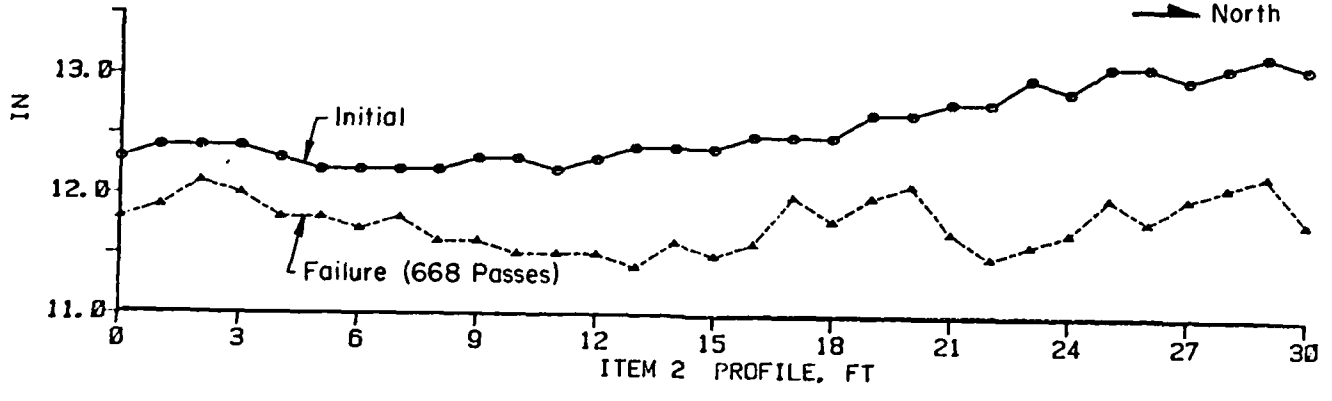

Figure A-12. Centerline Surface Profile, Items 1 and 2

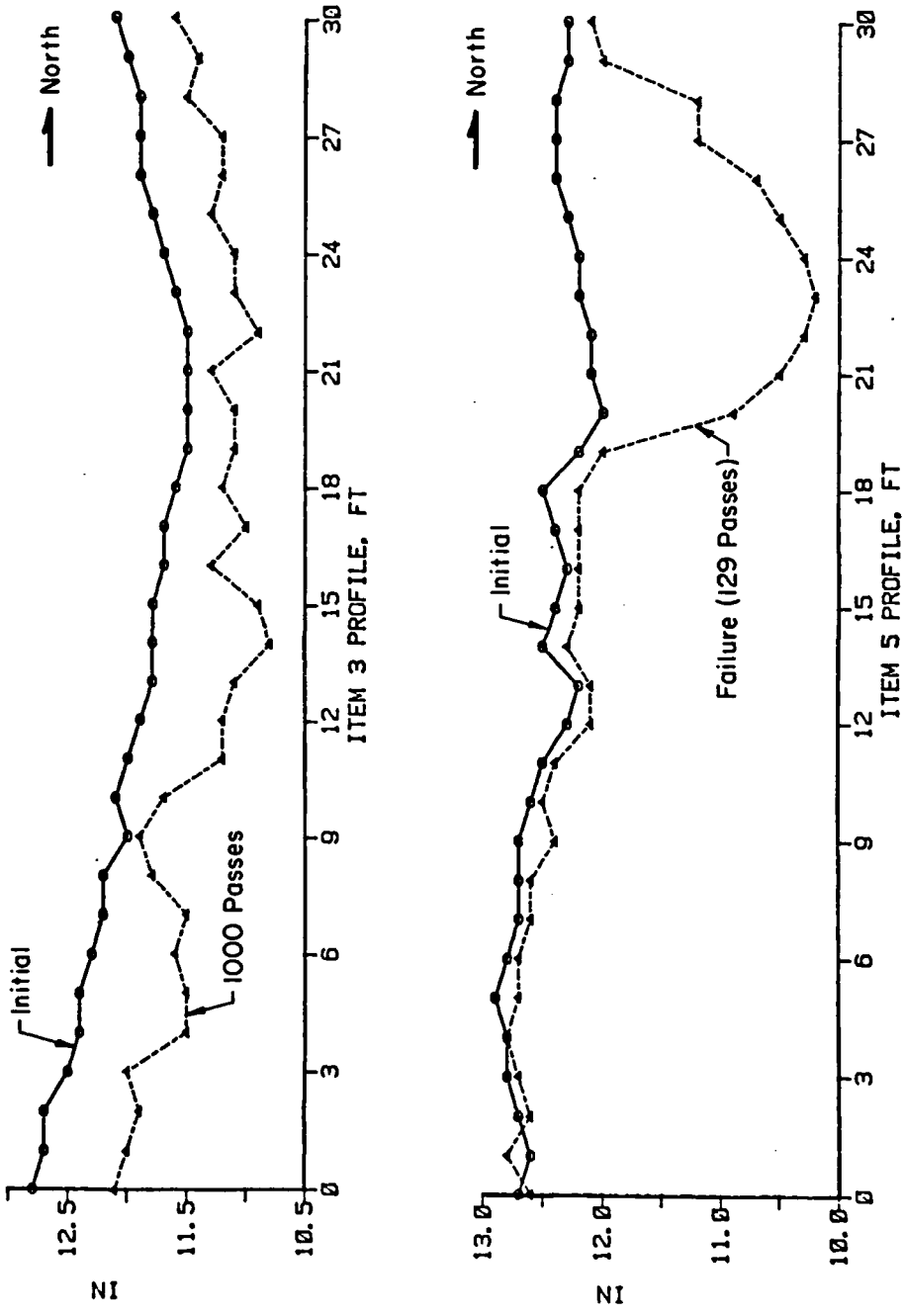

Figure A-13. Centerline Surface Profile, Items 3 and 5

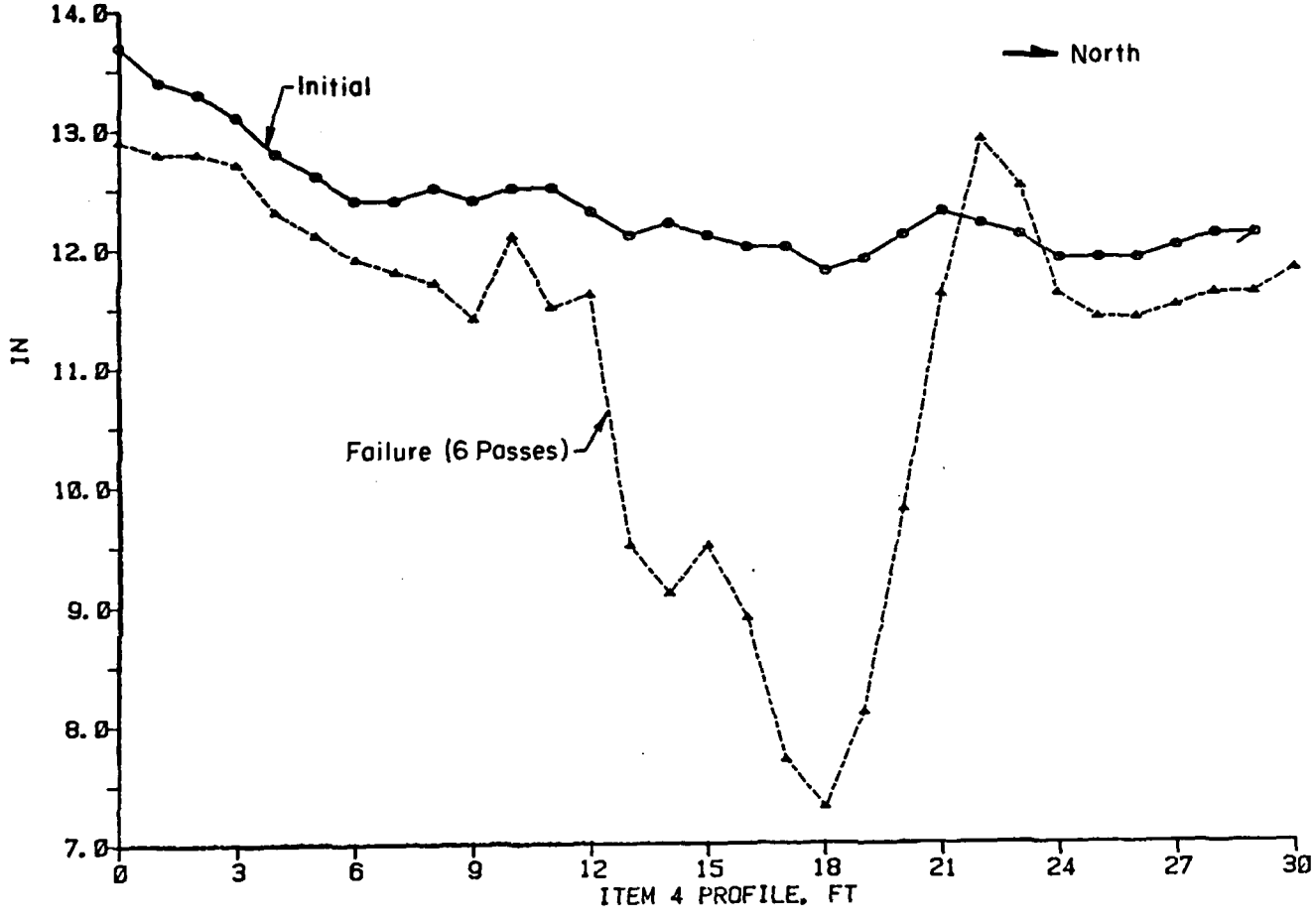

Figure A-14. Centerline Surface Profile, Item 4

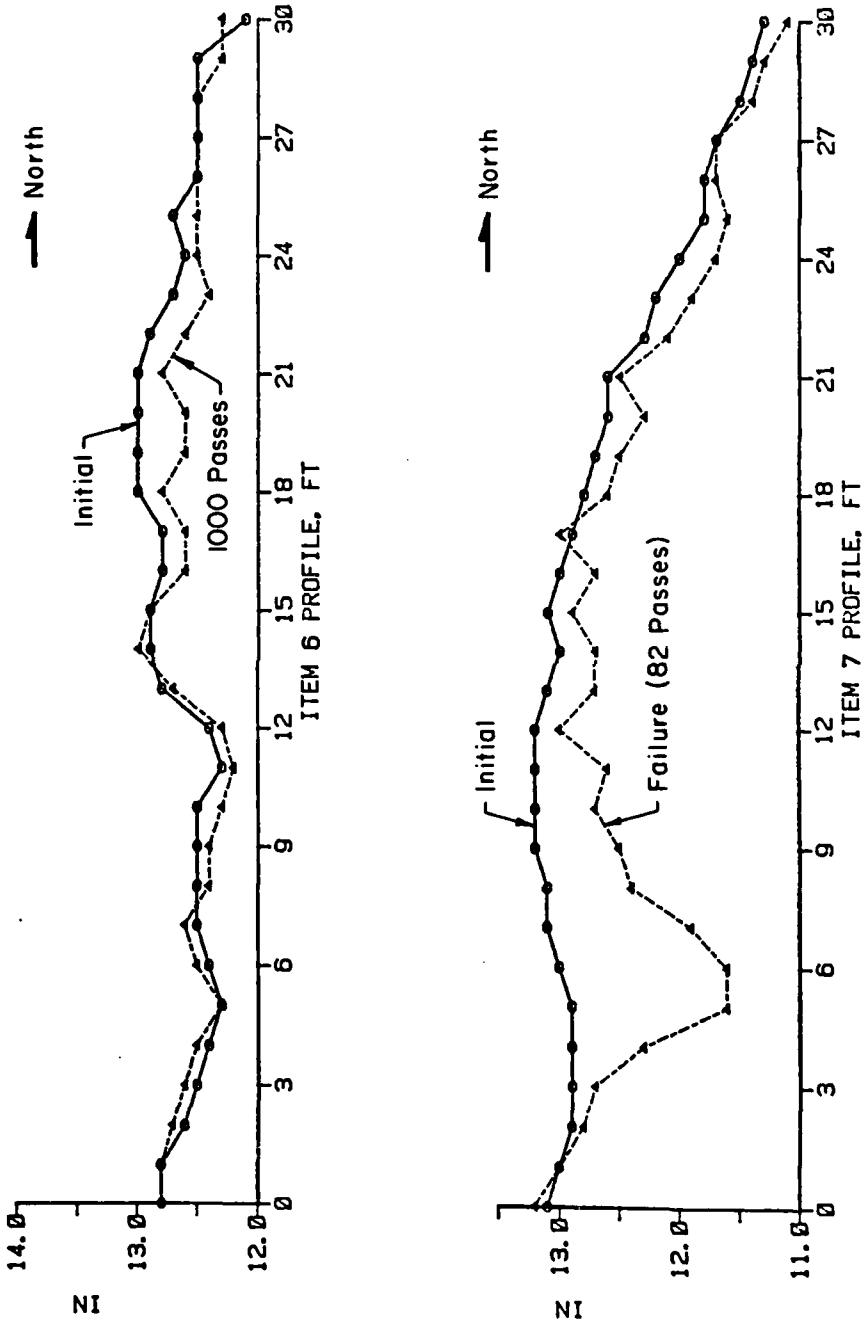

Figure A-15. Centerline Surface Profile, Items 6 and 7

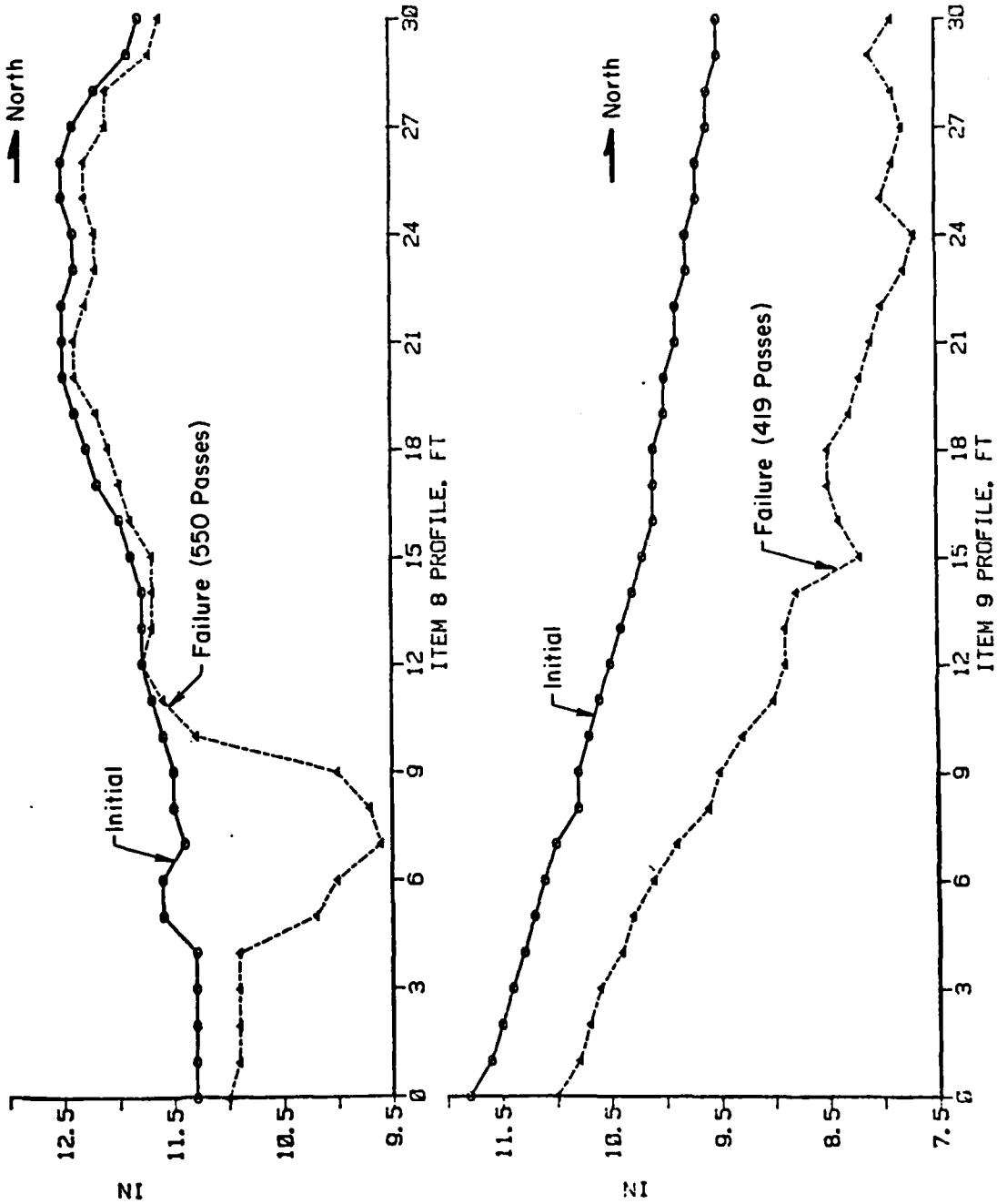

Figure A-16. Centerline Surface Profile, Items 8 and 9

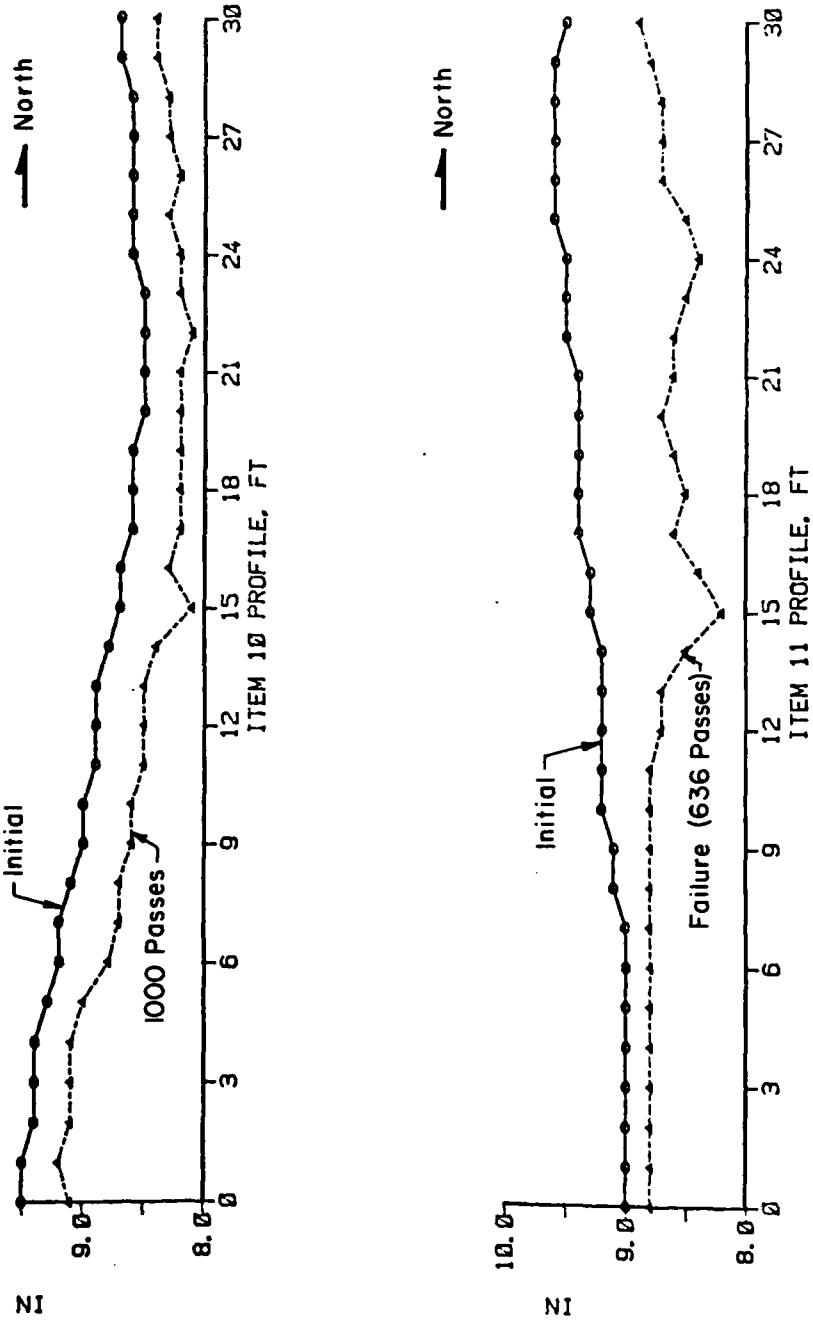

Figure A-17. Centerline Surface Profile, Items 10 and 11

APPENDIX B

SURFACE CRACKING DATA

TABLE B-1. TRANSVERSE CRACK LOAD TRANSFER EFFICIENCY (LTE) MEASURED ALONG ITEM CENTERLINE (REFERENCE 9)

Item	Station	Pass	FWD Load (kips)	LTE (%)
1	0+16	0	13.7	77
2	0+47	0	13.8	45
		48	8.3	43
		150	8.5	48
		500	8.8	44
3	0+84	0	14.0	38
		48	8.2	26
		150	8.5	27
		500	5.8	32
		750	8.8	38
6	2+09.5	0	11.7	45
		48	8.2	26
		150	8.5	25
		500	9.0	29
		750	8.8	36
		1000	8.6	42
7	0+06.8	0	13.7	62
		48	8.7	52

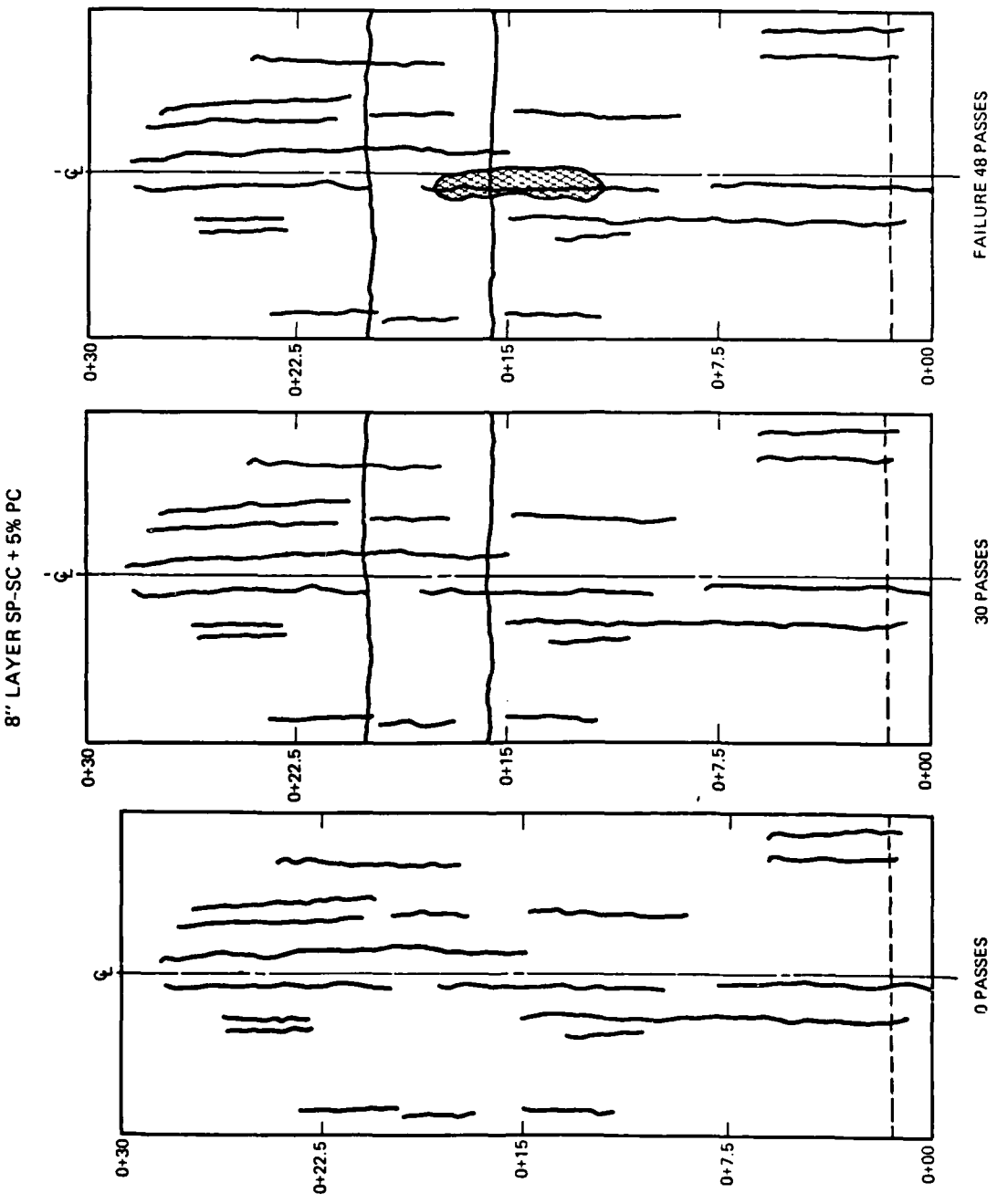

Figure B-1. Crack Survey, Item 1

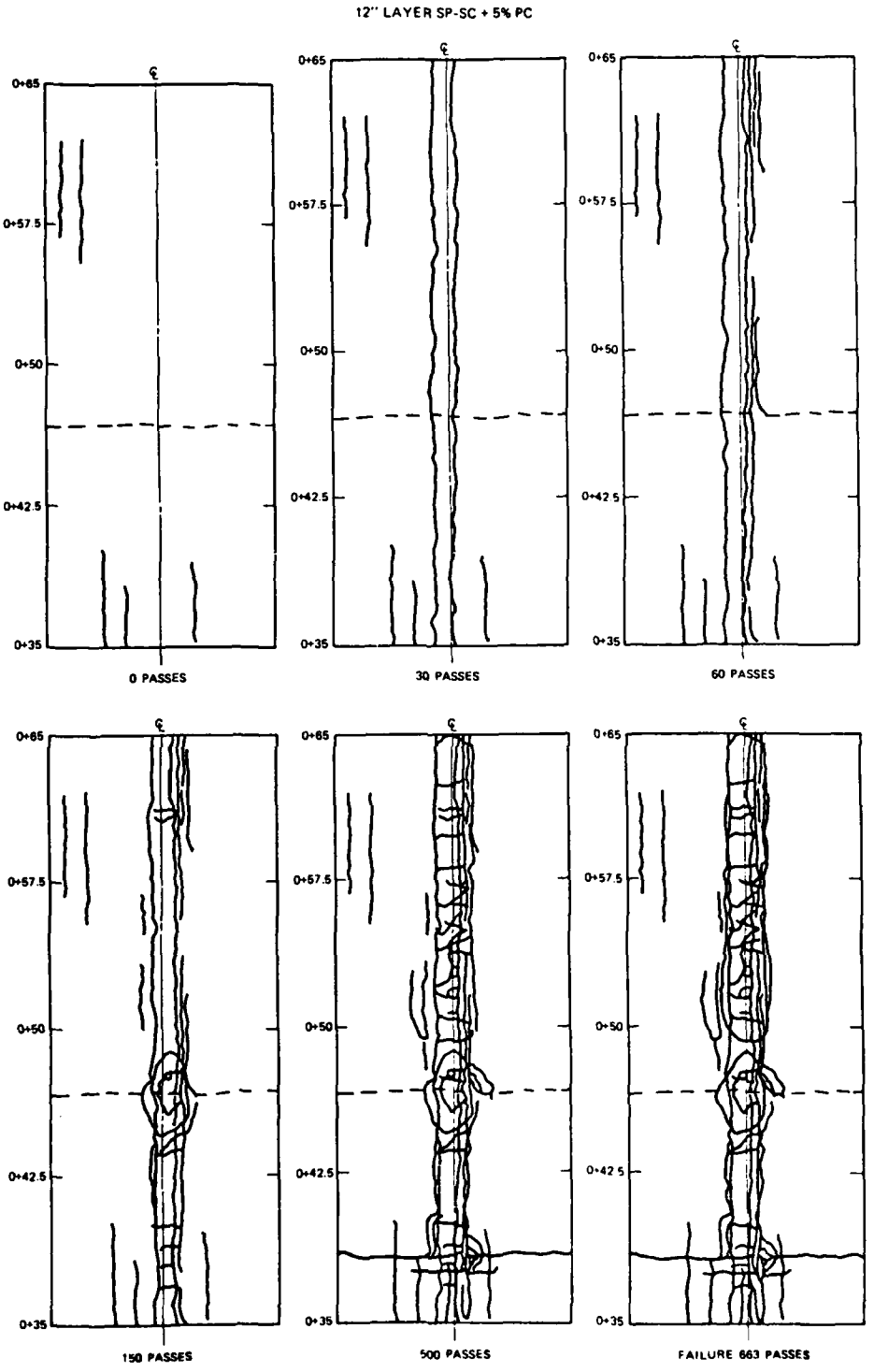

Figure B-2. Crack Survey, Item 2

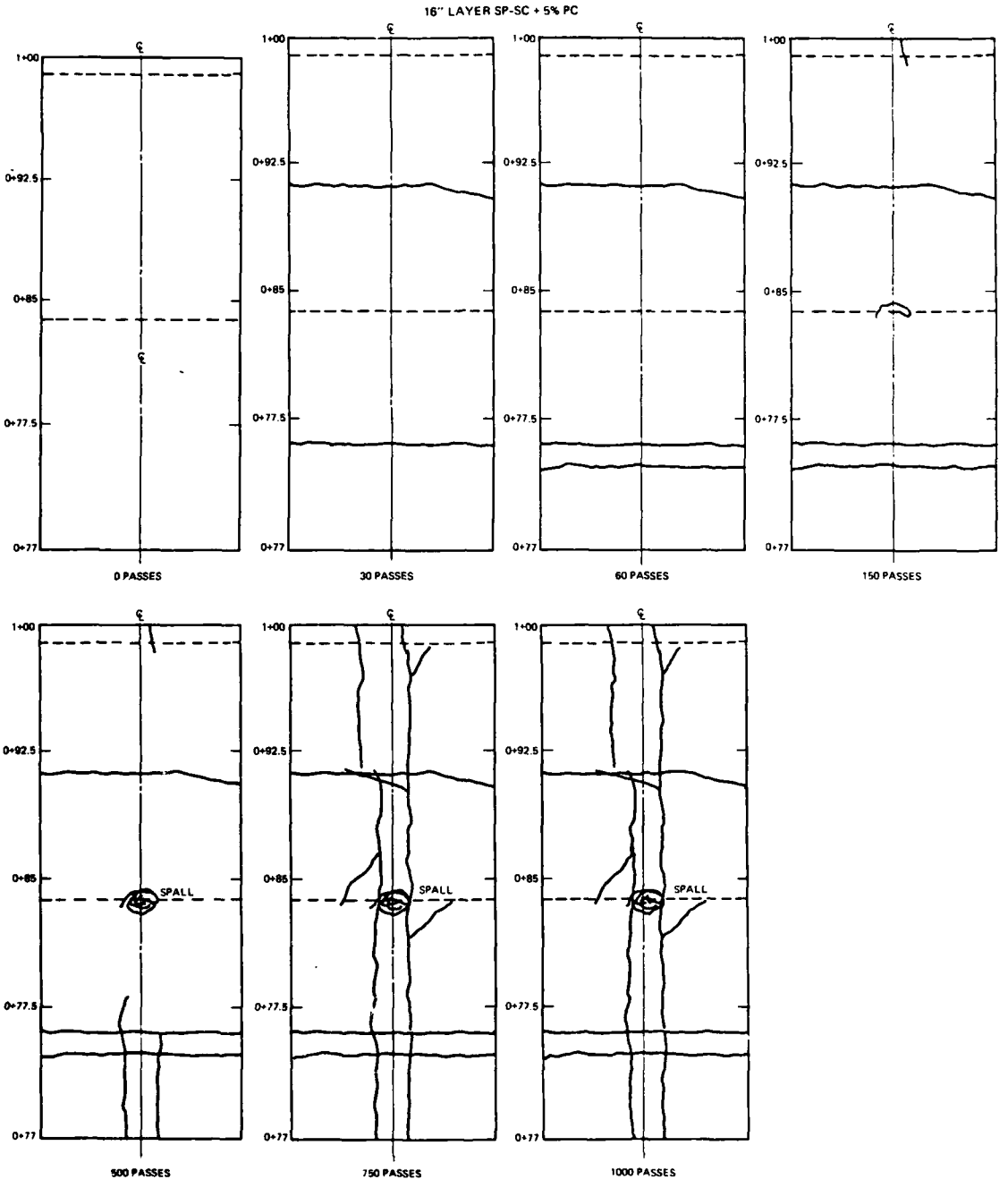

Figure B-3. Crack Survey, Item 3

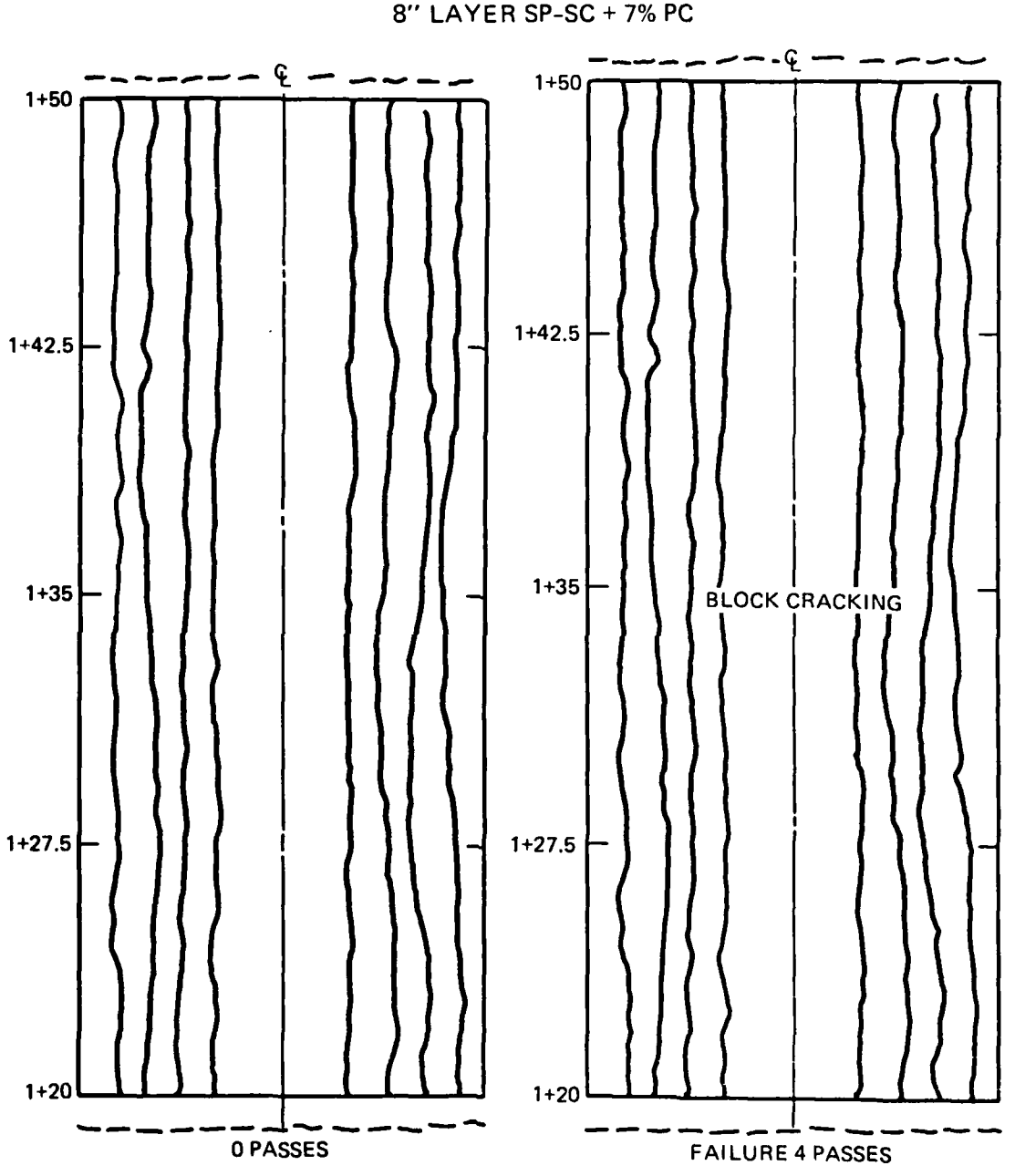

Figure B-4. Crack Survey, Item 4

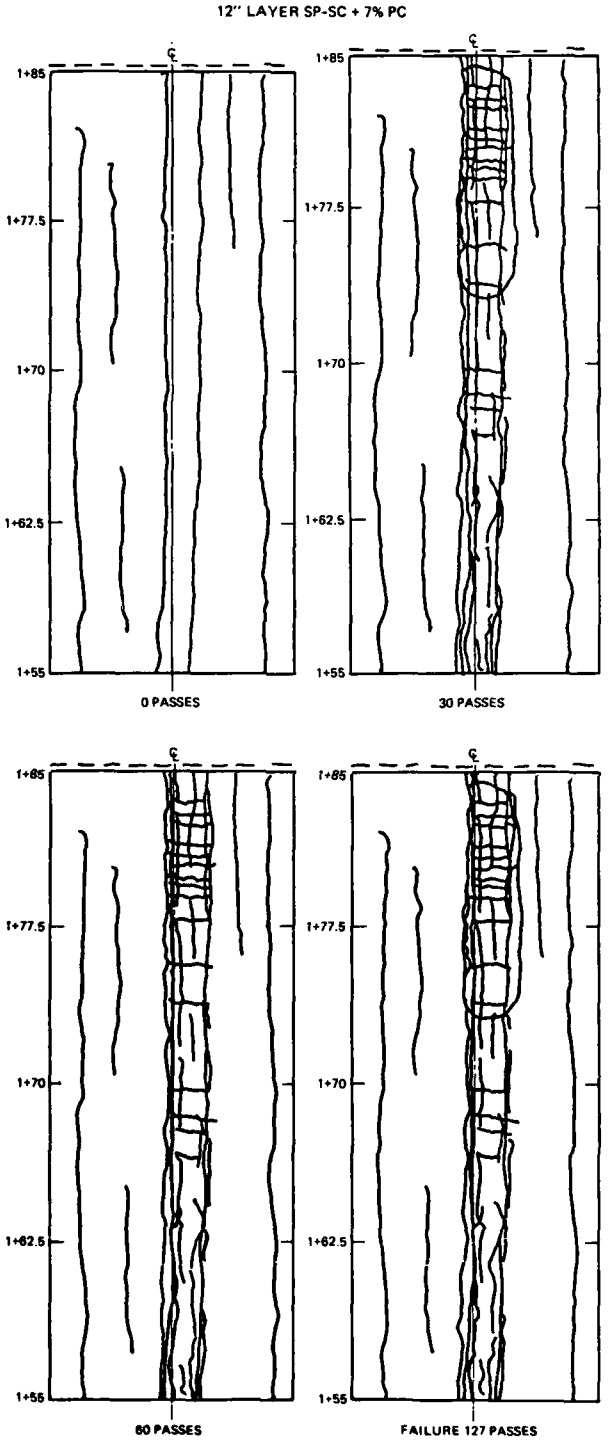

Figure B-5. Crack Survey, Item 5

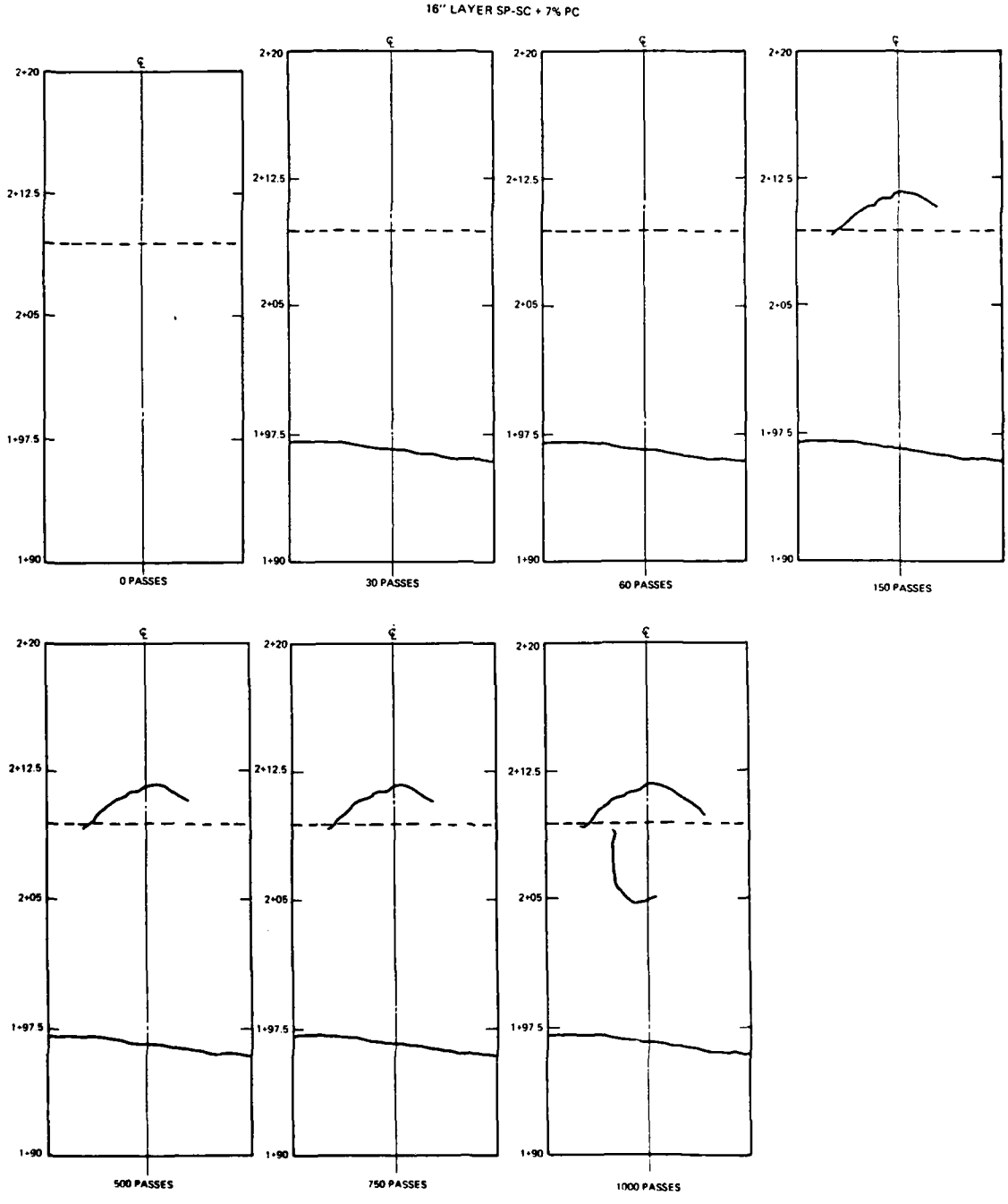

Figure B-6. Crack Survey, Item 6

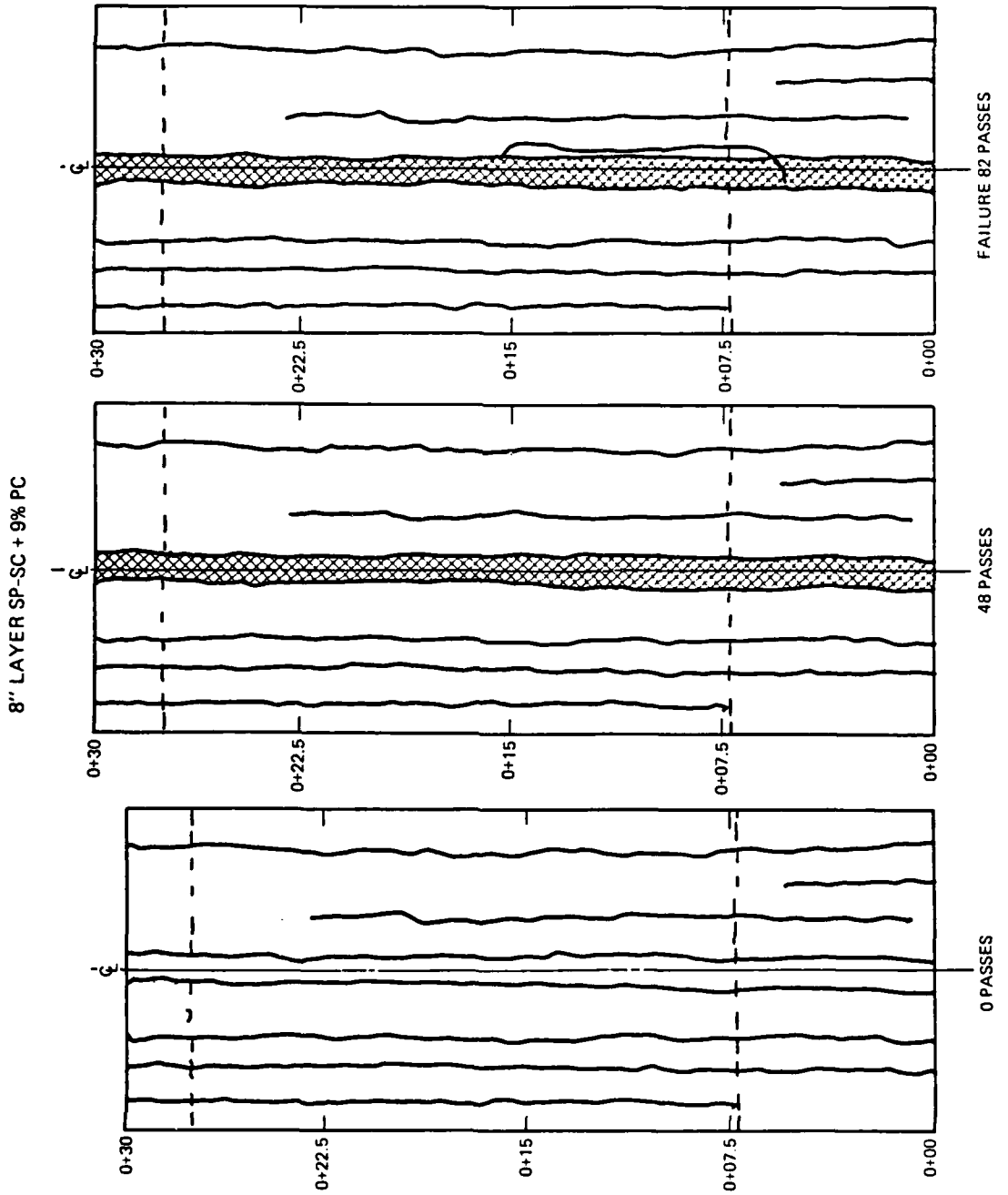

Figure B-7. Crack Survey, Item 7

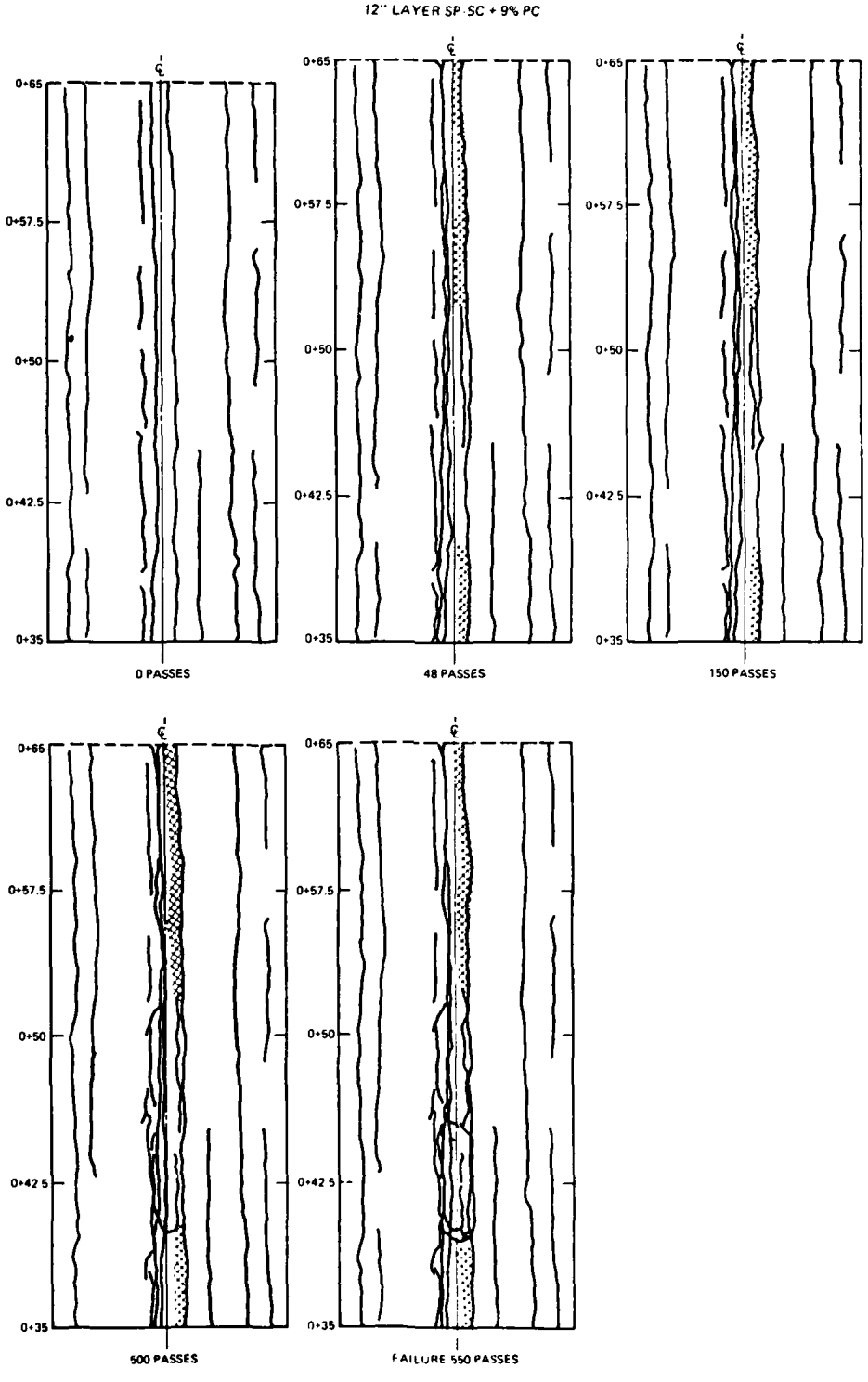

Figure B-8. Crack Survey, Item 8

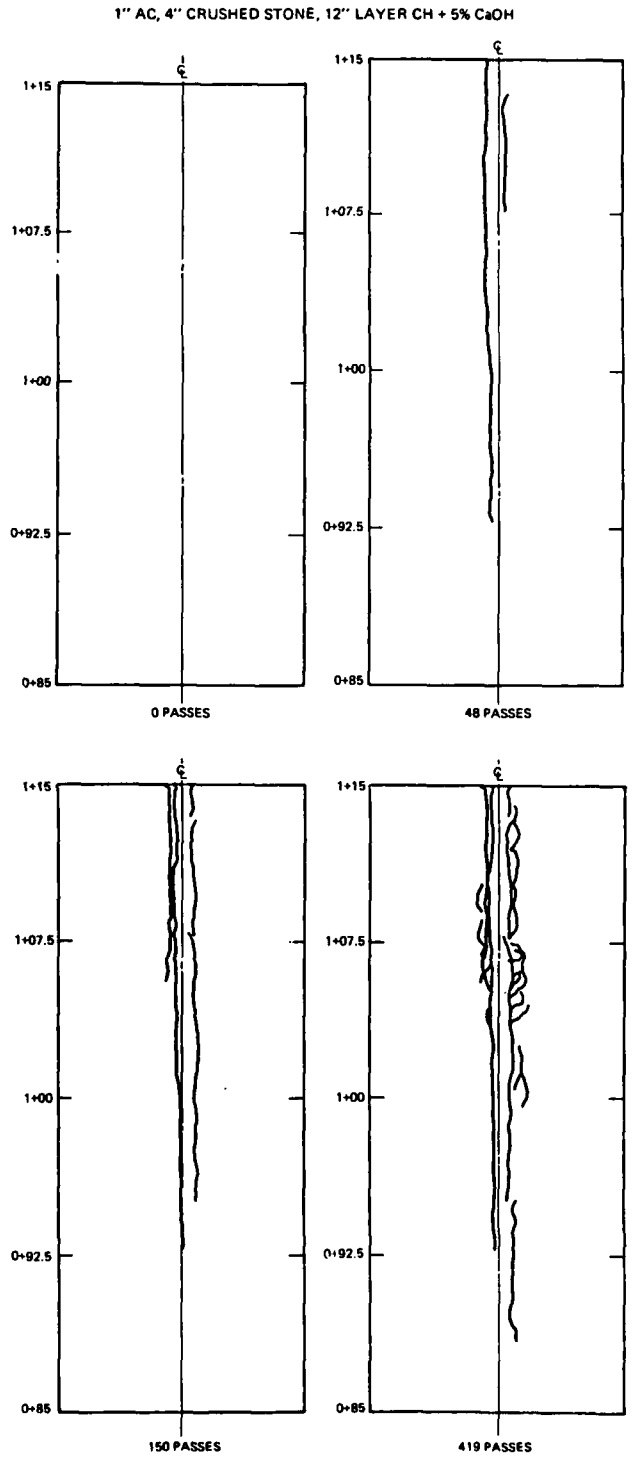

Figure B-9. Crack Survey, Item 9

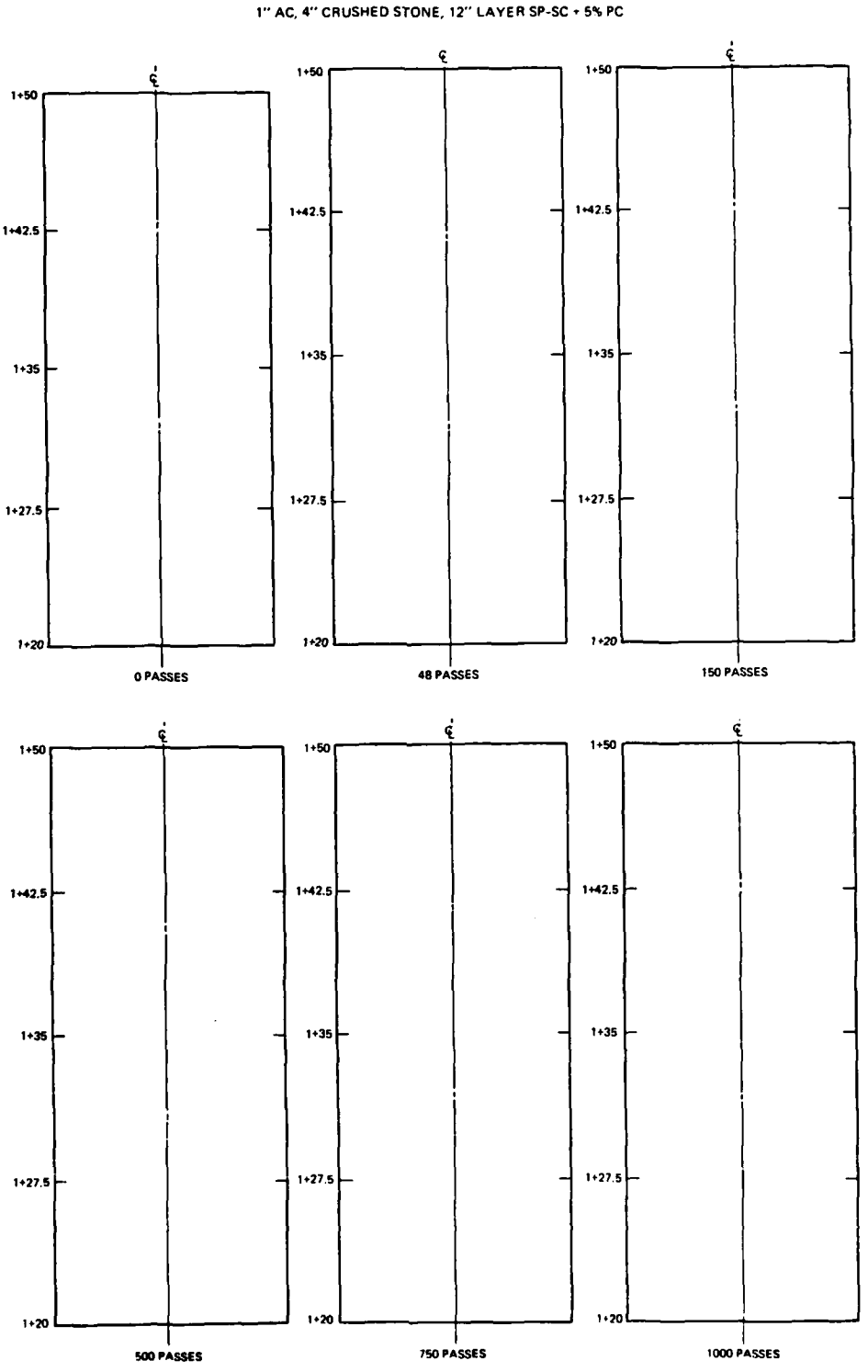

Figure B-10. Crack Survey, Item 10

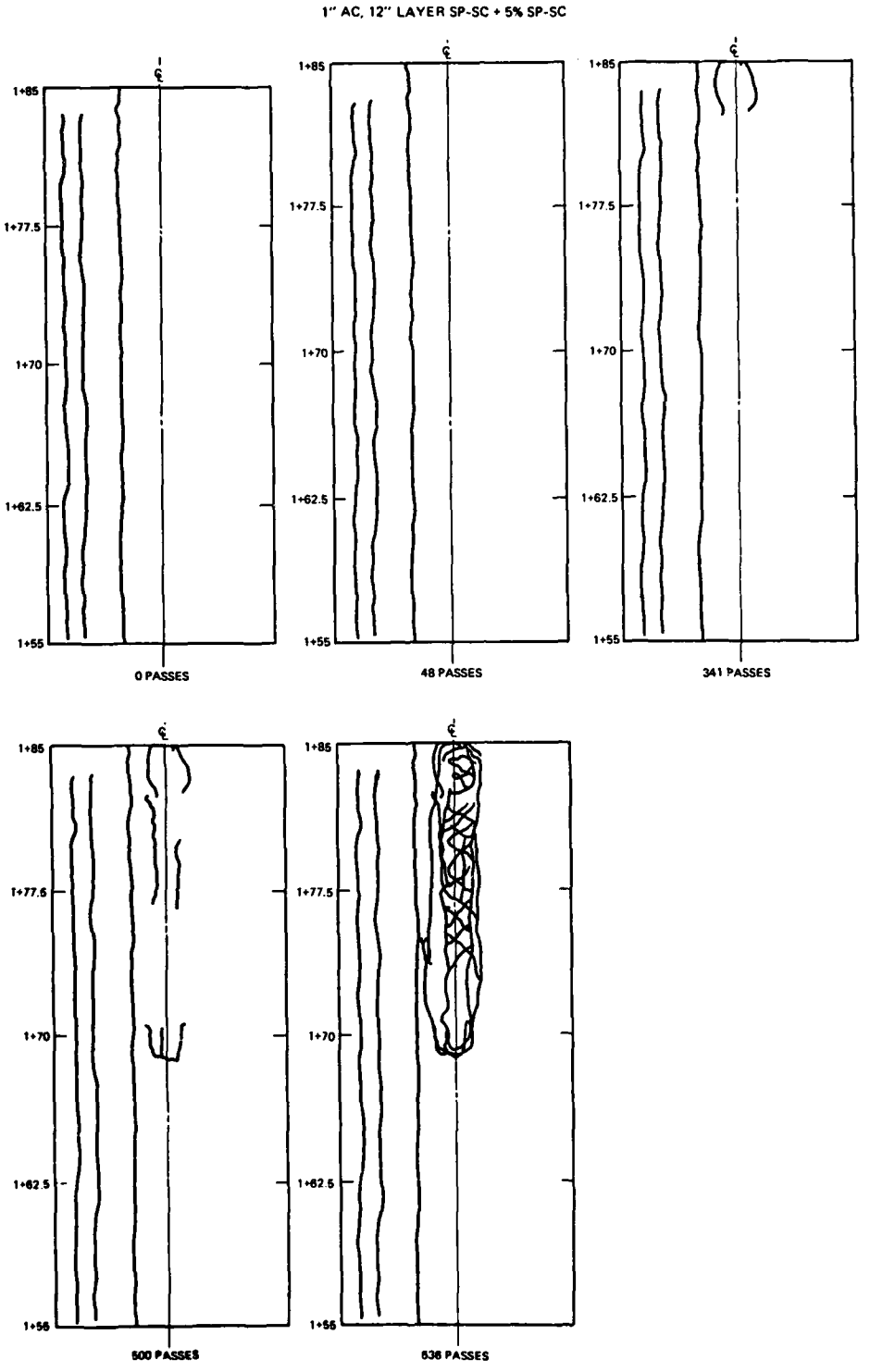

Figure B-11. Crack Survey, Item 11

APPENDIX C

F-4 ILLI-PAVE DATA BASE

TABLE C-1. SUMMARY OF SUBGRADE MATERIAL PROPERTIES IN ILLI-PAVE SOLUTIONS

Property	Standard Subgrade Types			
	Stiff	Medium	Soft	Very Soft
Unit Weight, pcf	125	120	115	110
Coefficient at Rest	0.82	0.82	0.82	0.82
Poisson's Ratio	0.45	0.45	0.45	0.45
Unconf. Comp. Strength, psi	32.80	22.85	12.90	6.21
Deviator Stress Upper Limit, psi	32.80	22.85	12.90	6.21
Deviator Stress Lower Limit, psi	2.00	2.00	2.00	2.00
E_{ri} at σ_{di}, ksi	12.34	7.68	3.02	1.00
σ_{di}, psi	6.20	6.20	6.20	6.20
E-Failure, ksi	7.61	4.72	1.83	1.00
Friction Angle	0.00	0.00	0.00	0.00
Cohesion, psi	16.40	11.43	6.45	3.11

TABLE C-2. F-4 ILLI-PAVE DATA BASE, STRUCTURAL RESPONSE TO 27 KIP, 265 PSI LOAD (REFERENCE 8)

THIS TABLE CONTAINS THE RESPONSE PARAMETERS IN CONJUNCTION WITH THE INDEPENDENT VARIABLES USED IN EACH PARAMETER'S CALCULATION. IT ALSO SUMMARIZES THE RESULTS OF USING THE ITERATIVE LOADING WITH STRESS MODIFICATION TECHNIQUE IN THE ILLI-PAVE PROGRAM.

LATEST REVIEW OF THE DATA: NOVEMBER 2 1981

	VARIABLE	UNIT
	.....	....
TST	THICKNESS OF STABILIZED LAYER	INCHES
EST	MODULUS OF ELASTICITY OF THE STABILIZED LAYER	KSI
ERI	SUBGRADE MODULUS AT THE INTERCEPT	KSI
MTST	MAXIMUM TENSILE STRESS AT BOTTOM OF STABILIZED LAYER	PSI
MEST	MAXIMUM RADIAL STRAIN AT BOTTOM OF STABILIZED LAYER	MICROSTRAIN
D0	DEFLECTION AT R= 0.0 IN. FROM LOAD	MILS
D1	DEFLECTION AT R=12.0 IN. FROM LOAD	MILS
D2	DEFLECTION AT R=24.0 IN. FROM LOAD	MILS
D3	DEFLECTION AT R=36.0 IN. FROM LOAD	MILS
DS	DEFLECTION AT TOP OF THE SUBGRADE	MILS
EZ	MAXIMUM STRAIN AT TOP OF THE SUBGRADE	0.0001 IN/IN
SZ	MAXIMUM SUBGRADE NORMAL STRESS	PSI
TS	MAXIMUM SUBGRADE SHEARING STRESS	PSI
SDEV	MAXIMUM SUBGRADE DEVIATOR STRESS	PSI
AREA	DEFLECTION BASIN AREA	INCHES

TABLE C-2. (CONTINUED)

TST	EST	ERI	AREA	D0	D1	D2	D3	DS	EZ	MEST	MTST	SZ	TS	SDEV
9.0	100	1.00	19.99	135.8	89.8	52.8	31.5	123.5	60.1	2166	249	9.4	2.9	5.8
9.0	200	1.00	22.63	88.7	64.4	43.6	29.8	82.6	27.4	1149	265	6.8	3.0	5.9
9.0	500	1.00	26.31	56.0	45.5	35.4	27.8	53.5	12.9	506	290	9.8	3.1	6.2
9.0	1000	1.00	29.05	42.5	37.0	31.3	26.7	41.3	7.9	274	314	6.8	1.8	3.7
9.0	2000	1.00	31.43	34.5	31.6	28.5	26.0	33.9	4.5	144	330	5.0	1.2	2.3
9.0	3000	1.00	32.55	31.5	29.5	27.4	25.6	31.1	3.2	98	337	4.2	0.9	1.8
12.0	100	1.00	21.15	98.4	65.4	43.9	29.8	83.2	36.7	1309	151	6.8	1.8	3.6
12.0	200	1.00	24.20	65.9	49.0	36.9	28.1	58.4	22.0	696	160	6.2	1.4	2.7
12.0	500	1.00	28.19	43.8	36.7	31.0	26.6	40.8	8.3	304	175	6.7	1.8	3.7
12.0	1000	1.00	30.89	35.0	31.4	28.3	25.8	33.5	4.7	161	185	5.1	1.2	2.4
12.0	2000	1.00	32.89	30.1	28.2	26.6	25.3	29.3	2.8	83	192	3.9	0.8	1.6
12.0	3000	1.00	33.74	28.4	27.1	26.0	25.1	27.8	2.1	56	194	3.5	0.6	1.2
15.0	100	1.00	21.83	79.0	52.1	38.0	28.2	61.9	25.2	840	96	5.9	1.2	2.5
15.0	200	1.00	25.18	54.2	40.5	32.7	26.9	45.6	12.6	444	102	7.1	1.8	3.5
15.0	500	1.00	29.35	37.7	32.0	28.5	25.7	34.2	5.4	194	111	5.4	1.4	2.7
15.0	1000	1.00	31.91	31.4	28.5	26.7	25.2	29.7	3.1	101	117	4.3	0.9	1.8
15.0	2000	1.00	33.69	28.0	26.6	25.6	24.8	27.2	2.0	52	120	3.6	0.6	1.2
15.0	3000	1.00	34.35	26.9	25.9	25.3	24.7	26.3	1.6	35	121	3.3	0.5	1.0
18.0	100	1.00	22.22	67.7	44.0	34.0	27.0	49.2	22.0	559	64	6.3	1.1	2.1
18.0	200	1.00	25.84	47.6	35.6	30.1	26.0	38.4	8.0	298	68	6.3	1.6	3.3
18.0	500	1.00	30.12	34.3	29.4	27.0	25.1	30.6	3.7	130	74	4.7	1.1	2.1
18.0	1000	1.00	32.55	29.4	27.0	25.7	24.7	27.6	2.3	67	77	3.9	0.7	1.4
18.0	2000	1.00	34.04	26.9	25.6	25.0	24.5	26.0	1.5	34	78	3.5	0.5	1.0
18.0	3000	1.00	34.71	26.0	25.2	24.8	24.4	25.4	1.3	23	79	3.4	0.4	0.8

TABLE C-2. (CONTINUED)

TST	EST	ERI	AREA	DO	D1	D2	D3	DS	EZ	MEST	MTST	SZ	TS	SDEV
9.0	100	3.02	18.60	112.3	68.8	38.2	21.8	99.6	54.4	1956	224	17.0	5.0	10.0
9.0	200	3.02	21.32	75.7	52.3	33.5	21.7	69.5	30.0	1091	250	12.7	3.8	7.6
9.0	500	3.02	24.98	47.1	36.8	27.4	20.6	44.6	13.4	490	281	9.8	2.9	5.8
9.0	1000	3.02	27.78	34.8	29.4	23.9	19.7	33.6	7.6	266	305	7.8	2.2	4.3
9.0	2000	3.02	30.31	27.3	24.4	21.4	19.0	26.7	4.2	141	324	5.7	1.4	2.8
9.0	3000	3.02	31.70	24.4	22.5	20.4	18.7	24.0	3.0	96	332	4.8	1.1	2.2
12.0	100	3.02	19.78	83.7	52.2	33.2	21.4	68.2	31.1	1190	136	12.3	3.8	7.6
12.0	200	3.02	22.76	56.3	39.8	28.5	20.7	48.6	18.4	661	152	9.2	2.5	5.0
12.0	500	3.02	26.79	36.1	29.1	23.7	19.5	33.0	8.0	294	169	7.6	2.1	4.2
12.0	1000	3.02	29.68	27.9	24.3	21.3	18.9	26.4	4.4	157	181	5.7	1.5	3.0
12.0	2000	3.02	31.97	23.2	21.3	19.7	18.4	22.4	2.5	82	189	4.4	1.0	1.9
12.0	3000	3.02	33.01	21.5	20.2	19.1	18.2	21.0	1.9	56	193	3.8	0.7	1.5
15.0	100	3.02	20.32	68.2	42.0	29.1	20.6	50.8	21.7	771	88	9.6	2.7	5.4
15.0	200	3.02	23.61	46.0	32.5	25.1	19.8	37.4	12.3	425	97	8.0	2.0	3.9
15.0	500	3.02	27.95	30.5	24.9	21.5	18.8	27.1	5.1	189	108	6.1	1.6	3.2
15.0	1000	3.02	30.76	24.5	21.6	19.8	18.3	22.8	2.9	100	115	4.7	1.1	2.2
15.0	2000	3.02	32.94	21.2	19.8	18.8	18.0	20.4	1.7	52	119	3.8	0.7	1.4
15.0	3000	3.02	33.87	20.0	19.1	18.4	17.9	19.5	1.4	35	120	3.5	0.6	1.1
18.0	100	3.02	20.55	59.0	35.5	26.1	19.9	40.3	14.4	520	59	8.3	2.1	4.2
18.0	200	3.02	24.15	40.1	28.2	22.9	19.1	30.8	7.5	286	65	7.1	1.9	3.9
18.0	500	3.02	28.75	27.3	22.5	20.1	18.3	23.7	3.5	127	72	5.2	1.3	2.6
18.0	1000	3.02	31.54	22.6	20.2	18.9	18.0	20.8	2.0	66	76	4.2	0.8	1.7
18.0	2000	3.02	33.46	20.1	18.9	18.2	17.8	19.2	1.3	34	78	3.6	0.6	1.1
18.0	3000	3.02	34.13	19.3	18.4	18.0	17.7	18.7	1.1	23	79	3.4	0.5	0.9

TABLE C-2. (CONTINUED)

TST	EST	ERI	AREA	D0	D1	D2	D3	DS	EZ	MEST	MTST	SZ	TS	SDEV
9.0	100	7.68	16.64	82.6	44.5	22.6	12.3	69.4	41.0	1577	178	29.7	9.9	19.9
9.0	200	7.68	19.35	57.5	36.2	21.3	12.9	51.0	24.5	939	214	21.8	7.2	14.5
9.0	500	7.68	23.04	36.2	26.6	18.4	12.8	33.7	12.2	452	258	13.7	4.2	8.5
9.0	1000	7.68	25.79	26.1	20.9	16.0	12.3	24.8	7.0	250	287	9.9	2.8	5.6
9.0	2000	7.68	28.47	19.6	16.8	14.0	11.8	19.0	4.0	136	311	7.2	1.9	3.8
9.0	3000	7.68	30.14	17.0	15.2	13.2	11.6	16.6	2.7	94	322	6.0	1.6	3.2
12.0	100	7.68	17.64	65.1	35.8	21.0	12.7	49.1	24.3	983	111	20.6	7.2	14.5
12.0	200	7.68	20.63	44.0	28.4	18.9	12.7	36.2	14.6	583	133	14.8	5.0	10.0
12.0	500	7.68	24.66	27.4	20.7	15.8	12.2	24.3	7.3	275	158	9.6	2.8	5.7
12.0	1000	7.68	27.65	20.2	16.7	13.9	11.7	18.7	4.1	150	173	7.2	2.0	4.0
12.0	2000	7.68	30.42	15.9	14.1	12.6	11.3	15.2	2.3	80	184	5.3	1.3	2.6
12.0	3000	7.68	31.76	14.3	13.1	12.0	11.2	13.8	1.6	55	189	4.5	1.0	2.0
15.0	100	7.68	18.02	55.0	29.8	19.0	12.6	37.2	15.7	650	73	15.1	5.3	10.7
15.0	200	7.68	21.25	36.4	23.3	16.8	12.3	27.7	9.6	384	87	11.0	3.6	7.1
15.0	500	7.68	25.61	22.8	17.3	14.1	11.7	19.3	4.6	178	102	7.6	2.2	4.4
15.0	1000	7.68	28.85	17.2	14.4	12.7	11.3	15.5	2.6	96	111	5.7	1.5	3.0
15.0	2000	7.68	31.53	14.1	12.7	11.8	11.0	13.3	1.5	50	116	4.4	1.0	1.9
15.0	3000	7.68	32.72	13.0	12.1	11.4	10.9	12.5	1.1	34	118	3.9	0.7	1.5
18.0	100	7.68	18.16	48.5	25.6	17.4	12.3	29.6	10.8	448	50	11.8	4.0	8.0
18.0	200	7.68	21.53	31.8	20.0	15.2	11.9	22.4	6.6	262	59	8.9	2.7	5.4
18.0	500	7.68	26.31	20.0	15.2	13.0	11.3	16.4	3.1	121	69	6.2	1.7	3.4
18.0	1000	7.68	29.46	15.6	13.1	11.9	11.0	13.7	1.8	64	74	4.9	1.1	2.3
18.0	2000	7.68	32.00	13.2	11.9	11.3	10.8	12.2	1.1	33	77	4.0	0.7	1.5
18.0	3000	7.68	33.27	12.3	11.5	11.1	10.7	11.7	0.8	23	78	3.7	0.6	1.2

TABLE C-2. (CONTINUED)

TST	EST	ERI	AREA	D0	D1	D2	D3	DS	EZ	MEST	MTST	SZ	TS	SDEV
9.0	100	12.34	15.38	67.8	33.0	15.8	8.4	54.1	33.9	1334	148	38.9	13.7	27.4
9.0	200	12.34	18.05	47.5	27.8	15.4	9.0	40.9	20.9	829	187	28.6	10.2	20.4
9.0	500	12.34	21.74	30.2	21.1	13.9	9.2	27.7	10.8	418	238	17.7	6.0	12.0
9.0	1000	12.34	24.53	21.7	16.8	12.2	9.0	20.5	6.4	238	272	12.2	3.8	7.5
9.0	2000	12.34	27.23	16.0	13.3	10.7	8.6	15.4	3.7	131	300	8.6	2.4	4.9
9.0	3000	12.34	28.69	13.7	11.8	9.9	8.4	13.3	2.6	91	314	7.0	1.9	3.8
12.0	100	12.34	16.23	55.4	27.6	15.2	8.9	39.0	20.2	842	93	26.7	10.1	20.2
12.0	200	12.34	19.11	37.4	22.2	14.1	9.1	29.5	12.8	524	118	19.0	7.0	13.9
12.0	500	12.34	23.22	23.1	16.6	12.1	8.9	20.0	6.6	259	148	11.9	3.9	7.8
12.0	1000	12.34	26.19	16.7	13.2	10.6	8.6	15.1	3.8	144	166	8.5	2.6	5.1
12.0	2000	12.34	29.06	12.7	10.9	9.4	8.2	11.9	2.2	78	179	6.1	1.6	3.3
12.0	3000	12.34	30.70	11.2	10.0	9.0	8.1	10.7	1.5	54	185	5.1	1.3	2.5
15.0	100	12.34	16.55	48.0	23.5	14.2	9.0	29.9	13.3	565	62	19.1	7.2	14.5
15.0	200	12.34	19.62	31.5	18.6	12.7	8.9	22.6	8.4	349	78	13.7	4.9	9.8
15.0	500	12.34	24.00	19.1	13.7	10.7	8.5	15.6	4.3	169	96	9.0	2.8	5.7
15.0	1000	12.34	27.26	14.0	11.2	9.5	8.2	12.3	2.4	93	107	6.5	1.9	3.7
15.0	2000	12.34	30.33	11.0	9.6	8.7	8.0	10.2	1.4	50	114	4.9	1.2	2.4
15.0	3000	12.34	31.62	10.0	9.0	8.4	7.9	9.4	1.0	34	117	4.3	0.9	1.8
18.0	100	12.34	16.62	43.1	20.6	13.1	8.9	23.9	9.2	393	43	14.5	5.3	10.7
18.0	200	12.34	19.89	27.6	16.0	11.6	8.7	18.2	5.8	241	54	10.7	3.6	7.2
18.0	500	12.34	24.54	16.7	11.9	9.8	8.2	13.0	2.9	115	65	7.2	2.2	4.3
18.0	1000	12.34	27.98	12.5	10.0	8.9	8.0	10.6	1.7	63	72	5.4	1.4	2.8
18.0	2000	12.34	31.07	10.1	8.9	8.3	7.8	9.2	1.0	33	76	4.4	0.9	1.8
18.0	3000	12.34	32.39	9.3	8.5	8.1	7.7	8.7	0.8	22	77	3.9	0.7	1.4

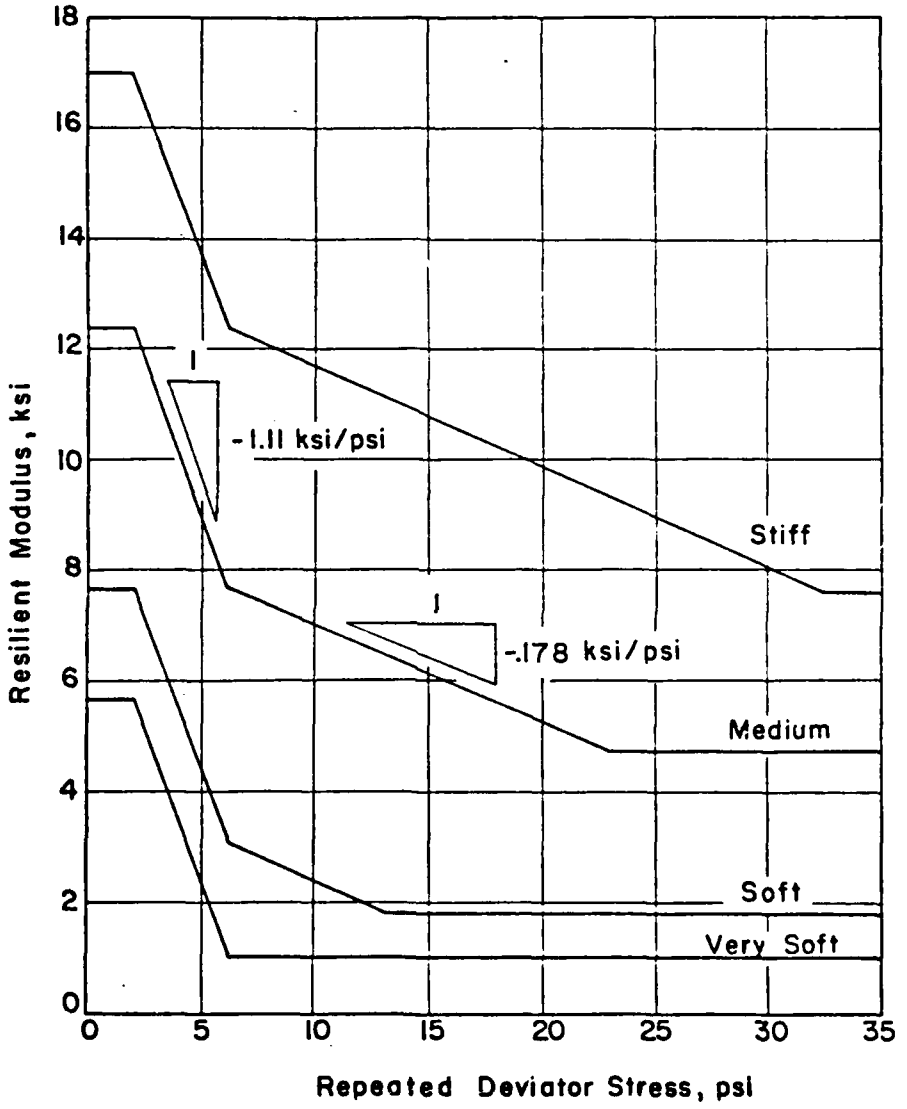

Figure C-1. Standard Soil Resilient Modulus Models for ILLI-PAVE Solutions (Reference 8)

APPENDIX D

ULTIMATE LOAD DATA BASE

TABLE D-1. ULTIMATE LOAD DATA BASE

REF	LOAD NO	LOAD TYPE	RADIUS A (IN)	H (IN)	FLEX STRG (PSI)	K (PCI)	CBR	MU	E (PSI)	A/H	FIELD ULTIMATE LOAD (KIPS)	FIELD ULTIMATE DEFL (MILS)	CALC ULT LOAD COLL (KIPS)	CALC ULT LOAD PUNCH (KIPS)	RATIOS LOAD COLL	RATIOS PUNCH
1	1	INT	3.5	4.0	98	43	2	.10	.24E+07	.875	8.75	164.0	3.46	6.77	2.53	1.29
1	2	INT	3.5	4.0	104	49	1	.10	.24E+07	.875	6.00	105.0	3.67	7.19	1.63	.83
1	3	INT	3.5	4.0	275	39	3	.10	.24E+07	.875	17.75	214.0	9.69	19.01	1.83	.93
1	4	INT	3.5	4.0	280	48	1	.10	.24E+07	.875	16.25	219.0	9.89	19.35	1.64	.84
1	7	INT	3.5	4.0	79	79	2	.10	.24E+07	.875	8.25	117.0	2.81	5.46	2.94	1.51
1	8	INT	3.5	4.0	86	88	3	.10	.24E+07	.875	10.00	151.0	3.06	5.94	3.26	1.68
1	5	EDG	3.5	4.0	290	30	2	.10	.24E+07	.875	8.25	288.0	6.08	-----	1.36	----
1	6	EDG	3.5	4.0	293	35	3	.10	.24E+07	.875	8.25	262.0	6.16	-----	1.34	----
2	11	INT	3.5	4.0	155	126	9	.10	.18E+07	.875	14.02	129.0	5.59	10.71	2.51	1.31
2	12	INT	3.5	4.0	133	126	9	.10	.12E+07	.875	7.01	65.0	4.83	9.19	1.45	.76
2	13	INT	3.5	5.5	155	126	9	.10	.18E+07	.640	15.98	73.0	10.39	16.74	1.54	.95
2	14	INT	3.5	5.5	133	126	9	.10	.12E+07	.640	9.98	64.0	8.97	14.36	1.11	.69
2	15	EDG	3.5	4.0	155	126	9	.10	.18E+07	.875	6.80	74.0	3.43	-----	1.98	----
2	16	EDG	3.5	4.0	155	126	9	.10	.18E+07	.875	8.30	138.0	3.43	-----	2.42	----
2	17A	EDG	3.5	5.5	155	126	9	.10	.18E+07	.640	10.07	66.0	6.27	-----	1.61	----
2	17B	EDG	3.5	5.5	155	126	9	.10	.18E+07	.640	9.51	127.0	6.27	-----	1.52	----
2	19	EDG	3.5	5.5	133	126	9	.10	.12E+07	.640	4.53	42.0	5.45	-----	.83	----
2	110	EDG	3.5	5.5	133	126	9	.10	.12E+07	.640	7.05	169.0	5.45	-----	1.29	----
2	111	EDG	3.5	4.0	133	126	9	.10	.12E+07	.875	4.53	120.0	3.00	-----	1.51	----
2	112	EDG	3.5	4.0	133	126	9	.10	.12E+07	.875	9.06	150.0	3.00	-----	3.02	----
2	111	INT	3.5	4.0	39	140	7	.10	.12E+06	.875	5.99	108.0	1.52	2.70	3.93	2.22
2	112	INT	3.5	5.5	39	140	7	.10	.12E+06	.640	8.90	274.0	2.78	4.21	3.20	2.11
2	113	INT	3.5	4.0	85	140	7	.10	.40E+06	.875	12.59	204.0	3.18	5.87	3.96	2.14
2	114	INT	3.5	5.5	85	140	7	.10	.40E+06	.640	17.01	270.0	5.87	9.18	2.90	1.85
2	116	EDG	3.5	5.5	39	140	7	.10	.12E+06	.640	6.60	130.0	1.81	-----	3.65	----

TABLE D-1. (CONTINUED)

REF	LOAD NO	LOAD TYPE	RADIUS A (IN)	H (IN)	FLEX STRG (PSI)	K (PCI)	CBR	MU	E (PSI)	A/H	FIELD ULTIMATE LOAD (KIPS)	DEFL (MILS)	CALC ULT LOAD COLL (KIPS)	PUNCH (KIPS)	LOAD COLL	RATIOS PUNCH
2	117	EDG	3.5	5.5	39	140	7	.10	.12E+06	.640	9.03	272.0	1.81	-----	5.00	----
2	118A	EDG	3.5	4.0	39	140	7	.10	.12E+06	.875	3.20	67.0	1.04	-----	3.09	----
2	118B	EDG	3.5	4.0	39	140	7	.10	.12E+06	.875	1.70	36.0	1.04	-----	1.64	----
2	119	EDG	3.5	5.5	85	140	7	.10	.40E+06	.640	10.15	226.0	3.67	-----	2.77	----
2	1110	EDG	3.5	4.0	85	140	7	.10	.40E+06	.875	4.00	97.0	2.05	-----	1.95	----
2	1111	EDG	3.5	4.0	85	140	7	.10	.40E+06	.875	5.80	158.0	2.05	-----	2.83	----
2	1112	EDG	3.5	5.5	85	140	7	.10	.40E+06	.640	6.10	95.0	3.67	-----	1.66	----
3	1	INT	6.0	6.0	55	50	3	.20	.22E+06	1.000	15.30	274.0	4.70	9.33	3.25	1.64
3	2	INT	6.0	6.0	55	450	*	.20	.22E+06	1.000	40.00	307.0	5.21	9.33	7.67	4.29
3	3	INT	6.0	9.0	55	50	3	.20	.22E+06	.670	22.00	400.0	10.22	16.33	2.15	1.35
3	4	INT	6.0	9.0	55	450	*	.20	.22E+06	.670	36.00	280.0	10.99	16.33	3.28	2.20
3	5	INT	6.0	12.0	55	50	3	.20	.22E+06	.500	36.50	350.0	17.84	24.88	2.05	1.47
3	6	INT	6.0	12.0	55	450	*	.20	.22E+06	.500	48.00	282.0	18.88	24.88	2.54	1.93

REF 1: BARENBERG AND AHLBERG, POZZOLANIC PAVEMENTS, BULLETIN 473, EES, U OF ILL., 1975.

REF 2: BARENBERG, EVALUATING STABILIZED MATERIALS, NCHRP NO 63-45-1, EES, U OF ILL, 1967.

REF 3: SUDDATH AND THOMPSON, LOAD-DEFLECTION BEHAVIOR OF LIME-STABILIZED LAYERS, TR-M-118, CERL, 1975.

MEYERHOF ULTIMATE LOAD EQUATIONS

Notation

a = Radius of loaded area, inches

E = Modulus of elasticity of slab material, psi

f_b = Modulus of rupture for slab material, psi

h = Slab thickness, inches

k = Modulus of subgrade reation, psi/inch

ℓ = Radius of relative stiffness, inches = $\sqrt[4]{\frac{E\,h^3}{(1-\mu^2)\,k}}$

$M_o = \frac{f_b\,h^2}{6}$

m = Center to center spacing of tandem gear assembly (circular load area of radius a)

P = Collapse load, pounds

μ = Poisson's ratio

Single-Wheel Load

Interior Loading

$$P_i = \left(\frac{4\pi}{1 - \frac{a}{3\ell}}\right) M_o$$

Edge Loading

$$P_e = \left[\frac{4 + \pi}{(1 - \frac{2a}{3\ell})}\right] M_o$$

Corner Loading

$$P_c = \left[\frac{4}{(1 - \frac{a}{\ell})}\right] M_o$$

Figure D-1. Meyerhof Ultimate Load Equations (Reference 35)

APPENDIX E

F-4 ILLI-PAVE INVERTED PAVEMENT DATA BASE

TABLE E-1. SUMMARY OF MATERIAL PROPERTIES, F-4 ILLI-PAVE INVERTED PAVEMENT STRUCTURAL RESPONSE DATA BASE

Property	Asphalt Concrete	Crushed Stone	Stabilized Material	Standard Medium Subgrade
Unit Weight, pcf	145	140	130	120
Coefficient at Rest	0.67	0.60	0.35	0.82
Poisson's Ratio	0.30	0.35	0.15	0.45
Unconf. Comp. Strength, psi	---	---	---	22.85
Friction Angle	---	45	---	0
Cohesion, psi	---	0	---	11.43
Modulus of Elasticity, ksi	700	(1)	Varies	---
Subgrade Modulus Response (2)				
E_{ri} at σ_{di}, ksi				7.68
σ_{di}, psi				6.20
E-Failure, ksi				4.72
Deviator Stress Lower Limit, psi				2.00
Deviator Stress Upper Limit, psi				22.85

(1) Resilient Modulus, $E_{cs} = 6.9750^{0.45}$

(2) See Figure C-1, Appendix C

TABLE E-2. F-4 ILLI-PAVE INVERTED PAVEMENT DATA BASE, STRUCTURAL RESPONSE TO 27 KIP, 265 PSI LOAD

Variable	Symbol
Thickness of Stabilized Layer, inches	t_{sm}
Modulus of Elasticity of Stabilized Layer, ksi	E_{sm}
Thickness of Crushed Stone Base Course, inches	t_{cs}
Surface Deflection Basin	
Deflection at R = 0 inches from load, mils	D0
Deflection at R = 12 inches from load, mils	D1
Deflection at R = 24 inches from load, mils	D2
Deflection at R = 36 inches from load, mils	D3
Deflection Basin Area, inches	Area
Radial Strain Bottom of Asphalt Concrete Wearing Course, microstrain	ac
Stress State in Crushed Stone Base Course (1)	
$(\sigma_1+\sigma_3)/2$, psi	p
$(\sigma_1-\sigma_3)/2$, psi	q
Shear Stress Ratio (q_f = ptan 35.3 degrees)	q/q_f
Stabilized Material Subbase (Bottom of Layer)	
Radial (Tensile) Stress, psi	σ_{sm}
Radial (Tensile) Strain, microstrain	ε_{sm}
Subgrade (Top of Layer)	
Vertical (Normal) Stress, psi	σ_v
Deviator Stress, psi	σ_d
Shear Stress Ratio	τ/c

(1) For 4 in. stone base, measured at 2.5 in. depth and radial distance of 0.5 in. For 6 and 8 in. stone base, measured at stone depth of 3.5 in. and radial distance of 0.5 in.

TABLE E-2. (CONTINUED)

t_{sm}	E_{sm}	t_{cs}	D0	D1	D2	D3	Area	ε_{ac}	p	q	q/q_f	σ_{sm}	ε_{sm}	σ_v	σ_d	τ/c
6	200	4	58.15	35.91	21.74	12.99	19.24	207	153.2	65.9	0.61	169	793	20.2	12.6	0.55
6	500	4	47.11	30.42	20.26	13.19	20.59	218	176.0	70.0	0.56	260	487	15.8	9.0	0.39
6	1000	4	39.41	25.63	18.37	12.98	21.37	233	186.0	78.0	0.59	340	319	12.5	6.6	0.29
6	200	6	57.58	34.06	21.10	12.99	18.85	247	126.5	75.6	0.85	142	664	18.2	11.2	0.49
6	500	6	48.82	29.32	19.67	13.08	19.65	260	142.3	81.8	0.81	224	418	14.6	8.2	0.36
6	1000	6	42.33	25.03	17.90	12.84	19.99	271	150.1	88.9	0.84	298	279	11.8	6.1	0.26
6	200	8	57.28	32.39	20.42	12.92	18.41	270	117.2	87.9	1.06	119	558	16.4	9.8	0.43
6	500	8	50.22	28.26	19.02	12.92	18.84	283	127.2	93.8	1.04	192	358	13.5	7.3	0.32
6	1000	8	44.81	24.51	17.37	12.64	18.91	293	131.1	98.9	1.07	260	243	11.2	5.5	0.24
9	200	4	47.03	29.09	19.44	12.90	20.03	219	162.8	72.2	0.63	116	538	14.5	9.3	0.40
9	500	4	36.78	23.33	17.22	12.65	21.29	234	183.0	79.0	0.61	170	313	10.9	6.2	0.26
9	1000	4	30.63	19.25	15.31	12.23	21.94	250	191.0	86.0	0.64	210	193	8.7	4.7	0.20
9	200	6	48.30	28.02	18.90	12.81	19.25	260	134.3	80.8	0.85	101	466	13.4	8.3	0.36
9	500	6	39.80	22.87	16.79	12.52	19.85	271	148.6	89.5	0.85	151	278	10.4	5.7	0.25
9	1000	6	34.44	19.10	14.97	12.08	19.98	282	154.6	95.5	0.87	190	174	8.5	4.4	0.19
9	200	8	49.36	26.97	18.24	12.63	18.53	284	123.4	92.6	1.06	87	401	12.8	7.6	0.33
9	500	8	42.32	22.44	16.28	12.30	18.72	293	145.3	109.8	1.07	132	242	10.2	5.3	0.23
9	1000	8	37.63	19.08	14.62	11.87	18.64	300	132.8	102.2	1.09	168	154	8.4	4.2	0.18
12	200	4	40.16	24.13	17.31	12.53	20.26	230	165.3	76.7	0.66	83	379	11.1	6.9	0.30
12	500	4	31.03	18.92	15.02	12.07	21.46	246	184.5	83.5	0.64	115	210	8.5	4.8	0.21
12	1000	4	26.25	15.78	13.46	11.66	22.03	258	192.0	90.0	0.66	137	124	6.7	3.5	0.15
12	200	6	42.29	23.52	16.85	12.40	19.21	269	137.2	84.8	0.87	73	335	10.6	6.4	0.29
12	500	6	34.56	18.75	14.68	11.92	19.68	280	150.1	93.0	0.88	104	189	8.3	4.5	0.20
12	1000	6	30.37	15.81	13.19	11.51	19.73	290	155.7	98.3	0.89	125	113	6.6	3.3	0.14
12	200	8	44.30	23.10	16.39	12.21	18.35	292	124.8	95.2	1.08	64	296	10.3	5.9	0.26
12	500	8	37.64	18.77	14.36	11.72	18.43	299	145.9	112.1	1.09	93	170	8.2	4.3	0.19
12	1000	8	33.89	16.05	12.95	11.32	18.27	306	133.4	103.7	1.10	114	103	6.6	3.2	0.14

LIST OF REFERENCES

1. Bittle, Darrel G., "Air Base Survivability," US Air Force Engineering and Services Quarterly, AFRP 85-1, Vol. 23, No. 1, Spring 1982, pp. 7-13.

2. Van Orman, James R. and Langford, Clarence E., "Can We Survive and Win," US Air Force Engineering and Services Quarterly, AFRP 85-1, Vol. 23, No. 1, Spring 1982, pp. 14-18.

3. Hammitt, G.M. II, Thickness Requirements for Unsurfaced Roads and Airfields, Technical Report S-70-5, US Army Engineer Waterways Experiment Station, Vicksburg, Mississippi, July 1970.

4. Grau, R.W., Stabilization of Soil and Aggregate Materials for Forward Area Operations, Instruction Report S-74-3, US Army Engineer Waterways Experiment Station, Vicksburg, Mississippi, September 1974.

5. Brabston, W.N. and Hammitt, G.W. II, Soil Stabilization for Roads and Airfields in the Theater of Operations, Misc Paper Report S-74-23, US Army Engineer Waterways Experiment Station, Vicksburg, Mississippi, September 1974.

6. Rone, C.L. "Alternate Launch and Recovery Surfaces State-of-the-Art Study," unpublished report, US Army Engineer Waterways Experiment Station, Vicksburg, Mississippi, October 1980.

7. Air Force Aeronautical Laboratory, Wright-Patterson AFB, Ohio, "Initial Aircraft Operation on Soil Prediction Routine Familiarization," AFWAL/FIEM, Wright-Patterson AFB, Ohio, 17 November 1983 (Mimeographed).

8. Thompson, M.R. and Dempsey, B.J., Development of a Preliminary ALRS Stabilization Material Pavement Analysis System (SPAS), Technical Report ESL-TR-83-84, US Air Force Engineering and Services Center, Tyndall AFB, Florida, March 1984.

9. Styron, C.R., Performance Data For F-4 Operations on Alternate Launch and Recovery Surfaces, unpublished report, US Army Engineer Waterways Experiment Station, Vicksburg, Mississippi, August 1983.

10. Raad, Lutfi and Figueroa, Jose L. "Load Response of Transportation Support Systems," Transportation Engineering Journal of the ASCE, Proceedings, Vol. 106, No. TE1, January 1980, pp. 111-128.

11. Ledbetter, R.H., Rice, J.L., Ulery, H.H., Kearney, F.W. and Gambill, J.B., Multiple-Wheel Heavy Gear Load Pavement Test, Vol. IIIA, Presentation and Initial Analysis of Stress-Strain-Deflection and Vibratory Measurements; Instrumentation, Technical Report S-71-17, US Army Engineer Waterways Experiment Station, Vicksburg, Mississippi, November 1971.

12. Thompson, M.R., Ioannides, A.M., Fischer, J.M., and Barenberg, E.J., Development of a Stress-Dependent Finite Element Slab Model, Report No. AFOSR-TR-83-1061, Air Force Office of Scientific Research (AFOSR), 1983., Report No. FAA-RD-79-4, November 1979.

13. Thompson, M.R. and Robnett, Q.L., "Final Report, Resilient Properties of Subgrade Soils," Civil Engineering Studies, Series No. 160, University of Illinois, Champaign-Urbana Illinois, June 1976.

14. Fossberg, P.E., Load-Deflection Characteristics of Three-Layer Pavements Containing Cement-Stabilized Bases, Ph.D. Thesis Dissertation, University of California, Berkley, California, 1970.

15. Duncan, J.M. Monismith, C.L. and Wilson, E.L., "Finite Element Analysis of Pavements," Highway Research Record, No. 228, Highway Research Board, Mashington, D.C., 1968, pp. 18-33.

16. Hicks, R.G. and Monismith, C.L., "Factors Influencing the Resilient Response of Granular Materials," Highway Research Record, No. 345, Highway Research Board, Washington, D.C., 1971, pp. 15-31.

17. US Army Engineer Waterways Experiment Station, Vicksburg, Mississippi, unpublished laboratory report from MX road study.

18. Rada, Gonzalo and Witczak, M.W., "Comprehensive Evaluation of Laboratory Resilient Moduli Results for Granular Material," Transportation Research Record, No. 810, 1981, pp. 23-33.

19. Lambe, T. William and Whitman, Robert V., Soil Mechanics, Massachusetts Institute of Technology, New York, John Wiley and Sons, 1969.

20. Transportation Research Board, Washington D.C., "State-of-the-Art: Lime Stabilization," Transportation Research Circular, Number 180, September 1976.

21. Mitchell, J.K., Dzwilewski, P and Monismith, C.L., Behavior of Stabilized Soils Under Repeated Loading; Report 6, A Summary Report with a Suggested Structural Pavement Design Procedure, Contract Report No. 3-145, US Army Engineer Waterways Experiment Station, Vicksburg, Mississippi, 1974.

22. Thompson, Marshall R. and Dempsey, Barry J., Final Report Durability Testing of Stabilized Materials, UILU-ENG-74-2010, Engineering Experiment Station, Urbana, Illinois, June 1974.

23. "Soil Stabilization with Portland Cement," Bulletin 292, Highway Research Board, Washington, D.C., 1961.

24. Witczak, M.W., Pavement Performance Models, Repeated Load Fracture of Pavement Systems, Contract Report No. S-76-15, Vol. I, US Army Engineer Waterways Experiment Station, Vicksburg, Mississippi, August 1976.

25. Otte, E., Van Wyk and Louw, Inc., "Analysis of a Cracked Pavement Base Layer," Transportation Research Record, No. 725, Transportation Research Board, Washington D.C., 1979, pp. 45-51.

26. Otte, Eddie. Savage, Philip F. and Monismith, Carl L., "Structural Design of Cemented Pavement Layers," Transportation Engineering Journal of the ASCE, Proceedings, Vol. 108, No. TE4, July 1982, pp. 428-445.

27. Westergaard, H.M., "New Formulas for Stresses in Concrete Pavements of Airfields," Transactions of American Society of Civil Engineers, May 1947, pp. 687-701.

28. Tabatabaie, A.M. and Barenberg, "Structural Analysis of Concrete Pavement Systems," American Society of Civil Engineers Paper 3563, presented at Spring Convention, Boston, Massachusetts, 1979.

29. Maree, J.H. and Freeme, C.R., The Mechanistic Design Method Used To Evaluate the Pavement Structures in the Catalogue of the Draft TRH4 1980, Technical Report RP/2/81, National Institute For Transportation and Road Research, CSIR, South Africa, March 1981.

30. Swanson, T.E. and Thompson, M.R., "Flexural Fatigue Strength of Lime-Soil Mixtures," Highway Research Record, No. 198, Highway Research Board, Washington, D.C., 1967.

31. Pretorious, P.C., Design Considerations for Pavements Containing Soil-Cement Bases, Ph.D. Dissertation, Civil Engineering, University of California, Berkley, California, 1970.

32. Shen, Chih-Kang and Mitchell, James K., "Behavior of Soil-Cement in Repeated Compression and Flexure. " Highway Research Record, No. 128, Highway Research Board, Washington, D.C., 1966.

33. Pell, P.S., "Characterization of Fatigue Behavior," Special Report 140, Highway Research Board, Washington, D.C.,1966.

34. Raad, L., Design Criteria for Soil-Cement Bases, Ph.D Thesis, Department of Civil Engineering, University of California, Berkley, California. 1976.

35. Meyerhof, G.G., "Load Carrying Capacity of Concrete Pavements," Journal, Soil Mechanics and Foundations Division, ACSE, Vol. 88, No. SM3, June 1962, pp. 89-116.

36. Barenberg, Ernest J. and Ahlberg, Harold L., Pozzolanic Pavements, Bulletin 473, Engineering Experiment Station, College of Engineering, University of Illinois, Champaign, Illinois, 1975.

37. Barenberg, Ernest J., Evaluating Stabilized Materials, Contract Report NO. HR-63-4-1, National Cooperative Highway Research Program, Engineering Experiment Station, University of Illinois, Champaign, Illinois, February 1967.

38. Suddath, L.P. and Thompson, M.R., Load-Deflection Behavior of Lime-Stabilized Layers, Technical Report M-118, Construction Engineering Research Laboratory, Champaign, Illinois, January 1975.

39. Barenberg, Ernest J., "The Behavior and Performance of Asphalt Pavements with Lime-Fly ash-Aggregate Bases," 2nd International Conference on the Structural Design of Asphalt Pavements, Proceedings, University of Michigan, Ann Arbor, Michigan, 1967, pp. 619-633.

40. Wang, M.C. and Kilareski, W.P., "Behavior and Performance of Aggregate-Cement Pavements," Transportation Research Record, No. 715, Transportation Research Board, Washington, D.C., 1979, pp. 67-73.

41. Berens, Alan P., Newman, Ronald, Analysis for the Determination of Significant Characteristics of Runway Roughness, Technical Report AFFDL-TR-73-109, Air Force Flight Dynamics Laboratory, Wright-Patterson AFB, Ohio, November 1973.

42. Sonnenburg, Paul N., Analysis of Airfield Roughness Criteria, Technical Report No. FAA-RD-75-110, Federal Aviation Administration, Washington, D.C., November 1976.

43. Gerardi, Anthony G., Digital Simulation of Flexible Aircraft Response to Symmetrical and Asymmetrical Runway Roughness, AFFDL-TR-77-37, Air Force Flight Dynamics Laboratory, Wright-Patterson AFB, Ohio, August 1977.

44. Gerardi, Anthony G., Dynamic Response of Aircraft to Pavement Unevenness, Special Report, Transportation Research Board, Washington, D.C., 1978.

45. Rapid Runway Repair Interim Planning Guidance, Engineering and Services Laboratory, Air Force Engineering and Services Center, Tyndall AFB, Florida, December 1981.

46. Larsen, T.J. and Nussbaum, P.J., "Fatigue of Soil-Cement," Portland Cement Association, Research and Development Laboratories Development Department, Bulletin D119, 1967, pp. 37-60.

47. Mitchell, J.K. and Monismith, C.L., "A Thickness Design Procedure for Pavements with Cement Stabilized Bases and Thin Asphalt Surfacings," Fourth International Conference on the Structural Design of Asphalt Pavement, University of Michigan, 1977, pp. 409-416.

VITA

PII Redacted

Robert Riddick Costigan was born in [redacted] In 1970, he received his B.S. in civil engineering from the Virginia Military Institute and also received a commission in the U.S. Air Force. He received a M.S. in civil engineering from the University of Missouri-Columbia in 1974. His master's degree thesis was entitled "The Effective Management of Professional Engineers." From 1974 to 1978 he served as chief of base level engineering design sections at U.S. Air Bases in Korea and Germany. He was an Air Force Institute of Technology Education With Industry student with Brown and Root, Inc. of Houston, Texas from 1978 to 1979. He was then transferred to the Engineering and Services Center, Tyndall AFB, Florida, where he was a research civil engineer in the Rapid Runway Repair Program. In 1981 he was selected for the Ph.D. program by the Air Force Institute of Technology. He expects to receive his Ph.D. from the University of Illinois at Urbana-Champaign in 1984.

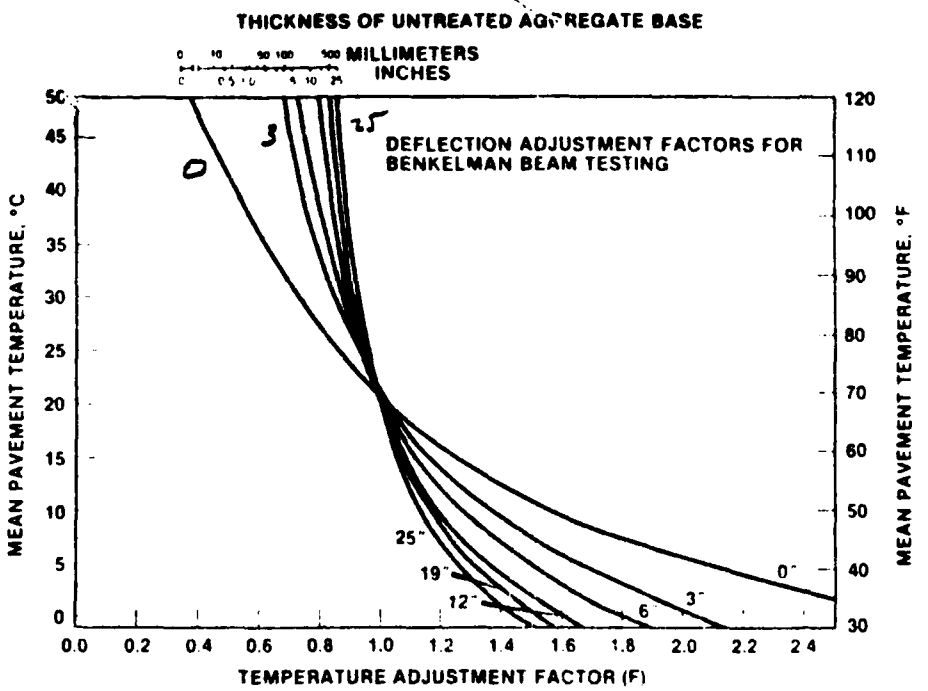

Figure IV-2—Average pavement temperature versus Benkelman Beam deflection adjustment factors for Full-Depth and three-layered asphalt concrete pavements